frontiers | Research Topics

Lung adenocarcinoma: From genomics to immunotherapy

Edited by
Yiming Meng and Elisa Frullanti

Published in
Frontiers in Genetics
Frontiers in Oncology
Frontiers in Immunology
Frontiers in Pharmacology

ISSN 1664-8714
ISBN 978-2-8325-4813-4
DOI 10.3389/978-2-8325-4813-4

About Frontiers

Frontiers is more than just an open access publisher of scholarly articles: it is a pioneering approach to the world of academia, radically improving the way scholarly research is managed. The grand vision of Frontiers is a world where all people have an equal opportunity to seek, share and generate knowledge. Frontiers provides immediate and permanent online open access to all its publications, but this alone is not enough to realize our grand goals.

Frontiers journal series

The Frontiers journal series is a multi-tier and interdisciplinary set of open-access, online journals, promising a paradigm shift from the current review, selection and dissemination processes in academic publishing. All Frontiers journals are driven by researchers for researchers; therefore, they constitute a service to the scholarly community. At the same time, the *Frontiers journal series* operates on a revolutionary invention, the tiered publishing system, initially addressing specific communities of scholars, and gradually climbing up to broader public understanding, thus serving the interests of the lay society, too.

Dedication to quality

Each Frontiers article is a landmark of the highest quality, thanks to genuinely collaborative interactions between authors and review editors, who include some of the world's best academicians. Research must be certified by peers before entering a stream of knowledge that may eventually reach the public - and shape society; therefore, Frontiers only applies the most rigorous and unbiased reviews. Frontiers revolutionizes research publishing by freely delivering the most outstanding research, evaluated with no bias from both the academic and social point of view. By applying the most advanced information technologies, Frontiers is catapulting scholarly publishing into a new generation.

What are Frontiers Research Topics?

Frontiers Research Topics are very popular trademarks of the *Frontiers journals series*: they are collections of at least ten articles, all centered on a particular subject. With their unique mix of varied contributions from Original Research to Review Articles, Frontiers Research Topics unify the most influential researchers, the latest key findings and historical advances in a hot research area.

Find out more on how to host your own Frontiers Research Topic or contribute to one as an author by contacting the Frontiers editorial office: frontiersin.org/about/contact

Lung adenocarcinoma: From genomics to immunotherapy

Topic editors
Yiming Meng — China Medical University, China
Elisa Frullanti — University of Siena, Italy

Citation
Meng, Y., Frullanti, E., eds. (2024). *Lung adenocarcinoma: From genomics to immunotherapy*. Lausanne: Frontiers Media SA. doi: 10.3389/978-2-8325-4813-4

Table of contents

frontiers | Frontiers in Genetics

TYPE Editorial
PUBLISHED 09 April 2024
DOI 10.3389/fgene.2024.1399127

OPEN ACCESS

EDITED AND REVIEWED BY
Anton A. Buzdin,
European Organisation for Research and Treatment of Cancer, Belgium

*CORRESPONDENCE
Elisa Frullanti,
elisa.frullanti@dbm.unisi.it

†These authors share last authorship

RECEIVED 11 March 2024
ACCEPTED 27 March 2024
PUBLISHED 09 April 2024

CITATION
Meng Y, Palmieri M and Frullanti E (2024), Editorial: Lung adenocarcinoma: from genomics to immunotherapy.
Front. Genet. 15:1399127.
doi: 10.3389/fgene.2024.1399127

Editorial: Lung adenocarcinoma: from genomics to immunotherapy

Yiming Meng[1], Maria Palmieri[2,3†] and Elisa Frullanti[2,3*†]

[1]Department of Central Laboratory, Cancer Hospital of Dalian University of Technology, Liaoning Cancer Hospital and Institute, Shenyang, China, [2]Cancer Genomics and Systems Biology Lab, Department of Medical Biotechnologies, University of Siena, Siena, Italy, [3]Department of Medical Biotechnologies, Med Biotech Hub and Competence Centre, University of Siena, Siena, Italy

KEYWORDS

solid cancer, cancer biomarkers, cancer prognosis, disease monitoring, lung cancer, precision medicine

Editorial on the Research Topic
Lung adenocarcinoma: from genomics to immunotherapy

Introduction

Lung cancer is the second most common type of cancer and is the leading cause of cancer death globally. In 2018, almost 2.1 million new cases were diagnosed, accounting for ~12% of the cancer burden worldwide (*Sung et al., 2021*). The malignant stage of lung cancer is known as lung adenocarcinoma, which is the most common and is diagnosed in both smokers and non-smokers.

There are two main types of lung cancer, the non-small cell lung cancer (NSCLC) and the small cell lung cancer (SCLC). Genomic studies have indicated that more than 80% of lung malignancies are classified as NSCLC, of which adenocarcinoma is the predominant subtype. In metastatic patients, although significant progress has been made for tumors harboring druggable mutations such as EGFR, the majority of those is lacking of such mutations and the prognosis remains poor. Platinum doublet chemotherapy has been the mainstay first-line treatment for patients who are diagnosed with metastatic lung adenocarcinoma without a targetable mutation (*Bodor et al., 2018*).

In recent years, immunotherapy has emerged as a treatment option that has shown a strong response in a subset of patients. The immune agents block crucial checkpoints and regulate the immune response, but the tumor cells evade the patient's immune system. By blocking these receptor–ligand interactions, a particular subset of T cells is activated to recognize and respond to tumor cells. While such responses to immunotherapy are promising, they have only been effective in ~20% of patients (*Murciano-Goroff et al., 2020*).

Therefore, there is an urgent need to understand the underlying mechanism of lung adenocarcinoma from genome to immunotherapy. To address this unmet need, this Research Topic will focus on advancements related to lung adenocarcinoma (LUAD) and the identification of novel biomarkers as new therapy-determining or

companion prognostic tools for the development of precise mechanism-based treatments.

Novel prognostic biomarkers for lung adenocarcinoma

The original articles published in the present Research Topic updated about novel prognostic biomarkers in lung adenocarcinoma patients through *in silico* approaches. In particular, Wang et al. F's group assessed the roles of unlocking phenotypic plasticity (UPP) in immune status, prognosis, and treatment in patients with LUAD based on the cancer genome atlas (TCGA) database (https://www.frontiersin.org/journals/genetics/articles/10.3389/fgene.2022.941567/full). They proposed UPP as a new and reliable prognosis indicator to predict the patient's overall survival and help the clinician to predict therapeutic responses and make individualized treatment plans.

Similarly, Zhou X et al. investigated the expression of indolethylamine N-methyltransferase (INMT) and its clinical value as a prognostic biomarker in LUAD based on TCGA and Gene Expression Omnibus (GEO) databases (https://www.frontiersin.org/journals/genetics/articles/10.3389/fgene.2022.946848/full). They found that INMT expression was significantly downregulated in LUAD, and the low expression of INMT was associated with poor prognosis but favorable immunotherapy response in LUAD.

Song Y et al. highlighted the association of necroptosis with LUAD and its potential use in guiding immunotherapy based on transcriptomic and clinical data of patients from TCGA and GEO databases (https://www.frontiersin.org/journals/genetics/articles/10.3389/fgene.2022.1027741/full). They analyzed 902 samples and identified a prognostic signature of five necroptosis-related genes that could be used to predict the prognosis of LUAD patients.

Additionally, Zhu X's group focused their attention on the role of basement membranes (BMs) and their related genes for prognosis prediction in LUAD patients from TCGA and GEO databases (https://www.frontiersin.org/journals/genetics/articles/10.3389/fgene.2023.1100560/full). They used a training set of data and a verification cohort and identified a prognostic signature of ten BM-associated genes that could be used to predict the prognosis of LUAD patients and guide personalized treatment.

Zhang et al. investigated the relationship between cuproptosis and long non-coding RNAs (lncRNAs) in carcinogenesis and prognosis/treatment of LUAD patients based on transcriptomic data of 507 samples from TCGA database (https://www.frontiersin.org/journals/pharmacology/articles/10.3389/fphar.2023.1236655/full). They constructed a prognostic model associated with the prognosis of patients with LUAD undergoing therapy and confirmed their results through *in-vitro* experiments.

Finally, Liu R's group has dedicated its work to studying the correlation between neutrophils and tumor development in LUAD based on data from the TCGA database and *in-vitro* experiments, identifying 30 hub genes that were significantly associated with neutrophil infiltration and developing a neutrophil scoring system associated with prognosis, and tumor immune microenvironment.

Relevant case reports

The present Research Topic also contains interesting, unusual, and noteworthy case reports that can help clinicians and scientists identify new trends, evaluate new therapeutic effects, as well as create new research questions. In particular, Hodges A et al. presented a 62-year female with Lynch syndrome, who developed an EGFR-positive lung adenocarcinoma highlighting the complex interplay of genetic cancer predisposition syndromes and the development of spontaneous driver mutations in the disease course and the subsequent management of tumors arising (https://www.frontiersin.org/journals/oncology/articles/10.3389/fonc.2023.1193503/full).

Li H et al. presented a 35-year female with a rare lung cancer exhibiting choriocarcinoma features demonstrating the potential of chemo-immunotherapy in treating this aggressive subtype of lung cancer (https://www.frontiersin.org/journals/oncology/articles/10.3389/fonc.2024.1324057/abstract).

Last but not least, Quanqing L et al. presented a 67-year female with a squamous cell carcinoma (NSCLC) that transforms into small cell carcinoma (SCLC) after five cycles of immunotherapy targeting PD-1 treatment (Sintilimab) of NSCLC (https://www.frontiersin.org/journals/oncology/articles/10.3389/fonc.2024.1329152/full). This histological transformation could represent a potential mechanism of cancer therapeutic resistance.

Conclusion

In conclusion, this Research Topic highlights the importance of good prognostic biomarkers in determining the most effective treatment and revolutionizing cancer precision medicine. The Research Topic of articles provides a comprehensive overview of current advancements in prognostic and therapeutic lung cancer biomarkers offering a substantive framework that informs ongoing scientific inquiry and clinical practice, aiming to improve the understanding and management of LUAD patients.

Author contributions

YM: Conceptualization, Validation, Writing–original draft, Writing–review and editing. MP: Conceptualization, Data curation, Validation, Writing–original draft, Writing–review and editing. EF: Conceptualization, Data curation, Supervision, Writing–original draft, Writing–review and editing.

Funding

The author(s) declare that no financial support was received for the research, authorship, and/or publication of this article.

Acknowledgments

We deeply thank all the authors and reviewers who have participated in this Research Topic.

Conflict of interest

The authors declare that the research was conducted in the absence of any commercial or financial relationships that could be construed as a potential conflict of interest.

The author(s) declared that they were an editorial board member of Frontiers, at the time of submission. This had no impact on the peer review process and the final decision.

Publisher's note

References

Bodor, J. N., Kasireddy, V., and Borghaei, H. (2018). First-line therapies for metastatic lung adenocarcinoma without a driver mutation. *J. Oncol. Pract.* 14 (9), 529–535. doi:10.1200/JOP.18.00250

Murciano-Goroff, Y. R., Warner, A. B., and Wolchok, J. D. (2020). The future of cancer immunotherapy: microenvironment-targeting combinations. *Cell Res.* 30 (6), 507–519. doi:10.1038/s41422-020-0337-2

Sung, H., Ferlay, J., Siegel, R. L., Laversanne, M., Soerjomataram, I., Jemal, A., et al. (2021). Global cancer statistics 2020: GLOBOCAN estimates of incidence and mortality worldwide for 36 cancers in 185 countries. *Ca. Cancer J. Clin.* 71 (3), 209–249. doi:10.3322/caac.21660

frontiers | Frontiers in Genetics

TYPE Original Research
PUBLISHED 06 September 2022
DOI 10.3389/fgene.2022.941567

OPEN ACCESS

EDITED BY
Yiming Meng,
China Medical University, China

REVIEWED BY
Xin Xie,
The First Affiliated Hospital of Xi'an Jiaotong University, China
Ming Yi,
Zhejiang University, China

*CORRESPONDENCE
Lei Zhu,
zhuleiZLei@163.com

†These authors have contributed equally to this work

SPECIALTY SECTION
This article was submitted to Cancer Genetics and Oncogenomics, a section of the journal Frontiers in Genetics

RECEIVED 11 May 2022
ACCEPTED 08 August 2022
PUBLISHED 06 September 2022

CITATION
Wang F, Du H, Li B, Luo Z and Zhu L (2022), Unlocking phenotypic plasticity provides novel insights for immunity and personalized therapy in lung adenocarcinoma.
Front. Genet. 13:941567.
doi: 10.3389/fgene.2022.941567

Unlocking phenotypic plasticity provides novel insights for immunity and personalized therapy in lung adenocarcinoma

Feng Wang[1†], Hongjuan Du[1†], Bibo Li[1], Zhibin Luo[1] and Lei Zhu[2*]

[1]Department of Oncology, Chongqing General Hospital, Chongqing, China, [2]Department of Thoracic Surgery, Shanghai Pulmonary Hospital, School of Medicine, Tongji University, Shanghai, China

Background: Unlocking phenotype plasticity (UPP) has been shown to have an essential role in the mechanism of tumor development and therapeutic response. However, the clinical significance of unlocking phenotypic plasticity in patients with lung adenocarcinoma is unclear. This study aimed to explore the roles of unlocking phenotypic plasticity in immune status, prognosis, and treatment in patients with lung adenocarcinoma (LUAD).

Methods: Differentially expressed genes (DEGs) and clinical information of UPP were selected from the cancer genome atlas (TCGA) database, and the GO, KEGG enrichment analyses were performed. The independent prognostic genes were determined by univariate and multivariate Cox regression, and the UPP signature score was constructed. Patients with LUAD were divided into high- and low-risk groups according to the median of score, and the immunocytes and immune function, the gene mutation, and drug sensitivities between the two groups were analyzed. Finally, the results were validated in the GEO database.

Results: Thirty-nine significantly DEGs were determined. Enrichment analysis showed that UPP-related genes were related to protein polysaccharides and drug resistance. The prognostic results showed that the survival of patients in the high-risk group was poorer than that in the low-risk group ($p < 0.001$). In the high- and low-risk groups, single nucleotide polymorphism (SNP) and C > T are the most common dissent mutations. The contents of immune cells were significantly different between high- and low-risk groups. And the immune functions were also significantly different, indicating that UPP affects the immunity in LUAD. The results from TCGA were validated in the GEO.

Conclusion: Our research has proposed a new and reliable prognosis indicator to predict the overall survival. Evaluation of the UPP could help the clinician to predict therapeutic responses and make individualized treatment plans in patients with LUAD.

KEYWORDS

unlocking phenotype plasticity (UPP), LUAD, drug sensitivities, immune, prognostic

Introduction

Lung cancer is a malignancy with the highest mortality and the second high incidence worldwide (Al-Dherasi et al., 2021; Zheng et al., 2021). Lung cancer mainly includes non-small cell lung cancer (NSCLC) and small cell lung cancer (SCLC). LUAD is one of the main subtypes of lung cancer. However, most patients with LUAD were usually diagnosed at advanced stages. EGFR-TKIs were the primary treatment for patients with EGFR sensitive mutation. However, about 20–30% of patients with EGFR mutant NSCLC have immediate resistance to EGFR-TKIs (Shi et al., 2022). The mechanism of the EGFR-TKI immediate resistance is still not fully clarified. LUAD is a group of mutant types of diseases, and patients in the same pathological stage may have different prognoses, so it is necessary to explore accurate and hopeful biomarkers to help clinicians promote the accuracy and early diagnosis of LUAD and improve the survival of and guide personalized therapy (Yoshizawa et al., 2011; Gandhi et al., 2018).

Phenotype plasticity means that genotypes produce different phenotypes under different environmental conditions and is a crucial mechanism to adapt to environmental heterogeneity. Although researchers have always believed that these biological characteristics have been plaguing this biometric character. However, this point of view has been controversial. Traditionally, phenotype plasticity is considered to be decentralized and differentiated during tissue regeneration or wound healing. Although the degeneration process is the main link of the organization, the decentralization itself has the risk of cancer. Therefore, phenotype plasticity provides a new paradigm to understand the occurrence, development of cancer, and resistance to treatment.

Plasticity exists in various fields of life, and the role of phenotypic plasticity is still seldom studied in mammalian (Matesanz et al., 2021). Recently, in January 2022, the Cancer Discovery released the third edition of Hallmarks of Cancer to explain the mechanism of occurrence, development, and treatment of response characteristics in malignant tumors (Haan, JC et al., 2022). Four new tumor iconic features were introduced based on the previous version, including unlocking phenotypic plasticity, which contributed to a unique point of view. In this study, we aimed to use the clinical, genomic, and transcriptome data of TCGA for prognosis and bioinformatics analysis, to clarify the predictive significance of UPP on the prognosis of LUAD patients and the relationship between UPP and immunity and treatment. This study provided a new insight for the prognosis and treatment of LUAD.

Materials and methods

Patient and data acquisition

The LUAD tissue sample was downloaded in the TCGA dataset (https://cancergenome.nih.gov/). TCGA provides 522 clinical, 569 genomes and mutated data, and the Illumina Hi-SEQ RNA SEQ platform provides 594 RNA sequencing (RNA SEQ) data. First, the expression of the unlocked phenotype plasticity-related gene is screened from the gene expression files for differential expression analysis. Then, the differentially expressed genes (DEGs) were analyzed by GO and KEGG. Finally, the data were analyzed for prognosis, immunity, drug resistance, and so on.

Analysis of DEGs

The key step is to obtain DEGs of the unlocking phenotype plastic-related genes between tumors and normal samples. This study used "limma" package (http://www.bioconductor.org/) to calculate the DEGs (Liu et al., 2021). Wilcox test was performed to obtain DEGs between tumor and normal samples with the standard of $|\log FC| > 1$ and false discovery rate (FDR) value <0.05. Then, the heatmap of DEGs was obtained to visualize their expression in different samples through the "ggplots" package in R. The longitudinal axis is displayed, and the color is used to distinguish between different differential expressions.

The verification of unlocking phenotypic plasticity-related genes by quantitative real-time polymerase chain reaction

To validate the expression profiles of UPP-related genes in LUAD, we performed quantitative real-time polymerase chain reaction (qRT-PCR) using the A549 cells and normal human bronchial epithelial (NHBE) cells. First, cells were cultured in DMEM (high glucose) + 10% fetal bovine serum +1% penicillin–streptomycin solution. Second, the A549 and NHBE cells were harvested when the confluence of cells is more than 90%. Then, cells were lysed with TRIzol reagent (Invitrogen, CA, United States). The concentrations of the total RNA of A549 and NHBE cells were measured by the NanoDrop 2000 spectrophotometer (Thermo Fisher Scientific, United States), and were synthesized into cDNA using the PrimeScript™ RT reagent kit (Takara, Japan). The qRT-PCR was conducted in the PCR apparatus (Applied Biosystems, Singapore) following the conditions: predenaturation at 95°C for 2 min, 95°C for 15 s, 60°C for 30 s, and 72°C for 30 s. Finally, the gene expression levels were calculated by the 2–Δ Ct method. The primers of genes were designed and synthesized by Sangon Biotech (Shanghai) Co., Ltd., and are available in Supplementary Table S1.

GO and KEGG enrichment analysis

The DEGs were analyzed by GO analysis through the "ClusterProfiler" package in R software. GO aims to solve the

problem of inconsistent gene description in different databases with strictly defined concepts. GO function annotation mainly annotates and classifies differential genes according to the biological process (BP), molecular function (MF), and cellular component (CC). The $p < 0.05$ and FDR <0.05 of the DEGs were used as the localization conditions to obtain the GO item with the highest correlation with the DEGs. The KEGG path with p-value <0.05 and at least five genes were selected as the enrichment condition of DEGs. Finally, the bubble map is drawn by the "ggplot"s package in the R software.

Prognosis-related analysis

We use univariate and multivariate Cox regression analyses to analyze the overall survival (OS) to determine the significant correlation phenotype plasticity-related gene prognosis significantly associated with LUAD. Survival analysis was performed between high- and low-risk groups, and the results were visualized by the Kaplan–Meier curve. To explore the two groups of genetic mutations, we also draw a waterfall map.

Unlocking phenotypic plasticity and immunity and drug sensitivity prediction

SsGSEA was used to evaluate the difference of immune cell content and function between high- and low-risk groups. p-value <0.05 and FDR <0.05 are considered statistically significant. "c2. cp.kegg.v7.1. Symbol" was set as the reference. "McPCounter" is an R-Package that quantifies the absolute abundance of eight immunocytes and two matrix cells using transcription group data. The Genomics of Drug Sensitivity in Cancer database (GDSC; https://www.cancerrxgene.org/) was used to estimate the sensitivity of each patient to chemotherapeutic drugs. The half-maximal inhibitory concentration (IC50) was quantified via the "pRRophetic" package in R (Geeleher et al., 2014).

Statistical analysis

OS is defined as the time from the diagnosis of LUAD to the patient's death or last follow-up. "Survival" package was used to draw the Kaplan–Meier survival curve, calculate the hazard ratio (HR), and evaluate the 95% confidence interval (CI) in R. Comparisons between two groups were calculated *via* Wilcoxon rank-sum test. Chi square test or Fisher exact test was used to compare categorical variables. $p < 0.05$ was considered to be statistically significant. All statistical analyses were performed in R (version 4.1.1).

Results

DEG screening and heat map

At present, there are a few researches about the unlocking phenotype plasticity genes. In order to clarify the difference of the gene transcription level of unlocking phenotypic plasticity, we obtained DEGs between tumor samples and normal samples using the data of expression profile. A total of 39 significant DEGs were retrieved, of which 20 genes were significantly up-regulated in tumor samples; 19 genes were significantly up-regulated in normal samples. Then, we cluster DEGs and visualize them in the heat map (Figure 1).

To further validate the UPP expression levels in LUAD, we selected the top 10 genes with the most significant expression differences to perform qRT-PCR, as described above. The results showed that ACAN (Figure 2A), CDKN3 (Figure 2C), GRIN2A (Figure 2D), IL17A (Figure 2E), KCNQ2 (Figure 2F), TIMP1 (Figure 2I), and UCHL1 (Figure 2J) were significantly up-regulated in lung adenocarcinoma cells. However, BMP2 (Figure 2B), SELP (Figure 2G), and SLC6A4 (Figure 2H) were significantly down-regulated in lung adenocarcinoma cells compared with NHBE cells. Collectively, these findings strongly suggested that UPP-related gene expressions were disturbed in LUAD.

GO and KEGG enrichment analyses

We use the gene expression of the ClusterProfiler in the R software to perform GO enrichment analysis. The results of BP analysis of GO enrichment suggest that DEGs are mainly enriched in the positive regulation of anion transport, the positive regulation of secretion, and the positive regulation of proteolysis. The CC results showed that DEGs are mainly enriched in the ion channel complex, transmembrane transporter complex, and cation channel complex; MF results showed that DEGs are mainly related to ubiquitin-like protein ligase binding, signaling receptor activator activity, histone acetyltransferase binding, ion transport, cell cycle regulation, and cell adhesion (Figure 3A).

Subsequently, the KEGG pathway enrichment analysis was carried out, and we only showed the first 10 pathways (Figure 3B). These DEGs are strongly correlated with the AGE–RAGE signaling pathway, EGFR tyrosine kinase inhibitor resistance, and other signaling pathways. It has an important impact on cancer progression through important biological processes related to drug resistance.

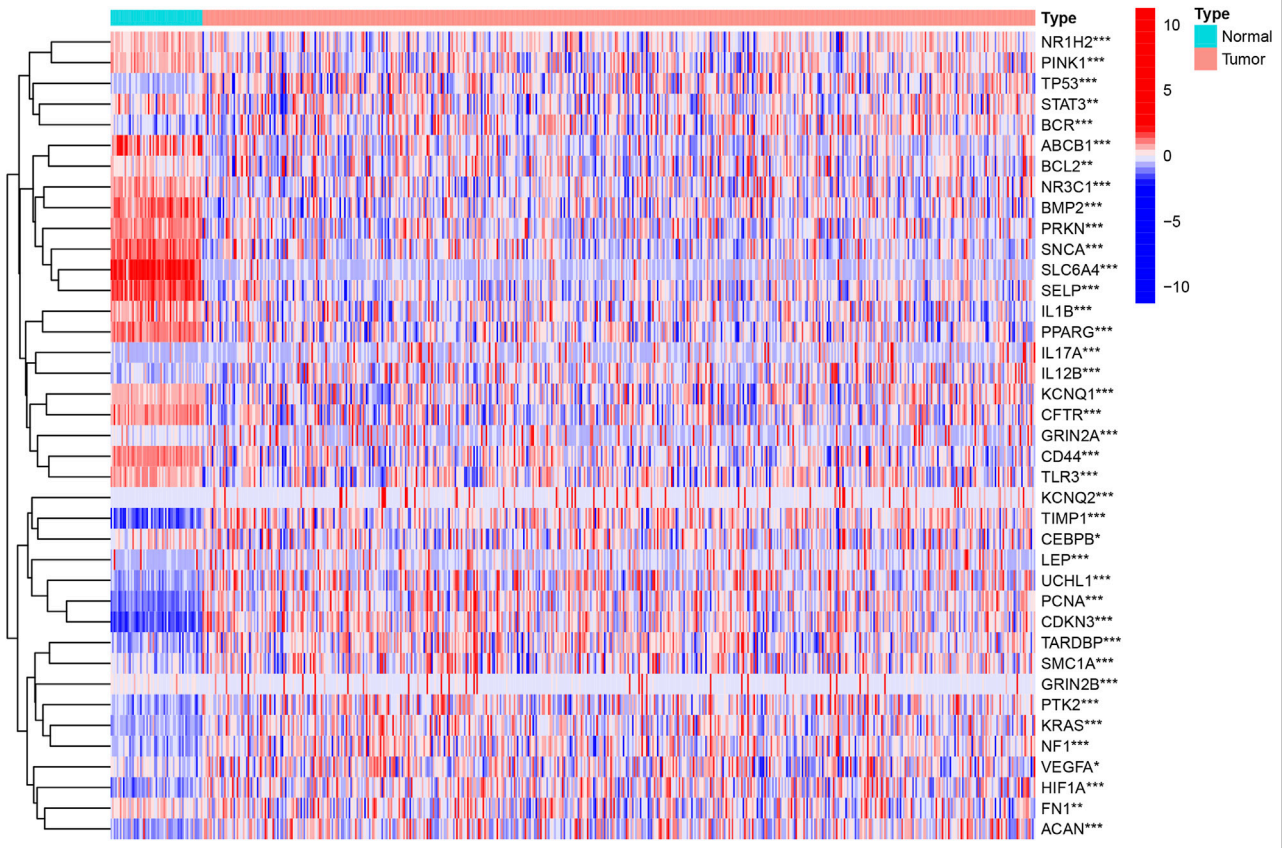

FIGURE 1
Identification of the UPP-related DEGs. The heatmap analysis of the top 39 DEGs between the tumor and normal samples.

Survival analysis

Eleven unlocked phenotype plastic-related genes (Figure 4A) were screened by univariate Cox analysis. Next, multivariate Cox analysis results showed that ABCB1, ADIPOQ, NGF, F9, CDKN3, ACAN, and CEBPB are independent prognostic genes. According to the expression level and coefficient of the separate prognostic gene, we constructed the signature following the formula: Risk Score = (1.267 × ADIPOQ) - (0.523 × ABCB1) - (0.233 × NGF) + (12.988 × F9) + (0.281 × CDKN3) + (0.605 × ACAN) + (0.168 × CEBPB). The samples were divided into two groups according to the median of the risk score (Table 1). Survival analysis was conducted for high- and low-risk groups. Compared to the low-risk group, patients in the high-risk group had worse prognoses ($p < 0.01$) (Figures 4B–D).

Mutations in high and low groups

In order to explore the cases of the genetic mutation of the two groups, the waterfall map was drawn. High- and low-risk groups are shown in Figures 3E,F, respectively (Figures 4E,F). TP53, TTN, and MUC16 also have a higher mutation rate. The top 20 mutation genes, PCDH15, MUC17, RPIL1, DAMTS12, and PAPPA219 mutations, exist only in the high-risk group, while ANK2, NAV3, ZNF536, APOB, and DANH9 mutations exist only in the low-risk group. Single nucleotide polymorphism (SNP) was responsible for such variants, and single nucleotide variants (SNVs) mostly occurred as C > A and C > T in the high- (Figures 5A–F) and low-risk (Figures 5G–L) groups.

Unlocking phenotypic plasticity and immune correlation

Immunocytes in tumor environments play important roles in tumor progression. We use ssGSEA to assess the correlation between immunocytocytes and related functions. The immune cells aDCs, B_cells, DCs, iDCs, Mast_cells, Neutrophils, T_helper_cells, and TIL have significant differences between two groups. The immune function is significantly different in HLA, MHC_class_I, and Type_II_IFN_Reponse (Figures 6A,B). The absolute abundance of eight immune cells and two stromal cells was evaluated using

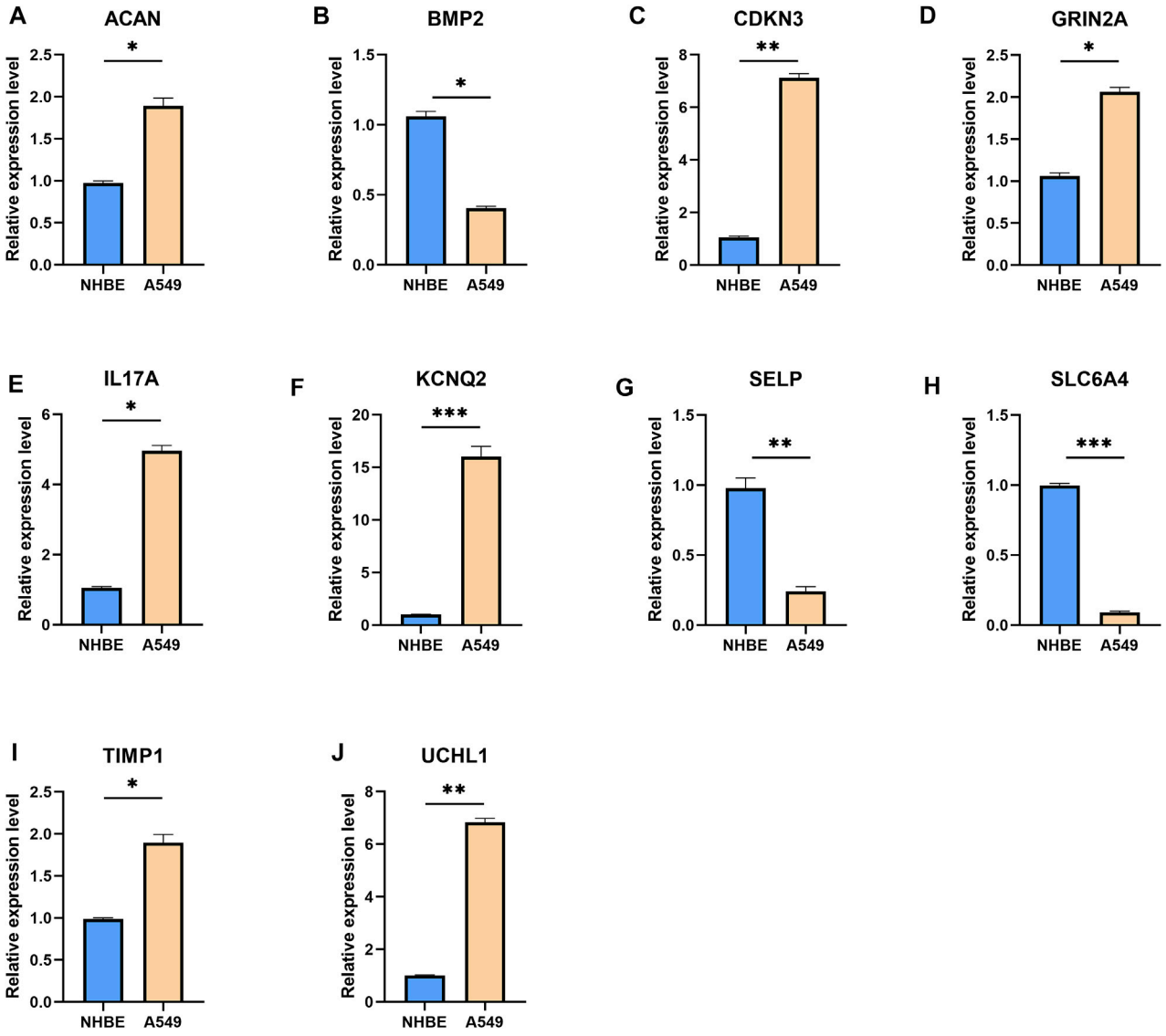

FIGURE 2
qRT-PCR results for the top 10 genes with the most significant expression differences. The mRNA expression levels of ACAN **(A)**, BMP2 **(B)**, CDKN3 **(C)**, GRIN2A **(D)**, IL17A **(E)**, KCNQ2 **(F)**, SELP **(G)**, SLC6A4 **(H)**, TIMP1 **(I)**, and UCHL1 **(J)**. Expression levels of the 10 genes were normalized against GAPDH expression. *$p < 0.05$, **$p < 0.01$, ***$p < 0.001$.

MCPcounter. The results showed that the abundance of B lineage, endothelial cells, myeloid dendritic cells, neutrophils, and T cells was higher in the low-risk group (Figures 6C–G), while the abundance of fibroblasts was higher in the high-risk group (Figure 6H).

Relations between unlocking phenotypic plasticity and therapeutic sensitivity

We compare the commonly used chemotherapy drugs, including paclitaxel (Figure 7A), cisplatin (Figure 7B), docetaxel (Figure 7C), etoposide (Figure 7D), gefitinib (Figure 7E), gemcitabine (Figure 7F), methotrexate (Figure 7G), sorafenib (Figure 7H), and sunitinib (Figure 7I)-estimated IC50 levels. Our data showed that the IC50 level of methotrexate in the low-risk group is significantly lower than that in the high-risk group, indicating that patients in the low-risk group are more sensitive to methotrexate. On the contrary, paclitaxel, cisplatin, docetaxel, etoposide, gefitinib, gemcitabine, sorafenib, and sunitinib were more sensitive in the high-risk group.

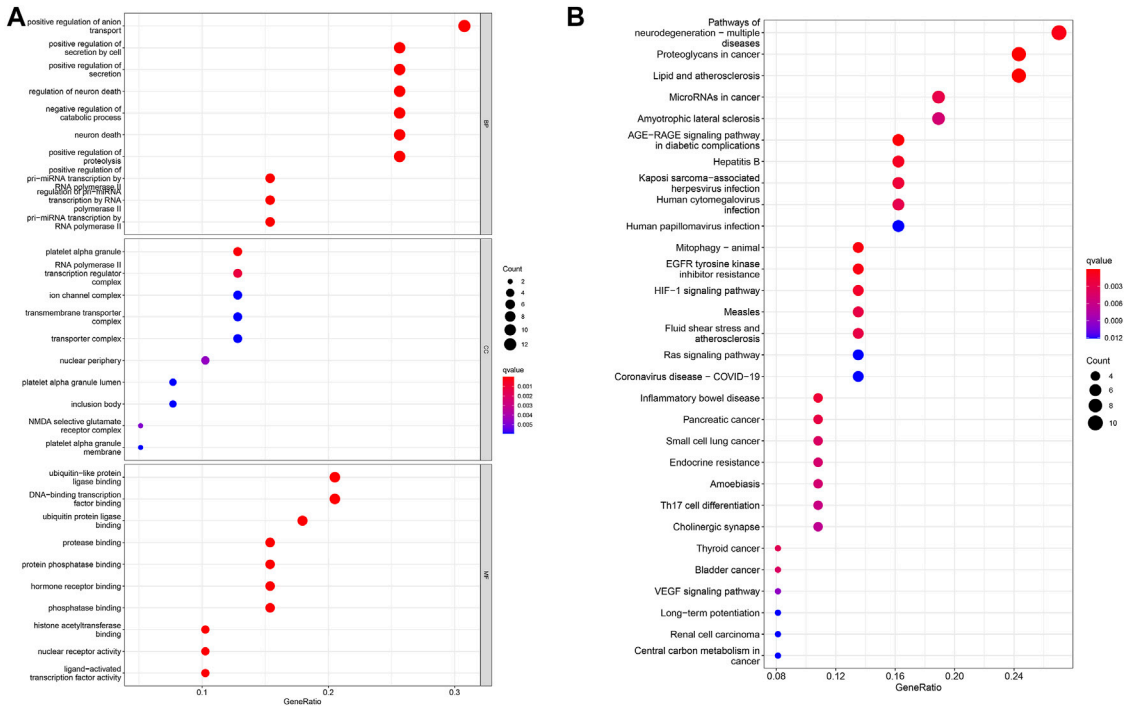

FIGURE 3
Analysis of DEG distribution and function in LUAD patients. **(A)** GO enrichment analysis of biological process (BP), cellular component (CC) and molecular function (MF) results ranked by the adjusted *p*-value. **(B)** KEGG enrichment analysis results showed that DEGs were strongly associated with the AGE-RAGE signaling pathway and EGFR tyrosine kinase inhibitor resistance pathways.

External verification

In the GSM72094 dataset of GEO database, we further verified the effectiveness of unlocking phenotypic plasticity score in predicting prognosis and drug sensitivity. Consistent with the results of the TCGA database, the prognosis of the high-risk group was significantly worse than that of the low-risk group in GSM72094 dataset (Figure 8A). In addition, the drug sensitivity of the prognostic score was further evaluated to speculate on the therapeutic benefits of LUAD patients. The results showed that the low-risk group was more sensitive to methotrexate, while the high-risk group was more sensitive to paclitaxel, docetaxel, and sorafenib (Figures 8B–E), which was consistent with the drug sensitivity results in the TCGA database.

Discussion

Previous findings have shown that phenotypic plasticity is directly related to the origin, progression, and treatment response of cancer cells (Healy and Schulte, 2015). The environmental factors affecting phenotype can be continuous or discontinuous, and the influence of environment can last for the whole life cycle of organism. Tumor heterogeneity stems, in part, from the ability of cancer cells to switch between phenotypic states, but the genetic of this cellular plasticity is still poorly understood.

In this study, we excavated the public database TCGA to explore the influence of unlocking phenotypic plasticity on the survival of LUAD patients, which proves that there is a worse clinical outcome in patients with unlocked phenotype plastic-related genetic mutations. The effect mechanism of unlocking the phenotypic plasticity on LUAD was discussed by bioinformatics for the first time. In what ways does unlocking the phenotypic plasticity affects the prognosis of LUAD patients? In this study, we were analyzed by the differential expression of the unlocked population plasticity and obtained 39 DEGs. GO and KEGG analyses were performed on DEGs to find the possible functions of DEGs and the metabolic and signaling pathways mainly involved.

The results of GO showed that the DEGs were related to the positive regulation of anion transport, positive regulation of secretion, positive regulation of proteolysis, and histone acetyltransferase binding. Studies have found that the most distinct group of protein modifiers is histone acetyltransferase (HATS). Most groups of histone acetylationase have substrate specificity to guide the acetylation of a particular residue within one or more core groups (Salutari et al., 2022). However, these substrate specificities are not fixed and can be changed by

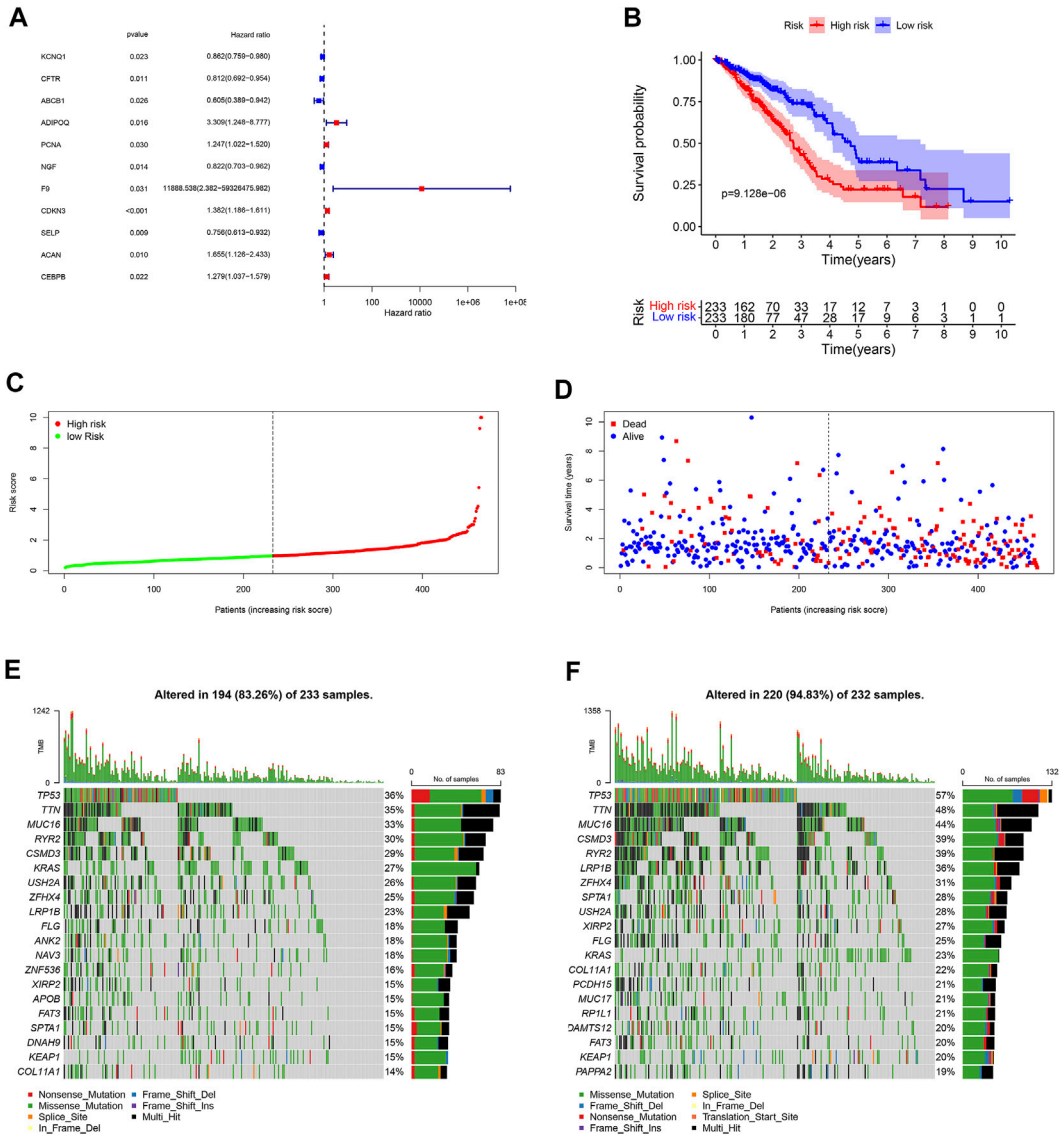

FIGURE 4
Landscape of UPP and prognosis in LUAD. **(A)** 11 UPP-related genes were obtained by univariate Cox analysis. **(B)** Survival analysis between high- and low-risk groups. **(C)** The risk score curve of all LUAD patients in the TCGA. **(D)** The scatter plot of LUAD survival time periods in the TCGA. **(E)** The Oncoplot of the low-risk group in LUAD. **(F)** The Oncoplot of the high-risk group in LUAD. Oncoplot shows the list of top 20 genes ordered by the number of samples with the gene variants, and the percentage represents the ratio of samples with gene variation to total samples.

catalytic subunits and protein complexes. The presence of many of HAT complexes expands the modified state of the chromosome template. Therefore, more and more evidence suggests that specific cellular processes are related to the precise model of histone modification (Zhao et al., 2022). Ion transport, protein catabolism, and other functions are also indispensable physiological mechanisms for tumor cell proliferation and metastasis. Tumor microenvironment is very important for the heterogeneity and the plasticity of tumor cells of LUAD.

We found that DEGs were mainly enriched in AGE-RAGE signaling pathway, and EGFR tyrosine kinase inhibitor resistance. The AGE-RAGE signal pathways promote autophagy flux while inhibiting apoptotic signals in cancer cells (Waghela, BN et al., 2021). The activation of autogenesis, such as beclin-1 passes through autophagy to promote cancer cell survival (Chhipa et al., 2019). The activation of the AGE-RAGE signal also produces oxygen-free radicals, leading to oxidative stress and activation of NF-κB. The latter secretes proinflammatory cytokines,

TABLE 1 Independent prognostic genes and coefficients.

Gene	Coef
ABCB1	−0.523
ADIPOQ	1.267
NGF	−0.233
F9	12.988
CDKN3	0.281
ACAN	0.605
CEBPB	0.168

growth factors, and adhesion molecules, such as intercellular adhesion molecule-1 and vascular cell adhesion molecule-1, which eventually lead to cancer progression. AGEs may change the extracellular matrix (ECM) through the production of cell surface receptors and proinflammatory cytokines. The overexpression of RAGE increases the migration, invasion, and epithelial mesenchymal transformation of human lung adenocarcinoma cells through the ERK signaling pathway (El-Far et al., 2020). Recent reports show that AGEs also promote cell proliferation and migration of breast cancer cells (Chen et al., 2020). Bhargav N. Waghela et al.'s recent studies have shown that AGE-RAGE signaling pathways are related to programmed cell death signal, apoptosis, and autophagy (Waghela, BN et al., 2021).

Although TKI-induced or selected genetic changes can drive drug resistance, drug resistance occurs in tumor cells without genetic changes. In the case of no gene changes, tumor cells are plasticity; from tumors, the various components of the microenvironment causing a change in tumor phenotypes may be the driving factor of drug resistance (Tsai and Nusinov et al., 2019; Gkountakos et al., 2022). A tumor microenvironment (TME) is a mixture of active ingredients and dynamic components, including a large number of metabolites, which interact to promote carcinogenic survival and proliferation. In particular, EGFR-TKI-resistant cell-secreted lactic acid is swallowed by cancer-related fibroblasts (CAFs), triggering the excess secretion of hepatocyte growth factor (HGF) and subsequent MET signal activation, indicating that there is a non-cellular autonomous metabolic EGFR-TkI drug resistance mechanism (Zhao et al., 2019). Recent studies have shown that extracellular matrix (ECM) has played a new role in malignant cancer progression and targeted therapeutic resistance (Levy et al., 2016; Chen W. et al., 2022). Yanan Yang et al. studied ECM as a unique role in obtaining EGFR TKIS drug resistance (Wang, et al., 2018).

Phenotype plasticity in the tumor process is also driven by the activation of the developmental differentiation procedure—epithelial–mesenchymal transition (EMT); an EMT is the broadest example of phenotype plasticity. Its role in tumor progression and metastasis has been fully confirmed. A transfer is the cause of most cancer patients (Yang et al., 2018).

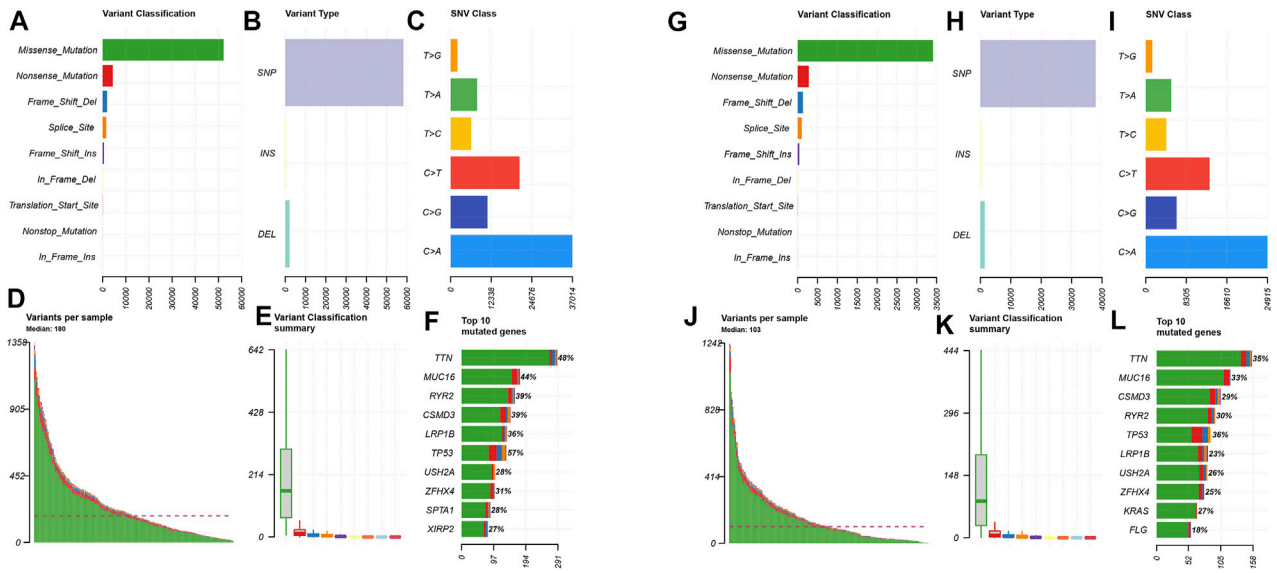

FIGURE 5
Distributions of mutant genes in high- and low-risk groups. **(A)** Variant classification and frequency of gene mutations in the high-risk group. **(B)** Variant type in the high-risk group. **(C)** Frequency of SNV classes in the high-risk group. **(D)** Median of variants per sample in the high-risk group. **(E)** Variant classification summary in the high-risk group. **(F)** List of top 10 mutated genes in the high-risk group. **(G)** Variant classification and frequency of gene mutations in the low-risk group. **(H)** Variant type in the low-risk group. **(I)** Frequency of SNV classes in the low-risk group. **(J)** Median of variants per sample in the low-risk group. **(K)** Variant classification summary in the low-risk group. **(L)** List of top 10 mutated genes in the low-risk group.

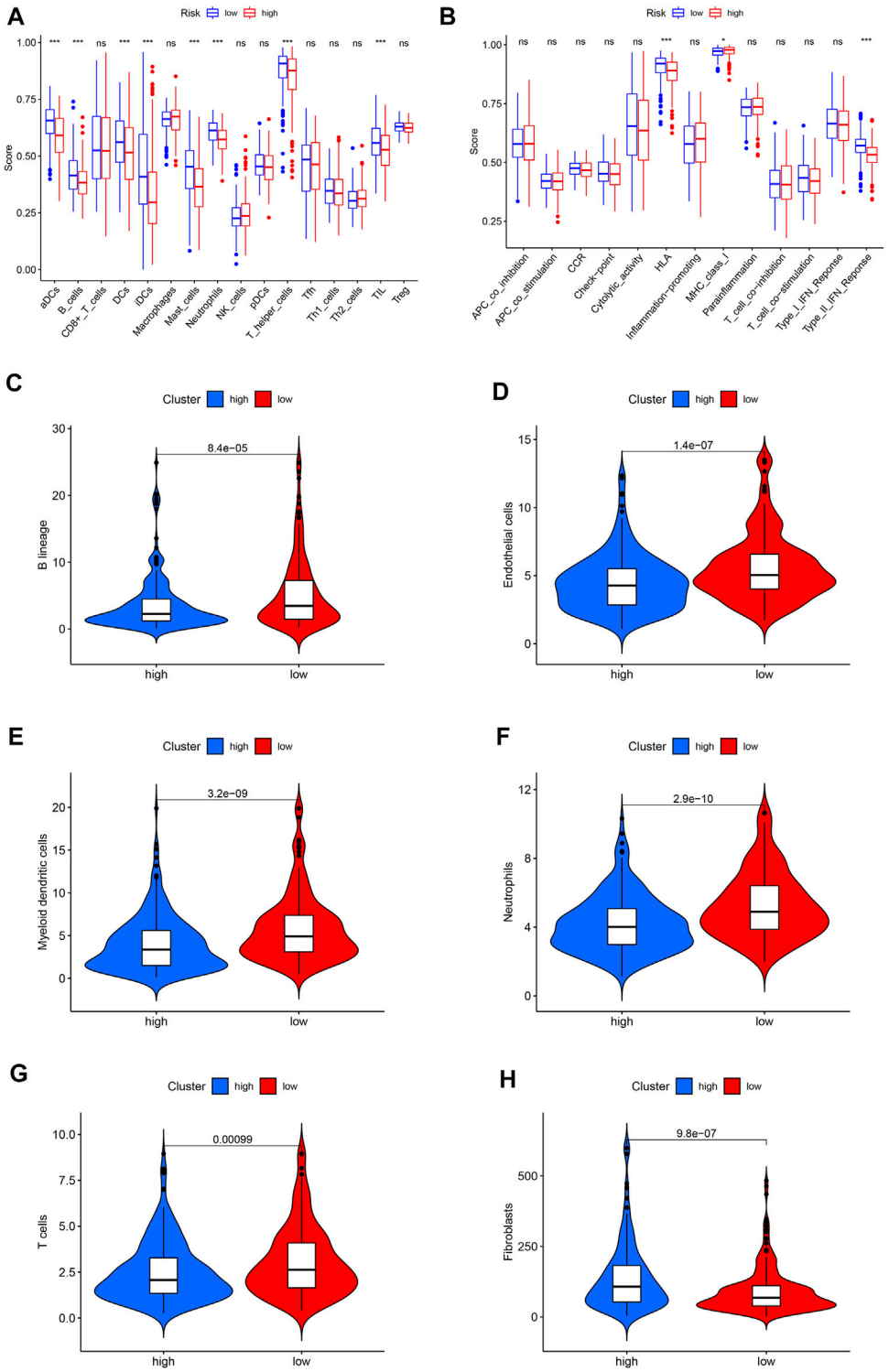

FIGURE 6
The landscape of immune infiltration in LUAD. **(A)** Differences of immune cells in the high- and low-risk groups. **(B)** Differences in the immune function between high- and low-risk groups. **(C)** Violin plot of B lineage. **(D)** Violin plot of endothelial cells. **(E)** Violin plot of myeloid dendritic cells. **(F)** Violin plot of neutrophils. **(G)** Violin plot of T cells. **(H)** Violin plot of fibroblasts. The horizontal line in the Violin plot represents the median, and blue and red represent the high-risk and low-risk groups, respectively. $p < 0.05$ shows the significant statistical difference between two groups.

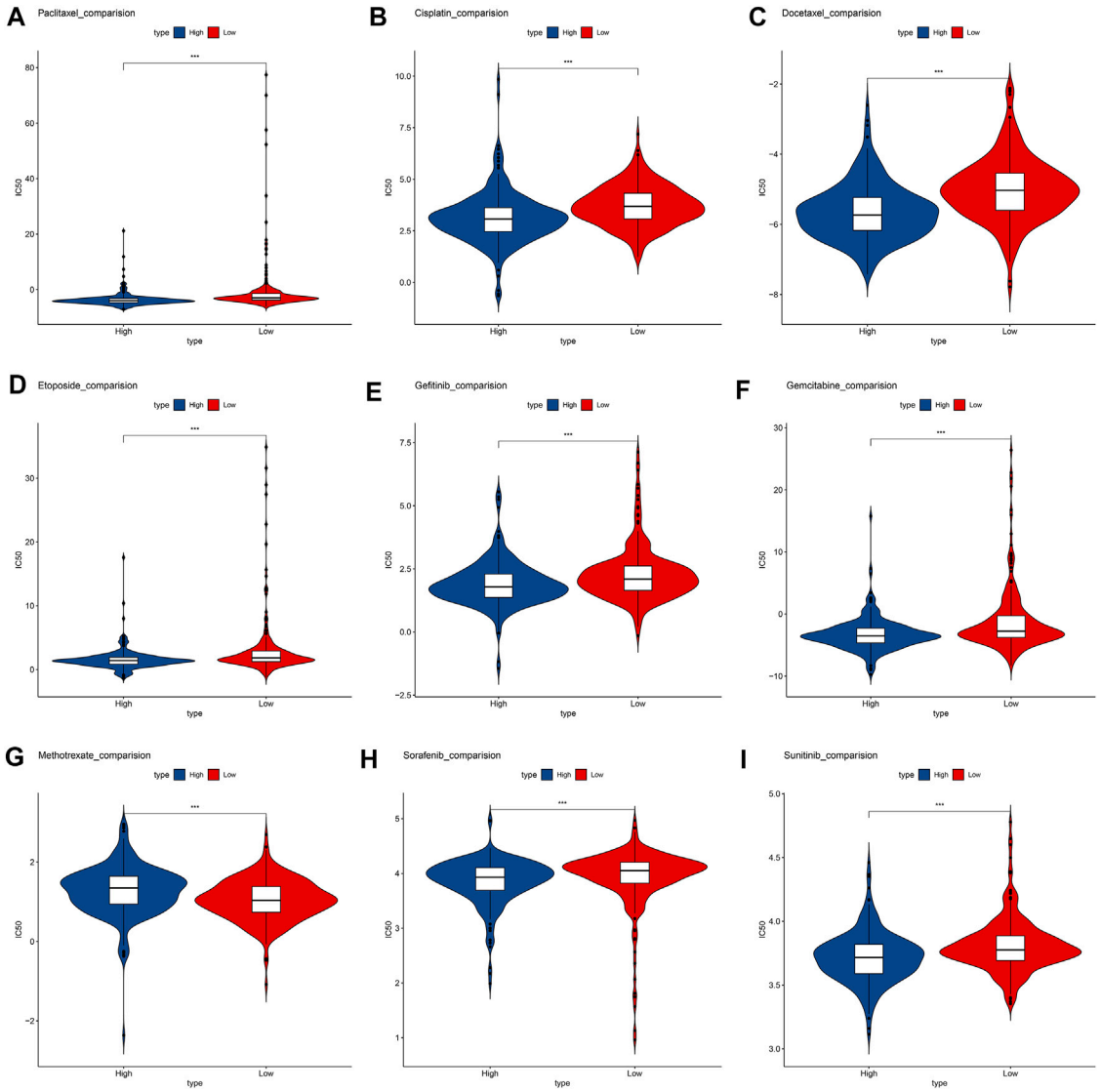

FIGURE 7
Box plots depicted the differences in the estimated IC50 levels of **(A)** Paclitaxel; **(B)** Cisplatin; **(C)** Docetaxel; **(D)** Etoposide; **(E)** Gefitinib; **(F)** Gemcitabine; **(G)** Methotrexate; **(H)** Sorafenib; **(I)** and Sunitinib between the high- and low-risk groups.

Recently, researchers have discovered several transition conditions that occurred during skin squamous cell carcinoma and breast tumors (Rubin, MA et al., 2020). Tumor cells in different differentiation stages, from epithelial to complete mesenchymal cells, exhibited similar tumor proliferation capabilities through intermediate hybridization. Tumor cell subsets show other cell plasticity and invasiveness.

We divide patients into high- and low-risk groups through univariate and multivariate Cox regression analyses, and the results show that the high-risk groups are poorer than the low-risk groups. After the differential expression gene is submitted to the associated prognostic gene, seven intersection genes are obtained, namely, ABCB1, ADIPOQ, NGF, F9, CDKN3, ACAN, and CEBPB. ABCB1 is a member of the ABCB subfamily located on chromosome 7q21. It consists of 28 exons, encoding 1280 amino acid glycoproteins (MDR1/PGP). MDR1/PGP produces different interactions with different drugs (Manna et al., 2015). In addition to a wide range of substrate specificity, the unique feature of MDR1/PGP is its base ATPase activity. MDR1/PGP can output most neutral and cationic hydrophobic compounds, and cancer cells can efficiently utilize this mechanism as the main barrier to chemotherapy. Cells with higher MDR1/PGP levels have selective advantages in adapting to harsh environments such

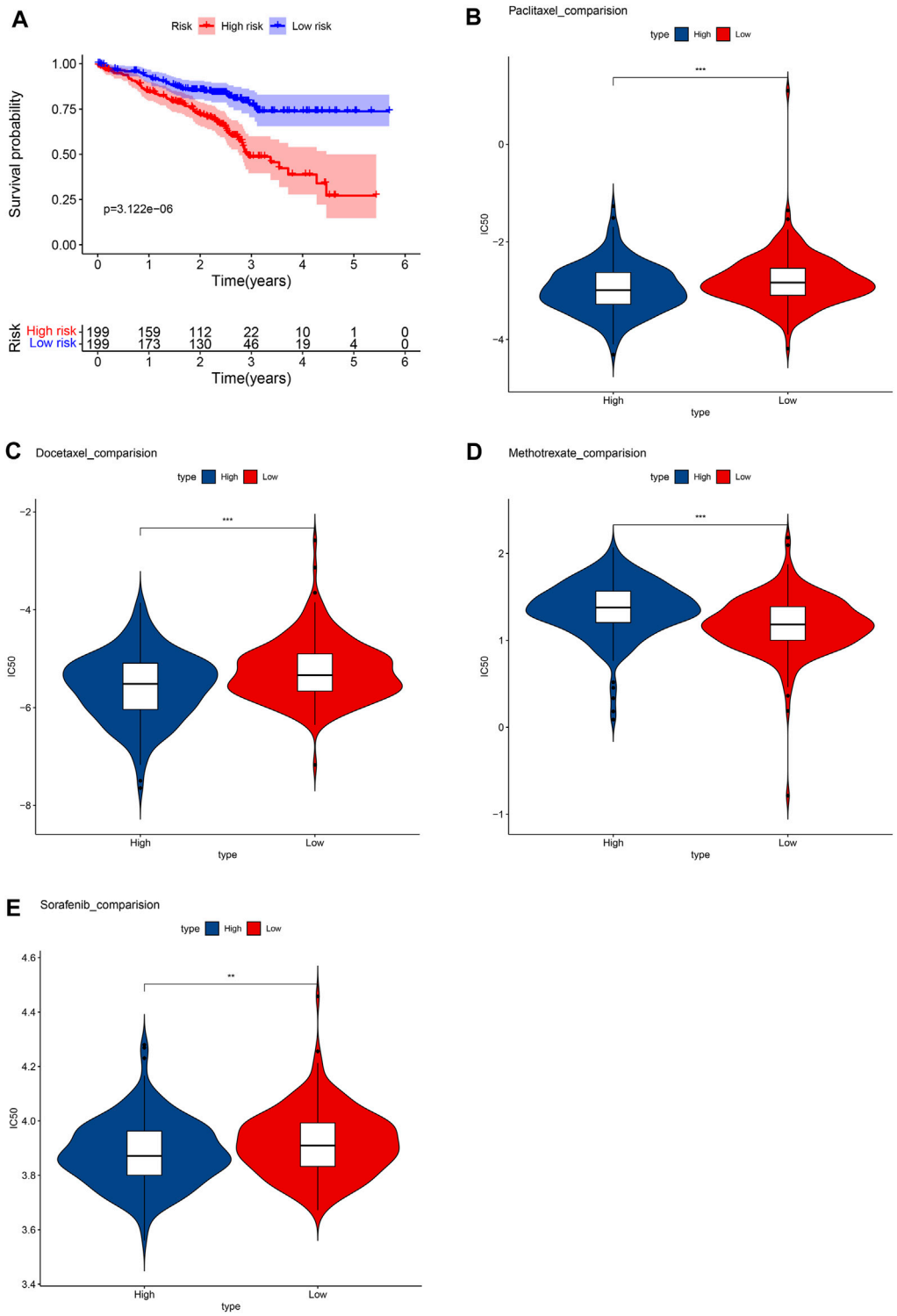

FIGURE 8
Verify the results in the GEO database. **(A)** Survival analysis between high- and low-risk groups. Box plots depicted the differences in the estimated IC50 levels of **(B)** Paclitaxel; **(C)** Docetaxel; **(D)** Methotrexate; **(E)** and Sorafenib between the high- and low-risk groups.

as hypoxia or inflammation. The study found that MDR1/PGP confers cancer cell resistance by inhibiting caspase-dependent apoptosis (Yang et al., 2022). The effectiveness of these interesting conjectures is to be further confirmed and confirmed by experiments such as the knockout model.

Human CDKN3 gene encodes cyclin-dependent kinase inhibitor 3, which is a bispecific protein tyrosine phosphatase of the CDC14 group. CDKN3 is used as CDK1 and CDK2 inhibitory proteins, which are conventionally considered a negative regulatory factor of the cell cycle process (Li et al., 2022). Although CDKN3 has a negative adjustment effect on CDK1 and CDK2, the carcinogenic effect of CDKN3 is abnormally expressed, which is related to a variety of human cancers. In esophageal cancer, CDKN3 affects the progress of cancer by promoting cell cycle and chemotherapy. Chao Fan found that CDKN3 has increased in NSCLC, and the CDKN3 high expression is always related to the total survival of these patients (Fan et al., 2015). There is also evidence to support that CDKN3 in cervical cancer (CC) can not only be used as a useful marker that survives and selects additional chemotherapy or specific targeted cancer treatment but also as a specific small drug for developing anti-CC potential target.

CCAAT/enhancer binding protein (CEBPS) is a leucine zipper transcription factor family to participate in cell proliferation and differentiation (Huang et al., 2020). Although it is well known that CEBPB is a transcription factor involved in adipocytes and immunocyte differentiation. Still, the function of CEBPB in NSCLC has been controversial, which may be because CEBPB depends on the synergistic transcription factor and/or the apparent genetic state of the respective gene sites in the intracellular environment. Studies have shown that under the transcription of CEBPB, long-coded RNA LOC102724169 can enhance cisplatin on the therapeutic effect of ovarian cancer cells (Lynch and May. 2011). CEBPS enhances the drug resistance of cisplatin to cisplatin by enhancing nasopharyngeal carcinoma cells in combination with the serine protease inhibitor Kazal 5-type promoter region. There is also evidence to support CEBPB-NRF2 synergies to drive cancer malignancy by improving the initial tumor activity and drug resistance (Perino et al., 2014).

Introduction to the mutation of high- and low-risk groups, in the top 20 mutation genes, PCDH15, MUC17, RPIL1, DAMTS12, and PAPPA219, exists only in the high-risk group, while ANK2, NAV3, ZNF536, APOB, and DANH9 exist only in the low-risk group. In the high- and low-risk groups, the most common mutation is missense mutation, followed by nonsense mutation. Single nucleotide polymorphism (SNP) was responsible for such variants, and single nucleotide variants (SNVs) mostly occurred as C > A and C > T. However, the role of PCDH15, MUC17, RPIL1, DAMTS12, and PAPPA219 expressed in a tumor microenvironment remains to be studied.

The anti-PD-1 and anti-PD-L1 antibodies have proven effective for certain LUAD patients (Zhang et al., 2020). Their therapeutic response is related to immune infiltration and related gene expression in the tumor environment. Therefore, it is very important to identify immune-related cells in the tumor environment. We found that aDCs, B_cells, DCs, iDCs, Mast_cells, Neutrophils, T_helper_cells, and TIL infiltration levels are related to the low-risk group. The immune function is different in HLA, MHC_class_I, and Type_II_IFN_Reponse. MCPcounter results show that B lineage, endothelial cells, myeloid dendritic cells, neutrophils, and T cells have higher abundance in the low-risk group, while fibroblasts are high in the high-risk groups. These results indicate that patients with the low-risk group may benefit from immune checkpoint inhibitors. Phenotype plasticity may be related to the adjustment of tumor microenvironment into fibroblast abundance, thereby affecting tumor growth and progression.

Although there are more and more treatment programs, in modern cancer medicine, the development of drug resistance is a major challenge and the cause of failure and disease recurrence. LUAD usually has chemotherapy to resist drug resistance (Dokla, EME et al., 2019). Our data show that low-risk patients are more sensitive to methotrexate. Methotrexate combined immunosuppressive treatment may alleviate the drug resistance mechanism. High-risk groups are more sensitive to paclitaxel, cisplatin, docetaxel, etoposide, gefitinib, gemcitabine, sorafenib, and sunitinib. Lowering the abundance of fibroblasts in a tumor microenvironment may be a targeted treatment direction (Chen J. et al., 2022).

Cancer cells have obtained two important malignant characteristics of metastasis and drug resistance during differentiation. The differentiation state of the tumor is a key determinant of therapeutic resistance. It was studied in an experiment that induced EMT or degeneration in a cancer cell line and mouse model (ScheelWeinberg. 2011). The results show that the deplified promotes drug resistance to various chemotherapeutic drugs, and the decimalization increases about 10 times the IC50 dose of chemotherapeutic drugs. This requires further *in vitro* and *in vivo* studies. In addition, further clinical research is needed to determine if phenotype plasticity is of independent prognostic biomarker, as well as their relationship with the therapeutic effect.

We first link the unlocked phenotype plasticity with LUAD. Our study shows that ABCB1, ADIPOQ, NGF, F9, CDKN3, ACAN, and CEBPB may be potential genes for resistance to drug resistance. It may be a useful biomarker that affects the plasticity of the phenotype. Phenotype plasticity may provide potential biomarkers between tumor microenvironments, ICIS, and treatment reactions, which may be valued for LUAD treatment and prognosis.

Similar to previous studies (Yi et al., 2021), we successfully divided patients with lung adenocarcinoma into high-risk and low-risk groups by constructing the UPP-related model through

gene signatures. This model can predict the prognosis and evaluate the content of immune cells. In addition, the model also evaluated the function of immune cells, the abundance of stromal cells, and drug sensitivity. Immune cells and this model can predict the sensitivity of patients to chemotherapy drugs and help clinical patients formulate personalized treatment plans.

However, our research still has some limitations: first, the lack of experiments to verify the association between ingredients such as immune cells and prognosis in microtumor environments. Second, the lack of large clinical samples to forward the predictive value of prognosis characteristics of LUAD patients. In addition, the experimental exploration of potential functions and mechanisms in the signal and immunization infiltration of unlocking phenotype plasticity-related genes in LUAD progression. Therefore, further study is required in a clinical trial of larger sample quantities to verify the value of unlocking phenotype plasticity in LUAD prognosis.

Data availability statement

The original contributions presented in the study are included in the article/Supplementary Material; further inquiries can be directed to the corresponding author.

Author contributions

FW: conceptualization; funding acquisition; project administration; resources; writing-original draft; writing review and editing. LZ: investigation; methodology; software; writing-original draft. HD: investigation; methodology; writing original draft. BL: validation; writing-review and editing. FW: validation; writing-review and editing. ZL: validation; writing review and editing.

Acknowledgments

The authors acknowledge TCGA and GEO databases for providing their platforms and contributors for uploading their meaningful datasets and would like to thank all the authors listed in this article.

Conflict of interest

The authors declare that the research was conducted in the absence of any commercial or financial relationships that could be construed as a potential conflict of interest.

Publisher's note

All claims expressed in this article are solely those of the authors and do not necessarily represent those of their affiliated organizations, or those of the publisher, the editors, and the reviewers. Any product that may be evaluated in this article, or claim that may be made by its manufacturer, is not guaranteed or endorsed by the publisher.

Supplementary material

The Supplementary Material for this article can be found online at: https://www.frontiersin.org/articles/10.3389/fgene.2022.941567/full#supplementary-material

References

Al-Dherasi, A., Huang, Q. T., Liao, Y., Al-Mosaib, S., Hua, R., Wang, Y., et al. (2021). A seven-gene prognostic signature predicts overall survival of patients with lung adenocarcinoma (LUAD). *Cancer Cell. Int.* V21N1, 294. doi:10.1186/s12935-021-01975-z

Chen, J., Fu, Y., Hu, J., and He, J. (2022b). Hypoxia-related gene signature for predicting LUAD patients' prognosis and immune microenvironment. *Cytokine* 152, 155820. doi:10.1016/j.cyto.2022.155820

Chen, M-C., Chen, K-C., Chang, G-C., Lin, H., Wu, C-C., Kao, W-H., et al. (2020). RAGE acts as an oncogenic role and promotes the metastasis of human lung cancer. *Cell. Death Dis.* 11, 265. doi:10.1038/s41419-020-2432-1

Chen, W., Li, W., Liu, Z., Ma, G., Deng, Y., Zhu, L., et al. (2022a). Identification of tumor microenvironment-based genes associated with acquired resistance to EGFR Tyrosine Kinase Inhibitor in Lung Adenocarcinoma. *J. Cancer* 13 (3), 877–889. doi:10.7150/jca.57008

Chhipa, A. S., Borse, S. P., Baksi, R., Lalotra, S., and Nivsarkar, M. (2019). Targeting receptors of advanced glycation end products (RAGE): Preventing diabetes induced cancer and diabetic complications. *Pathol. Res. Pract.* 215, 152643. doi:10.1016/j.prp.2019.152643

Dokla, E. M. E., Fang, C. S., Abouzid, K. A. M., and Chen, C. S. (2019). 1, 2, 4-Oxadiazole derivatives targeting EGFR and c-Met degradation in TKI resistant NSCLC. *Eur. J. Med. Chem.* 2019V182N, 111607. doi:10.1016/j.ejmech.2019.111607

El-Far, A. H., Sroga, G., Jaouni, S. K. A., and Mousa, S. A. (2020). Role and mechanisms of RAGE-ligand complexes and RAGE-inhibitors in cancer progression. *Int. J. Mol. Sci.* 21, E3613. doi:10.3390/ijms21103613

Fan, C., Chen, L., Huang, Q., Shen, T., Welsh, E. A., Teer, J. K., et al. (2015). Overexpression of major CDKN3 transcripts is associated with poor survival in lung adenocarcinoma. *Br. J. Cancer* 113 (12), 1735–1743. doi:10.1038/bjc.2015.378

Gandhi, L., Rodríguez-Abreu, D., Gadgeel, S., Esteban, E., FelipE De Angelis, F., Domine, M., et al. (2018). Pembrolizumab plus chemotherapy in metastatic non–small-cell lung cancer. *N. Engl. J. Med.* 378 (22), 2078–2092. doi:10.1056/NEJMoa1801005

Geeleher, P., Cox, N., and Huang, R. S. (2014). pRRophetic: an R package for prediction of clinical chemotherapeutic response from tumor gene expression levels. *PLoS One* 583 9, e107468. doi:10.1371/journal.pone.0107468

Gkountakos, A., Centonze, G., Vita, E., Belluomini, L., Milella, M., Bria, E., et al. (2022). Identification of targetable liabilities in the dynamic metabolic profile of EGFR-mutant lung adenocarcinoma: Thinking beyond genomics for overcoming EGFR TKI resistance. *Biomedicines* 10, 277. doi:10.3390/biomedicines10020277

Haan, J. C., Bhaskaran, R., Ellappalayam, A., Bijl, Y., Griffioen, C. J., Lujinovic, E., et al. (2022). MammaPrint and BluePrint comprehensively capture the cancer hallmarks in early-stage breast cancer patients. *Genes. Chromosom. Cancer* 61 (3), 148–160. doi:10.1002/gcc.23014

Healy, T. M., and Schulte, P. M. (2015). Phenotypic plasticity and divergence in gene expression. *Mol. Ecol.* 24 (13), 3220–3222. doi:10.1111/mec.13246

Huang, Y., Lin, L., Shen, Z., Li, Y., Cao, H., Peng, L., et al. (2020). CEBPG promotes esophageal squamous cell carcinoma progression by enhancing PI3K-AKT signaling. *Am. J. Cancer Res.* 10 (10), 3328–3344. PMID:33163273.

Levy, B. P., Rao, P., Becker, D. J., and Becker, K. (2016). Attacking a moving target: Understanding resistance and managing progression in EGFR-positive lung cancer patients treated with tyrosine kinase inhibitors. *Oncol. Willist. Park)* 30 (7), 601–612. PMID: 27432364.

Li, M., Che, N., Jin, Y., Li, J., and Yang, W. (2022). CDKN3 overcomes bladder cancer cisplatin resistance via LDHA-dependent glycolysis reprogramming. *Onco. Targets. Ther.* 15, 299–311. doi:10.2147/OTT.S358008

Liu, S., Wang, Z., Zhu, R., Wang, F., Cheng, Y., and Liu, Y. (2021). Three differential expression analysis methods for RNA sequencing: Limma, EdgeR, DESeq2. *J. Vis. Exp.* VN175. doi:10.3791/62528

Lynch, V. J., May, G., and Wagner, G. P. (2011). Regulatory evolution through divergence of a phosphoswitch in the transcription factor CEBPB. *Nature* 480, 383–386. doi:10.1038/nature10595

Manna, I., Gambardella, A., Labate, A., Mumoli, L., Ferlazzo, E., Pucci, F., et al. (2015). Polymorphism of the multidrug resistance 1 gene MDR1/ABCB1 C3435T and response to antiepileptic drug treatment in temporal lobe epilepsy. *Seizure* 24, 124–126. doi:10.1016/j.seizure.2014.09.010

Matesanz, S., Blanco-Sánchez, M., Ramos-Muñoz, M., de la Cruz, M., Benavides, R., and Escudero, A. (2021). Phenotypic integration does not constrain phenotypic plasticity: Differential plasticity of traits is associated to their integration across environments. *New Phytol.* 231 (6), 2359–2370. doi:10.1111/nph.17536

Perino, A., Pols, T. W., Nomura, M., Stein, S., Pellicciari, R., and Schoonjans, K. (2014). TGR5 reduces macrophage migration through mTOR-induced C/EBPβ differential translation. *J. Clin. Investig.* 124 (12), 5424–5436. doi:10.1172/JCI76289

Rubin, M. A., Bristow, R. G., Thienger, P. D., Dive, C., and Imielinski, M. (2020). Impact of lineage plasticity to and from a neuroendocrine phenotype on progression and response in prostate and lung cancers. *Mol. Cell.* 80 (4), 562–577. doi:10.1016/j.molcel.2020.10.033

Salutari, I., and Caflisch, A. (2022). Dynamics of the histone acetyltransferase lysine-rich loop in the catalytic core of the CREB-binding protein. *J. Chem. Inf. Model.* 62 (4), 1014–1024. doi:10.1021/acs.jcim.1c01423

Scheel, C., and Weinberg, R. A. (2011). Phenotypic plasticity and epithelial-mesenchymal transitions in cancer and normal stem cells? *Int. J. Cancer* 129 (10), 2310–2314. doi:10.1002/ijc.26311

Shi, Y., Xu, Y., Xu, Z., Wang, H., Zhang, J., Wu, Y., et al. (2022). TKI resistant-based prognostic immune related gene signature in LUAD, in which FSCN1 contributes to tumor progression. *Cancer Lett.* 532, 215583. doi:10.1016/j.canlet.2022.215583

Tsai, C. J., and Nussinov, R. (2019). Emerging allosteric mechanism of EGFR activation in physiological and pathological contexts. *Biophys. J.* 117, 5–13. doi:10.1016/j.bpj.2019.05.021

Waghela, B. N., Vaidya, F. U., Ranjan, K., Chhipa, A. S., Tiwari, B. S., and Pathak, C. (2021). AGE-RAGE synergy influences programmed cell death signaling to promote cancer. *Mol. Cell. Biochem.* 476 (2), 585–598. doi:10.1007/s11010-020-03928-y

Wang, Y., Zhang, T., Guo, L., Ren, T., and Yang, Y. (2018). Stromal extracellular matrix is a microenvironmental cue promoting resistance to EGFR tyrosine kinase inhibitors in lung cancer cells. *Int. J. Biochem. Cell. Biol.* 106, 96–106. doi:10.1016/j.biocel.2018.11.001

Yang, X., Liang, X., Zheng, M., and Tang, Y. (2018). Cellular phenotype plasticity in cancer dormancy and metastasis. *Front. Oncol.* 8, 505. doi:10.3389/fonc.2018.00505

Yang, Y., Teng, Q. X., Wu, Z. X., Wang, J. Q., Lei, Z. N., Lusvarghi, S., et al. (2022). PBK/TOPK inhibitor OTS964 resistance is mediated by ABCB1-dependent transport function in cancer: *In vitro* and *in vivo* study. *Mol. Cancer* 21 (1), 40. doi:10.1186/s12943-022-01512-0

Yi, M., Li, A., Zhou, L., Chu, Q., Luo, S., and Wu, K. (2021). Immune signature-based risk stratification and prediction of immune checkpoint inhibitor's efficacy for lung adenocarcinoma. *Cancer Immunol. Immunother.* 70 (6), 1705–1719. doi:10.1007/s00262-020-02817-z

Yoshizawa, A., Motoi, N., Riely, G. J., Sima, C. S., Gerald, W. L., Kris, M. G., et al. (2011). Impact of proposed IASLC/ATS/ERS classification of lung adenocarcinoma: Prognostic subgroups and implications for further revision of staging based on analysis of 514 stage I cases. *Mod. Pathol.* 24 (5), 653–664. doi:10.1038/modpathol.2010.232

Zhang, L., Chen, J., Cheng, T., Yang, H., Li, H., and Pan, C. (2020). Identification of the key genes and characterizations of tumor immune microenvironment in lung adenocarcinoma (LUAD) and lung squamous cell carcinoma (LUSC). *J. Cancer* 11 (17), 4965–4979. doi:10.7150/jca.42531

Zhao, W., Mo, H., Liu, R., Chen, T., Yang, N., and Liu, Z. (2022). Matrix stiffness-induced upregulation of histone acetyltransferase KAT6A promotes hepatocellular carcinoma progression through regulating SOX2 expression. *Br. J. Cancer* 127, 202–210. doi:10.1038/s41416-022-01784-9

Zhao, Z., Xie, L., and Bourne, P. E. (2019). Structural insights into characterizing binding sites in epidermal growth factor receptor kinase mutants. *J. Chem. Inf. Model.* 59, 453–462. doi:10.1021/acs.jcim.8b00458

Zheng, Q., Min, S., and Zhou, Q. (2021). Identification of potential diagnostic and prognostic biomarkers for LUAD based on TCGA and GEO databases. *Biosci. Rep.* 41, BSR20204370. doi:10.1042/BSR20204370

frontiers | Frontiers in Genetics

TYPE Original Research
PUBLISHED 10 November 2022
DOI 10.3389/fgene.2022.946848

OPEN ACCESS

EDITED BY
Lei Yang,
Guangzhou Medical University, China

REVIEWED BY
Jinshuo Fan,
Huazhong University of Science and Technology, China
Wei Tang,
National Institutes of Health (NIH), United States
Yuannyu Zhang,
The University of Texas at Dallas, United States

*CORRESPONDENCE
Qiang Tan,
dr_tanqiang@sina.cn
Chunyu Ji,
chunyuji2022@163.com

†These authors have contributed equally to this work and share first authorship

‡These authors have contributed equally to this work and share last authorship

SPECIALTY SECTION
This article was submitted to Cancer Genetics and Oncogenomics, a section of the journal Frontiers in Genetics

RECEIVED 18 May 2022
ACCEPTED 25 October 2022
PUBLISHED 10 November 2022

CITATION
Zhou X, Zou B, Wang J, Wu L, Tan Q and Ji C (2022), Low expression of INMT is associated with poor prognosis but favorable immunotherapy response in lung adenocarcinoma.
Front. Genet. 13:946848.
doi: 10.3389/fgene.2022.946848

Low expression of INMT is associated with poor prognosis but favorable immunotherapy response in lung adenocarcinoma

Xincheng Zhou[1†], Bing Zou[2†], Jian Wang[3], Lihong Wu[3], Qiang Tan[4*‡] and Chunyu Ji[5*‡]

[1]Department of Experimental Pathology, Ningbo Clinical Pathological Diagnosis Center, Ningbo, China, [2]Department of Radiation Oncology, Cancer Hospital of Shandong Province, Jinan, China, [3]Burning Rock Biotech, Guangzhou, China, [4]Shanghai Lung Tumor Clinical Medical Center, Shanghai Chest Hospital, Shanghai Jiao Tong University, Shanghai, China, [5]Department of Thoracic Surgery, Shanghai Chest Hospital, Shanghai Jiao Tong University, Shanghai, China

Background: The expression of INMT (indolethylamine N-methyltransferase) has been reported to be downregulated in non-small-cell lung cancer (NSCLC). However, the role of INMT in NSCLC remains elusive. We aim to investigate the underlying mechanisms and clinical value of INMT in NSCLC, especially in lung adenocarcinoma (LUAD).

Methods: Gene expression cohorts from The Cancer Genome Atlas (TCGA) and Gene Expression Omnibus (GEO) were analyzed to assess the effect of INMT on NSCLC. Gene expression data from an immunotherapy cohort were used to investigate the association of INMT with immunotherapy in NSCLC.

Results: INMT expression was significantly downregulated in NSCLC compared with adjacent normal tissues. Downregulated INMT was associated with poor overall survival in LUAD, but not in lung squamous carcinoma. Multivariate Cox regression analysis suggested that INMT was an independent prognostic marker in LUAD. INMT had a reference value in the diagnosis and prognostic estimation of LUAD. Gene set enrichment analysis showed that pathways of the cell cycle and DNA damage response were enriched in the INMT low-expression group. The top 10 hub genes upregulated in the INMT low-expression group mainly activated the cell cycle pathway. In addition, more frequently mutated *TP53* genes, higher aneuploidy scores, a fraction of genomes altered, MANTIS

Abbreviations: AUC, area under the curve; CTRP, Cancer Therapeutics Response Portal; DCB, durable clinical benefit; DDR, DNA damage response; DEGs, differentially expressed genes; GDC, Genomic Data Commons; GEO, Gene Expression Omnibus; GEP, gene expression profiling; GSEA, gene set enrichment analysis; HR, hazard ratio; ICIs, immune checkpoint inhibitors; INMT, indolethylamine N-methyltransferase; IOBR, Immuno-Oncology Biological Research; LUAD, lung adenocarcinoma; LUSC, lung squamous cell carcinoma; MCC, maximal clique centrality; MSI, microsatellite instability; MSigDB, Molecular Signatures Database; NSCLC, non-small-cell lung cancer; OS, overall survival; PD-1, programmed cell death-1; PFS, progression-free survival; PPI, protein–protein interaction; ROC, receiver operating characteristic; STRING, Search Tool for Retrieval of Interacting Genes; TCGA, The Cancer Genome Atlas; TMB, tumor mutation burden; TPM, transcripts per million mapped reads.

scores, and tumor mutation burden were found in tumors with low expression of INMT. Furthermore, patients with low expression of INMT showed favorable clinical benefits to anti-PD-1 treatment with higher enrichment scores of immune-related signatures.

Conclusion: The low expression of INMT was associated with poor prognosis but favorable immunotherapy response in LUAD. INMT may affect the progression of LUAD by regulating the cell cycle and may serve as a valuable independent prognostic biomarker in patients with LUAD.

KEYWORDS

INMT, lung adenocarcinoma, prognosis, immunotherapy, cell cycle

Introduction

Non-small-cell lung cancer (NSCLC) is a malignant cancer that has the highest mortality rate of all cancers worldwide (Siegel et al., 2020; Sung et al., 2021). Lung adenocarcinoma (LUAD) is the largest subtype of NSCLC (Little et al., 2007). Advances in recent years, such as the identification of multiple oncogenic drivers and the use of immunotherapies, have changed the treatment of LUAD (Kleczko et al., 2019). However, the survival rates remain low. Therefore, it is urgent to find more effective biomarkers to smooth the way for novel therapeutic methods.

In recent years, immunotherapy, especially immune checkpoint inhibitors (ICIs) targeting programmed cell death-1 (PD-1) and its ligand PD-L1, has revolutionized cancer treatment and substantially improved patient outcomes in NSCLC (Suresh et al., 2018). However, only a limited subset of patients could benefit from immunotherapy, and immunotherapy lacks precise biomarkers to predict efficacy (Brahmer et al., 2012). Therefore, identifying biomarkers to screen dominant populations for ICI efficacy is particularly important. Multiple factors associated with the clinical outcome of immunotherapy are discovered, such as PD-L1 expression (Herbst et al., 2014; Shukuya and Carbone, 2016), tumor mutation burden (TMB) (Rizvi et al., 2015), DNA mismatch repair deficiency (Le et al., 2015), the degree of cytotoxic T-cell infiltration (Tang et al., 2016), mutational signature (Miao et al., 2018), antigen presentation defects (Chowell et al., 2018), interferon signaling (Ayers et al., 2017), and tumor aneuploidy (Davoli et al., 2017). These biomarkers show different accuracies and utilities, and identifying robust ICI-response biomarkers remains a critical challenge in the field (Nishino et al., 2017).

Indolethylamine N-methyltransferase (INMT) is a methyltransferase that regulates the tryptophan metabolic pathway by catalyzing the N-methylation of tryptamine and structurally related compounds (Chu et al., 2014; Torres et al., 2019). As a thioether S-methyltransferase, it also plays an important role in the detoxification of selenium compounds (Kuehnelt et al., 2015). It is specifically expressed in the lung and expressed as supplemental in the liver, kidneys, prostate, and other tissues (Fukumoto et al., 2020). It has been reported that the expression of INMT is downregulated in lung cancer, prostate cancer, and meningioma (Kopantzev et al., 2008; Larkin et al., 2012; Schulten et al., 2016). However, the role of INMT and its molecular mechanism in cancer, especially lung cancer, remain unknown. The study of the molecular mechanism of INMT would help us better understand the process of tumorigenesis and development and find new targets in cancers. Herein, using data from The Cancer Genome Atlas (TCGA) project and the Gene Expression Omnibus (GEO) database, we performed a secondary analysis to thoroughly analyze the INMT expression level, determine its prognostic role, and explore its potential functions in NSCLC.

Materials and methods

Genomic data sources

The transcriptome sequencing data (including 962 NSCLC samples and 103 adjacent nontumor samples), somatic mutation data (including 486 LUAD samples), and clinical information of TCGA data were downloaded from the Genomic Data Commons (GDC) data portal (https://portal.gdc.cancer.gov/). The samples from primary lesions that had a follow-up time of more than 1 month were included in this study. The following gene expression profiles were downloaded from GEO (www.ncbi.nlm.nih.gov/geo/): GSE19188 (including 65 tumor samples and 72 adjacent nontumor samples), GSE72094 (including 398 LUAD samples), and GSE41271 (including 183 LUAD samples); these were used to further validate our results. The PD-1 immunotherapy gene expression profiling dataset GSE135222 (including 27 NSCLC samples) was downloaded from GEO and used to analyze the association between INMT expression and immunotherapy response. The detailed data sources used in this study are summarized in Supplementary Table S1.

Establishment and evaluation of the nomogram for lung adenocarcinoma survival prediction

In this study, all independent prognostic factors were selected using multivariate Cox regression analysis and used to construct the nomogram to evaluate the 3- and 5-year overall survival (OS) probabilities of LUAD patients. Covariates in the nomogram were assessed for the patient and given a point. A higher total number of points represented a lower expected survival. By comparing the predicted probability of the line chart with the observed actual probability through a calibration curve, the accuracy of the line chart was verified. The overlapping reference lines show that the model is accurate.

Differential gene expression analysis

The "limma" package (version 3.46.0), using R software, was used to screen differentially expressed genes (DEGs) between INMT low- and high-expression groups. INMT-related DEGs were identified when the adjusted p-value < 0.05 and $|\log_2(\text{Fold Change})| > 1$.

Gene set enrichment analysis and functional annotation

Gene set enrichment analysis (GSEA) was performed to explore the biological functions of INMT in LUAD (Subramanian et al., 2005). First, we ranked all the mRNAs according to the fold change between INMT high- and low-expression groups. Then, the ordered mRNAs were imported to the R package "clusterProfiler" (version 3.18.1) for GSEA, containing KEGG and Reactome pathways from a Molecular Signatures Database (MSigDB) (https://software.broadinstitute.org/gsea/msigdb). Benjamini–Hochberg standard false discovery rate correction was used for multiple testing corrections. The gene set was considered significantly enriched when the adjusted p-value < 0.05.

Protein–protein interaction network construction and hub gene identification

The protein–protein interaction (PPI) data were extracted from the Search Tool for the Retrieval of Interacting Genes (STRING) database (https://string-db.org/), an online tool allowing users to upload the data of DEGs. It is used to analyze the PPI information and to evaluate the interaction relationships among DEGs (Szklarczyk et al., 2015). After downloading INMT-related DEG interactions, the PPI network was visualized using Cytoscape (3.7.2) software (http://www.cytoscape.org/). In Cytoscape, module screening and connection degree computation were performed using the maximal clique centrality (MCC) method in the cytoHubba plugin. Nodes with a higher degree of connection were more essential for maintaining the stability of the entire network; usually, nodes with a degree of connection ≥10 were considered to be core candidate genes. In this study, the top 10 hub genes were selected for further functional analysis. The GeneMANIA database (http://www.genemania.org) was also applied to construct the INMT interaction network.

The relationship between gene expression and pathway activity in GSCALite

Gene Set Cancer Analysis (GSCALite) (http://bioinfo.life.hust.edu.cn/web/GSCALite/) is a web-based platform for dynamic analysis and visualization of gene sets from the point of view of the expression of malignant tumor genes correlations with drug sensitivity (Liu et al., 2018). The correlation between gene expression and pathway activity groups (activation and inhibition) defined by pathway scores was analyzed in GSCALite. Pathway activation (red) represents the percentage of cancers in which the pathway may be activated by given genes, and inhibition in a similar way is shown as pathway inhibition (blue).

The relationship between gene expression and drug sensitivity in GSCALite

The drug sensitivity analysis of GSCALite has collected 481 small molecules from the Cancer Therapeutics Response Portal (CTRP) (https://portals.broadinstitute.org/ctrp/) (Rees et al., 2016). Drug sensitivity and gene expression profiling data on cancer cell lines in CTRP are integrated for investigation (Garnett et al., 2012). The expression profiling of each gene in a given gene set is performed by Spearman's correlation analysis with small molecule/drug sensitivity (IC_{50}). The Spearman correlation represents the gene expression that correlates with the drug. A negative correlation means that the gene's high expression is sensitive to the drug and *vice versa*.

Mutational analysis

The R package "maftools" (version 2.6.05) was used to analyze the frequently mutated genes in the TCGA-LUAD cohort. Aneuploidy scores, a fraction of genome altered, MANTIS scores, and TMB scores were downloaded from cBioPortal (https://www.cbioportal.org/study/clinicalData?id=luad_tcga_pan_can_atlas_2018). TMB scores of the

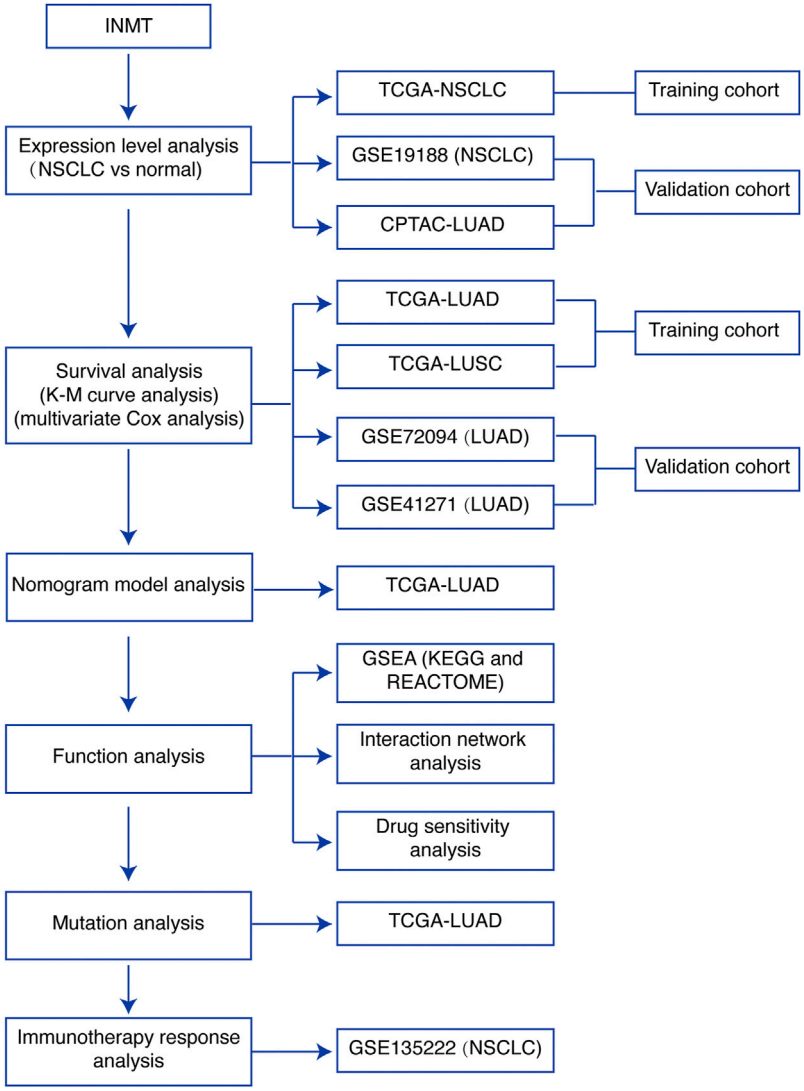

FIGURE 1
Study flowchart. INMT, indolethylamine N-methyltransferase; NSCLC, non-small-cell lung cancer; LUAD, lung adenocarcinoma; LUSC, lung squamous cell carcinoma; TCGA, The Cancer Genome Atlas; K-M curve, Kaplan–Meier survival; GSEA, gene set enrichment analysis.

immunotherapy cohort were downloaded from GEO (https://www.ncbi.nlm.nih.gov/geo/query/acc.cgi?acc=GSE135222). The aneuploidy score is the total number of arm-level gains and losses for a tumor, adjusted for ploidy. The fraction of genome altered is the percentage of copy number-altered chromosome regions out of measured regions. The MANTIS score is a score that predicts a patient's microsatellite instability (MSI) status (Bonneville et al., 2017). TMB is broadly defined as the number of nonsynonymous somatic mutations per megabase of the interrogated genomic sequence as previously described (Chalmers et al., 2017).

Immune gene signature calculation

Immuno-Oncology Biological Research (IOBR) is a tool for leveraging multi-omics data to facilitate immuno-oncology exploration and unveil tumor–immune interactions (Zeng et al., 2021). The gene sets utilized for the immune signature score in this study are defined as previously reported (Ayers et al., 2017; Charoentong et al., 2017; Mariathasan et al., 2018) and are presented in Supplementary Table S2. The enrichment scores of these immune gene signatures were calculated using the "IOBR" R package (version 0.99.9).

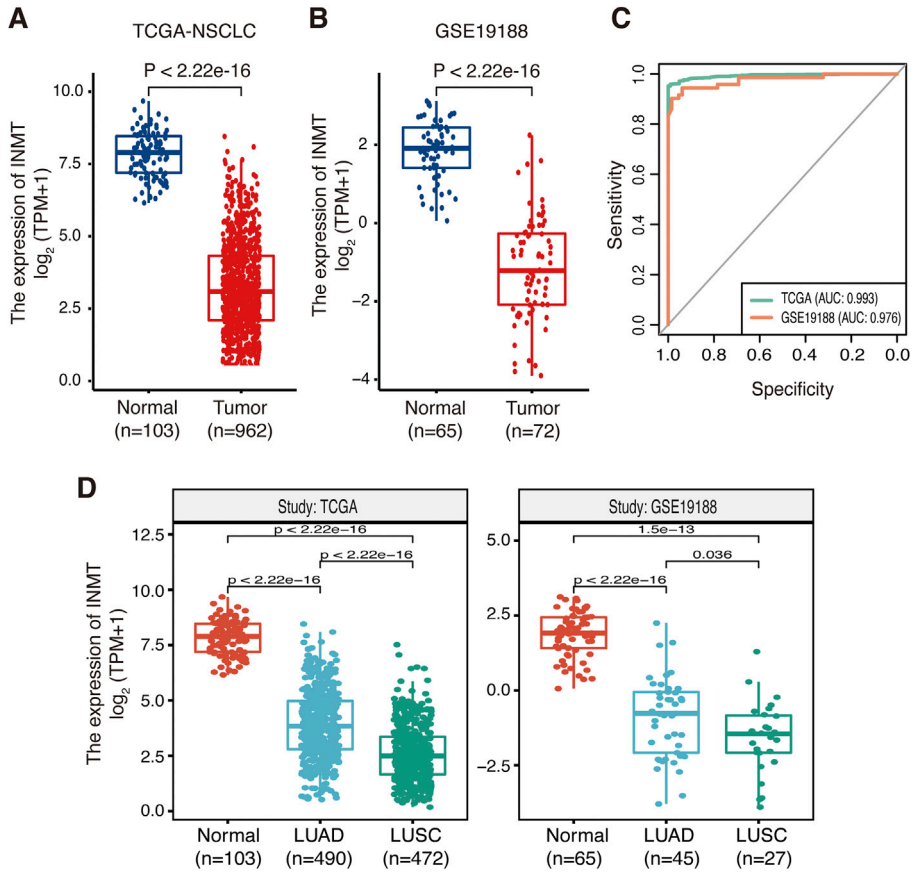

FIGURE 2
Expression of INMT in normal lung and NSCLC tissues. **(A,B)** Differential expression of INMT in normal lung and NSCLC tissues in TCGA dataset **(A)** and the GSE19188 dataset **(B)**. **(C)** Evaluation of the sensitivity and specificity of NSCLC diagnosis by ROC curves in TCGA dataset and the GSE19188 dataset. **(D)** Differential expression of INMT in normal lung, LUAD, and LUSC tissues in TCGA dataset (left) and the GSE19188 dataset (right), respectively. NSCLC, non-small-cell lung cancer; LUAD, lung adenocarcinoma; LUSC, lung squamous cell carcinoma; ROC, receiver operator characteristic; AUC, area under the curve; TPM, transcripts per million mapped reads.

Statistical analysis

The Student *t*-test or Wilcoxon rank-sum test was used to compare two groups of continuous variables, depending on whether the data were normally distributed. The Chi-squared test or Fisher's exact test was used to compare categorical variables. The Spearman correlation test was applied to evaluate the correlation between sample factors. Receiver operating characteristic (ROC) analysis was performed to assess the diagnostic value of INMT expression in NSCLC. The Kaplan–Meier method was applied for survival analysis, and the log-rank test was used to estimate statistical significance. Multivariate Cox regression analysis was used to screen potential prognostic factors. The level of significance was set at $p < 0.05$, and all statistical tests were two-sided. All statistical data analyses were implemented using R software, version 4.0.2.

Results

Indolethylamine N-methyltransferase was significantly downregulated in patients with NSCLC

A brief flowchart of our study is shown in Figure 1. We first used the TCGA-NSCLC database to evaluate the mRNA expression levels of INMT in NSCLC patients and adjacent normal tissues. The result showed that the expression level of INMT in NSCLC was significantly lower than that in normal tissues ($p < 0.001$) (Figure 2A). This result was verified in GSE19188 and CPTAC-LUAD cohorts at a transcription level and protein level, respectively (Figure 2B and Supplementary Figure S1A). According to ROC curve analysis, INMT was a robust predictor of NSCLC, with an area under the curve (AUC) = 0.976 (Figure 2C). Furthermore, we found that the

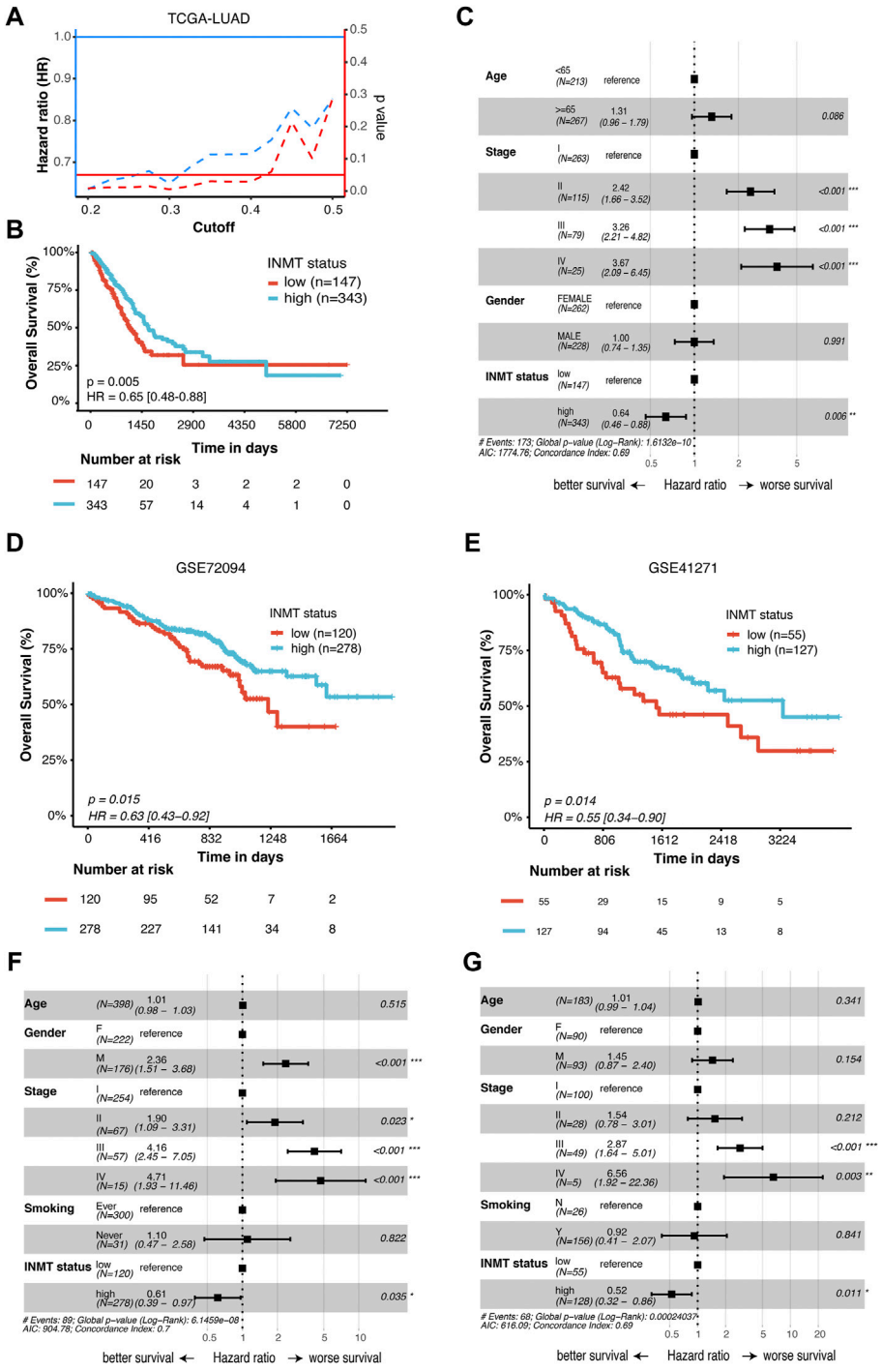

FIGURE 3
Prognostic significance of INMT in LUAD patients. **(A)** Hazard ratio (HR) and statistical results of the INMT high-expression group *versus* low-expression group at different cutoffs in TCGA-LUAD cohort. The blue dashed line represents the HR value, the red dashed line represents the *p*-value, and the solid red line represents $p = 0.05$. **(B)** Kaplan–Meier curve analysis of the prognostic significance of high- and low-expression of INMT in TCGA-LUAD cohorts. **(C)** Multivariate Cox analysis of the clinical characteristics and INMT associated with overall survival (OS) in TCGA-LUAD cohort. **(D,E)** Kaplan–Meier curve analysis of the prognostic significance of high and low expression of INMT in two GEO-LUAD cohorts (GSE72094 and GSE41271), respectively. **(F,G)** Multivariate Cox analysis of the clinical characteristics and INMT associated with OS in two GEO-LUAD cohorts (GSE72094 and GSE41271), respectively. The cutoff of 30% quantile was used to divide patients into low- and high-expression groups. LUAD, lung adenocarcinoma; HR, hazard ratio; OS, overall survival.

expression of INMT in LUSC was significantly lower than that in LUAD (Figure 2D). Additionally, based on the TCGA cohort, we used the Spearman rank correlation test to analyze the correlation of INMT expression with a pathological stage in LUAD and LUSC. We observed a weak but significant negative correlation between INMT expression and pathological stage in both LUAD and LUSC, i.e., INMT expression decreases as the stage increases (Supplementary Figures S1B, S1C). These results showed that INMT was significantly downregulated in patients with NSCLC and was a robust predictor of NSCLC.

Low indolethylamine N-methyltransferase expression is associated with poor prognosis of patients with lung adenocarcinoma

To identify whether INMT expression affects patient survival, Kaplan–Meier survival analysis was conducted on the TCGA-NSCLC cohort. As shown in Figure 3A, low INMT expression was associated with poor prognosis in LUAD patients. At the cutoff value of a quantile of 30%, the survival difference between the low-INMT group and the high-INMT group was the most significant in LUAD patients. So, we used this cutoff to classify LUAD patients into a low INMT expression group (30% of samples with the lowest expression) and a high INMT expression group (the remaining 70% of the samples) in this study. The Kaplan–Meier survival analysis showed that the low expression of INMT was significantly related to the poor OS of LUAD patients [Hazard ratio (HR), 1.54; 95% CI, 1.14-2.08; p-value = 0.005] (Figure 3B). Multivariate Cox regression analysis results suggested that INMT expression was an independent prognosis factor in the TCGA-LUAD cohort, after adjusting age, gender, and pathological stage (Figure 3C). Similarly, we also checked the association between INMT expression and survival in LUSC patients. However, the Kaplan–Meier survival analysis failed to show a significant difference between low and high INMT expression groups in LUSC patients (Supplementary Figures S2A, S2B). Furthermore, we validated the relationship between INMT expression and OS using two GEO-LUAD cohorts (GSE72094 and GSE41271) and demonstrated that INMT was an independent prognosis factor in LUAD patients through multivariate Cox analysis (Figures 3D–G).

Prognostic nomogram model for lung adenocarcinoma overall survival

To better predict the prognosis of LUAD patients in the clinic, we developed a prognostic nomogram model by integrating two independent predictors of mortality from the aforementioned analyses, INMT expression and pathological stage, into a multivariate Cox regression model, which was evaluated and validated using TCGA, GSE72094, and GSE41271 data (Figures 3C, F, G). A score based on the nomogram developed in the current study was calculated to predict the 3- and 5-year survival probabilities for individual patients (Figure 4A). The calibration plot showed that the nomogram performed well in predicting patient OS according to an ideal model (Figure 4B).

Low indolethylamine N-methyltransferase expression is closely related to the cell cycle, DNA replication, and DNA damage response pathways

To investigate the possible signaling pathways in which INMT might be involved, GSEA was performed on the TCGA-LUAD cohort. Supplementary Tables S3 and S4 illustrate GSEA results of KEGG and Reactome gene sets between high- and low-INMT groups, respectively. As shown in Figure 5A, KEGG gene sets of the cell cycle, DNA replication, and DNA damage response (DDR) pathways, such as mismatch repair, Fanconi anemia pathway, and homologous recombination, were enriched in the INMT low-expression group. GSEA of Reactome gene sets showed similar results that the INMT low-expression group was closely associated with cell cycle, DNA replication, and DDR pathways (Figure 5B).

Hub genes upregulated in the indolethylamine N-methyltransferase low-expression group are associated with cell cycle, apoptosis, and DDR pathways

Considering that downregulated INMT was associated with the worse prognosis in LUAD, we further explored the functions of hub genes that were upregulated in the INMT low-expression group of the TCGA-LUAD cohort to find the potential drugs that were inhibitors of hub genes for these INMT-related high-risk patients. As shown in Figure 6A, 111 upregulated genes in the INMT low-expression group were used to construct a PPI network based on the STRING database and thus formed 56 nodes and 553 edges. The top 10 hub genes were identified from these complex interactomes using the MCC method in Cytoscape, namely, ASPM, BUB1, BUB1B, TTK, CDC20, CDK1, CCNA2, CCNB2, DLGAP5, and KIF2C (Figure 6B). The chord plot result confirmed that the expression of each hub gene was negatively correlated with the expression of INMT (Figure 6C). Furthermore, pathway activity analysis of hub genes indicated that the pathways of the cell cycle, apoptosis, and DDR, the vital steps in tumor progression, were mainly activated by these 10 hub genes (Figures 6D,E). In addition, high expression of each hub gene was significantly associated with a worse OS in

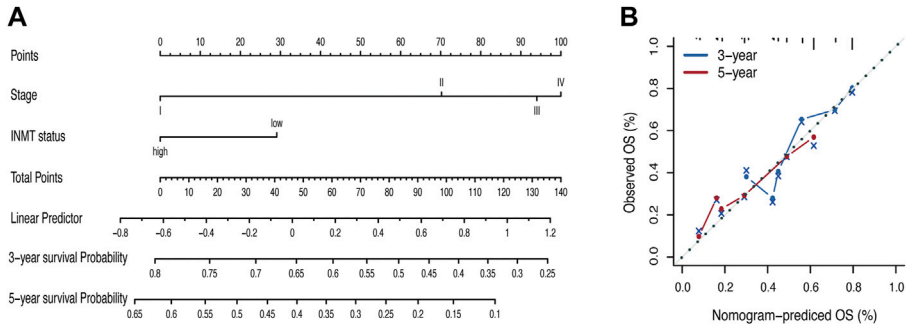

FIGURE 4
Nomogram for the prediction of survival in LUAD. **(A)** Nomogram by multivariate Cox regression analysis for predicting the proportion of patients with overall survival (OS). **(B)** Plots depict the calibration of the model in terms of the agreement between predicted and observed OS. Model performance is shown by the plot, relative to the 45-degree line, which represents perfect prediction. OS, overall survival.

LUAD (Figure 6F), which was consistent with the association of low INMT with poor OS. Additionally, we used CTRP IC_{50} drug data from the GSCALite database to analyze the correlation between the expression of these 10 hub genes and the sensitivity of the small-molecule drugs in LUAD cell lines. We found that LUAD cell lines with hub gene overexpression were sensitive to the cell cycle and DNA replication-related drugs, such as topotecan, etoposide, doxorubicin, and gemcitabine (Figure 6G). Our aforementioned results found that these hub genes upregulated in the INMT low-expression group were mainly involved in the activation of the cell cycle, apoptosis, and DDR pathways and might provide the basis for drug-targeted therapy for these INMT-related high-risk LUAD patients.

Low indolethylamine N-methyltransferase indicates high-frequency somatic alterations

It has been reported that somatic mutations were involved in the development of cancer (Martincorena and Campbell, 2015). Here, we used the TCGA-LUAD cohort to investigate the difference in somatic mutations between low- and high-INMT groups in LUAD. Common tumor-related mutations were shown in the waterfall plot and stratified by the INMT expression level (Figure 7A). Somatic mutation profiles revealed that the tumor-suppressor gene TP53 was more frequently mutated in the low INMT expression group (Figure 7B). We then compared the differences in the distribution of aneuploidy scores, a fraction of genome altered scores, MANTIS scores, and TMB scores between low- and high-INMT groups. We found that the low INMT expression group had higher aneuploidy scores, a fraction of genome altered scores, MANTIS scores, and TMB scores (Figures 7C–F).

Low indolethylamine N-methyltransferase is associated with a favorable immunotherapy response

We previously found that mutated *TP53* genes and higher TMB and MANTIS scores were enriched in tumors with the low expression of INMT, and we therefore speculated on whether these high-risk patients would benefit from immunotherapy. We then investigated the correlation between INMT expression and immunotherapy response in a GEO public PD-1 immunotherapy cohort of advanced NSCLC (GSE135222). As shown in Figures 8A, B, patients with low INMT expression had a higher durable clinical benefit (DCB) rate (50% vs. 0%, $p = 0.008$) and more improved progression-free survival (PFS) (HR, 0.14; 95% CI, 0.05–0.40; $p < 0.001$) than those with high INMT expression, with median PFS of 5.70 months vs. 1.73 months. We also checked the distribution of TMB in low-and high-INMT groups and found that tumors with low INMT expression had higher TMB (Figure 8C). Previous studies have confirmed that CD8 effector T cells, MHC Class I, IFN-gamma signaling, and T-cell-inflamed gene expression profiling (GEP) play roles in anticancer immunity and immunotherapeutic effects (Ayers et al., 2017; Charoentong et al., 2017; Mariathasan et al., 2018). Here, we analyzed the relationship between INMT and these immune signatures and found that the signature scores of CD8 effector T cells, IFN-gamma signaling, and MHC Class I signature were significantly higher in the INMT low-expression group (Figure 8D).

Discussion

In this study, we used data from TCGA and GEO to thoroughly analyze the INMT expression level, determine its prognostic role, and explore its potential functions in NSCLC.

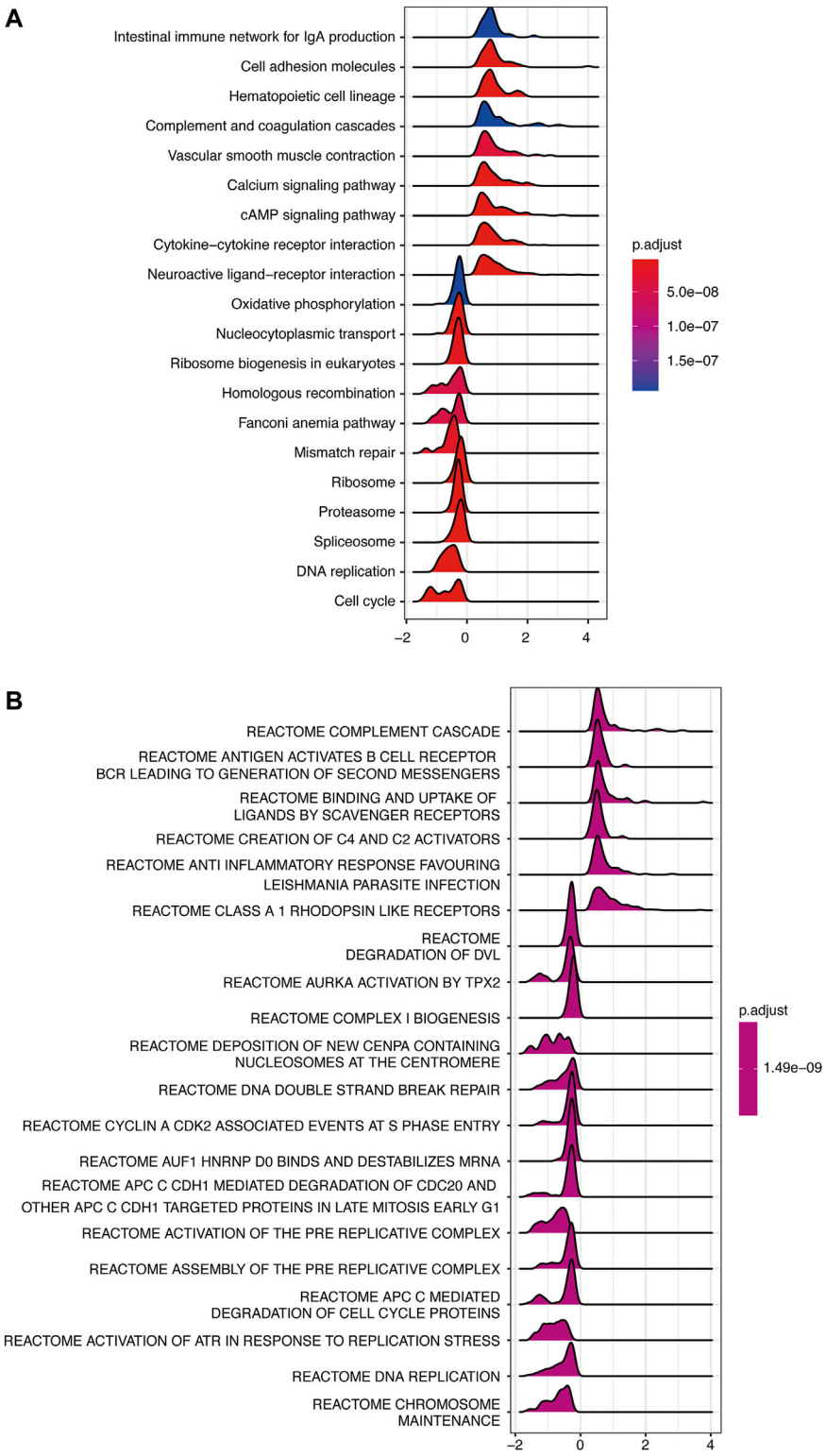

FIGURE 5
GSEA of samples between high- and low-INMT groups in TCGA-LUAD cohort. Ridge plot of gene sets of KEGG **(A)** and Reactome **(B)** enriched in the high- or low-INMT group in TCGA-LUAD cohort. The X-axis represents the normalized enrichment score (NES), and the color represents the *p*-value adjusted by FDR. The top enriched signaling pathways are shown in the figures. GSEA, gene set enrichment analysis.

10.3389/fgene.2022.946848

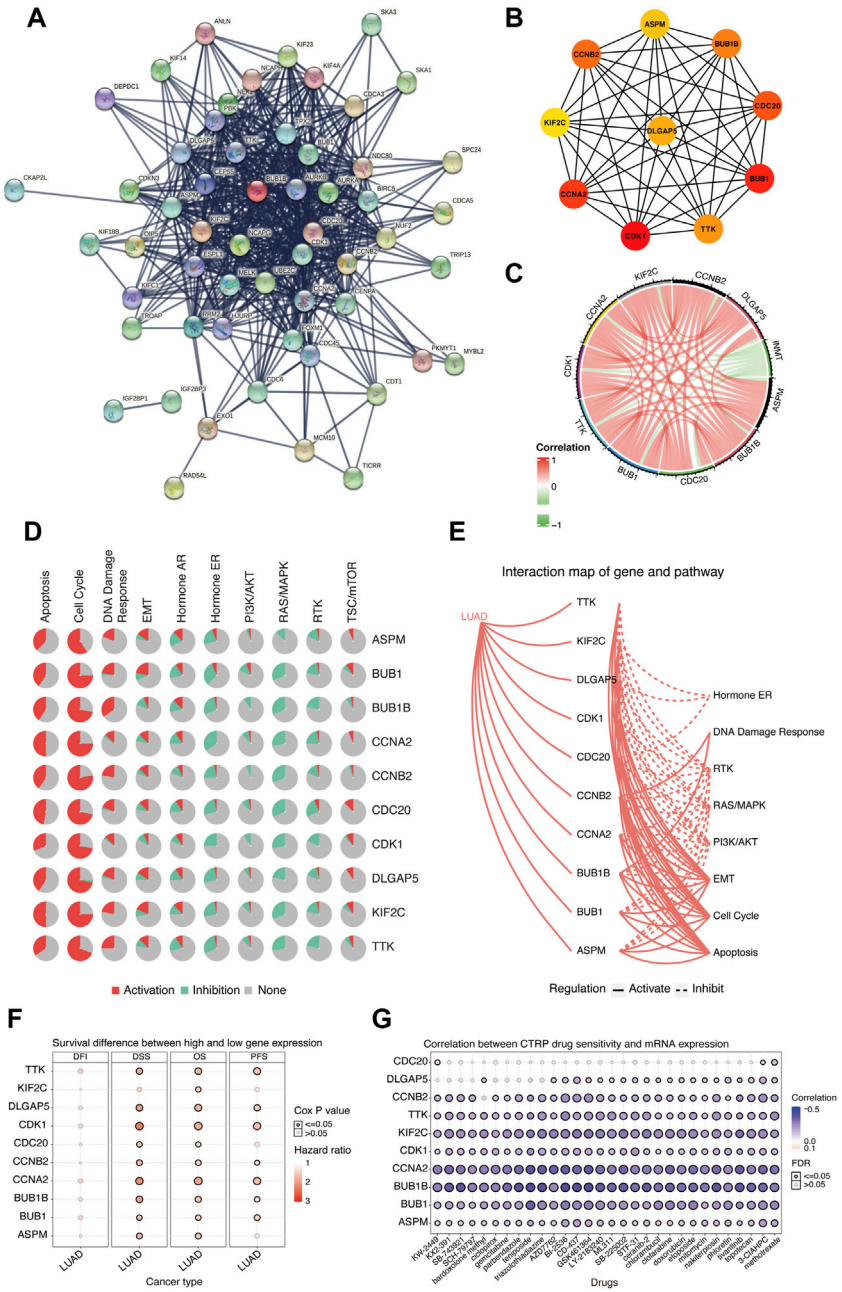

FIGURE 6
Biological function analysis of hub genes that were upregulated in the INMT low-expression group of TCGA-LUAD cohort. **(A)** Protein–protein interaction (PPI) network of upregulated genes in the INMT low-expression group constructed based on the STRING database. **(B)** Top 10 hub genes identified using the MCC method in the cytoHubba plugin of Cytoscape. **(C)** Chord plot for the correlation of INMT and its hub genes. **(D)** Pathway activity analysis of hub genes. Pathway activation (red) represents the percentage of cancers in which pathways may be activated by given genes, and inhibition in a similar way showed as pathway inhibition (blue). **(E)** Interaction map of hub genes and pathway conducted. A solid line indicates that the hub gene activates the pathway, and a dashed line indicates that the hub gene inhibits the pathway. **(F)** Survival difference between the high and low expression of hub genes. **(G)** Correlation between the expression of hub genes and CTRP drug sensitivity. The analyses of Figures 5D–G were performed online in GSCALite. LUAD, lung adenocarcinoma; PPI, protein–protein interaction.

We found that INMT expression was significantly downregulated in NSCLC, and downregulated INMT was associated with poor OS in LUAD, but not in LUSC. Multivariate Cox regression analysis further demonstrated that INMT is a promising independent prognostic biomarker in LUAD in three independent datasets. In addition, INMT has

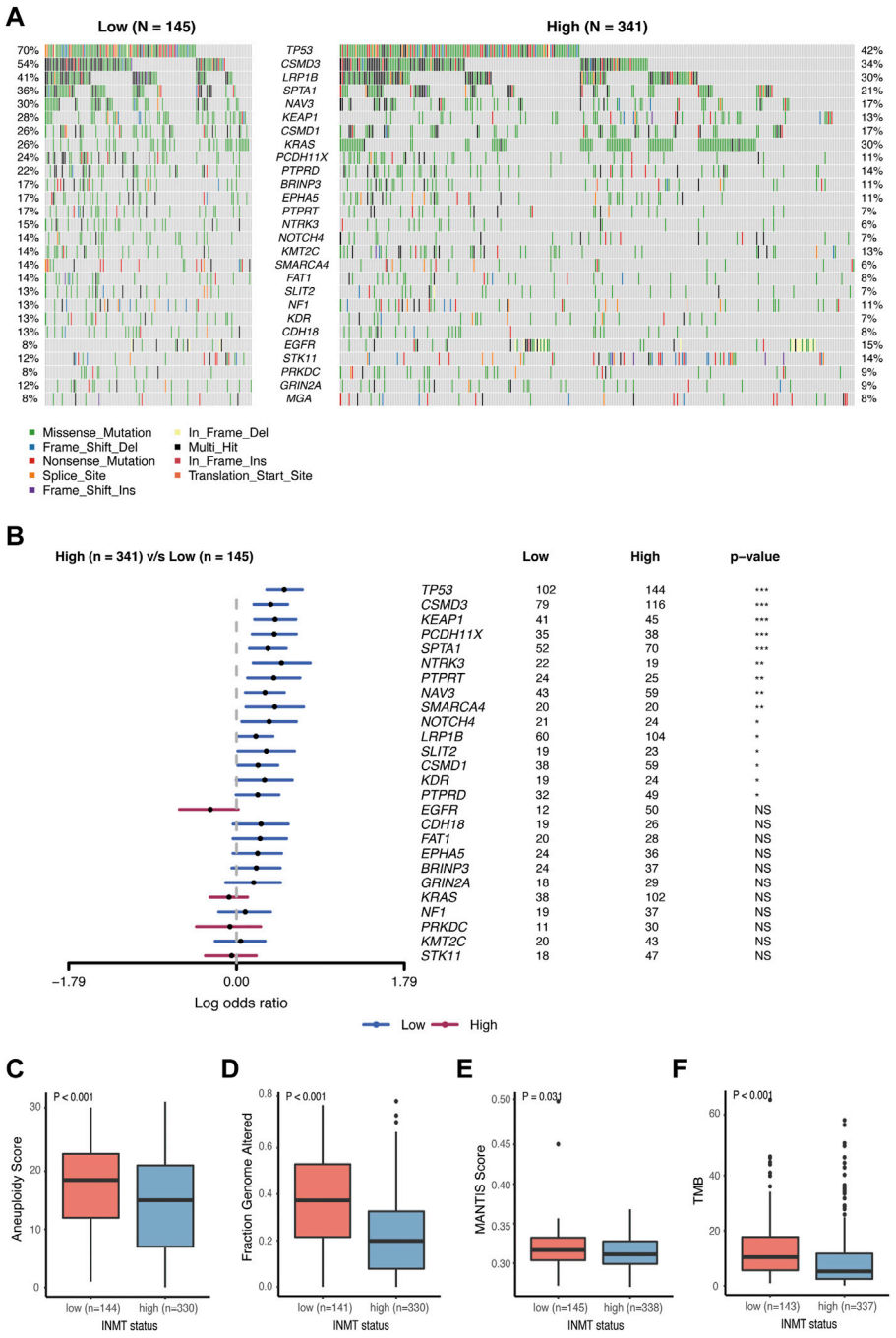

FIGURE 7
Association between INMT and gene alterations in TCGA-LUAD cohort. **(A)** Common tumor-related gene mutation information illustrated in the somatic mutation spectrum in low- and high-INMT groups, respectively. The genes in the top 20 of the population mutation frequency are shown in the figure. **(B)** Forest plot examined the difference in the population frequency of mutant genes between the high- and low-INMT groups. **(C–F)** Distribution of the aneuploidy score **(C)**, a fraction of genome altered score **(D)**, MANTIS score **(E)**, and TMB score **(F)** between low- and high-INMT groups. TMB, tumor mutation burden.

a certain reference value for the diagnosis and prognosis of LUAD. GSEA results found that pathways of the cell cycle, DNA replication, and DDR were enriched in the INMT low-expression group. The top 10 hub genes upregulated in the INMT low-expression group mainly activated the cell cycle pathway, and LUAD cell lines with hub gene overexpression were sensitive

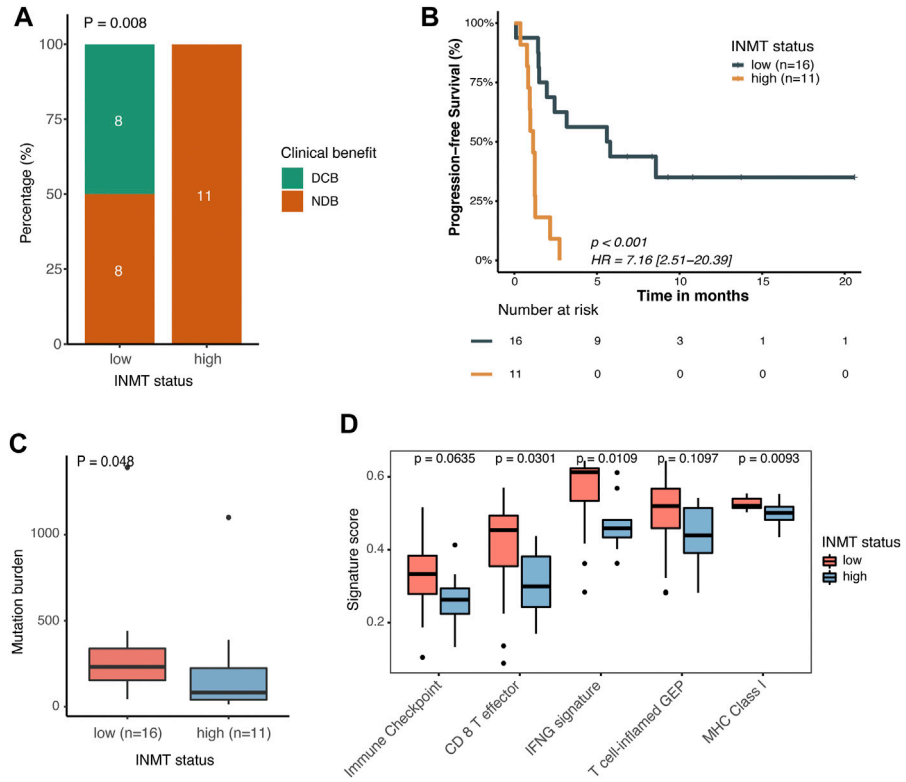

FIGURE 8
Association between INMT and immunotherapy response in a PD-1 immunotherapy cohort of NSCLC (GSE135222). **(A)** Clinical benefit rate among INMT low-and high-expression groups. Fisher's exact test was used for the analysis. **(B)** Kaplan–Meier curve for progression-free survival according to an INMT expression status. The log-rank test was used for the analysis. **(C)** TMB distribution between INMT low- and high-expression groups. The Wilcoxon rank-sum test was used for the analysis. **(D)** Boxplot of enrichment scores of immune-related signatures among INMT low- and high-expression groups. The Wilcoxon rank-sum test was used for the analysis. DCB, durable clinical benefit; NDB, non-durable clinical benefit; HR, hazard ratio; TMB, tumor mutation burden.

to the cell cycle and DNA replication-related drugs. More mutated *TP53* genes and higher aneuploidy scores, a fraction of genome altered scores, MANTIS scores, and TMB scores were found in the INMT low-expression group. Furthermore, a GEO public PD-1 immunotherapy cohort of NSCLC suggested that patients in the INMT-related high-risk group could benefit from immunotherapy. Our study has provided new insights into INMT that could be a potential prognostic marker of survival and a potential predictive marker of immunotherapy in LUAD patients.

As a methyltransferase, INMT detoxifies selenium compounds and regulates the tryptophan metabolic pathway by catalyzing the N-methylation of tryptamines and structure-related compounds (Kuehnelt et al., 2015). INMT is downregulated in NSCLC and prostate cancer (Kopantzev et al., 2008; Larkin et al., 2012; Jianfeng et al., 2022). To the best of our knowledge, no previous study has assessed the relationship between INMT and prognosis in cancers. In this work, using TCGA-NSCLC data, we found that the low expression of INMT was associated with poor OS in LUAD, but not in LUSC. We further demonstrated that INMT was an independent prognostic biomarker in LUAD using multivariate Cox regression analysis in TCGA-LUAD and another two GEO cohorts. We found that INMT expression decreased as the pathological stage increased; this supported that there was a correlation between low INMT and poor prognosis in LUAD. ROC curve analysis and the nomogram model showed that INMT had a certain reference value in the diagnosis and prognostic estimation of LUAD. Our work is the first report on the association between INMT and the prognosis of patients with LUAD, providing new insights into INMT as a potential prognostic marker in LUAD.

Previous studies on INMT have mainly focused on its role in regulating the tryptophan metabolic pathway and detoxifying selenium compounds by catalyzing the methylation of several substrates (Chu et al., 2014; Kuehnelt et al., 2015; Torres et al., 2019). Only a few studies have reported on its biological function in prostate cancer but not in lung cancer. For instance, Zhong et al. (2021) found that INMT was highly increased in castration-resistant

prostate cancer, and further *in vitro* experiments suggested that INMT might promote prostate cancer castration resistance through detoxification of anticancer metabolites. Wang et al. found that INMT may inhibit proliferation and promote apoptosis of human prostate cancer cells (Jianfeng et al., 2022). In our study, we showed that the cell cycle and DNA replication pathways were enriched in the INMT low-expression group. Cell cycle disorder is one of the key features of cancer that cause genomic instability (Hanahan and Weinberg, 2011). Our GSEA results indicated that downregulated INMT may lead to an acceleration of cell cycle and DNA replication to increase the probability of genome instability. Further hub gene analysis also showed that the top 10 hub genes that were upregulated in the INMT low-expression group played key roles in the control of the cell cycle, including mitotic spindle regulation and G1/S and G2/M transition. The drug sensitivity analysis revealed that LUAD cell lines with hub gene overexpression were sensitive to the cell cycle and DNA replication-related drugs, indicating that these INMT-related high-risk patients might benefit from cell cycle-related drugs. Our results revealed that INMT may affect the progression of LUAD by regulating the cell cycle and might provide the basis for drug-targeted therapy for these INMT-related high-risk LUAD patients. However, our results are only analyzed based on the public data, and further molecular experiments on cancer cell lines are needed to explore the mechanism of INMT in tumorigenesis and the development of LUAD.

Our analysis of the relationship between INMT expression and immunotherapy response found that NSCLC patients with low INMT expression showed favorable clinical benefits to anti-PD-1 treatment. More mutated TP53 genes, higher TMB, and higher enrichment scores of immune-related signatures of MHC Class I, $CD8^+$ effector T cells, and IFN-gamma signaling were found in the INMT low-expression group. A TP53 gene mutation has been reported to boost PD-L1 expression, facilitate T-cell infiltration, and augment tumor immunogenicity and is a potential predictive marker for response to ICIs in LUAD (Dong et al., 2017). TMB reflects cancer mutation quantity. The more mutations there are, the higher the number of neoantigens and the higher the chances that one or more of the neoantigens will be immunogenic and trigger a T-cell response. Many studies have reported a connection between higher TMB and ICI efficacy across a wide variety of cancer types (Snyder et al., 2014; Goodman et al., 2017; Cristescu et al., 2018; Samstein et al., 2019). A number of predicted MHC Class I-associated neoantigens have been shown to be correlated with a cytolytic activity (Rooney et al., 2015), and the anti-tumor activity of ICIs is dependent on MHC Class I presentation of specific tumor-derived peptides (Gubin et al., 2014; Tran et al., 2015). $CD8^+$ T cells are primed and activated toward $CD8^+$ T effector cells in a process called the cancer immunity cycle to make durable and efficient anti-tumor immune responses (Chen and Mellman, 2013). It has been reported that the IFN-γ–related mRNA profile could predict clinical response to a PD-1 blockade in many types of cancers (Ayers et al., 2017). The higher scores of biomarkers in the INMT low-expression group may explain why patients in the INMT low-expression group have a better response to immunotherapy in NSCLC. Although our result is based on a small cohort, it provides these INMT-related high-risk patients with a treatment option.

There are several limitations to our work. First, we did not investigate the exact mechanisms of INMT with *in vivo/in vitro* experiments, and further experiments are required to demonstrate the effect of INMT on the tumor cell cycle to improve the reliability of our results. Second, we obtained data on the anti-PD-1 response in a small NSCLC cohort from a public database, and further immunotherapy data on LUAD are needed to verify the role of INMT.

Conclusion

In summary, INMT is downregulated in LUAD, and the low expression of INMT is closely associated with poor prognosis in LUAD. INMT has a certain reference value for the diagnosis and prognosis of LUAD. Furthermore, INMT may affect the progression of LUAD by regulating the cell cycle. With further exploration, patients with low INMT expression showed favorable clinical benefits to anti-PD-1 treatment. This is the first study to reveal that INMT influences prognosis and immunotherapy responses in LUAD. These findings provide a new perspective on LUAD progression and treatment.

Data availability statement

The original contributions presented in the study are included in the article/Supplementary Material; further inquiries can be directed at the corresponding authors.

Author contributions

CJ and QT conceived and designed the work. XZ, BZ, and JW acquired, analyzed, and interpreted the data. XZ and LW drafted and revised the manuscript. All authors contributed to the manuscript and approved the submitted version.

Acknowledgments

The authors gratefully acknowledge The Cancer Genome Atlas and Gene Expression Omnibus databases.

Conflict of interest

JW and LW were employed by Burning Rock Biotech.

The remaining authors declare that the research was conducted in the absence of any commercial or financial relationships that could be construed as a potential conflict of interest.

Publisher's note

All claims expressed in this article are solely those of the authors and do not necessarily represent those of their affiliated organizations, or those of the publisher, the editors, and the reviewers. Any product that may be evaluated in this article, or claim that may be made by its manufacturer, is not guaranteed or endorsed by the publisher.

Supplementary material

The Supplementary Material for this article can be found online at: https://www.frontiersin.org/articles/10.3389/fgene.2022.946848/full#supplementary-material

References

Ayers, M., Lunceford, J., Nebozhyn, M., Murphy, E., Loboda, A., Kaufman, D. R., et al. (2017). IFN-gamma-related mRNA profile predicts clinical response to PD-1 blockade. *J. Clin. Invest.*. 127 (8), 2930–2940. doi:10.1172/JCI91190

Bonneville, R., Krook, M. A., Kautto, E. A., Miya, J., Wing, M. R., Chen, H. Z., et al. (2017). Landscape of microsatellite instability across 39 cancer types. *JCO Precis. Oncol.* 2017, 1–15. doi:10.1200/PO.17.00073

Brahmer, J. R., Tykodi, S. S., Chow, L. Q. M., Hwu, W. J., Topalian, S. L., Hwu, P., et al. (2012). Safety and activity of anti-PD-L1 antibody in patients with advanced cancer. *N. Engl. J. Med.* 366 (26), 2455–2465. doi:10.1056/NEJMoa1200694

Chalmers, Z. R., Connelly, C. F., Fabrizio, D., Gay, L., Ali, S. M., Ennis, R., et al. (2017). Analysis of 100, 000 human cancer genomes reveals the landscape of tumor mutational burden. *Genome Med.* 9 (1), 34. doi:10.1186/s13073-017-0424-2

Charoentong, P., Finotello, F., Angelova, M., Mayer, C., Efremova, M., Rieder, D., et al. (2017). Pan-cancer immunogenomic analyses reveal genotype-immunophenotype relationships and predictors of response to checkpoint blockade. *Cell Rep.* 18 (1), 248–262. doi:10.1016/j.celrep.2016.12.019

Chen, D. S., and Mellman, I. (2013). Oncology meets immunology: The cancer-immunity cycle. *Immunity* 39 (1), 1–10. doi:10.1016/j.immuni.2013.07.012

Chowell, D., Morris, L. G. T., Grigg, C. M., Weber, J. K., Samstein, R. M., Makarov, V., et al. (2018). Patient HLA class I genotype influences cancer response to checkpoint blockade immunotherapy. *Science* 359 (6375), 582–587. doi:10.1126/science.aao4572

Chu, U. B., Vorperian, S. K., Satyshur, K., Eickstaedt, K., Cozzi, N. V., Mavlyutov, T., et al. (2014). Noncompetitive inhibition of indolethylamine-N-methyltransferase by N, N-dimethyltryptamine and N, N-dimethylaminopropyltryptamine. *Biochemistry* 53 (18), 2956–2965. doi:10.1021/bi500175p

Cristescu, R., Mogg, R., Ayers, M., Albright, A., Murphy, E., Yearley, J., et al. (2018). Pan-tumor genomic biomarkers for PD-1 checkpoint blockade-based immunotherapy. *Science* 362 (6411), eaar3593. doi:10.1126/science.aar3593

Davoli, T., Uno, H., Wooten, E. C., and Elledge, S. J. (2017). Tumor aneuploidy correlates with markers of immune evasion and with reduced response to immunotherapy. *Science* 355 (6322), eaaf8399. doi:10.1126/science.aaf8399

Dong, Z. Y., Zhong, W. Z., Zhang, X. C., Su, J., Xie, Z., Liu, S. Y., et al. (2017). Potential predictive value of TP53 and KRAS mutation status for response to PD-1 blockade immunotherapy in lung adenocarcinoma. *Clin. Cancer Res.* 23 (12), 3012–3024. doi:10.1158/1078-0432.CCR-16-2554

Fukumoto, Y., Yamada, H., Matsuhashi, K., Okada, W., Tanaka, Y. K., Suzuki, N., et al. (2020). Production of a urinary selenium metabolite, trimethylselenonium, by thiopurine S-methyltransferase and indolethylamine N-methyltransferase. *Chem. Res. Toxicol.* 33 (9), 2467–2474. doi:10.1021/acs.chemrestox.0c00254

Garnett, M. J., Edelman, E. J., Heidorn, S. J., Greenman, C. D., Dastur, A., Lau, K. W., et al. (2012). Systematic identification of genomic markers of drug sensitivity in cancer cells. *Nature* 483 (7391), 570–575. doi:10.1038/nature11005

Goodman, A. M., Kato, S., Bazhenova, L., Patel, S. P., Frampton, G. M., Miller, V., et al. (2017). Tumor mutational burden as an independent predictor of response to immunotherapy in diverse cancers. *Mol. Cancer Ther.* 16 (11), 2598–2608. doi:10.1158/1535-7163.MCT-17-0386

Gubin, M. M., Zhang, X., Schuster, H., Caron, E., Ward, J. P., Noguchi, T., et al. (2014). Checkpoint blockade cancer immunotherapy targets tumour-specific mutant antigens. *Nature* 515 (7528), 577–581. doi:10.1038/nature13988

Hanahan, D., and Weinberg, R. A. (2011). Hallmarks of cancer: The next generation. *Cell* 144 (5), 646–674. doi:10.1016/j.cell.2011.02.013

Herbst, R. S., Soria, J. C., Kowanetz, M., Fine, G. D., Hamid, O., Gordon, M. S., et al. (2014). Predictive correlates of response to the anti-PD-L1 antibody MPDL3280A in cancer patients. *Nature* 515 (7528), 563–567. doi:10.1038/nature14011

Jianfeng, W., Yutao, W., and Jianbin, B. (2022). Indolethylamine-N-Methyltransferase inhibits proliferation and promotes apoptosis of human prostate cancer cells: A mechanistic exploration. *Front. Cell Dev. Biol.* 10, 805402. doi:10.3389/fcell.2022.805402

Kleczko, E. K., Kwak, J. W., Schenk, E. L., and Nemenoff, R. A. (2019). Targeting the complement pathway as a therapeutic strategy in lung cancer. *Front. Immunol.* 10, 954. doi:10.3389/fimmu.2019.00954

Kopantzev, E. P., Monastyrskaya, G. S., Vinogradova, T. V., Zinovyeva, M. V., Kostina, M. B., Filyukova, O. B., et al. (2008). Differences in gene expression levels between early and later stages of human lung development are opposite to those between normal lung tissue and non-small lung cell carcinoma. *Lung Cancer* 62 (1), 23–34. doi:10.1016/j.lungcan.2008.02.011

Kuehnelt, D., Engstrom, K., Skroder, H., Kokarnig, S., Schlebusch, C., Kippler, M., et al. (2015). Selenium metabolism to the trimethylselenonium ion (TMSe) varies markedly because of polymorphisms in the indolethylamine N-methyltransferase gene. *Am. J. Clin. Nutr.* 102 (6), 1406–1415. doi:10.3945/ajcn.115.114157

Larkin, S. E., HolmeS, S., Cree, I. A., Walker, T., Basketter, V., Bickers, B., et al. (2012). Identification of markers of prostate cancer progression using candidate gene expression. *Br. J. Cancer* 106 (1), 157–165. doi:10.1038/bjc.2011.490

Le, D. T., Uram, J. N., Wang, H., Bartlett, B. R., Kemberling, H., Eyring, A. D., et al. (2015). PD-1 blockade in tumors with mismatch-repair deficiency. *N. Engl. J. Med.* 372 (26), 2509–2520. doi:10.1056/NEJMoa1500596

Little, A. G., Gay, E. G., Gaspar, L. E., and Stewart, A. K. (2007). National survey of non-small cell lung cancer in the United States: Epidemiology, pathology and patterns of care. *Lung Cancer* 57 (3), 253–260. doi:10.1016/j.lungcan.2007.03.012

Liu, C. J., Hu, F. F., Xia, M. X., Han, L., Zhang, Q., and Guo, A. Y. (2018). GSCALite: A web server for gene set cancer analysis. *Bioinformatics* 34 (21), 3771–3772. doi:10.1093/bioinformatics/bty411

Mariathasan, S., Turley, S. J., Nickles, D., Castiglioni, A., Yuen, K., Wang, Y., et al. (2018). TGFβ attenuates tumour response to PD-L1 blockade by contributing to exclusion of T cells. *Nature* 554 (7693), 544–548. doi:10.1038/nature25501

Martincorena, I., and Campbell, P. J. (2015). Somatic mutation in cancer and normal cells. *Science* 349 (6255), 1483–1489. doi:10.1126/science.aab4082

Miao, D., Margolis, C. A., Vokes, N. I., Liu, D., Taylor-Weiner, A., Wankowicz, S. M., et al. (2018). Genomic correlates of response to immune checkpoint blockade in microsatellite-stable solid tumors. *Nat. Genet.* 50 (9), 1271–1281. doi:10.1038/s41588-018-0200-2

Nishino, M., Ramaiya, N. H., Hatabu, H., and Hodi, F. S. (2017). Monitoring immune-checkpoint blockade: Response evaluation and biomarker development. *Nat. Rev. Clin. Oncol.* 14 (11), 655–668. doi:10.1038/nrclinonc.2017.88

Rees, M. G., Seashore-Ludlow, B., Cheah, J. H., Adams, D. J., Price, E. V., Gill, S., et al. (2016). Correlating chemical sensitivity and basal gene expression reveals mechanism of action. *Nat. Chem. Biol.* 12 (2), 109–116. doi:10.1038/nchembio.1986

Rizvi, N. A., Hellmann, M. D., Snyder, A., Kvistborg, P., Makarov, V., Havel, J. J., et al. (2015). Cancer immunology. Mutational landscape determines sensitivity to PD-1 blockade in non-small cell lung cancer. *Science* 348 (6230), 124–128. doi:10.1126/science.aaa1348

Rooney, M. S., Shukla, S. A., Wu, C. J., Getz, G., and Hacohen, N. (2015). Molecular and genetic properties of tumors associated with local immune cytolytic activity. *Cell* 160 (1-2), 48–61. doi:10.1016/j.cell.2014.12.033

Samstein, R. M., Lee, C. H., Shoushtari, A. N., Hellmann, M. D., Shen, R., Janjigian, Y. Y., et al. (2019). Tumor mutational load predicts survival after immunotherapy across multiple cancer types. *Nat. Genet.* 51 (2), 202–206. doi:10.1038/s41588-018-0312-8

Schulten, H. J., Hussein, D., Al-Adwani, F., Karim, S., Al-Maghrabi, J., Al-Sharif, M., et al. (2016). Microarray expression data identify DCC as a candidate gene for early meningioma progression. *PLoS One* 11 (4), e0153681. doi:10.1371/journal.pone.0153681

Shukuya, T., and Carbone, D. P. (2016). Predictive markers for the efficacy of anti-PD-1/PD-L1 antibodies in lung cancer. *J. Thorac. Oncol.* 11 (7), 976–988. doi:10.1016/j.jtho.2016.02.015

Siegel, R. L., Miller, K. D., and Jemal, A. (2020). Cancer statistics. *Ca. Cancer J. Clin.* 70 (1), 7–30. doi:10.3322/caac.21590

Snyder, A., Makarov, V., Merghoub, T., Yuan, J., Zaretsky, J. M., Desrichard, A., et al. (2014). Genetic basis for clinical response to CTLA-4 blockade in melanoma. *N. Engl. J. Med.* 371 (23), 2189–2199. doi:10.1056/NEJMoa1406498

Subramanian, A., Tamayo, P., Mootha, V. K., Mukherjee, S., Ebert, B. L., Gillette, M. A., et al. (2005). Gene set enrichment analysis: A knowledge-based approach for interpreting genome-wide expression profiles. *Proc. Natl. Acad. Sci. U. S. A.* 102 (43), 15545–15550. doi:10.1073/pnas.0506580102

Sung, H., Ferlay, J., Siegel, R. L., Laversanne, M., Soerjomataram, I., Jemal, A., et al. (2021). Global cancer statistics 2020: GLOBOCAN estimates of incidence and mortality worldwide for 36 cancers in 185 countries. *Ca. Cancer J. Clin.* 71 (3), 209–249. doi:10.3322/caac.21660

Suresh, K., Naidoo, J., Lin, C. T., and Danoff, S. (2018). Immune checkpoint immunotherapy for non-small cell lung cancer: Benefits and pulmonary toxicities. *Chest* 154 (6), 1416–1423. doi:10.1016/j.chest.2018.08.1048

Szklarczyk, D., Franceschini, A., Wyder, S., Forslund, K., Heller, D., Huerta-Cepas, J., et al. (2015). STRING v10: Protein-protein interaction networks, integrated over the tree of life. *Nucleic Acids Res.* 43, D447–D452. doi:10.1093/nar/gku1003

Tang, H., Wang, Y., Chlewicki, L. K., Zhang, Y., Guo, J., Liang, W., et al. (2016). Facilitating T cell infiltration in tumor microenvironment overcomes resistance to PD-L1 blockade. *Cancer Cell* 29 (3), 285–296. doi:10.1016/j.ccell.2016.02.004

Torres, B., Tyler, J. S., Satyshur, K. A., and Ruoho, A. E. (2019). Human indole(ethyl)amine-N-methyltransferase (hINMT) catalyzed methylation of tryptamine, dimethylsulfide and dimethylselenide is enhanced under reducing conditions - a comparison between 254C and 254F, two common hINMT variants. *PLoS One* 14 (7), e0219664. doi:10.1371/journal.pone.0219664

Tran, E., Ahmadzadeh, M., Lu, Y. C., Gros, A., Turcotte, S., Robbins, P. F., et al. (2015). Immunogenicity of somatic mutations in human gastrointestinal cancers. *Science* 350 (6266), 1387–1390. doi:10.1126/science.aad1253

Zeng, D., Ye, Z., Shen, R., Yu, G., Wu, J., Xiong, Y., et al. (2021). Iobr: Multi-Omics immuno-oncology biological research to decode tumor microenvironment and signatures. *Front. Immunol.* 12, 687975. doi:10.3389/fimmu.2021.687975

Zhong, S., Jeong, J. H., Huang, C., Chen, X., Dickinson, S. I., Dhillon, J., et al. (2021). Targeting INMT and interrupting its methylation pathway for the treatment of castration resistant prostate cancer. *J. Exp. Clin. Cancer Res.* 40 (1), 307. doi:10.1186/s13046-021-02109-z

frontiers | Frontiers in Genetics

TYPE Original Research
PUBLISHED 25 November 2022
DOI 10.3389/fgene.2022.1027741

OPEN ACCESS

EDITED BY
Andrey Ivanov,
Emory University, United States

REVIEWED BY
Yuan Liu,
Emory University, United States
Wahafu Alafate,
Guangdong Provincial People's Hospital, China

*CORRESPONDENCE
Linan Fang,
fanglinan_jdyy@jlu.edu.cn
Wei Liu,
l_w01@jlu.edu.cn

†These authors have contributed equally to this work and share first authorship

SPECIALTY SECTION
This article was submitted to Cancer Genetics and Oncogenomics, a section of the journal Frontiers in Genetics

RECEIVED 25 August 2022
ACCEPTED 16 November 2022
PUBLISHED 25 November 2022

CITATION
Song Y, Zhang J, Fang L and Liu W (2022), Prognostic necroptosis-related gene signature aids immunotherapy in lung adenocarcinoma.
Front. Genet. 13:1027741.
doi: 10.3389/fgene.2022.1027741

Prognostic necroptosis-related gene signature aids immunotherapy in lung adenocarcinoma

Yuqi Song[1†], Jinming Zhang[2†], Linan Fang[1*] and Wei Liu[1*]

[1]Department of Thoracic Surgery, First Hospital of Jilin University, Changchun, China, [2]First Hospital of Jilin University, Changchun, China

Background: Necroptosis is a phenomenon of cellular necrosis resulting from cell membrane rupture by the corresponding activation of Receptor Interacting Protein Kinase 3 (RIPK3) and Mixed Lineage Kinase domain-Like protein (MLKL) under programmed regulation. It is reported that necroptosis is closely related to the development of tumors, but the prognostic role and biological function of necroptosis in lung adenocarcinoma (LUAD), the most important cause of cancer-related deaths, is still obscure.

Methods: In this study, we constructed a prognostic Necroptosis-related gene signature based on the RNA transcription data of LUAD patients from The Cancer Genome Atlas (TCGA) and Gene Expression Omnibus (GEO) databases as well as the corresponding clinical information. Kaplan-Meier analysis, receiver operating characteristic (ROC), and Cox regression were made to validate and evaluate the model. We analyzed the immune landscape in LUAD and the relationship between the signature and immunotherapy regimens.

Results: Five genes (RIPK3, MLKL, TLR2, TNFRSF1A, and ALDH2) were used to construct the prognostic signature, and patients were divided into high and low-risk groups in line with the risk score. Cox regression showed that risk score was an independent prognostic factor. Nomogram was created for predicting the survival rate of LUAD patients. Patients in high and low-risk groups have different tumor purity, tumor immunogenicity, and different sensitivity to common antitumor drugs.

Conclusion: Our results highlight the association of necroptosis with LUAD and its potential use in guiding immunotherapy.

KEYWORDS

lung adenocarcinoma, necroptosis, gene signature, prognosis, immunotherapy, chemotherapy

Introduction

As the most important cause of cancer death, lung cancer has been a major research topic for clinicians and researchers (Sung et al., 2021). Non-small cell lung cancer (NSCLC), the most important type of lung cancer, accounts for 85% of the total incidence of the disease (Chen et al., 2014). Slow-growing, insidious-developing lung adenocarcinoma (LUAD) is the most common pathological type of NSCLC. It is prone to hematogenous metastasis, so some patients are often diagnosed at a late stage, which deprives them of the opportunity for surgery and their clinical prognosis is poor (Devarakonda et al., 2015). The advent of targeted therapies and immunotherapy has brought better options for such patients, but most of them have no mutation in the driver gene or do not respond to a single immune checkpoint inhibitor (ICI) (Matter et al., 2020; Santarpia et al., 2020). In recent years, with the development of RNA sequencing, microarrays, and other "Omics" technologies, a series of new potential markers driving tumor cell formation have been identified and progressively applied in the clinic. The average 5-year survival rate of LUAD patients, although significantly improved, is still less than optimal.

Necroptosis is a phenomenon of cellular necrosis resulting from cell membrane rupture by the corresponding activation of Receptor Interacting Protein Kinase 3 (RIPK3) and Mixed Lineage Kinase domain-Like protein (MLKL) under programmed regulation (Degterev et al., 2005). It has a proper regulatory mechanism. With the advancement of basic research, necroptosis has been found to be not only involved in the inflammatory pathological mechanism of the body (Khoury et al., 2020) but also closely related to the development of tumors and drug resistance. Preliminary studies suggest that necroptosis has a "double-edged sword" role in tumor pathology, which can exert either tumor-suppressive or tumor-promoting effects (Raposo et al., 2015; Liu et al., 2016; Hänggi et al., 2017). On the one hand, inducing necroptosis can remove chemotherapy-resistant tumor cells; on the other hand, it may also kill normal cells and lead to inflammatory responses that promote tumor progression and metastasis (Gong et al., 2019).

Immunotherapies, represented by ICIs such as various antibodies against cytotoxic T lymphocyte-associated antigen 4 (CTLA-4), programmed cell death 1 (PD-1), and programmed cell death ligand 1 (PD-L1), are designed to stimulate the patient's immune system to trigger an effective anti-tumor immune response (Rosenberg, 2014). Despite its emerging and encouraging results, increased immune tolerance is frequently documented in many cancer types (Bonavida and Chouaib, 2017). Furthermore, a large proportion of studies have also highlighted the potentially enormous impact of necroptosis-driven immunogenic features in tumor immunology, for example, the induction of necroptosis can act synergistically with ICIs to enhance their antitumor activity in drug-resistant tumors (Tang et al., 2020). These close and complex relationships suggest that necroptosis may be an important target for tumor progression and may provide new strategies for tumor immunotherapy and prognosis (Philipp et al., 2016). However, to date, the mechanism of the role of necroptosis in LUAD is unclear, and its relationship with immunotherapy and prognosis has been little studied.

The aim of this study was to construct a robust prognostic model of Necroptosis-Related Genes (NRGs) by bioinformatics algorithms to predict the survival probability of LUAD patients at different periods. We will also explore the functional pathways and signaling pathways involved in key genes and their relationship with immune cell infiltration, tumor mutation burden, immunotherapy, and drug sensitivity, to assist in individualized and precise treatment.

Materials and methods

Data acquisition

RNA transcriptome information and clinical information of LUAD patients were obtained from The Cancer Genome Atlas (TCGA) database and the GSE72094, GSE50081 datasets in Gene Expression Omnibus (GEO) database, respectively. The RNA-seq transcriptome data were converted to transcript volume per million (TPM) values, and the R "limma" and "sav" packages were applied for batch correction and normalization of RNA-seq from both platforms. After excluding samples with incomplete clinical information or gene expression data, 504 patients from TCGA and 398 patients from the GSE72094 dataset with LUAD were included in the downstream analysis, and 127 patients from the GSE50081 dataset were used for external validation. 17 NRGs (RIPK1, RIPK3, MLKL, TLR2, TLR3, TLR4, TNFRSF1A, PGAM5, ZBP1, NR2C2, HMGB1, CXCL1, USP22, TRAF2, ALDH2, EZH2, NDRG2) were obtained from literature reviews of previous related studies (Petersen et al., 2015; Choi et al., 2019; Lou et al., 2019; Malireddi et al., 2019; Wen et al., 2020; Xia et al., 2020; Zhu et al., 2020; Cheng et al., 2021; Roedig et al., 2021). The relative position of these genes to the chromosomes was visualized using the R "RCircos" package. The Human Protein Atlas database (https://www.proteinatlas.org/) was used to display the expression of proteins encoded by NRGs.

Construction and validation of a necroptosis-related prognostic signature

Sample data from the TCGA and GSE72094 dataset was combined, including expression data of NRGs and patients' survival data. A univariate Cox regression analysis was performed to obtain genes significantly associated with

prognosis. After that, we randomly divided the patients into Train and Test sets (632 in the Train set and 270 in the Test set). The R "glmnet" package was used to perform LASSO regression analysis on the prognostic data and to optimize the penalty function using cross-validation. A prognostic signature consisting of genes related to necroptosis was developed to predict the prognosis of LUAD patients. The formulae are as follows:

$$\begin{aligned} Risk\ Score = {} & coefficients * expressing\ values\ of\ A\ gene \\ & + coefficients * expressing\ values\ of\ B\ gene \\ & + \ldots \end{aligned}$$

Using the "CatPredi" software package, an R package allows the user to categorize a continuous predictor variable in a logistic or a Cox proportional hazards regression setting by maximizing the discriminative ability of the model, we determined the optimal two cut-off values for the Train and Test sets separately, splitting each set into a low-risk group and a high-risk group. Kaplan-Meier analysis was used to plot the overall survival (OS) curves for each set. In this study, OS was defined as the duration from the date of diagnosis to death or last follow-up, with no restriction on the cause of death. The R "timeROC" package was used to generate subject operating characteristic (ROC) curves, and the area under the curve (AUC) of the ROC curves was measured to show the sensitivity and specificity of the model.

In addition, we performed univariate and multivariate Cox regression analyses of the validity of the risk score as an independent prognostic indicator. The clinical characteristics of high and low-risk patients were compared using the R "pheatmap" package to explore the correlation between risk scores and clinicopathological variables.

Nomogram construction and verification

We constructed a nomogram based on 902 samples from all TCGA + GSE72094 datasets to predict the survival rate of patients at 1, 2, and 3 years using pathological staging and risk score information. We then plotted ROC curves and calibration curves to test the validity and robustness of the nomogram.

Gene Ontology and Kyoto Encyclopedia of Genes and Genomes analysis

Eleven prognosis-related NRGs were annotated and functionally analyzed using the R "DOSE" package, including Gene Ontology (GO) and Kyoto Encyclopedia of Genes and Genomes (KEGG), with a corrected p-value (q-value) < 0.05 as the filter.

Correlation between risk score and immune landscape

To reveal the correlation between risk scores and tumor-infiltrating immune cells, we assessed the immune infiltration of tumors using the CIBERSORT algorithm. We uploaded the full gene expression data of all samples to the CIBERSORTx portal and later ran the algorithm for 1,000 permutations based on the LM22 signature. LUAD samples with output p-values < 0.05 were selected for further analysis to explore the relationship between risk score and necroptosis-related prognostic gene expression and immune cell infiltration. The "estimate" software package was used to calculate the immune score and stromal score for each sample to quantify the relative enrichment of immune and stromal cells in each sample. Violin plots were applied to visualize the differences in enrichment between high and low-risk groups.

Predicting patient response to immunotherapy

We further explored the potential role of risk scores in the prediction of immunotherapy using the immunophenoscore (IPS). Based on relevant data from The Cancer Imaging Archive (TCIA) database (https://www.cancerimagingarchive.net), we evaluated the differences in four IPS scores between high and low-risk groups. The scoring scheme integrates the four major classes of genes that determine tumor immunogenicity (effector cells, immunosuppressive cells, MHC molecules, and immunomodulators) and the gene expression of these cell types (e.g., activated $CD4^+$ T cells, activated $CD8^+$ T cells, effector memory $CD4^+$ T cells, Tregs, MDSCs) to derive specific scores without bias using machine learning that is viewed as a new and reliable predictor of response to immunotherapy regimens (Givechian et al., 2018).

Tumor mutational burden (TMB) is broadly defined as the number of somatic mutations per megabase of interrogated genomic sequence. TMB reflects the total number of mutations carried by tumor cells. It is now generally accepted that TMB is positively correlated with the effect of immunotherapy and can be used as a potential molecular diagnostic marker for tumor immune checkpoint inhibitor therapy (Mayakonda et al., 2018). We obtained TMB information for the corresponding TCGA-LUAD cohort from the TCGA database. Spearman's method was used for correlation analysis.

Assessment of patients' sensitivity to chemotherapy

With the "pRRophetic" software package, we reliably predicted the response to chemotherapy in each LUAD sample. The package works by using gene expression and

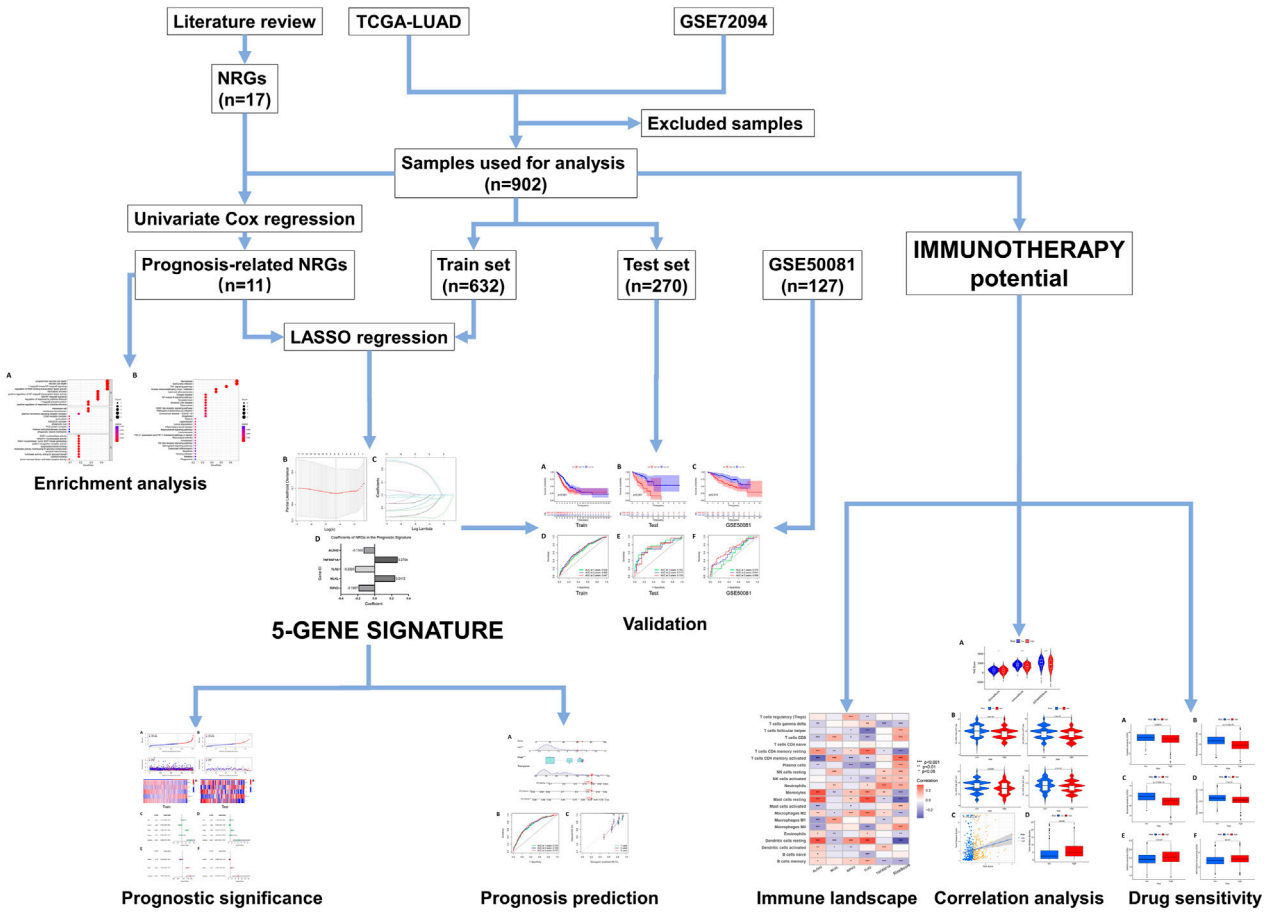

FIGURE 1
The framework and workflow of this study.

drug sensitivity data from a very large panel of cancer cell lines in the Genomics of Drug Sensitivity in Cancer (GDSC) database (www.cancerrxgene.org/) as training data for developing statistical models (Yang et al., 2013). These models were then applied to gene expression data from other tumor biopsies to predict the clinical drug response of other samples to different anticancer drugs, with the half maximal inhibitory concentration (IC50) value of the target drug as the predicted outcome variable. The robustness of the model has been extensively validated (Geeleher et al., 2014a). After that, we reflected the difference in chemotherapy sensitivity between high and low-risk groups by box-line plots.

Statistical methods

The study was statistically analyzed using R programming language (version 4.0.3). The Wilcoxon test was used to analyze continuous variables. Categorical variables were analyzed using Fisher's exact test or Chi-square test. Survival differences were analyzed using Kaplan-Meier curves and log-ranch tests. p-values < 0.05 were considered statistically significant.

Results

The design and workflow of this study are shown in Figure 1.

Identification of necroptosis-related genes in lung adenocarcinoma

We obtained 17 NRGs (RIPK1, RIPK3, MLKL, TLR2, TLR3, TLR4, TNFRSF1A, PGAM5, ZBP1, NR2C2, HMGB1, CXCL1, USP22, TRAF2, ALDH2, EZH2, NDRG2) from previous literature reviews. The positions of these genes on the chromosomes are shown in Figure 2A. Immunohistochemical (IHC) staining results provided expression levels of 13 (RIPK1,

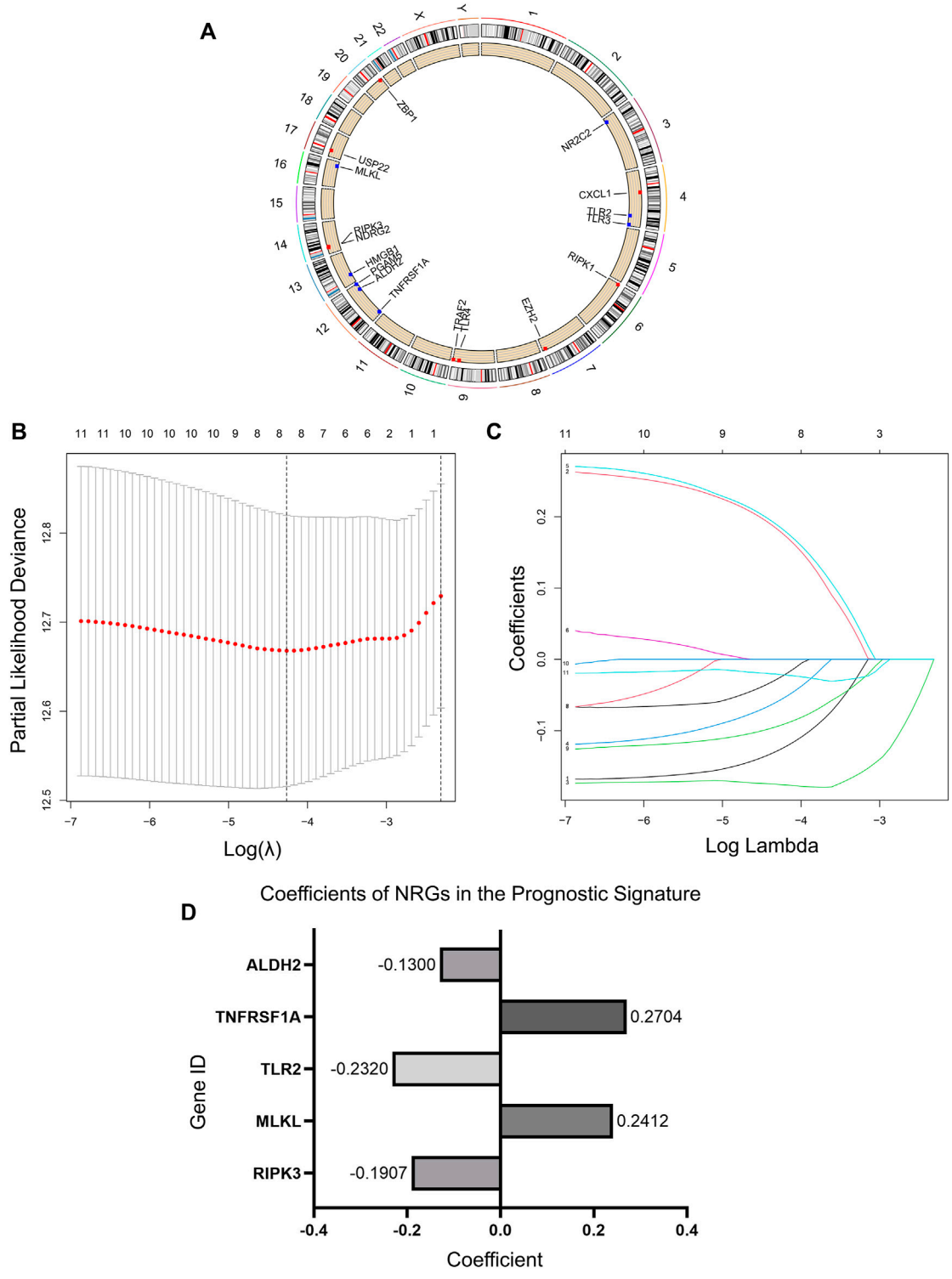

FIGURE 2
Necroptosis regulators in LUAD and an NRG signature. **(A)** Location of NRGs on chromosomes. **(B)** Ten-fold cross-validation for tuning parameter selection in the lasso regression. The vertical lines are plotted based on the optimal data according to the minimum criteria and 1-standard error criterion. The left vertical line represents the five genes finally identified. **(C)** LASSO coefficient profiles of 11 candidate genes and an optimal model derived from them. **(D)** 5 NRGs and their coefficients in the prognostic signature.

TABLE 1 Univariate Cox analysis of prognostic NRGs.

ID	HR	HR.95L	HR.95H	*p*-value
RIPK3	0.775939	0.655868	0.917991	0.003101
MLKL	1.22469	1.01345	1.479959	0.035881
TLR2	0.786491	0.707495	0.874307	8.70E-06
TLR4	0.838561	0.736965	0.954162	0.007539
TNFRSF1A	1.534057	1.218781	1.930888	0.000267
PGAM5	1.513917	1.248294	1.836062	2.52E-05
NR2C2	0.794317	0.646461	0.97599	0.028436
TRAF2	1.313365	1.08852	1.584655	0.004437
ALDH2	0.74703	0.654351	0.852836	1.59E-05
EZH2	1.198274	1.0576	1.35766	0.004527
NDRG2	0.790279	0.696952	0.896103	0.000242

TLR3, TLR4, TNFRSF1A, PGAM5, ZBP1, NR2C2, HMGB1, USP22, TRAF2, ALDH2, EZH2, NDRG2) of the 17 necroptotic proteins between LUAD and normal lung tissues (Supplementary Figure S1). For some reason, the remaining four genes could not be found in the HPA database with evidence of corresponding IHC staining.

By univariate Cox regression analysis of RNA transcriptome data, we identified 11 NRGs that were significantly associated with OS in LUAD patients. These genes and their HR, and *p*-values were listed in Table 1 and the clinical-pathological characteristics of 902 LUAD patients in TCGA + GSE72094 dataset were shown in Table 2.

Identification and validation of necroptosis-related gene prognostic signature

We randomized 902 patients included in the study into the Train and Test sets. Then LASSO regression analysis was performed in the Train set samples to construct a prognostic signature that included five NRGs (Figures 2B,C). These five genes and their correlation coefficients in the signature were shown in Figure 2D. Risk scores were calculated based on the expression profile data for all patients according to the formula provided by the model.

We divided each set into low-risk and high-risk groups bounded by the optimal cut-off values calculated by "CatPredi" package and then we plotted Kaplan-Meier survival curves and ROC curves separately for the Train set, Test set, and GSE50081 to verify the robustness of the model.

The K-M curves showed that the OS of the high-risk group is much lower than that of the low-risk group in both the Train and Test sets, with *p*-values of < 0.001 (Figures 3A,B). The AUC values for the Test set exceeded 0.7 in each of the first 3 years (Figures 3D,E). To further test the reliability of our model, we selected GSE50081 as external data for validation, and both results also showed that the label performed well in assessing prognosis (Figures 3C,F), with a survival curve of $p = 0.015$ and an AUC > 0.69 at year 3, demonstrating the good performance of the signature in assessing prognosis.

Risk score has independent prognostic significance

Figures 4A,B demonstrated the relationship between risk score, patient survival, and gene expression of necroptosis regulators in the Train set and Test set, respectively. The heat map showed that RIPK3, TLR2, and ALDH2 were lowly expressed in the high-risk group, which corresponds to their correlation coefficients in the predictive signature (Figure 2D).

We performed Cox analyses to test whether the 5-gene signature was an independent predictor of OS in patients with LUAD. Univariate Cox regression analysis (Figures 4C,D) showed a significant association between risk score and OS. [Train set: HR 2.089, 95% confidence interval (CI) 1.657–2.633, $p < 0.001$; Test set: HR 6.481, 95% CI 3.095–13.572, $p < 0.001$]. After adjusting for other confounding variables, the five-gene signature remained an independent indicator of OS in multivariate Cox regression studies (Figures 4E,F) (Train set: HR 1.883, 95% CI 1.464–2.421, $p < 0.001$; Test set: HR 5.725, 95% CI 2.527–12.973, $p < 0.001$).

Construction of a nomogram to quantitatively predict patient prognosis

To quantitatively predict the prognosis of LUAD patients, we developed a risk score-based nomogram (Figure 5A) that included tumor stages. The AUCs of curves at years 1, 2, and 3 were 0.724, 0.729, and 0.737, respectively (Figure 5B). Combined with the calibration curves of the nomogram shown in Figure 5C, the results show that the nomogram model has very good predictive performance for prognosis.

Gene Ontology analysis and Kyoto Encyclopedia of Genes and Genomes analysis

To explore the preliminary function of the 11 prognosis-related NRGs, we did GO functional analysis and KEGG pathway enrichment analysis using the "ClusterProfiler" R package (adjusted $p < 0.05$, $|\log FC| > 1$). GO analysis showed significant enrichment of genes in programmed necrotic cell death, necrotic cell death, I-kappaB kinase/NF-kappaB signaling, regulation of DNA-binding transcription factor activity, and

TABLE 2 The clinical characteristics of LUAD patients in the TCGA and GSE72094 datasets.

Clinical characteristics		Total	%
TCGA		504	100
Survival status	Alive	321	63.69
	Dead	183	36.31
Age	≥60 years old	358	71.03
	<60 years old	136	26.98
	Unknown	10	1.98
Gender	Male	234	46.43
	Female	270	53.57
Stage	I	270	53.57
	II	119	23.61
	III	81	16.07
	IV	26	5.16
	Unknown	8	1.59
T classification	T1	168	33.33
	T2	269	53.37
	T3	45	8.93
	T4	19	3.77
	Tx	3	0.60
N classification	N0	325	64.48
	N1	94	18.65
	N2	71	14.09
	N3	2	0.40
	Nx	12	2.38
M classification	M0	335	66.47
	M1	25	4.96
	Mx	144	28.57
Pharmaceutical therapy	YES	61	12.10
	NO	68	13.49
	Unknown	375	74.41
Radiation therapy	YES	61	12.10
	NO	71	14.09
	Unknown	372	73.81
Locoregional surgery	YES	9	1.78
	NO	96	19.05
	Unknown	399	79.17
Metastatic surgery	YES	20	3.97
	NO	78	15.48
	Unknown	406	80.55
GSE72094		398	100
Survival status	Alive	285	71.61
	Dead	113	28.39
Age	≥60 years old	340	85.43
	<60 years old	58	14.57
Gender	Male	176	44.22
	Female	222	55.78
Race	White	377	94.72
	Others	21	5.28
Stage	I	254	63.82
	II	67	16.83
	III	57	14.32
	IV	15	3.77
	Unknown	5	1.26

other functions (Figure 6A). In KEGG pathway analysis, we learned that these genes are mainly concentrated in Necroptosis, Salmonella infection, and TNF signaling pathway (Figure 6B).

Immune landscape and immunotherapy-related analysis

Figure 7 suggested that a variety of immune cells such as cytotoxic $CD8^+$ T cells, Natural killer T cells, regulatory T cells, and macrophages are highly correlated with the risk score as well as key genes in the process of necroptosis and may play an important role in this prognostic signature.

We then performed the ESTIMATE analysis (Figure 8A), and the immune score and ESTIMATE score were significantly lower in the high-risk group. Considering that patients in high and low-risk groups may respond differently to immunotherapy, we further investigated the response to ICI therapy represented by CTLA4/PD-1 inhibitors in both groups by ImmunoPhenoScore (IPS). Regardless of whether the CTLA4 and PD-1 status was positive or negative, patients in the low-risk group had higher IPS than those in the low-risk group, and the difference was statistically significant (Figure 8B).

Furthermore, we performed a TMB correlation analysis, Figures 8C,D, showing that the Tumor Mutation Burden differed significantly between the two groups of high and low risk according to the risk score. The risk score and TMB were positively correlated, $r = 0.3$.

High-risk groups are more sensitive to chemotherapy

Finally, we tested the sensitivity of patients in high and low-risk groups to familiar drugs based on a database of the GDSC. The R package "pRRophetic" (Geeleher et al., 2014a; Geeleher et al., 2014b) allows us to calculate IC50 for common chemotherapeutic agents in the cohort, including cisplatin, paclitaxel, and doxorubicin, rapamycin, etc. The lower the IC50 value, the higher the drug sensitivity. So, patients with LUAD in the high-risk group were significantly more sensitive to

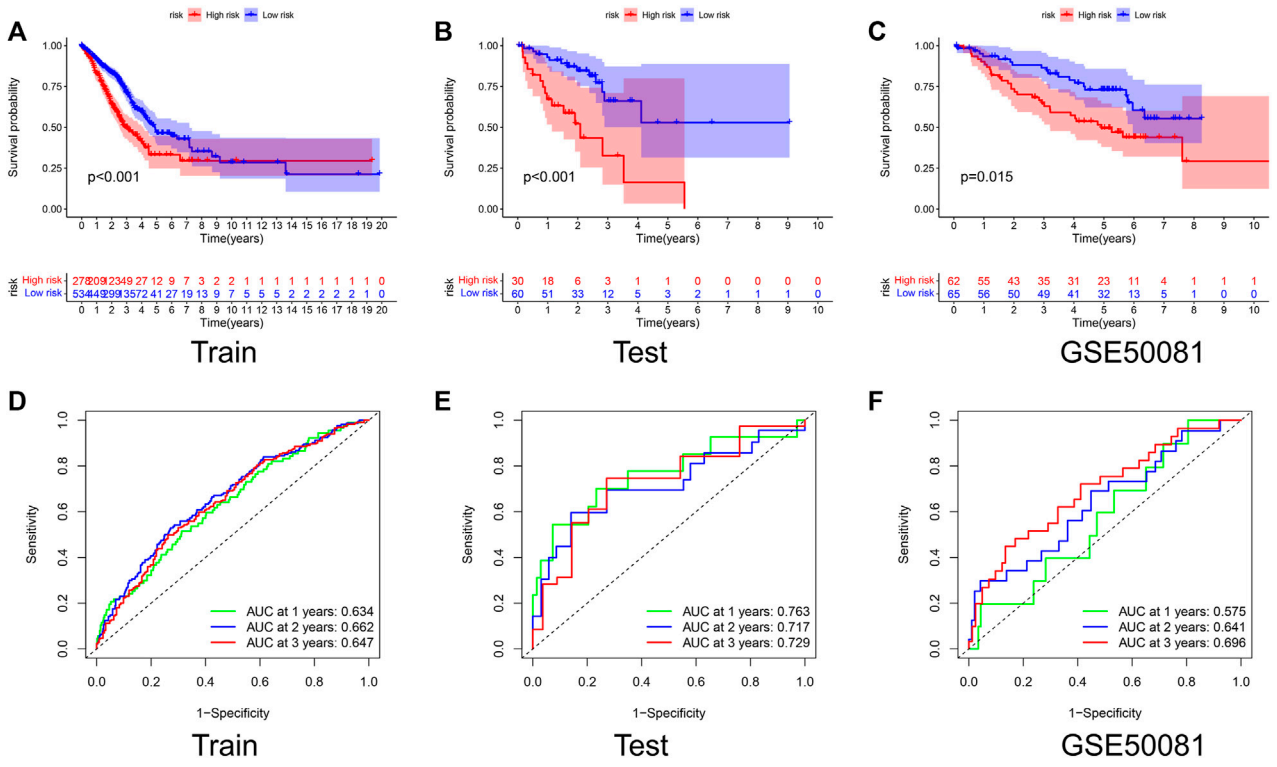

FIGURE 3
Validation of the prognostic signature. Kaplan–Meier curve presents differences in overall survival between the high-risk and low-risk groups in the Train set **(A)**, Test set **(B)**, and GSE50081 **(C)**. ROC curves of the NRG signature for predicting the 1/2/3-year survival in the Train set **(D)**, Test set **(E)**, and GSE50081 **(F)**. All results were statistically significant, demonstrating the good performance of the signature in assessing prognosis.

common chemotherapeutic agents such as cisplatin, paclitaxel, docetaxel, and doxorubicin (Figures 9A–D). Additionally, for the targeted drug of lung cancer, Gefitinib had a favorable response in the low-risk group (Figure 9E) and so did AKT inhibitor VIII (Figure 9F), suggesting that targeted therapy may provide benefit to these patients.

Discussion

Necroptosis, as a form of programmed cell death, is a regulated form of necrosis. It has biological changes like that of cell necrosis, such as a dramatic increase in intracellular peroxides, highly phosphorylated mitochondrial membranes, and cell swelling, but the mechanisms of their initiation are not the same. Necrosis is defined as a non-programmed form of cell death characterized by cellular rupture. This allows the leakage of biomolecules such as damage-associated molecular patterns (DAMP), which are recognized by immune cells and trigger an inflammatory response. In contrast, necroptosis is controlled by a unique signaling pathway, which requires RIPK3-dependent MLKL phosphorylation. This phosphorylation event causes MLKL to produce a pore complex at the plasma membrane, which leads to DAMP secretion, cell swelling, and membrane rupture.

In this study, we constructed a prognostic signature associated with NRGs and demonstrated its good and accurate prognostic prediction ability using a combination of internal validation (Test set) and external validation (GSE50081). Cox regression analysis showed that our risk score could be used as a strong predictor of prognosis for LUAD patients. Interestingly, the fact that smoking was not an independent prognostic factor for patients was also confirmed in our study. According to Jemal et al. (2018), an increasing proportion of patients diagnosed with lung cancer are non-smokers, especially among those diagnosed with LUAD, despite that smoking has long been recognized as one of the important risk factors for lung cancer (Gould et al., 2013).

A total of five NRGs were included in the prognostic prediction model, which were RIPK3, MLKL, TLR2, TNFRSF1A, and ALDH2. Several studies have been conducted to explore the function of these genes, especially the relationship between these genes and cancer. RIPK3 is thought to be a key molecular switch for the initiation of

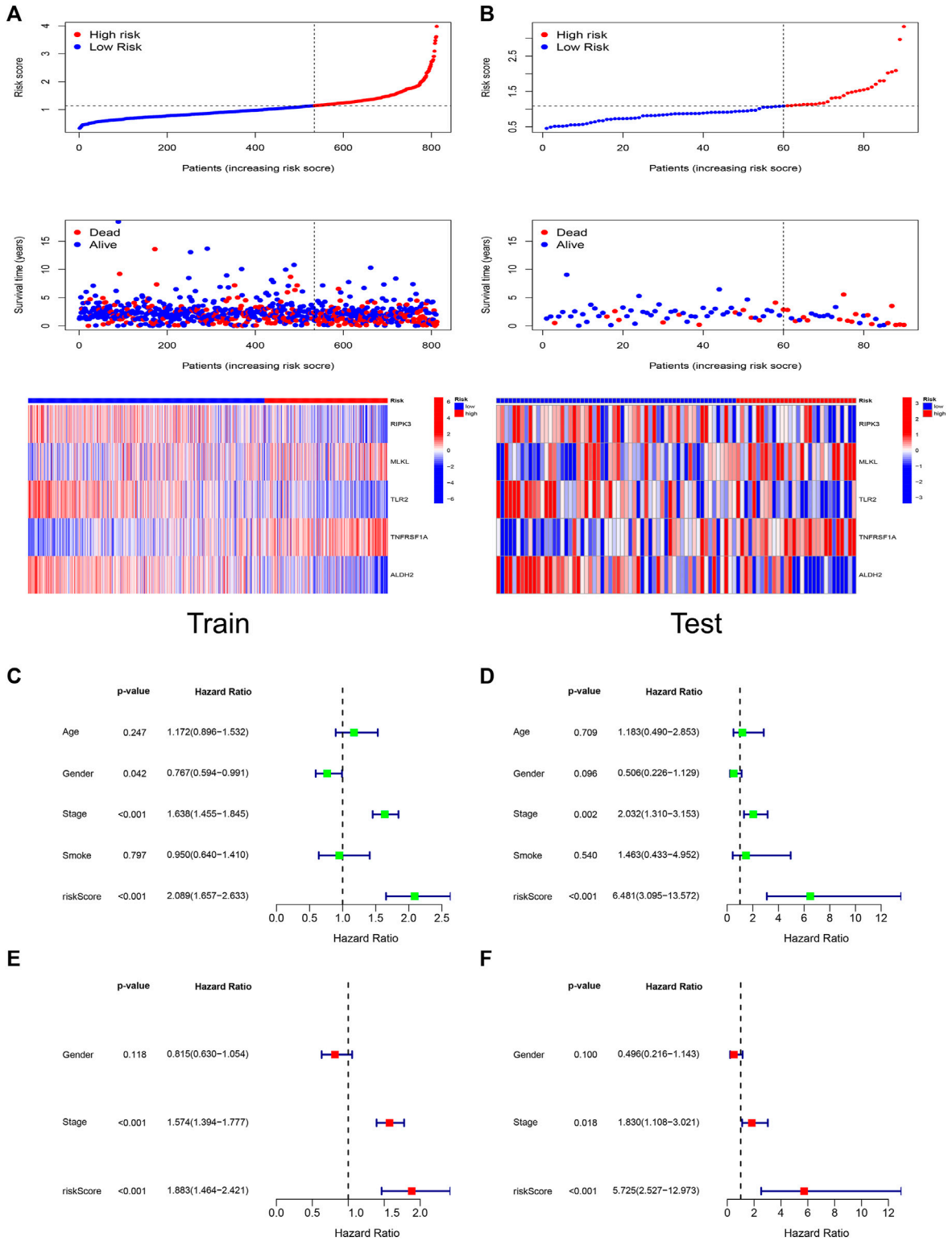

FIGURE 4
Risk score has independent prognostic significance. The trends of risk scores, the distribution of survival status, and the expression of the five genes included in the signature in Train set **(A)** and Test set **(B)**. The prognostic ability and clinical characteristics of the signature were analyzed by univariate Cox regression **(C)**, multivariate Cox regression **(E)** in Train set and validated by univariate Cox regression **(D)**, multivariate Cox regression **(F)** in Test set. The five-gene signature and stage were statistically significant in the Cox regression analysis.

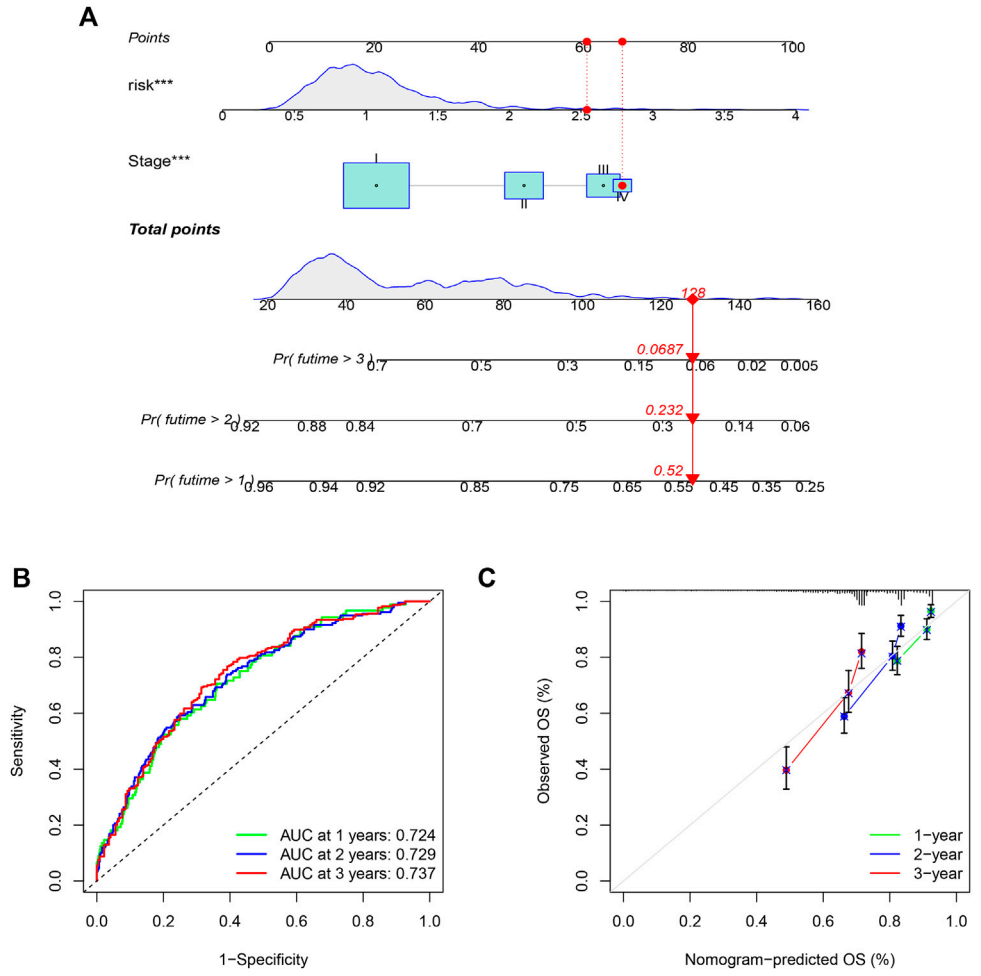

FIGURE 5
Nomogram was assembled by stage, and risk score for predicting the survival rate of LUAD patients **(A)**. ROC curves of the nomogram for predicting the 1/2/3-year survival **(B)**. 1/2/3-year nomogram calibration curves **(C)**. The results show that the nomogram model has very good predictive performance for prognosis (***$p < 0.001$).

necroptosis in cells. In the classical necroptotic pathway, deubiquitinated RIPK1 interacts with RIPl3 *via* exposure of the RIP homotypic interaction motif (RHIM) structural domain and conformational changes to phosphorylate and form amyloid signaling complex necrosomes together with FADD/caspase8 (Anderton et al., 2019). Then, MLKL is recruited and phosphorylated to mediate the execution of necroptosis. When RIPK1 is deficient, DNA-dependent activator of interferon regulatory factors (DAI), lipopolysaccharide, and chemical inducers can directly activate RIPK3 through a non-caspase-dependent mechanism, and activated RIPK3 phosphorylates MLKL to mediate necrosis signaling (Brault and Oberst, 2017). Multiple cancers suppress necroptosis through epigenetic silencing of RIPK3, which is consistent with our obtained finding that the mRNA expression of RIPK3 in the model is negatively correlated with the patient's risk score.

Although activation of MLKL is the executor of the necroptotic process, the expression of MLKL varies much across cancers, which is related to its complex cytological function. Recent studies have revealed that MLKL has an important role in a variety of non-necroptotic processes such as axonal repair, receptor internalization, extracellular vesicle formation, ligand-receptor degradation, and even in the inhibition of necroptosis (Martens et al., 2021). Unfortunately, the exact role of MLKL in cancer progression and metastasis is still unclear.

TLR2 induces TNF expression mainly through the Myeloid differentiation factor 88 (MyD88)-dependent pathway, which can indirectly trigger apoptosis or triggers the classical pathway

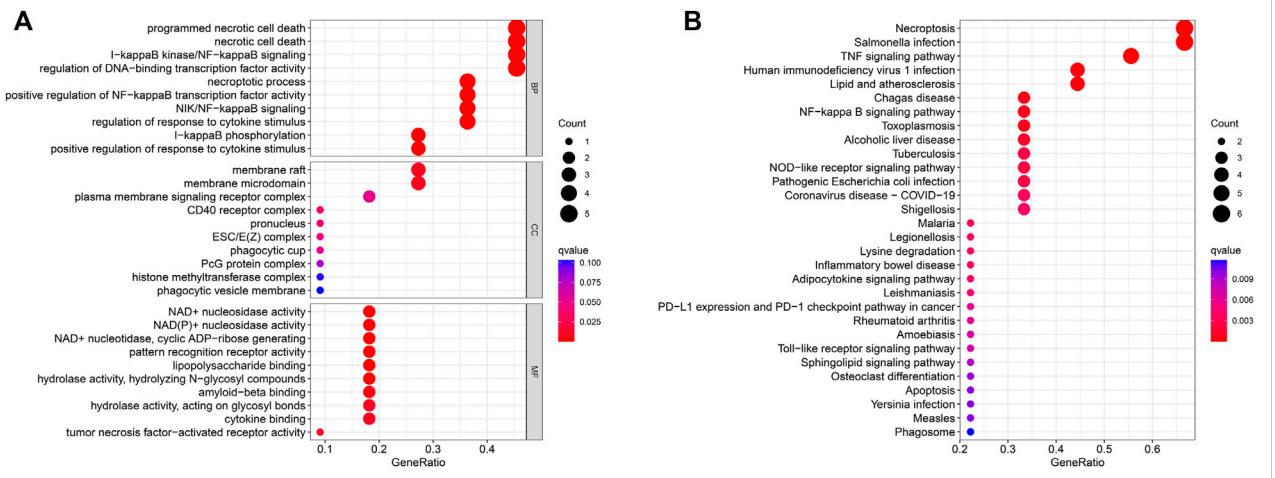

FIGURE 6
GO enrichment analysis **(A)** and KEGG enrichment analysis **(B)** of the 11 prognostic NRGs. The size of the circles in the graph indicates the number of genes enriched in the mechanism or pathway, and the color of the circles indicates the *q*-value.

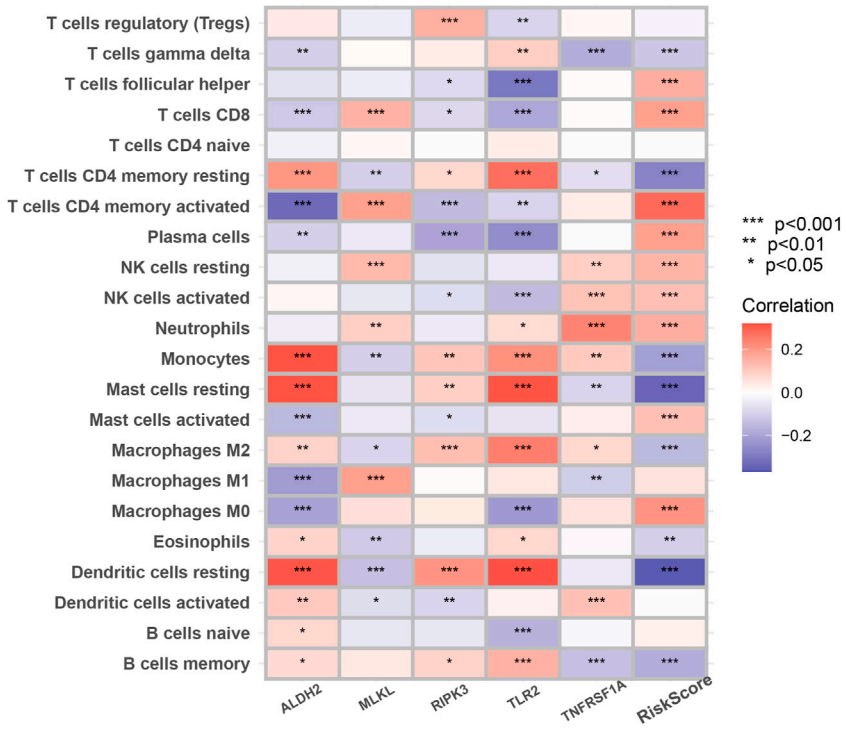

FIGURE 7
The correlation between infiltrating immune cells and NRGs in the signature. The change in the color of blocks implies the strength of the correlation (*$p < 0.05$; **$p < 0.01$; ***$p < 0.001$).

of necroptosis through RIP1-RIP3 activation (Kaiser et al., 2013). Interestingly, TNF is generally recognized to inhibit or kill tumor cells through multiple links, TNF receptors (TNFR), especially TNFR1, have been found to be upregulated in a variety of tumors, such as ovarian cancer (Le Page et al., 2006), renal clear cell carcinoma (Diegmann et al., 2006) and acute myeloid leukemia

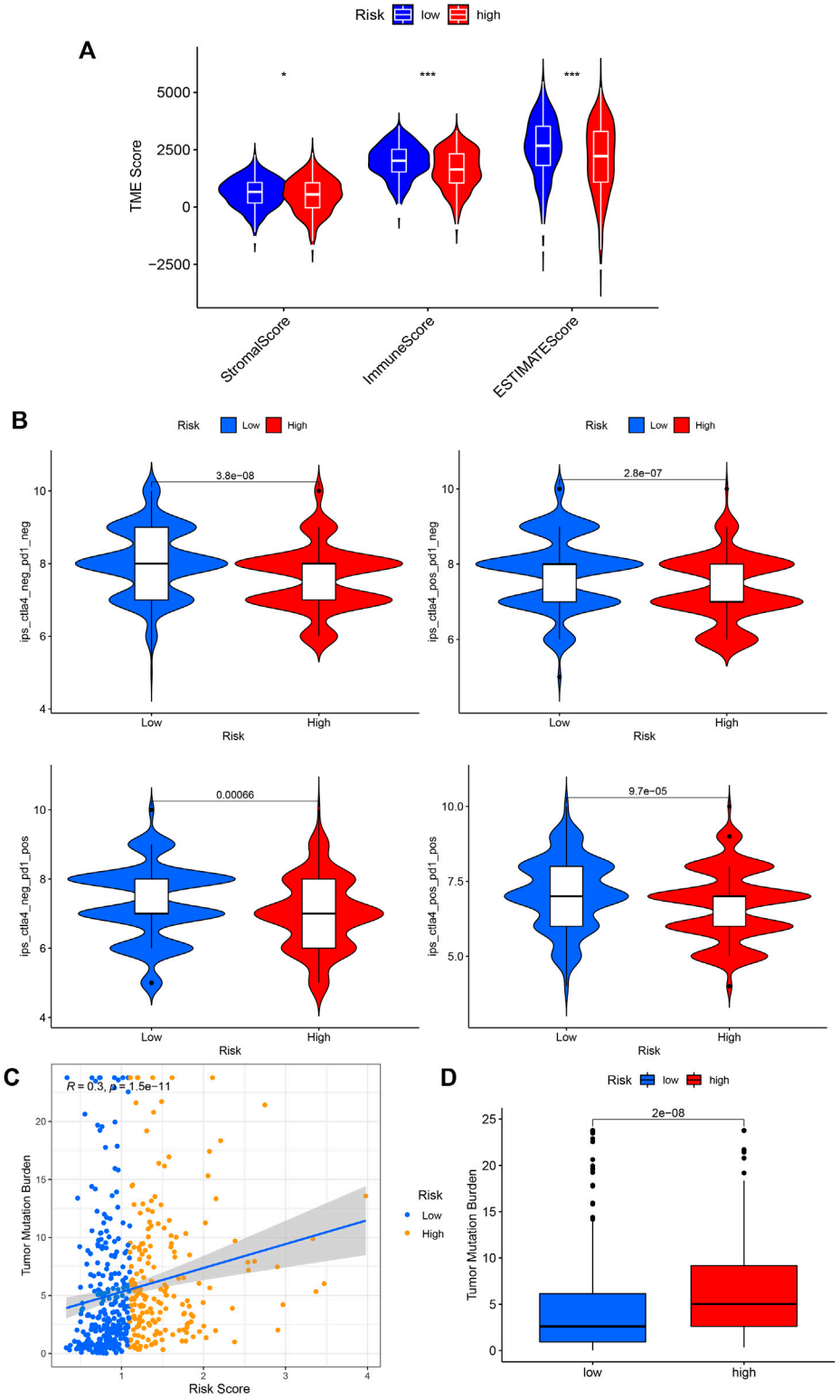

FIGURE 8
Application of risk score in predicting the immunotherapeutic effect. **(A)** Differential analysis of the tumor microenvironment for relative enrichment of immune cells and stromal cells. The low-risk group had a higher degree of immune cell infiltration and lower tumor purity. **(B)** The immunophenoscore (IPS) distribution was compared between high and low-risk groups. **(C,D)** Tumor Mutation Burden correlation analysis showed a positive correlation between risk score and TMB. (*$p < 0.05$; **$p < 0.01$; ***$p < 0.001$; pos means positive; neg means negative).

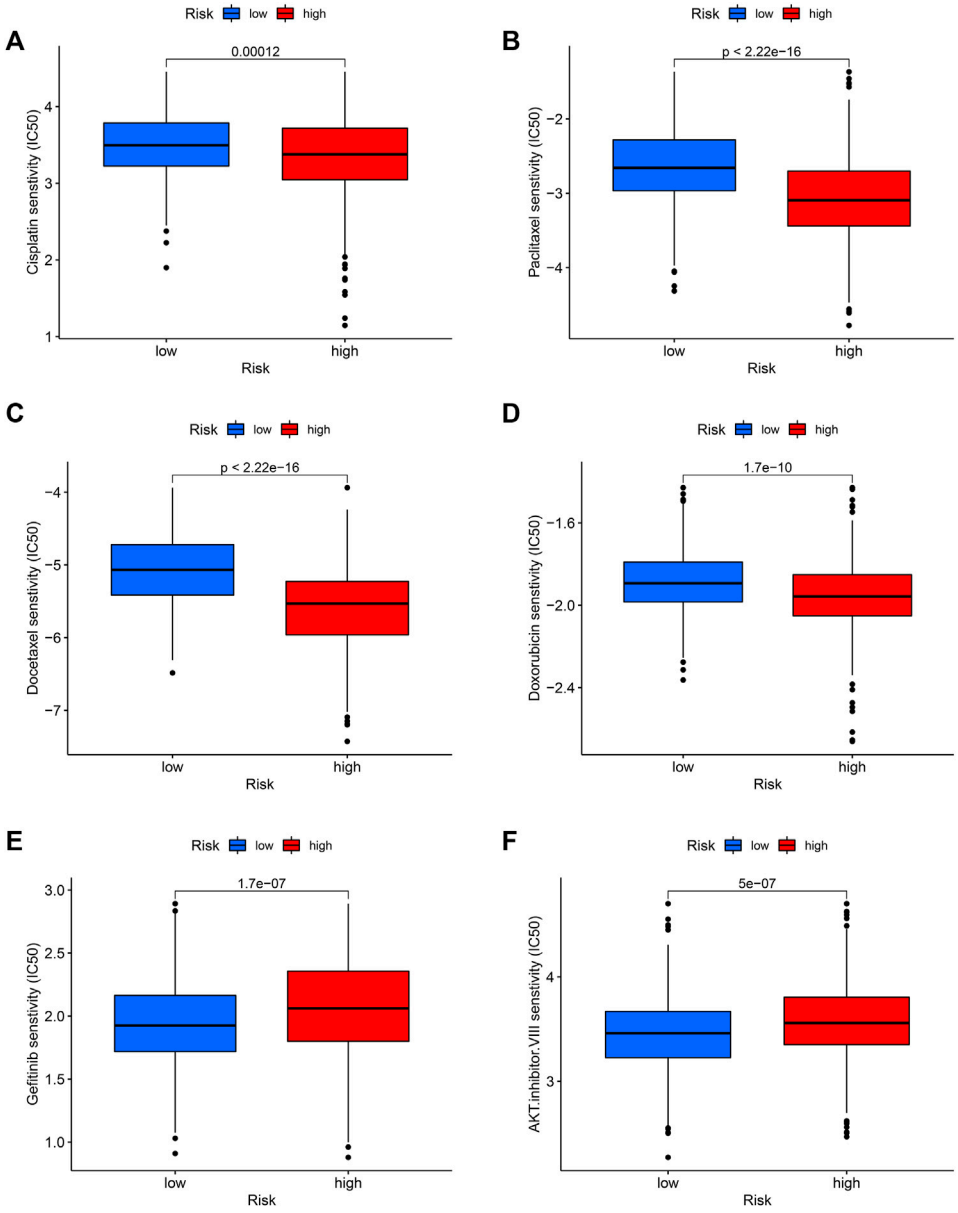

FIGURE 9
Potential drug sensitivity of common drugs in high and low-risk groups. The high-risk group had a higher sensitivity to chemotherapeutic agents such as cisplatin **(A)**, paclitaxel **(B)**, docetaxel **(C)**, and doxorubicin **(D)** compared to the low-risk group. However, the low-risk group was more sensitive to targeted therapeutic agents gefitinib **(E)** and AKT inhibitor VIII **(F)**.

(Brouwer et al., 2001). This may be related to the fact that TNFR1, in addition to being involved in mediating apoptosis and necroptosis, can also mediate cell activation signals and proliferation signals that drive the expression of pro-survival genes (Dondelinger et al., 2016). TNFRSF1A, the gene encoding the TNFR1 protein, was similarly found to be highly expressed in the high-risk group of LUAD patients in our present study. ALDH2 belongs to the acetaldehyde dehydrogenase family, and its reduction not only induces proliferation and stem cell properties of LUAD cells but also may induce DNA damage, which will promote tumor recurrence, drug resistance, and metastasis, leading to poor prognosis of LUAD (Li et al., 2019).

Many studies have shown that cancer cells undergoing necroptosis mediate immune responses by promoting interactions between dying cancer cells and immune cells through the release of damage-associated molecular patterns (DAMPs), chemokines, cytokines, and/or cancer antigens (Krieser and White, 2002; Park et al., 2009; McCracken et al.,

2015; Sprooten et al., 2020). In terms of tumor suppression, DAMPs can eliminate cancer cells by stimulating the initial sensors of infection or damage (e.g., pattern recognition receptors on myeloid cells) and activating adaptive immune cells such as antigen-specific cytotoxic $CD8^+$ T cells (Yatim et al., 2015). A significant positive correlation of MLKL with cytotoxic $CD8^+$ T cells was also demonstrated in our study. In addition to this, RIPK3 can induce the production of cytokines to activate natural killer T cells, which also help to kill cancer cells (Sprooten et al., 2020). However, regarding tumor promotion, necroptotic cancer cells can also attract myeloid or lymphocytes, triggering tumor-associated immunosuppression (Cohen et al., 2010; Vandenberk et al., 2016; Wauters et al., 2021). For example, in Figure 7, RIPK3 exhibited a significant positive correlation with regulatory T cell and Macrophages M2. Besides, cytokines released from necrotic apoptotic cancer cells can promote angiogenesis, reactive oxygen species release, and genomic instability, thus promoting tumor progression (Singh et al., 2017).

Furthermore, in addition to these biological insights, our study plays an important role in guiding the use of immunotherapy in patients with LUAD. The background features of the immunobiology of necroptosis, combined with a more complex tumor immune landscape, can produce highly unpredictable outcomes for immunotherapy of tumors. ICIs do greatly improve the prognosis of cancer patients, but a minority still does not respond adequately to these immunotherapies, as treatment efficacy is largely influenced by immune cell abundance, tumor mutation burden, and other biomolecules (He et al., 2015; Sharma et al., 2017; Herbst et al., 2018). Combined results, our study has important implications for the use of single ICIs as well as combined ICIs in patients with LUAD. Therefore, it will be interesting to systematically decipher whether ICI-based immunotherapy can synergize with necroptosis and produce unknown benefits. More importantly, we predicted the sensitivity of chemotherapeutic agents, which helps physicians choose the right combination of chemotherapy and immunotherapy to improve the survival rate of LUAD patients. This is because the efficacy of ICIs can be greatly improved when co-administered with cytotoxic therapy (Judd and Borghaei, 2020).

Of course, our study has many drawbacks. Firstly, necroptosis is a new and rapidly developing field, and more and more NRGs will be discovered and fully studied over time. Our findings will be fleshed out then. Secondly, all data samples in this study were obtained from public open-source databases. Due to the relatively small number of LUAD patients in public databases and the duplication of transcriptome data in different databases, the sample size covered in the randomized grouping of this study was relatively insufficient, resulting in the low significance of some results. On the other hand, some important clinical details were not available in the open-source dataset, including chemotherapy regimens, drug information, and tumor TNM grading. And the lack of these data limits more in-depth analysis of the dataset. In addition, some of the prognostic NRG-associated immunohistochemical slides in the HPA database were not available, which also left us with a regret for our study. Finally, the role of some NRGs in non-small cell lung cancer is unclear and still needs to be revealed by further *in vivo* or *in vitro* experiments.

In conclusion, we constructed a robust NRG-related prognostic signature that could be used to predict the prognosis of LUAD patients. We also analyzed the sensitivity of different immunotherapy and chemotherapy regimens, which could provide a reference to improve patient prognosis and achieve personalized medicine. Meanwhile, we believe that this study provides insight into the potential role of necroptosis in lung adenocarcinoma.

Data availability statement

The original contributions presented in the study are included in the article/Supplementary Material, further inquiries can be directed to the corresponding authors.

Author contributions

YS, JZ, and LF made contributions to the study's conception and design. YS and JZ collected the clinical information and gene expression data, analysed the data, and wrote the manuscript. YS, JZ, LF, and WL revised the manuscript. All authors contributed to the article and approved the submitted manuscript.

Funding

This work was supported by the National Natural Science Foundation of China (#82003284 to LF) and the Scientific Research Foundation of The First Hospital of Jilin University (#JDYY11202015 to LF).

Acknowledgments

The TCGA and GEO database is gratefully acknowledged for the availability of the raw research data.

Conflict of interest

The authors declare that the research was conducted in the absence of any commercial or financial relationships that could be construed as a potential conflict of interest.

Publisher's note

Supplementary material

The Supplementary Material for this article can be found online at: https://www.frontiersin.org/articles/10.3389/fgene.2022.1027741/full#supplementary-material

SUPPLEMENTARY FIGURE S1
Immunohistochemical (IHC) staining results of expression levels of the 13 necroptotic proteins (RIPK1, TLR3, TLR4, TNFRSF1A, PGAM5, ZBP1, NR2C2, HMGB1, USP22, TRAF2, ALDH2, EZH2, NDRG2) between LUAD and normal lung tissues.

References

Anderton, H., Bandala-Sanchez, E., Simpson, D. S., Rickard, J. A., Ng, A. P., Di Rago, L., et al. (2019). RIPK1 prevents TRADD-driven, but TNFR1 independent, apoptosis during development. *Cell Death Differ.* 26 (5), 877–889. doi:10.1038/s41418-018-0166-8

Bonavida, B., and Chouaib, S. (2017). Resistance to anticancer immunity in cancer patients: Potential strategies to reverse resistance. *Ann. Oncol.* 28 (3), 457–467. doi:10.1093/annonc/mdw615

Brault, M., and Oberst, A. (2017). Controlled detonation: Evolution of necroptosis in pathogen defense. *Immunol. Cell Biol.* 95 (2), 131–136. doi:10.1038/icb.2016.117

Brouwer, R. E., Hoefnagel, J., Borger van Der Burg, B., Jedema, I., Zwinderman, K. H., Starrenburg, I. C., et al. (2001). Expression of co-stimulatory and adhesion molecules and chemokine or apoptosis receptors on acute myeloid leukaemia: High CD40 and CD11a expression correlates with poor prognosis. *Br. J. Haematol.* 115 (2), 298–308. doi:10.1046/j.1365-2141.2001.03085.x

Chen, Z., Fillmore, C. M., Hammerman, P. S., Kim, C. F., and Wong, K. K. (2014). Non-small-cell lung cancers: A heterogeneous set of diseases. *Nat. Rev. Cancer* 14 (8), 535–546. doi:10.1038/nrc3775

Cheng, M., Lin, N., Dong, D., Ma, J., Su, J., and Sun, L. (2021). PGAM5: A crucial role in mitochondrial dynamics and programmed cell death. *Eur. J. Cell Biol.* 100 (1), 151144. doi:10.1016/j.ejcb.2020.151144

Choi, M. E., Price, D. R., Ryter, S. W., and Choi, A. M. K. (2019). Necroptosis: A crucial pathogenic mediator of human disease. *JCI Insight* 4 (15), 128834. doi:10.1172/jci.insight.128834

Cohen, I., Rider, P., Carmi, Y., Braiman, A., Dotan, S., White, M. R., et al. (2010). Differential release of chromatin-bound IL-1alpha discriminates between necrotic and apoptotic cell death by the ability to induce sterile inflammation. *Proc. Natl. Acad. Sci. U. S. A.* 107 (6), 2574–2579. doi:10.1073/pnas.0915018107

Degterev, A., Huang, Z., Boyce, M., Li, Y., Jagtap, P., Mizushima, N., et al. (2005). Chemical inhibitor of nonapoptotic cell death with therapeutic potential for ischemic brain injury. *Nat. Chem. Biol.* 1 (2), 112–119. doi:10.1038/nchembio711

Devarakonda, S., Morgensztern, D., and Govindan, R. (2015). Genomic alterations in lung adenocarcinoma. *Lancet. Oncol.* 16 (7), e342–e351. doi:10.1016/S1470-2045(15)00077-7

Diegmann, J., Tomiuk, S., Sanjmyatav, J., Junker, K., Hindermann, W., and Von Eggeling, F. (2006). Comparative transcriptional and functional profiling of clear cell and papillary renal cell carcinoma. *Int. J. Mol. Med.* 18 (3), 395–403. doi:10.3892/ijmm.18.3.395

Dondelinger, Y., Darding, M., Bertrand, M. J., and Walczak, H. (2016). Poly-ubiquitination in TNFR1-mediated necroptosis. *Cell. Mol. Life Sci.* 73 (11-12), 2165–2176. doi:10.1007/s00018-016-2191-4

Geeleher, P., Cox, N., and Huang, R. S. (2014). pRRophetic: an R package for prediction of clinical chemotherapeutic response from tumor gene expression levels. *PLoS One* 9 (9), e107468. doi:10.1371/journal.pone.0107468

Geeleher, P., Cox, N. J., and Huang, R. S. (2014). Clinical drug response can be predicted using baseline gene expression levels and *in vitro* drug sensitivity in cell lines. *Genome Biol.* 15 (3), R47. doi:10.1186/gb-2014-15-3-r47

Givechian, K. B., Wnuk, K., Garner, C., Benz, S., Garban, H., Rabizadeh, S., et al. (2018). Identification of an immune gene expression signature associated with favorable clinical features in Treg-enriched patient tumor samples. *NPJ Genom. Med.* 3, 14. doi:10.1038/s41525-018-0054-7

Gong, Y., Fan, Z., Luo, G., Yang, C., Huang, Q., Fan, K., et al. (2019). The role of necroptosis in cancer biology and therapy. *Mol. Cancer* 18 (1), 100. doi:10.1186/s12943-019-1029-8

Gould, M. K., Donington, J., Lynch, W. R., Mazzone, P. J., Midthun, D. E., Naidich, D. P., et al. (2013). Evaluation of individuals with pulmonary nodules: When is it lung cancer? Diagnosis and management of lung cancer, 3rd ed: American college of chest physicians evidence-based clinical practice guidelines. *Chest* 143 (5), e93S–e120S. doi:10.1378/chest.12-2351

Hänggi, K., Vasilikos, L., Valls, A. F., Yerbes, R., Knop, J., Spilgies, L. M., et al. (2017). RIPK1/RIPK3 promotes vascular permeability to allow tumor cell extravasation independent of its necroptotic function. *Cell Death Dis.* 8 (2), e2588. doi:10.1038/cddis.2017.20

He, J., Hu, Y., Hu, M., and Li, B. (2015). Development of PD-1/PD-L1 pathway in tumor immune microenvironment and treatment for non-small cell lung cancer. *Sci. Rep.* 5, 13110. doi:10.1038/srep13110

Herbst, R. S., Morgensztern, D., and Boshoff, C. (2018). The biology and management of non-small cell lung cancer. *Nature* 553 (7689), 446–454. doi:10.1038/nature25183

Jemal, A., Miller, K. D., Ma, J., Siegel, R. L., Fedewa, S. A., Islami, F., et al. (2018). Higher lung cancer incidence in young women than young men in the United States. *N. Engl. J. Med.* 378 (21), 1999–2009. doi:10.1056/NEJMoa1715907

Judd, J., and Borghaei, H. (2020). Combining immunotherapy and chemotherapy for non-small cell lung cancer. *Thorac. Surg. Clin.* 30 (2), 199–206. doi:10.1016/j.thorsurg.2020.01.006

Kaiser, W. J., Sridharan, H., Huang, C., Mandal, P., Upton, J. W., Gough, P. J., et al. (2013). Toll-like receptor 3-mediated necrosis via TRIF, RIP3, and MLKL. *J. Biol. Chem.* 288 (43), 31268–31279. doi:10.1074/jbc.M113.462341

Khoury, M. K., Gupta, K., Franco, S. R., and Liu, B. (2020). Necroptosis in the pathophysiology of disease. *Am. J. Pathol.* 190 (2), 272–285. doi:10.1016/j.ajpath.2019.10.012

Krieser, R. J., and White, K. (2002). Engulfment mechanism of apoptotic cells. *Curr. Opin. Cell Biol.* 14 (6), 734–738. doi:10.1016/s0955-0674(02)00390-3

Le Page, C., Ouellet, V., Madore, J., Ren, F., Hudson, T. J., Tonin, P. N., et al. (2006). Gene expression profiling of primary cultures of ovarian epithelial cells identifies novel molecular classifiers of ovarian cancer. *Br. J. Cancer* 94 (3), 436–445. doi:10.1038/sj.bjc.6602933

Li, K., Guo, W., Li, Z., Wang, Y., Sun, B., Xu, D., et al. (2019). ALDH2 repression promotes lung tumor progression via accumulated acetaldehyde and DNA damage. *Neoplasia* 21 (6), 602–614. doi:10.1016/j.neo.2019.03.008

Liu, X., Zhou, M., Mei, L., Ruan, J., Hu, Q., Peng, J., et al. (2016). Key roles of necroptotic factors in promoting tumor growth. *Oncotarget* 7 (16), 22219–22233. doi:10.18632/oncotarget.7924

Lou, X., Zhu, H., Ning, L., Li, C., Li, S., Du, H., et al. (2019). EZH2 regulates intestinal inflammation and necroptosis through the JNK signaling pathway in intestinal epithelial cells. *Dig. Dis. Sci.* 64 (12), 3518–3527. doi:10.1007/s10620-019-05705-4

Malireddi, R. K. S., Kesavardhana, S., and Kanneganti, T. D. (2019). ZBP1 and TAK1: Master regulators of NLRP3 inflammasome/pyroptosis, apoptosis, and necroptosis (PAN-optosis). *Front. Cell. Infect. Microbiol.* 9, 406. doi:10.3389/fcimb.2019.00406

Martens, S., Bridelance, J., Roelandt, R., Vandenabeele, P., and Takahashi, N. (2021). MLKL in cancer: More than a necroptosis regulator. *Cell Death Differ.* 28 (6), 1757–1772. doi:10.1038/s41418-021-00785-0

Matter, M. S., Chijioke, O., Savic, S., and Bubendorf, L. (2020). Narrative review of molecular pathways of kinase fusions and diagnostic approaches for their detection in non-small cell lung carcinomas. *Transl. Lung Cancer Res.* 9 (6), 2645–2655. doi:10.21037/tlcr-20-676

Mayakonda, A., Lin, D. C., Assenov, Y., Plass, C., and Koeffler, H. P. (2018). Maftools: Efficient and comprehensive analysis of somatic variants in cancer. *Genome Res.* 28 (11), 1747–1756. doi:10.1101/gr.239244.118

McCracken, M. N., Cha, A. C., and Weissman, I. L. (2015). Molecular pathways: Activating T cells after cancer cell phagocytosis from blockade of CD47 "don't eat me" signals. *Clin. Cancer Res.* 21 (16), 3597–3601. doi:10.1158/1078-0432.CCR-14-2520

Park, S., Hatanpaa, K. J., Xie, Y., Mickey, B. E., Madden, C. J., Raisanen, J. M., et al. (2009). The receptor interacting protein 1 inhibits p53 induction through NF-kappaB activation and confers a worse prognosis in glioblastoma. *Cancer Res.* 69 (7), 2809–2816. doi:10.1158/0008-5472.CAN-08-4079

Petersen, S. L., Chen, T. T., Lawrence, D. A., Marsters, S. A., Gonzalvez, F., and Ashkenazi, A. (2015). TRAF2 is a biologically important necroptosis suppressor. *Cell Death Differ.* 22 (11), 1846–1857. doi:10.1038/cdd.2015.35

Philipp, S., Sosna, J., and Adam, D. (2016). Cancer and necroptosis: Friend or foe? *Cell. Mol. Life Sci.* 73 (11-12), 2183–2193. doi:10.1007/s00018-016-2193-2

Raposo, T. P., Beirão, B. C., Pang, L. Y., Queiroga, F. L., and Argyle, D. J. (2015). Inflammation and cancer: Till death tears them apart. *Vet. J.* 205 (2), 161–174. doi:10.1016/j.tvjl.2015.04.015

Roedig, J., Kowald, L., Juretschke, T., Karlowitz, R., Ahangarian Abhari, B., Roedig, H., et al. (2021). USP22 controls necroptosis by regulating receptor-interacting protein kinase 3 ubiquitination. *EMBO Rep.* 22 (2), e50163. doi:10.15252/embr.202050163

Rosenberg, S. A. (2014). Decade in review-cancer immunotherapy: Entering the mainstream of cancer treatment. *Nat. Rev. Clin. Oncol.* 11 (11), 630–632. doi:10.1038/nrclinonc.2014.174

Santarpia, M., Aguilar, A., Chaib, I., Cardona, A. F., Fancelli, S., Laguia, F., et al. (2020). Non-small-cell lung cancer signaling pathways, metabolism, and PD-1/PD-L1 antibodies. *Cancers (Basel)* 12 (6), E1475. doi:10.3390/cancers12061475

Sharma, P., Hu-Lieskovan, S., Wargo, J. A., and Ribas, A. (2017). Primary, adaptive, and acquired resistance to cancer immunotherapy. *Cell* 168 (4), 707–723. doi:10.1016/j.cell.2017.01.017

Singh, R., Mishra, M. K., and Aggarwal, H. (2017). Inflammation, immunity, and cancer. *Mediat. Inflamm.* 2017, 6027305. doi:10.1155/2017/6027305

Sprooten, J., De Wijngaert, P., Vanmeerbeerk, I., Martin, S., Vangheluwe, P., Schlenner, S., et al. (2020). Necroptosis in immuno-oncology and cancer immunotherapy. *Cells* 9 (8), E1823. doi:10.3390/cells9081823

Sung, H., Ferlay, J., Siegel, R. L., Laversanne, M., Soerjomataram, I., Jemal, A., et al. (2021). Global cancer statistics 2020: GLOBOCAN estimates of incidence and mortality worldwide for 36 cancers in 185 countries. *Ca. Cancer J. Clin.* 71 (3), 209–249. doi:10.3322/caac.21660

Tang, R., Xu, J., Zhang, B., Liu, J., Liang, C., Hua, J., et al. (2020). Ferroptosis, necroptosis, and pyroptosis in anticancer immunity. *J. Hematol. Oncol.* 13 (1), 110. doi:10.1186/s13045-020-00946-7

Vandenberk, L., Garg, A. D., Verschuere, T., Koks, C., Belmans, J., Beullens, M., et al. (2016). Irradiation of necrotic cancer cells, employed for pulsing dendritic cells (DCs), potentiates DC vaccine-induced antitumor immunity against high-grade glioma. *Oncoimmunology* 5 (2), e1083669. doi:10.1080/2162402X.2015.1083669

Wauters, E., Van Mol, P., Garg, A. D., Jansen, S., Van Herck, Y., Vanderbeke, L., et al. (2021). Discriminating mild from critical COVID-19 by innate and adaptive immune single-cell profiling of bronchoalveolar lavages. *Cell Res.* 31 (3), 272–290. doi:10.1038/s41422-020-00455-9

Wen, S., Li, X., Ling, Y., Chen, S., Deng, Q., Yang, L., et al. (2020). HMGB1-associated necroptosis and Kupffer cells M1 polarization underlies remote liver injury induced by intestinal ischemia/reperfusion in rats. *Faseb J.* 34 (3), 4384–4402. doi:10.1096/fj.201900817R

Xia, X., Lei, L., Wang, S., Hu, J., and Zhang, G. (2020). Necroptosis and its role in infectious diseases. *Apoptosis* 25 (3-4), 169–178. doi:10.1007/s10495-019-01589-x

Yang, W., Soares, J., Greninger, P., Edelman, E. J., Lightfoot, H., Forbes, S., et al. (2013). Genomics of drug sensitivity in cancer (GDSC): A resource for therapeutic biomarker discovery in cancer cells. *Nucleic Acids Res.* 41, D955–D961. doi:10.1093/nar/gks1111

Yatim, N., Jusforgues-Saklani, H., Orozco, S., Schulz, O., Barreira da Silva, R., Reis e Sousa, C., et al. (2015). RIPK1 and NF-κB signaling in dying cells determines cross-priming of CD8$^+$ T cells. *Science* 350 (6258), 328–334. doi:10.1126/science.aad0395

Zhu, J., Yang, L. K., Wang, Q. H., Lin, W., Feng, Y., Xu, Y. P., et al. (2020). NDRG2 attenuates ischemia-induced astrocyte necroptosis via the repression of RIPK1. *Mol. Med. Rep.* 22 (4), 3103–3110. doi:10.3892/mmr.2020.11421

frontiers | Frontiers in Genetics

TYPE Original Research
PUBLISHED 09 February 2023
DOI 10.3389/fgene.2023.1100560

OPEN ACCESS

EDITED BY
Guojun Li,
University of Texas MD Anderson Cancer Center, United States

REVIEWED BY
Jian Gu,
University of Texas MD Anderson Cancer Center, United States
Peng Sun,
The First Affiliated Hospital of Soochow University, China
Kristina Dahlstrom,
Baylor College of Medicine, United States

*CORRESPONDENCE
Yipeng Song,
Syp1972@sina.com

†These authors have contributed equally to this work and share first authorship

SPECIALTY SECTION
This article was submitted to Cancer Genetics and Oncogenomics, a section of the journal Frontiers in Genetics

RECEIVED 16 November 2022
ACCEPTED 31 January 2023
PUBLISHED 09 February 2023

CITATION
Zhu X, Liu X, Qiu X, Niu Z, Dong W and Song Y (2023), Prognostic roles of a novel basement membranes-related gene signature in lung adenocarcinoma. *Front. Genet.* 14:1100560. doi: 10.3389/fgene.2023.1100560

Prognostic roles of a novel basement membranes-related gene signature in lung adenocarcinoma

Xingzhuang Zhu[1,2†], Xiaoyan Liu[2†], Xiaowen Qiu[3], Zihao Niu[4], Wei Dong[2] and Yipeng Song[2*]

[1]Department of Oncology, Qingdao University, Qingdao, China, [2]Department of Radiation Oncology, Yantai Yuhuangding Hospital, Affiliated Hospital of Qingdao University, Yantai, China, [3]Department of Oncology, Binzhou Medical University, Yantai, China, [4]Ministry of Education Key Laboratory of Otolaryngology Head and Neck Surgery, Department of Otolaryngology Head and Neck Surgery, Beijing Tongren Hospital, Capital Medical University, Beijing, China

Background: The basement membranes (BMs) are involved in tumor progression, while few comprehensive analyses to date are performed on the role of BM-related gene signatures in lung adenocarcinoma (LUAD). Thus, we aimed to develop a novel prognostic model in LUAD based on BMs-related gene profiling.

Methods: The LUAD BMs-related gene profiling and corresponding clinicopathological data were obtained from the basement membrane BASE, The Cancer Genome Atlas (TCGA) and gene expression omnibus (GEO) databases. The Cox regression and least absolute shrinkage and selection operator (LASSO) methods were used to construct a BMs-based risk signature. The concordance index (C-index), receiver operating characteristic (ROC), and calibration curves were generated to evaluate the nomogram. The GSE72094 dataset was used to validate prediction of the signature. The differences in functional enrichment, immune infiltration, and drug sensitivity analyses were compared based on risk score.

Results: In TCGA training cohort, 10 BMs-related genes were found, (e.g., ACAN, ADAMTS15, ADAMTS8, BCAN, etc). The signal signature based on these 10 genes was categorized into high- and low-risk groups regarding survival differences ($p < 0.001$). Multivariable analysis showed that the signature of combined 10 BMs-related genes was an independent prognostic predictor. Such a prognostic value of BMs-based signature in validation cohort of the GSE72094 were further verified. The GEO verification, C-index, and ROC curve showed that the nomogram had accurate prediction performance. The functional analysis suggested that BMs were mainly enriched in extracellular matrix-receptor (ECM-receptor) interaction. Moreover, the BMs-based model was correlated with immune checkpoint.

Abbreviations: BMs, Basement membranes; ECM, Extracellular matrix; LUAD, Lung adenocarcinoma; TCGA, The Cancer Genome Atlas; GEO, Gene expression omnibus; LASSO, Least absolute shrinkage and selection operator; ROC, Receiver operating characteristic; OS, Overall survival; TME, Tumor microenvironment; FDR, False discovery rate; C-index, Concordance index; GO, Gene ontology; MF, Molecular function; BP, Biological processes; CC, Cellular components; KEGG, Kyoto encyclopedia of genes and genomes; PPI, Protein-protein interaction; ITGB4, Integrin subunit β4; EMT, Epithelial mesenchymal transition; NSCLC, Non-small-cell lung cancer; LAD1, Ladinin-1; CAFs, Cancer-associated fibroblasts; TIL, Infiltrating lymphocytes.

Conclusion: This study identified BMs-based risk signature genes and demonstrated their ability to predict prognosis and guide personalized treatment of patients with LUAD.

KEYWORDS

basement membranes, lung adenocarcinoma, TCGA, GEO, prognosis

Introduction

Lung cancer is the second most common cancer and causes a high mortality in the world (Abe and Tanaka, 2016). Lung adenocarcinoma (LUAD) was the predominant type of lung cancer, consisted of approximately 40% cases of lung cancer (Sung et al., 2021). Although great progress has been made in diagnosis and treatment of LUAD, especially in targeting and immunotherapy, the 5-year overall survival (OS) of patients with LUAD remains poor, with approximately 15% only (Wang et al., 2021). LUAD had high molecular heterogeneity and a tendency of early metastasis (Devarakonda et al., 2015). Current methods are still difficult to accurately predict the occurrence and prognosis of LUAD (Calvayrac et al., 2017). Therefore, there is an urgent need to develop more effective and reliable prognostic biomarkers to identify beneficiary patients.

The basement membranes (BMs) are the oldest animal extracellular matrix (ECM), forming a flaky structure that lies under the epithelial cells and surrounds most tissues (Pozzi et al., 2017). The respective planar networks of laminin and type IV collagen molecules are associated with cell surface interactions, providing a scaffold structure for building BMs along the tissue (Yurchenco, 2011). The BMs can not only be used to resist mechanical stress, determine tissue shape and create diffusion barriers, but also provide clues to guide cell polarity, differentiation, migration and survival (Jayadev et al., 2022). The variation of more than 20 BMs genes emphasizes the diversity and basic function of the BM (Nyström et al., 2017). BM protein expression and turnover defects are related to the occurrence of cancer (Naba et al., 2014).

The altered expression of ECM macromolecules in tumor microenvironment (TME) affects the growth, survival, adhesion and migration of cancer cells (Fares et al., 2020). Recently, the study has found that BMs play a critical role in the development of human diseases (Jayadev et al., 2022). For example, In the early development of breast cancer, cancer cells invade through the BM foramen, which is one of the key steps of metastasis (Sikic et al., 2022). At present, the research of BMs in LUAD is relatively few, and thus further research in this filed is needed.

Because the prediction of multi-gene model is better than that of single-gene one, we carried out this study (Srivastava and Gopal-Srivastava, 2002). In this study, we downloaded data from The Cancer Genome Atlas (TCGA) to build a BMs-related genes signature in order to predict the clinical outcome in LUAD patients. The predictive ability of the signature is then verified using data from the Gene Expression Omnibus (GEO). Finally, a risk prognosis model based on the BMs-related genes signature was established, which offered a more accurate prediction of LUAD prognosis than simple clinicopathologic nomograms.

Materials and methods

Data collection and determination of BMs differential expression

The RNA-seq data expression and clinical information of 59 normal lung and 539 LUAD tissues were obtained from TCGA database (https://portal.gdc.cancer.gov). The LUAD RNA-seq data of 398 cases were downloaded from GEO database (https://www.ncbi.nlm.nih.gov/geo/). After the data were integrated, 449 cases in TCGA database were used as training cohort, while 398 cases in GSE72094 database were used as validation cohort. BMs were downloaded from hallmark gene sets in the basement membrane BASE database (https://bmbase.manchester.ac.uk) (Jayadev et al., 2022). Different gene expression data sets were normalized by R software. The differentially expressed BMs were identified by "limma" package based on R software according to the criteria of $|\log FC| > 1$ and false discovery rate (FDR) < 0.05.

Construction and validation of a predictive model based on BMs

In the training cohort, univariate Cox regression analysis was used to analyze the differentially expressed BMs-related genes ($p < 0.05$). Then, the regression analysis of least absolute shrinkage and selection operator (LASSO) was used, and the candidate BMs-related genes with predictive significance were screened by "glmnet" R package. Next, the optimal weighting coefficient of each prognostic candidate BM gene was determined by multivariable Cox regression analysis. All differentially expressed and prognostically significant BM-related genes were included by BM features. This specific risk score is calculated by the following formula: (Coef1 expression *mRNA1) + (Coef2 expression *mRNA2) + (Coef n expression *mRNAn), where Coef is the corresponding coefficient of mRNA in the LASSO regression model.

According to the median of risk score, patients with LUAD were divided into high-risk group and low-risk group. To assess the prognosis of both groups, the OS was performed by the Kaplan-Meier curve. The prognostic ability of the risk model was evaluated by time-dependent ROC analysis using the "survival ROC" software package (Janssens and Martens. 2020). To verify the BM signature, use the risk score of LUAD cases in the GSE72094 dataset to verify the accuracy of the model. In order to verify the BM signature, the risk score of LUAD cases in the GSE72094 data set was used by the same method to verify the accuracy of the model.

Establishment of a prognostic nomogram in LUAD

In TCGA training set, the association between BMs-related genes signature and clinical variables was performed. In addition, both univariate and multivariable Cox regression analysis were conducted to explore whether the risk score had an independent prognostic value in patients with LUAD. The probability of 1-year, 3-year and 5-year OS in LUAD patients were assessed by clinical variables and risk score. The accuracy of nomogram was performed to evaluated by concordance index (C-index) and calibration curve.

Analysis of prognosis and immune value of BMs-related genes signature

The prognostic survival value of BMs-related genes signature mRNAs in LUAD was analyzed by Kaplan-Meier survival analyses. Then, mRNAs with high prognostic potential were chosen for the next stage of evaluation. The correlation between the immune function and immune cells of prognostic signature genes was analyzed and scored by ssGESA algorithm.

Functional enrichment analyses and protein-protein interaction (PPI)

Gene ontology (GO) analysis, including molecular function (MF), biological processes (BP), and cellular components (CC), and the Kyoto Encyclopedia of Genes and Genomes (KEGG) pathway analysis was performed by the "clusterProfiler" package (Kanehisa and Goto, 2000). FDR and p-value < 0.05 were considered to be significantly enriched. By submitting the differentially expressed BMs information to the STRING database (http://www.string-db.org/), the protein-protein interaction information was obtained (Szklarczyk et al., 2019). The construction and visualization of PPI network was realized by the Cytoscape software (Otasek et al., 2019). According to the MCODE plug-in, we selected the MCODE score > 10 to filter out the most significant module in the PPI network.

Immune cell infiltration analysis

We utlized a series of algorithms, including CIBERSORT, CIBERSORT-ABS, QUANTISEQ, MCP-counter, XCELL, TIMER, and EPIC algorithms, to evaluate the level of immune cell permeability between the high-risk group and the low-risk group according to the differentially expressed BMs-based signature (Newman et al., 2015). We explored the expression of several immune checkpoints, such as CD276, TNFSF9, CD200R1, CD28, CD80, CD48, TNFS18, TNFS15 and CD40LG, for immune checkpoint blockade therapy.

Statistics analysis

All statistical analyses were performed using R software (version 4.1.3). Continuous variables are tested by the student T test, while classified variables are tested by chi-square test. A p-value < 0.05 was considered significant.

Results

Identification of a BM-related genes signature

In 539 tumor and 59 normal tissues, we found 81 differentially expressed BMs genes (p < 0.05, and logFC | > 1), including 47 up-regulated and 34 down-regulated differential expression ones (Figure 1A). The differential expression of each sample was shown in the heatmap (Figure 1B). After excluding 72 patients without appropriate follow-up or lack of important clinical information, 449 patients were included in the TCGA training set to identify the prognosis-related BMs genes for constructing a BMs-based signature. The clinicopathological information of LUAD in the TCGA database was shown in Table 1.

We used the univariate Cox regression to analyze individually the differentially expressed BMs gene profile, 20 BMs genes were found from TCGA training cohort (Figure 1C). Lasso regression analysis was carried out among 20 BMs genes, of which 10 BMs genes were found to be significant and selected as the BM signature candidates genes (Figures 1D, E). The multivariate Cox regression analysis was used to determine the corresponding regression coefficients of each candidate in this BM-related risk gene signature (Table 2). Finally, according to 449 LUAD cases in TCGA training cohort, the 10 BM-related risk gene signature was constructed, and the risk score was calculated based on the linear combination of gene expression levels and corresponding regression coefficients. Among them, the calculation formula of correlation coefficient among 10 BM-related genes was as following (Table 2): risk score= (0.1021 × ACAN expression) +(0.0162 × ADAMTS15 expression) + (−0.010 × ADAMTS8 expression) + (0.0058 × BCAN expression) + (−0.0070 × COL4A3 expression) + (−0.0405 × ITGA8 expression) + (0.0017 × ITGB4 expression) + (0.0043 ×LAD1expression) + (−0.0891 × TENM3 expression) + (0.0003 × TIMP1 expression).

Prognostic value of BM-related risk gene signature in the training cohort

According to the median of risk score, the patients with LUAD were divided into high- and low-risk groups. The LUAD patients in the low-risk group had significantly longer OS time than those in the high-risk group (p < 0.001) (Figure 2A). From the distribution of risk score (Figure 2B), the number of deaths in the high-risk group was significantly higher than that in the low-risk group. The heatmap showed the differential expression of these 10 BM-related risk genes between the low-risk group and the high-risk group (Figure 2C). The area under the time-dependent ROC curve at 1-, 3-, and 5 years was 0.673, 0.709, and 0.722 in the two groups of patients, respectively, indicating a good performance of the risk model for predicting the survival of LUAD patients (Figure 2D).

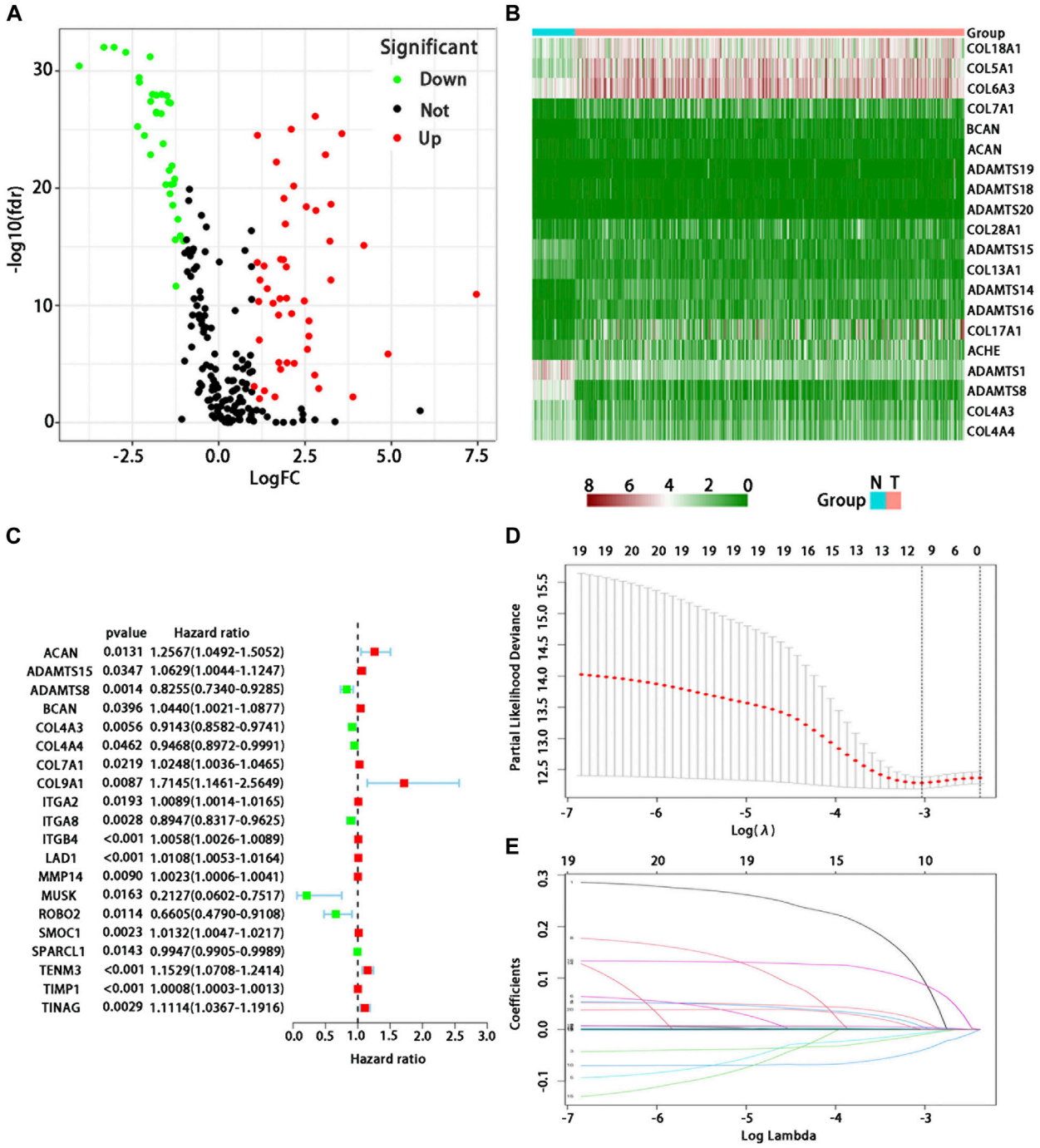

FIGURE 1
Analysis of differential expression and establishment of prognostic model of BMs-related genes in LUAD. **(A)** Volcano map showed differential expression BMs-related genes. Red dots represent upregulated BMs-associated mRNAs, green dots represent downregulated ones, and black dots represent mRNAs with no significant differential expression; **(B)** Heatmap showed differential expression BMs-related genes. Red represents high expression and green represents low expression. Acronym: N = normal tissue, T = tumor tissue. **(C)** Determination of prognostic BMs-related genes under univariate Cox regression analysis. **(D)** LASSO coefficient profiles of the 10 genes in LUAD. A coefficient profile plot was generated against the log (lambda) sequence. **(E)** Selection of the optimal parameter (lambda) in the LASSO model for LUAD.

Prognostic value of BMs-related genes signature in validation cohort

We used the same method to verify the prognostic value of BMs-based signature in GSE72094 verification cohort. The survival curve showed that the OS of patients in the low-risk group was better than that in the high-risk group ($p = 0.015$) (Figure 2E), and there were more deaths in the high-risk group than that in the low-risk group (Figure 2F). The expression profiles of 10-BMs between the low-risk group and the high-risk group were drawn in the heatmap

TABLE 1 Summary of the Clinicopathological characteristics of patients with LUAD.

Covariates	Group	Patient number (%)	*p*-value[1]	*p*-value[2]
Age	≤65	218 (48.6)	0.271	0.182
	>65	231 (51.4)		
Gender	Female	248 (55.2)	0.832	0.942
	Male	201 (44.8)		
Chemotherapy	Yes	181 (40.3)	0.091	0.209
	No	268 (59.7)		
Radiotherapy	Yes	106 (23.6)	4.20e-05	0.008
	No	343 (76.4)		
Stage	Stage I-II	358 (79.7)	4.28e-07	<0.001
	Stage III-IV	91 (20.3)		

1 *p*-value of univariate Cox regression.
2 *p*-value of multivariable Cox regression.

TABLE 2 The 10 BMs-related gene list and coefficient.

Genes	Coefficient
ACAN	0.1021
ADAMTS15	0.0162
ADAMTS8	−0.010
BCAN	0.0058
COL4A3	−0.0070
ITGA8	−0.0405
ITGB4	0.0017
LAD1	0.0043
TENM3	0.0891
TIMP1	0.0003

(Figure 2G). Compared with the training cohort, the area under the time-dependent ROC of the validation cohort at 1-, 3-, and 5 years was 0.667, 0625, and 0.614, respectively, which also showed a good verification (Figure 2H).

Prognostic significance and immune infiltration of differential expression BMs genes

From the 10 BMs genes which were used to construct the risk score model, four of them based on survival significance were screened. After we draw the survival curve of these four genes, the high expression group of ITGB4 ($p < 0.001$), LAD1 ($p = 0.009$), BCAN ($p = 0.017$), and ADAMTS15 ($p = 0.043$) had a worse prognosis than the low expression group (Figures 3A–D), respectively, suggesting that the high expression of ITGB4, LAD1, BCAN and ADAMTS15 might be related to the progression of the tumor. Moreover, the correlation analysis of differential expression genes in immune cells and function showed that TIMP1, TENM3, ITGA8 and ADAMTS8 were positively correlated with most immune cells and immune function (Figure 3E), while ACAN, BCAN, and LAD1 were negatively correlated, suggesting that these genes may play significant roles in LUAD immunity and deserve further study. Taken together, these results suggested that above genes with differential expression could play a crucial role in the immune regulation of LUAD.

Stratified analysis of association between BMs-based signature and prognosis by clinical features in patients with LUAD

We further confirmed the association between risk score and clinical characteristics of LUAD patients. From the heatmap (Figure 4A), we found that sex ($p = 0.022$), stage ($p < 0.001$), radiotherapy ($p = 0.008$) and chemotherapy ($p = 0.014$) had significantly statistical differences between the high-risk and low-risk groups, while the age ($p = 0.493$) had no significant statistical significance (Figures 4B–F). Thus, we performed the stratified analysis of risk score on survival by clinical factors. We found that there were significant survival differences between low-risk and high-risk groups in different subgroups with different clinical factors, including as age (≤65 *vs.* > 65 years) ($p < 0.001$), sex (male *vs.* Female) ($p < 0.001$), with chemotherapy ($p = 0.011$), without chemotherapy ($p < 0.001$), with radiotherapy ($p = 0.014$) and stage (I/II *vs.* III/IV) ($p < 0.001$), while no significant survival difference in patients without radiotherapy ($p > 0.068$) (Figures 4G–K).

Multivariable analysis of prognosis of risk score in LUAD

Multivariable Cox regression analysis was used to analyze whether risk score could be regarded as independent prognostic

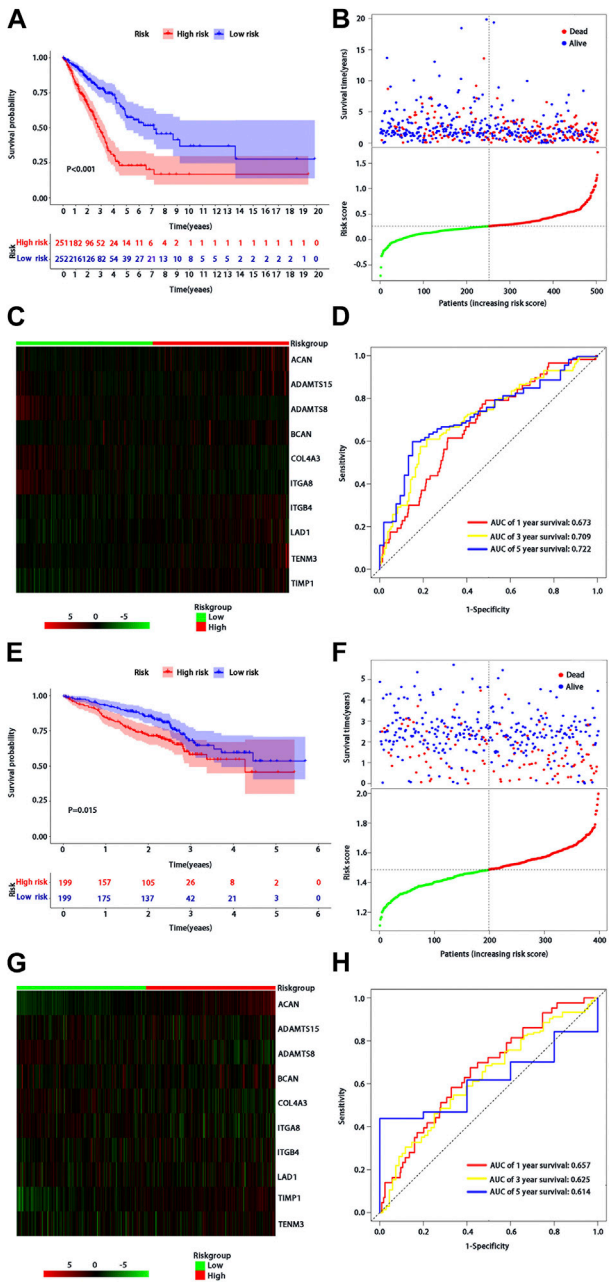

FIGURE 2
Assessment of BMs-related genes signature. **(A)** Kaplan-Meier survival analysis of patients with LUAD in high and low risk groups of TCGA training cohort; **(B)** Survival status distribution based on the median risk score in TCGA training cohort; Red represents high risk and green represents low risk; **(C)** Heatmap showed differential expression of BMs in high and low risk groups of TCGA training cohort; **(D)** ROC curve analysis of risk score predicting overall survival in TCGA training cohort. **(E)** Kaplan-Meier survival analysis of patients with LUAD in high and low risk groups of the GSE72094 validation cohort; **(F)** Survival status distribution based on the median risk score of the GSE72094 validation cohort; Red represents high risk and green represents low risk; **(G)** Heatmap showed differential expression of BMs in high and low risk groups in the GSE72094 validation cohort t; **(H)** ROC curve analysis of risk score predicting overall survival in the GSE72094 validation cohort.

indicators of LUAD after adjustment with other prognostic factors. We first found that risk score ($p < 0.001$), stage ($p < 0.001$), and radiotherapy ($p < 0.001$) were significantly associated with survival in patients with LUAD by the univariate analysis (Figure 5A). We then performed the multivariable Cox regression analysis to show a significant association between risk score and prognosis ($p < 0.001$) (Figure 5B), indicating that risk score may serve as an independent predictor of prognosis of patients with LUAD.

Nomogram of BMs-related genes signature in patients with LUAD

In the training cohort, we used BMs-based signature risk score, age, sex, stage, radiotherapy and chemotherapy to develop a visual nomogram for 1-, 3- and 5-year individual survival prediction (Figure 5C). Bootstrap verification was performed to verify the accuracy of the nomogram. The C-index of the training cohort was 0.663, which showed that the nomogram had good prediction ability in LUAD. We then draw the calibration curve (Figure 5D) to verify the accuracy of the nomogram. The calibration curve showed that the survival probability of the actual observation and prediction was satisfactory in terms of 1-, 3- and 5-year consistency.

Functional enrichment analysis and PPI of the BMs-related genes

To investigate the function and potential pathway of BMs genes in LUAD, we performed the GO and KEGG analysis for differentially expressed BMs genes. Based on the results of biological process (BP)'s analysis, we found that 81 BMs genes were involved in extracellular matrix organization, extracellular structure organization, and external encapsulating structure organization. The cellular component (CC) analysis demonstrated that collagen-containing extracellular matrix and basement membrane. Molecular function (MF) analysis also showed that 81 BMs were mainly related to extracellular matrix structural constituent, extracellular matrix structural constituent conferring tensile strength, metalloendopeptidase activity, glycosaminoglycan binding, and extracellular matrix binding (Figure 6A). Moreover, the KEGG pathway enrichment analysis found that the main enrichment pathways of BMs differentially expressed genes included ECM-receptor interaction, focal adhesion, protein digestion and absorption, human papillomavirus infection, PI3K-Akt signaling pathway, small cell lung cancer, axon guidance, arrhythmogenic right ventricular cardiomyopathy, hypertrophic cardiomyopathy, and dilated cardiomyopathy (Figure 6B). From the STRING database, we found that the PPI network based on differentially expressed BMs genes was mainly composed of 62 nodes and 173 edges (Figure 6C).

Analysis of immune checkpoint analysis for BMs-related genes signature in patients with LUAD

The relationship between risk score and immune checkpoint is worthy of our investigation as the immune checkpoints play important roles in immunotherapy. We found that there were differences in the expression of CD276, TNFSF9, CD200R1,

10.3389/fgene.2023.1100560

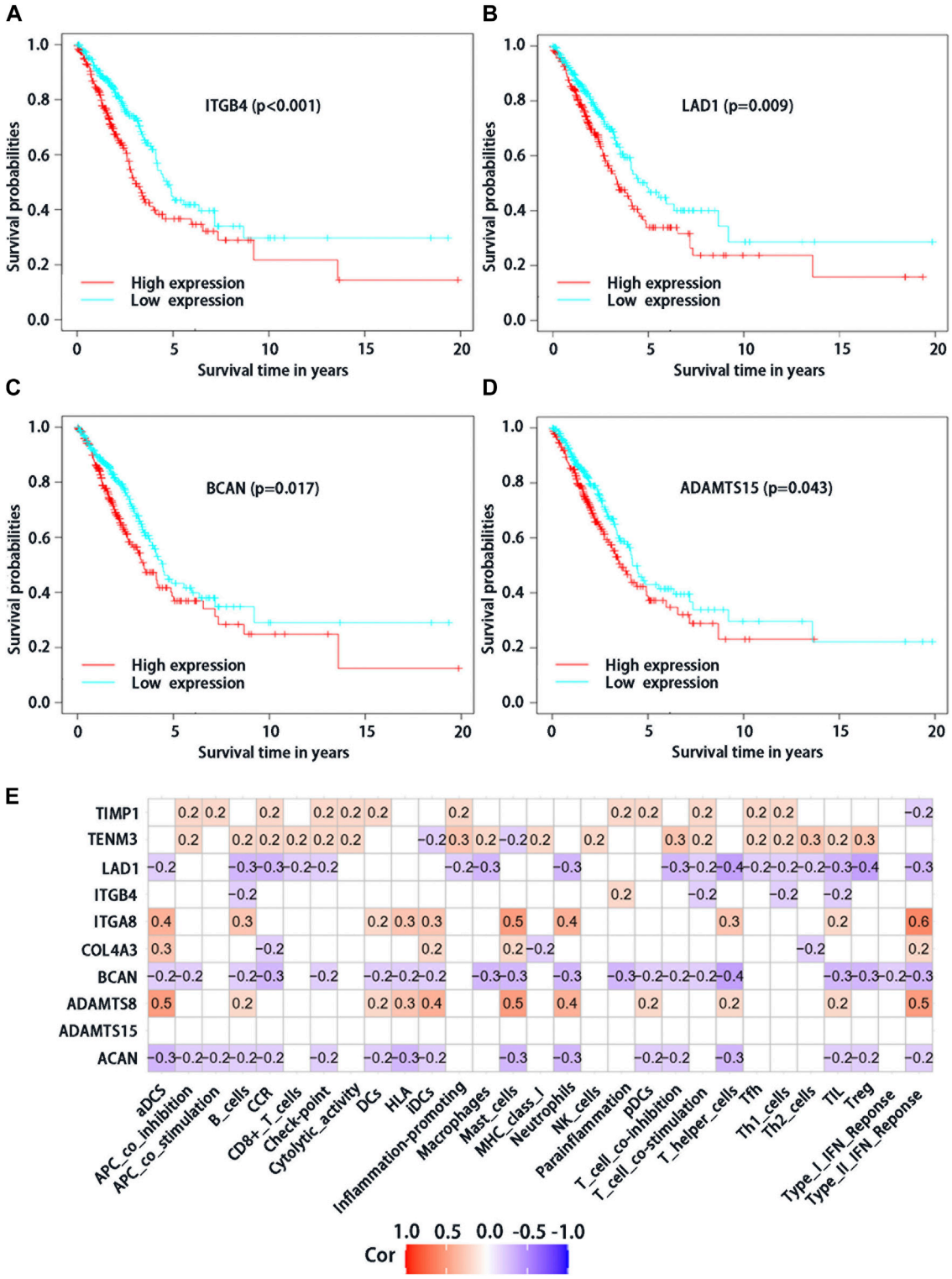

FIGURE 3
Analysis of survival significance of differential expression BMs-related genes signature in high-risk group and low-risk group including high expression of ITGB4 **(A)**, LAD1 **(B)**, BCAN **(C)** and ADAMTS15 **(D)**. The red curve represents the high expression of mRNA and the blue curve represents the low expression. **(E)** Analysis of immune cells and immunology functions associated with differential expression genes. Correlation analysis of differential expression genes with immune cells and immunology functions. The red color represents positive correlations, the blue color represents negative correlations, and the white indicates relationships without a statistical difference.

10.3389/fgene.2023.1100560

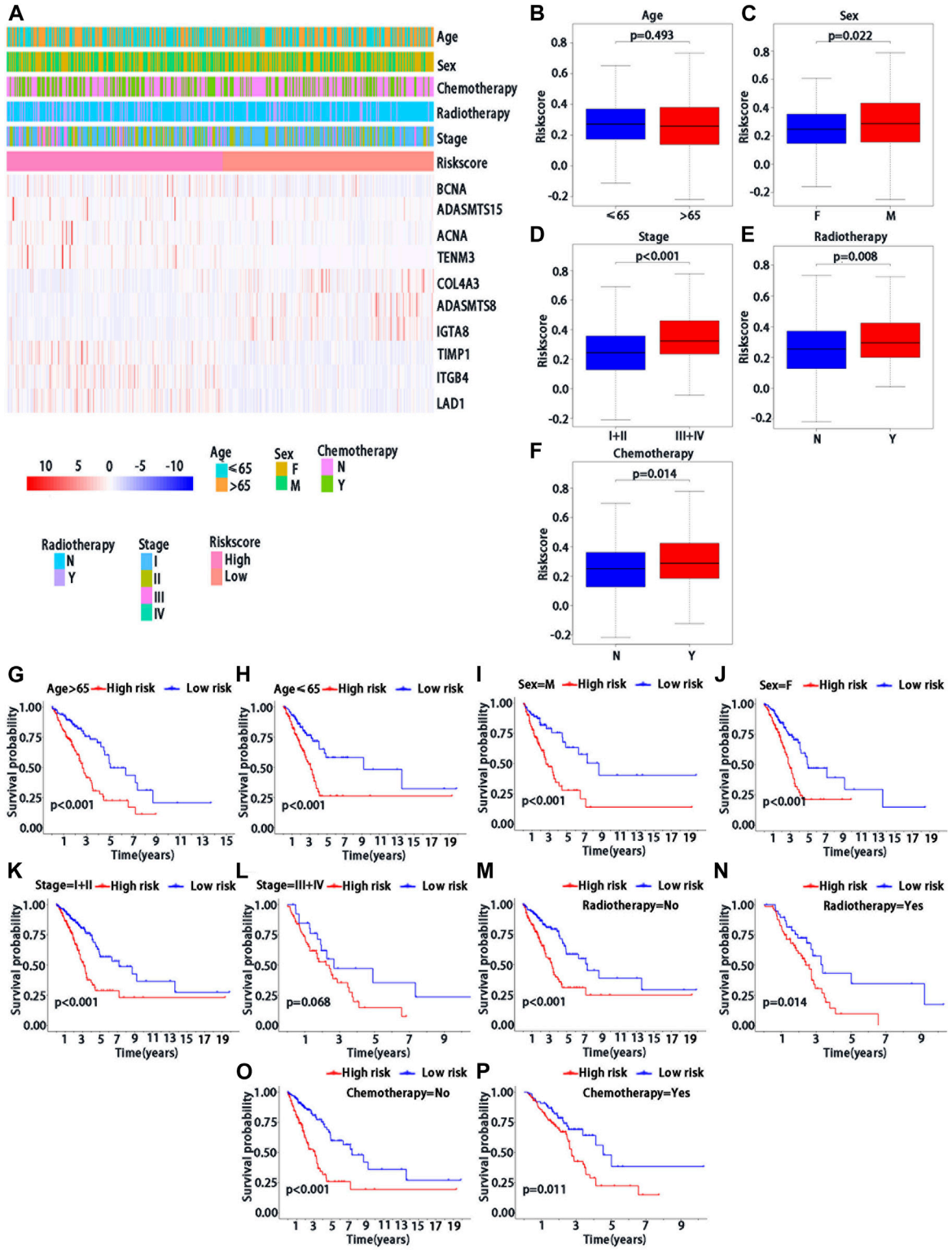

FIGURE 4
Clinical characteristics of BMs-related genes signature with LUAD. **(A)** The heatmap of clinical factors and BM genes in high and low-risk with LUAD. Differential expression in clinical factors of age**(B)**, sex **(C)**, stage **(D)**, radiotherapy **(E)** and chemotherapy **(F)** under high and low-risk with LUAD. Prognostic analysis of different clinical factors, including age>65 **(G)**, age≤65 **(H)**, sex = M **(I)**, sex = F **(J)**, stage = I + II **(K)**, stage = III + IV **(L)**, radiotherapy = No **(M)**, radiotherapy = Yes **(N)**, chemotherapy = No **(O)** and chemotherapy = Yes **(P)** in K-M survival analysis of high and low risk. Red curve represents the high-risk group and blue curve represents the low-risk group. Abbreviations: F = female, M = male, I + II = I and II stage, III + IV = III and IV stage.

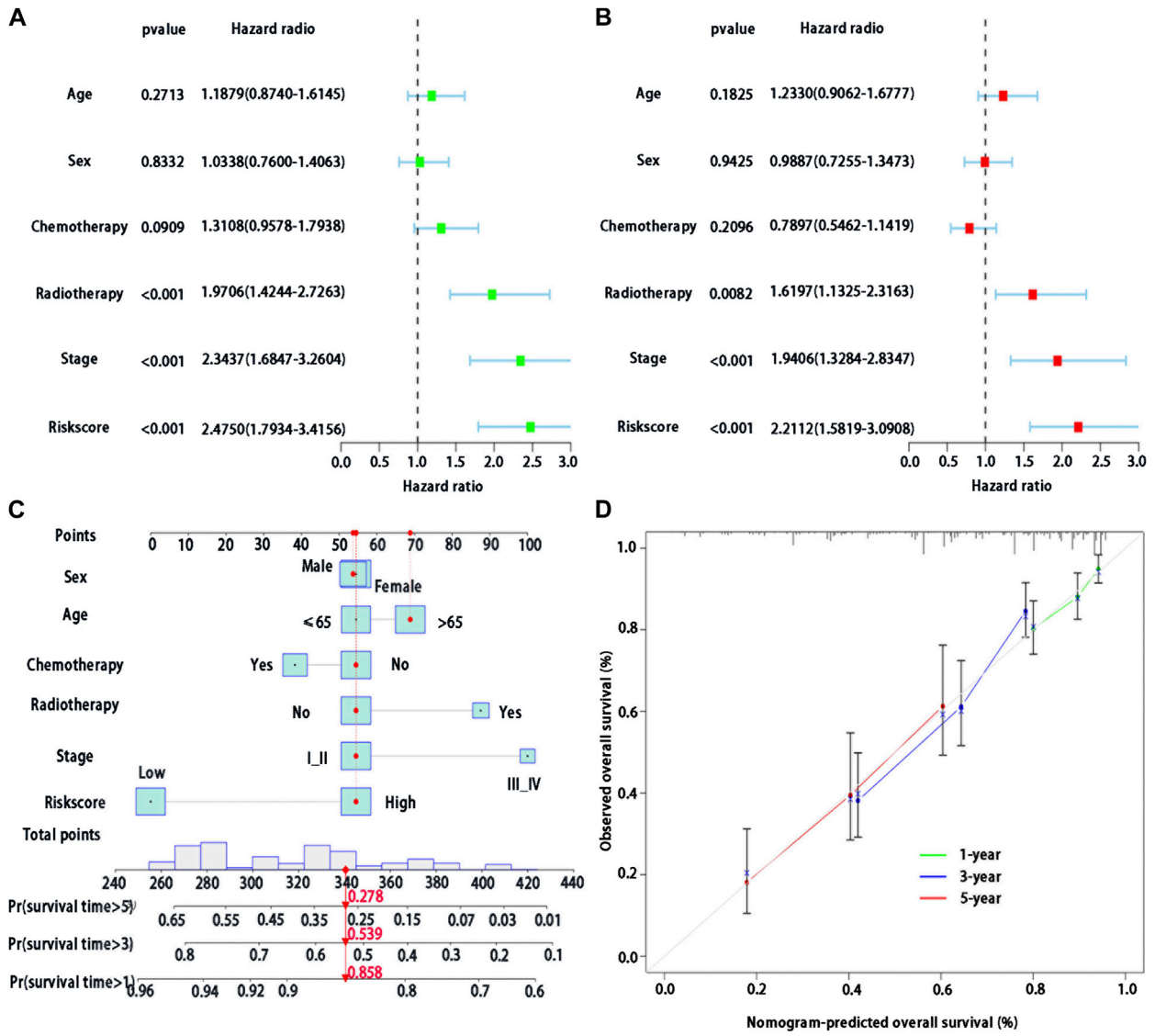

FIGURE 5
Development of a BMs-related genes signature nomogram with LUAD. **(A)** Univariate Cox regression analysis of the clinical features and the risk score in patients with LUAD; **(B)** Multivariate Cox regression analysis of the clinical features and the risk score in patients with LUAD. **(C)** Nomogram for BMs risk score and clinical features; **(D)** The calibration plots for predicting 1-,3- or 5-year survival probability.

CD28, CD80, CD48, TNFS18, TNFS15 and CD40LG between high-risk and low-risk groups. Among them, CD276, and TNFSF9 were highly expressed in the high-risk group (Supplementary Figures S1 A, B), while CD200R1, CD28, CD80, CD48, TNFS18, TNFS15, and CD40LG were highly expressed in the low-risk group (Supplementary Figures S1 C–L).

Discussion

Based on the data from open access public databases, many studies have focused on the link between RNA-seq data of specific genomes and prognosis of individual patients (Sun et al., 2022; Zhao et al., 2022), while few studies were focused on the prognosis of LUAD with specific genomes, particularly on clinical application, immune infiltration and other related areas. There was growing evidence that the response of extracellular matrix to TME drives the potential carcinogenic mechanisms of many cancers, including lung cancer (Li et al., 2021). At present, there were few reports on the prognostic value of BMs-related genes in LUAD. In this study, we have developed a comprehensive model with multi-genes for prediction of prognosis in the patients with LUAD. This study was aimed to investigate the relationship between the expression of BMs-related gene signature and the prognosis of patients with LUAD. We constructed a new prognostic model based on the BMs-based signature which included 10-BMs-related genes, such as ACAN, ADAMTS15, ADAMTS8, BCAN, COL4A3, ITGA8, ITGB4, LAD1, TENM3, and TIMP1. Furthermore, we confirmed the prognostic value of BMs-based signature, and established a

10.3389/fgene.2023.1100560

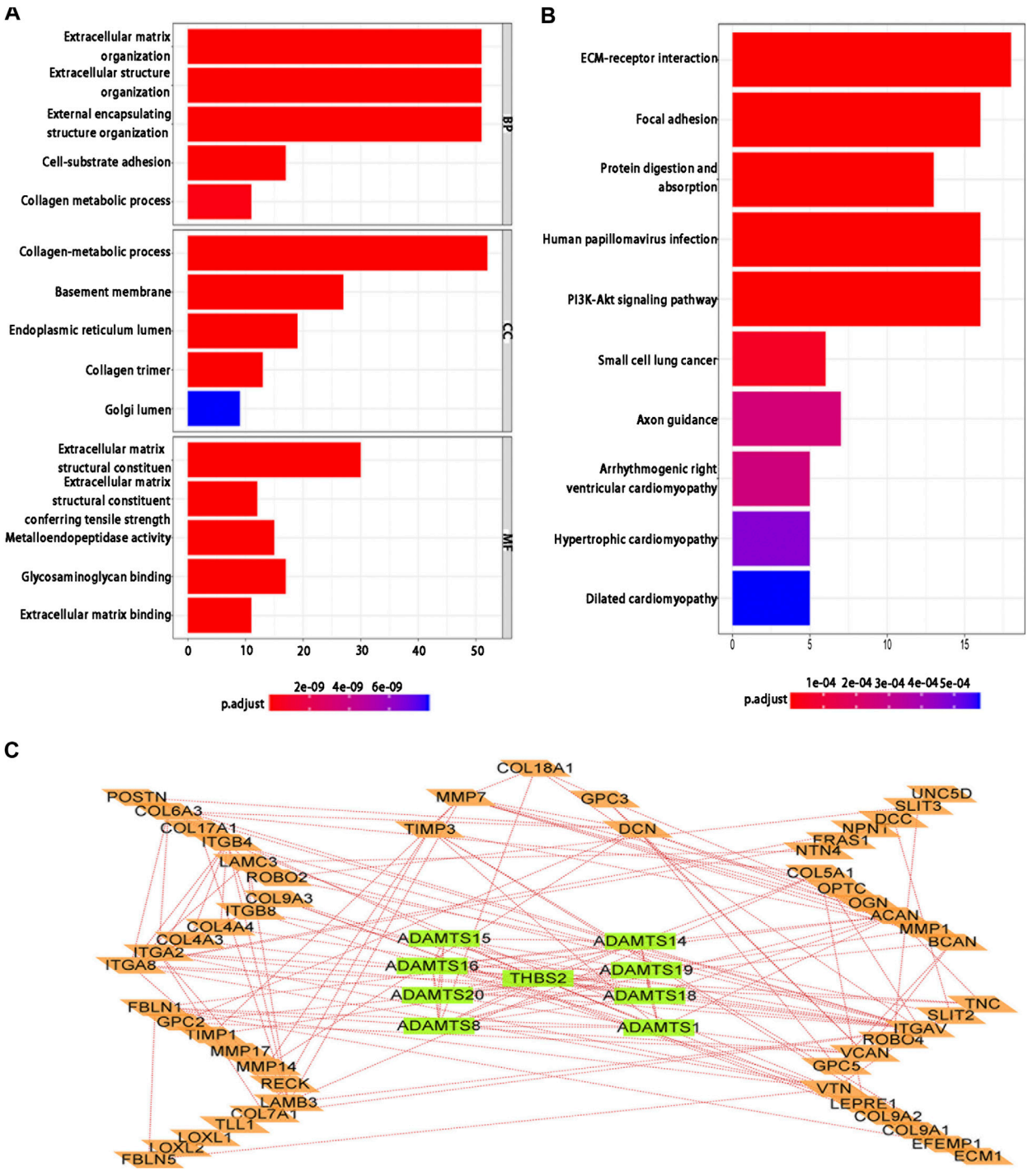

FIGURE 6
Differentially expressed BMs-related genes analysis of enrichment function in LUAD. **(A)** GO function analysis; **(B)** KEGG pathway analysis; **(C)** PPI network.

survival prediction nomogram involving risk score, age, sex, staging, radiotherapy and chemotherapy, and verified its predictive ability with GSE72094 data sets. In this study, we have demonstrated that the nomogram was verified to have good prediction performance. We further investigated the relationship between BMs-based signatures and clinical features. Finally, we explored the relationship between the differential expression of BMs-related genes and immune checkpoints in patients with LUAD.

In the current study, the risk score was constructed based on 10 BMs-related genes and used to demonstrate its value in clinical research. The ITGB4, LAD1, BCAN and ADAMTS15 were found

to have significance in OS of patients with LUAD, of which the integrin subunit β4 (ITGB4) is one of the most characteristic integrins and is involved in regulation of various cellular functions (Giancotti, 2007). Previous studies have shown that integrin regulates angiogenesis, connective tissue proliferation and immune response of tumor host cells by affecting tumor cell migration, invasion, proliferation and survival. Thus it affects epithelialmesenchymal transition (EMT), tumor occurrence, metastasis and even treatment outcome (Xiong et al., 2021). For example, the overexpression of ITGB4 was associated with invasive behavior and poor prognosis of NSCLC (Zheng et al., 2013; Wu et al., 2019). In this study, we found that the high expression of ITGB4 contributes to the poor prognosis of LUAD, which was consistent with previous studies. The LAD1 (Ladinin-1) was a collagen-anchored filament protein on the BM, which was used to maintain the cohesion of the dermis-epidermal junction (Teixeira et al., 2015). It helped to stabilize the connection between the epithelium and the underlying mesenchyme (Motoki et al., 1997). In addition to its structural role, LAD1 also participates in the regulation of mitotic signals by acting as a connexin in EGF-induced ERK5 cascade activation (Yao et al., 2010). Comparative proteomic studies showed that the expression of LAD1 in LUAD was more abundant than that in normal lung tissue (Codreanu et al., 2017). Similarly, we found that the overexpression of LAD1 leads to the poorly prognostic value in the progression of LUAD. The ADAMTS-15 acted as a tumor suppressor in breast and prostate cancer (Porter et al., 2006; Binder et al., 2020). Enhanced expression of ADAMTS-15 might reduce the motor ability of breast cancer cells and angiogenesis, rather than rely on its catalytic activity. Binder et al. found that ADAMTS-15 combined with androgen could inhibit tumor (Binder et al., 2020). However, in our current study, the overexpression of ADAMTS-15 led to a poor prognosis of patients with LUAD. Recent study has found that the expression of BCNA gene can protect bacterial cell capsule from lipid peroxidation free radicals; however, its exact roles in cancer require to be further studied (Naguib et al., 2022). In our study, BCNA was risk factors, and the patients with highexpression had a poor prognosis, which provided evidence for further study in the future.

Our understanding of BMs in normal and disease states remains limited due to the lack of adequate understanding of the role of BM proteins in LUAD. However, in the GO enrichment analysis, we found that BMs was an important part of EMC in the process of BP, CC and MF, which was consistent with previous studies (Baghban et al., 2020; Sahai et al., 2020). The EMC macromolecules exist in all extracellular tissues, coordinating a variety of cellular processes and tumor metastasis (Jayadev et al., 2022). The KEGG analysis showed that BMs-related genes played a significant role in ECM-receptor interaction. The TME, apart from ECM, included fibroblasts, immune cells, and blood vessels. Composition and network organization of EMC were synthesized and modified by cancer-associated fibroblasts (CAFs) and cancer cells (Baghban et al., 2020; Sahai et al., 2020). In this way, the nature of TME is altered, and conversely, the TME can dictate the growth and spread of the tumor. This showed that BMs might play a certain role in the transformation between TME and ECM, which needs futher study to be explored in the future.

Tumor infiltrating lymphocytes (TIL) were indispensable for the occurrence and development of tumors (Kuninty et al., 2022). Although the monotherapy of PD-1 or PD-L1 was generally well tolerated and the efficacy is limited, combination therapy increased the risk of immune-related adverse events. Therefore, new predictive biomarkers were needed to maximize the benefit of patients, reduce toxicity, and guide combination therapy (Ni et al., 2022). We used immune algorithm to find immune checkpoints with differences between high-risk and low-risk groups of BMs. Moreover, LUAD patients in high-risk groups might benefit from immune checkpoint therapy. However, so far, there have been no studies on the association between BMs and drug sensitivity or resistance. Using the CellMine database, we found that the expression of BMs-related genes was related to the sensitivity of Vemurafeni, Dabrafenib, Selumetinib and Cobimetinib, which were targeted drugs for gene mutations. Therefore, we speculated that BMs might play a role in targeted therapy, which might increase the drug sensitivity.

Although this study has found the relationship between BMs-related genes signature and the prognosis of LUAD and clinical significance of prognosis prediction of patients with LUAD, it remains certain limitations. For example, since this study collected the data of LUAD patients from TCGA and GEO public databases and lacked actual laboratory research data, the model was constructed based on such data, the findings are needed to be verified or validated with the real data from the prospectively designed clinical trials.

In conclusion, we determined whether the BMs genes risk characteristics related to the OS of LUAD patients; and constructed and verified the prognostic nomogram of LUAD, including BMs-related risk score, age, sex, stage, radiotherapy and chemotherapy for prediction of individual survival. Moreover, we comprehensively analyzed the differentially expressed BMs-related genes by enrichment analysis, immunity and drug susceptibility. Thus, this study may identify a new BMs-related prognostic marker, demonstrate the clinical significance of BMs in LUAD, and provide some evidence for the future study on the role of BMs in LUAD.

Data availability statement

The original contributions presented in the study are included in the article/Supplementary Material, further inquiries can be directed to the corresponding author.

Author contributions

XZ and YS Designed and coordinated the study. XL, XQ, WD, and XZ Performed the analysis. XL, XQ, and ZN Collected the dataset. YS Reviewed and revised the manuscript.

Acknowledgments

All authors would like to appreciate the TCGA database and the GEO database for sharing data.

Conflict of interest

The authors declare that the research was conducted in the absence of any commercial or financial relationships that could be construed as a potential conflict of interest.

Publisher's note

All claims expressed in this article are solely those of the authors and do not necessarily represent those of their affiliated organizations, or those of the publisher, the editors and the reviewers. Any product that may be evaluated in this article, or claim that may be made by its manufacturer, is not guaranteed or endorsed by the publisher.

Supplementary material

The Supplementary Material for this article can be found online at: https://www.frontiersin.org/articles/10.3389/fgene.2023.1100560/full#supplementary-material

SUPPLEMENTARY FIGURE S1
Differential expression analysis of immune checkpoints such as the CD276 **(F)**, TNFSF9 **(G)**, CD200R1 **(H)**, CD28 **(I)**, CD80 **(J)**, CD48 **(K)**, TNFS18 **(L)**, TNFS15 **(M)** and CD40LG **(N)** in high- and low-risk groups.

References

Abe, Y., and Tanaka, N. (2016). The hedgehog signaling networks in lung cancer: The mechanisms and roles in tumor progression and implications for cancer therapy. *Biomed. Res. Int.* 2016, 7969286. doi:10.1155/2016/7969286

Baghban, R., Roshangar, L., Jahanban-Esfahlan, R., Seidi, K., Ebrahimi-Kalan, A., Jaymand, M., et al. (2020). Tumor microenvironment complexity and therapeutic implications at a glance. *Cell Commun. Signal* 18 (1), 59. doi:10.1186/s12964-020-0530-4

Binder, M. J., McCoombe, S., Williams, E. D., McCulloch, D. R., and Ward, A. C. (2020). ADAMTS-15 has a tumor suppressor role in prostate cancer. *Biomolecules* 10 (5), 682. doi:10.3390/biom10050682

Calvayrac, O., Pradines, A., Pons, E., Mazières, J., and Guibert, N. (2017). Molecular biomarkers for lung adenocarcinoma. *Eur. Respir. J.* 49 (4), 1601734. doi:10.1183/13993003.01734-2016

Codreanu, S. G., Hoeksema, M. D., Slebos, R. J. C., Zimmerman, L. J., Rahman, S. M. J., Li, M., et al. (2017). Identification of proteomic features to distinguish benign pulmonary nodules from lung adenocarcinoma. *J. Proteome Res.* 16 (9), 3266–3276. doi:10.1021/acs.jproteome.7b00245

Devarakonda, S., Morgensztern, D., and Govindan, R. (2015). Genomic alterations in lung adenocarcinoma. *Lancet Oncol.* 16 (7), e342–e351. doi:10.1016/s1470-2045(15)00077-7

Fares, J., Fares, M. Y., Khachfe, H. H., Salhab, H. A., and Fares, Y. (2020). Molecular principles of metastasis: A hallmark of cancer revisited. *Signal Transduct. Target Ther.* 5 (1), 28. doi:10.1038/s41392-020-0134-x

Giancotti, F. G. (2007). Targeting integrin beta4 for cancer and anti-angiogenic therapy. *Trends Pharmacol. Sci.* 28 (10), 506–511. doi:10.1016/j.tips.2007.08.004

Janssens, A. C. J. W., and Martens, F. K. (2020). Reflection on modern methods: Revisiting the area under the ROC Curve. *Int. J. Epidemiol.* 49, 1397–1403. doi:10.1093/ije/dyz274

Jayadev, R., Morais, M., Ellingford, J. M., Srinivasan, S., Naylor, R. W., Lawless, C., et al. (2022). A basement membrane discovery pipeline uncovers network complexity, regulators, and human disease associations. *Sci. Adv.* 8 (20), eabn2265. doi:10.1126/sciadv.abn2265

Kanehisa, M., and Goto, S. (2000). Kegg: Kyoto encyclopedia of genes and genomes. *Nucleic Acids Res.* 28, 27–30. doi:10.1093/nar/28.1.27

Kuninty, P. R., Binnemars-Postma, K., Jarray, A., Pednekar, K. P., Heinrich, M. A., Pijffers, H. J., et al. (2022). Cancer immune therapy using engineered 'tail-flipping' nanoliposomes targeting alternatively activated macrophages. *Nat. Commun.* 13 (1), 4548. doi:10.1038/s41467-022-32091-9

Li, M., Wang, Y., Li, M., Wu, X., Setrerrahmane, S., and Xu, H. (2021). Integrins as attractive targets for cancer therapeutics. *Acta Pharm. Sin. B* 11 (9), 2726–2737. doi:10.1016/j.apsb.2021.01.004

Motoki, K., Megahed, M., LaForgia, S., and Uitto, J. (1997). Cloning and chromosomal mapping of mouse ladinin, a novel basement membrane zone component. *Genomics* 39 (3), 323–330. doi:10.1006/geno.1996.4507

Naba, A., Clauser, K. R., Whittaker, C. A., Carr, S. A., Tanabe, K. K., and Hynes, R. O. (2014). Extracellular matrix signatures of human primary metastatic colon cancers and their metastases to liver. *BMC Cancer* 14, 518. doi:10.1186/1471-2407-14-518

Naguib, M., Feldman, N., Zarodkiewicz, P., Shropshire, H., Biamis, C., El-Halfawy, O. M., et al. (2022). An evolutionary conserved detoxification system for membrane lipid-derived peroxyl radicals in Gram-negative bacteria. *PLoS Biol.* 20 (5), e3001610. doi:10.1371/journal.pbio.3001610

Newman, A. M., Liu, C. L., Green, M. R., Gentles, A. J., Feng, W., Xu, Y., et al. (2015). Robust enumeration of cell subsets from tissue expression profiles. *Nat. Methods* 12, 453–457. doi:10.1038/nmeth.3337

Ni, J. J., Zhang, Z. Z., Ge, M. J., Chen, J. Y., and Zhuo, W. (2022). Immune-based combination therapy to convert immunologically cold tumors into hot tumors: An update and new insights. *Acta Pharmacol. Sin.* 44, 288–307. doi:10.1038/s41401-022-00953-z

Nyström, A., Bornert, O., and Kühl, T. (2017). Cell therapy for basement membrane-linked diseases. *Matrix Biol.* 57, 124–139. doi:10.1016/j.matbio.2016.07.012

Otasek, D., Morris, J. H., Bouças, J., Pico, A. R., and Demchak, B. (2019). Cytoscape automation: Empowering workflow-based network analysis. *Genome Biol.* 20, 185. doi:10.1186/s13059-019-1758-4

Porter, S., Span, P. N., Sweep, F. C., Tjan-Heijnen, V. C., Pennington, C. J., Pedersen, T. X., et al. (2006). ADAMTS8 and ADAMTS15 expression predicts survival in human breast carcinoma. *Int. J. Cancer* 118 (5), 1241–1247. doi:10.1002/ijc.21476

Pozzi, A., Yurchenco, P. D., and Iozzo, R. V. (2017). The nature and biology of basement membranes. *Matrix Biol.* 57, 1–11. doi:10.1016/j.matbio.2016.12.009

Sahai, E., Astsaturov, I., Cukierman, E., DeNardo, D. G., Egeblad, M., Evans, R. M., et al. (2020). A framework for advancing our understanding of cancer-associated fibroblasts. *Nat. Rev. Cancer* 20 (3), 174–186. doi:10.1038/s41568-019-0238-1

Sikic, L., Schulman, E., Kosklin, A., Saraswathibhatla, A., Chaudhuri, O., and Pokki, J. (2022). Nanoscale tracking combined with cell-scale microrheology reveals stepwise increases in force generated by cancer cell protrusions. *Nano Lett.* 22 (18), 7742–7750. doi:10.1021/acs.nanolett.2c01327

Srivastava, S., and Gopal-Srivastava, R. (2002). Biomarkers in cancer screening: A public health perspective. *J. Nutr.* 132 (8), 2471S–2475s. doi:10.1093/jn/132.8.2471S

Sun, N., Chu, J., Hu, W., Chen, X., Yi, N., and Shen, Y. (2022). A novel 14-gene signature for overall survival in lung adenocarcinoma based on the Bayesian hierarchical Cox proportional hazards model. *Sci. Rep.* 12 (1), 27. doi:10.1038/s41598-021-03645-6

Sung, H., Ferlay, J., Siegel, R. L., Laversanne, M., Soerjomataram, I., Jemal, A., et al. (2021). Global cancer statistics 2020: GLOBOCAN estimates of incidence and mortality worldwide for 36 cancers in 185 countries. *CA Cancer J. Clin.* 71 (3), 209–249. doi:10.3322/caac.21660

Szklarczyk, D., Gable, A. L., Lyon, D., Junge, A., Wyder, S., Huerta-Cepas, J., et al. (2019). STRING v11: Protein-protein association networks with increased coverage, supporting functional discovery in genome-wide experimental datasets. *Nucleic Acids Res.* 47, D607–D613. doi:10.1093/nar/gky1131

Teixeira, J. C., de Filippo, C., Weihmann, A., Meneu, J. R., Racimo, F., Dannemann, M., et al. (2015). Long-term balancing selection in LAD1 maintains a missense trans-species polymorphism in humans, chimpanzees, and bonobos. *Mol. Biol. Evol.* 32 (5), 1186–1196. doi:10.1093/molbev/msv007

Wang, Z., Embaye, K. S., Yang, Q., Qin, L., Zhang, C., Liu, L., et al. (2021). Establishment and validation of a prognostic signature for lung adenocarcinoma based on metabolism-related genes. *Cancer Cell Int.* 21 (1), 219. doi:10.1186/s12935-021-01915-x

Wu, P., Wang, Y., Wu, Y., Jia, Z., Song, Y., and Liang, N. (2019). Expression and prognostic analyses of ITGA11, ITGB4 and ITGB8 in human non-small cell lung cancer. *PeerJ* 7, e8299. doi:10.7717/peerj.8299

Xiong, J., Yan, L., Zou, C., Wang, K., Chen, M., Xu, B., et al. (2021). Integrins regulate stemness in solid tumor: An emerging therapeutic target. *J. Hematol. Oncol.* 14 (1), 177. doi:10.1186/s13045-021-01192-1

Yao, Z., Yoon, S., Kalie, E., Raviv, Z., and Seger, R. (2010). Calcium regulation of EGF-induced ERK5 activation: Role of lad1-MEKK2 interaction. *PLoS One* 5 (9), e12627. doi:10.1371/journal.pone.0012627

Yurchenco, P. D. (2011). Basement membranes: Cell scaffoldings and signaling platforms. *Cold Spring Harb. Perspect. Biol.* 3 (2), a004911. doi:10.1101/cshperspect.a004911

Zhao, R., Ding, D., Ding, Y., Han, R., Wang, X., and Zhu, C. (2022). Predicting differences in treatment response and survival time of lung adenocarcinoma patients based on a prognostic risk model of glycolysis-related genes. *Front. Genet.* 13, 828543. doi:10.3389/fgene.2022.828543

Zheng, Y., de la Cruz, C. C., Sayles, L. C., Alleyne-Chin, C., Vaka, D., Knaak, T. D., et al. (2013). A rare population of CD24(+)ITGB4(+)Notch(hi) cells drives tumor propagation in NSCLC and requires Notch3 for self-renewal. *Cancer Cell* 24 (1), 59–74. doi:10.1016/j.ccr.2013.05.021

frontiers | Frontiers in Pharmacology

TYPE Original Research
PUBLISHED 07 September 2023
DOI 10.3389/fphar.2023.1236655

OPEN ACCESS

EDITED BY
Peixin Dong,
Hokkaido University, Japan

REVIEWED BY
Xiao Song,
Northwestern University, United States
Tianyue Zhai,
Hokkaido University, Japan
Jiaqi Li,
Macau University of Science and Technology, Macao SAR, China

*CORRESPONDENCE
Lianmin Zhang,
zhanglianmin1031@163.com
Zhenfa Zhang,
zhangzhenfa1973@163.com

†These authors have contributed equally to this work

RECEIVED 08 June 2023
ACCEPTED 23 August 2023
PUBLISHED 07 September 2023

CITATION
Zhang M, Xiao Z, Xie Y, Li Z, Zhang L and Zhang Z (2023), A cuproptosis-related lncRNA signature-based prognostic model featuring on metastasis and drug selection strategy for patients with lung adenocarcinoma.
Front. Pharmacol. 14:1236655.
doi: 10.3389/fphar.2023.1236655

A cuproptosis-related lncRNA signature-based prognostic model featuring on metastasis and drug selection strategy for patients with lung adenocarcinoma

Mengzhe Zhang[1†], Zengtuan Xiao[1,2†], Yongjie Xie[3], Zekun Li[3], Lianmin Zhang[1*] and Zhenfa Zhang[1*]

[1]Department of Lung Cancer Surgery, Tianjin Lung Cancer Center, Tianjin Medical University Cancer Institute and Hospital, National Clinical Research Center for Cancer, Key Laboratory of Cancer Prevention and Therapy, Tianjin's Clinical Research Center for Cancer, Tianjin, China, [2]Department of Immunology, Biochemistry and Molecular Biology, Collaborative Innovation Center of Tianjin for Medical Epigenetics, Tianjin Medical University, Tianjin, China, [3]Department of Pancreatic Cancer, Tianjin Medical University Cancer Institute and Hospital, National Clinical Research Center for Cancer, Key Laboratory of Cancer Prevention and Therapy, Tianjin's Clinical Research Center for Cancer, Tianjin, China

Introduction: Lung adenocarcinoma is a common cause of mortality in patients with cancer. Recent studies have indicated that copper-related cell death may not occur in the same way as previously described. Long non-coding RNAs (lncRNAs) play a key role in the occurrence and development of tumors; however, the relationship between cuproptosis and lncRNAs in tumorigenesis and lung adenocarcinoma (LUAD) treatment has not been well established. Our study aimed to construct a model to analyze the prognosis of lung adenocarcinoma in patients using a carcinogenesis-related lncRNA (CR) signature.

Methods: The transcriptional profiles of 507 samples from The Cancer Genome Atlas were assessed. Cox regression and co-expression analyses, and the least absolute shrinkage and selection operator (LASSO) were used to filter the CR and develop the model. The expression status of the six prognostic CRs was used to classify all samples into high- and low-risk groups. The overall disease-free survival rate was compared between the two groups. The Gene Ontology and the Kyoto Encyclopedia of Genes and Genomes were used to identify the pathways and mechanisms involved in this model. Subsequently, immunotherapy response, sensitivity, and correlation analyses for several anti-tumor medications were performed. *In vitro* experiments, including qPCR, were conducted in nine lung adenocarcinoma cell lines and 16 pairs of lung adenocarcinoma and para-carcinoma tissues.

Results: After confirmation using the ROC curve, patients in the low-risk category benefited from both overall and disease-free survival. Gene Ontology analysis highlighted cell movement in the model. In the *in vitro* experiments, qPCR results showed the expression levels of six CRs in 16 pairs of carcinoma and para-carcinoma tissues, which were in accordance with the results of the model. AL138778.1 is a protective factor that can weaken the invasion and migration of A549 cells, and AL360270.1 is a hazardous factor that promotes the invasion

and migration of A549 cells. According to this model, targeted treatments such as axitinib, gefitinib, linsitinib, pazopanib, and sorafenib may be more appropriate for low-risk patients.

Conclusion: Six CR profiles (AL360270.1, AL138778.1, CDKN2A-DT, AP003778.1, LINC02718, and AC034102.8) with predictive values may be used to evaluate the prognosis of patients with lung adenocarcinoma undergoing therapy.

KEYWORDS

lung cancer, cuproptosis, lung adenocarcinoma, lncRNA, prognostic model, biofunction, anti-cancer drug, metastasis

1 Introduction

Lung adenocarcinoma (LUAD) is a malignancy of the respiratory system and is highly prevalent worldwide (Sequist et al., 2013). To better understand and develop more therapeutic mechanisms for patients with LUAD, researchers have established risk models to classify patients and implement proper treatment plans and drug selection strategies (Gautschi et al., 2020). Copper (Cu) elements are involved in various biological functions (van den Berghe and Klomp, 2009). Recent studies have revealed that Cu concentrations are strongly enriched in tumor tissues when compared to that of normal tissues (Tsang et al., 2020). Negative effects, such as cancer pathogenesis, have been associated with high concentrations of Cu that exceed the threshold (Ishida et al., 2013). Dysregulation of Cu has been linked to cancer development (Sciegienka et al., 2017). Cu-based promoters and antagonists have therefore been used as anti-tumor agents (Brady et al., 2017). It has been noted that Cu molecules bind compactly to the tricarboxylic acid cycle, resulting in the

TABLE 1 The basic characteristic of the samples (age, gender, and TNMstage) in our baseline analysis. Data were presented as numbers (Percentage %).

Characteristics	Type	Total (n = 507)	Test group (n = 168)	Training group (n = 339)	*p*-Value
Age	≤65	239 (47.14%)	72 (42.86%)	167 (49.26%)	0.1378
	>65	258 (50.89%)	95 (56.55%)	163 (48.08%)	
	Unknown	10 (1.97%)	1 (0.6%)	9 (2.65%)	
Gender	Female	272 (53.65%)	89 (52.98%)	183 (53.98%)	0.9051
	Male	235 (46.35%)	79 (47.02%)	156 (46.02%)	
TNM Stage	I	272 (53.65%)	88 (52.38%)	184 (54.28%)	0.5459
	II	120 (23.67%)	38 (22.62%)	82 (24.19%)	
	III	81 (15.98%)	32 (19.05%)	49 (14.45%)	
	IV	26 (5.13%)	7 (4.17%)	19 (5.6%)	
	Missing/unknown	8 (1.58%)	3 (1.79%)	5 (1.47%)	
T stage	T1	169 (33.33%)	57 (33.93%)	112 (33.04%)	0.9926
	T2	271 (53.45%)	88 (52.38%)	183 (53.98%)	
	T3	45 (8.88%)	15 (8.93%)	30 (8.85%)	
	T4	19 (3.75%)	6 (3.57%)	13 (3.83%)	
	Unknown	3 (0.59%)	2 (1.19%)	1 (0.29%)	
N stage	N0	327 (64.5%)	104 (61.9%)	223 (65.78%)	0.6264
	N1	95 (18.74%)	33 (19.64%)	62 (18.29%)	
	N2	71 (14%)	26 (15.48%)	45 (13.27%)	
	N3	2 (0.39%)	0 (0%)	2 (0.59%)	
	Unknown	12 (2.37%)	5 (2.98%)	7 (2.06%)	
M stage	M0	338 (66.67%)	114 (67.86%)	224 (66.08%)	0.7141
	M1	25 (4.93%)	7 (4.17%)	18 (5.31%)	
	Unknown	144 (28.4%)	47 (27.98%)	97 (28.61%)	

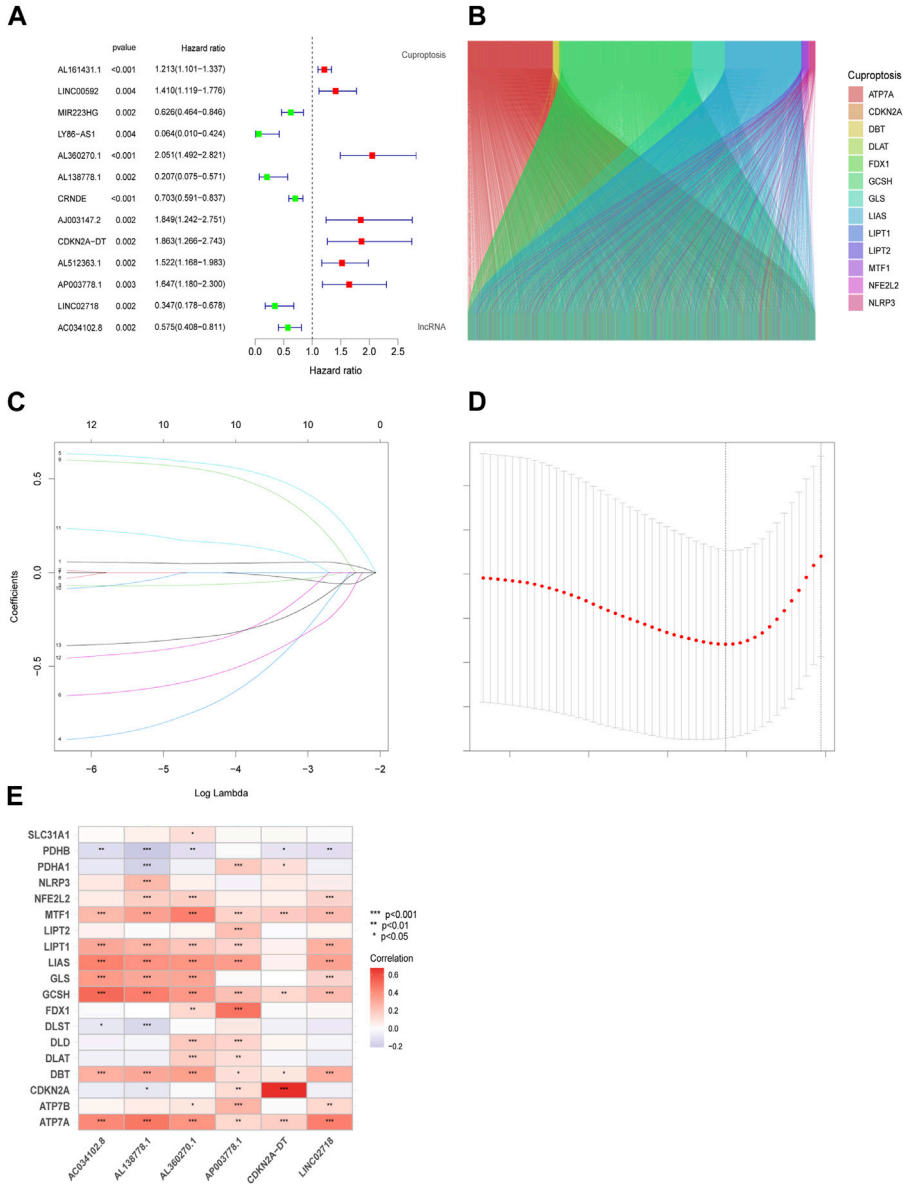

FIGURE 1
Prognostic features in the identification of Cuproptosis-associated lncRNA (CR). Thirteen eligible CRs with a $p < 0.05$ were chosen by uniforest plot **(A)**. The Sankey diagram revealed the corelation in cuproptosis genes and CRs **(B)**. Variable selection based on 10-fold cross-validation with the least absolute shrinkage and selection operator (LASSO) algorithm **(C)**. Coefficient LASSO patterns for CRs **(D)**. Heatmap of the corelation between CRs and CGs in risk models **(E)**.

accumulation of toxic proteins and cell death (Solmonson et al., 2022). A previous study also demonstrated that cuproptosis-related genes (CG) could induce many cell-related pathways, including apoptosis, autophagy and anti-angiogenesis (Xie et al., 2023). DNA is extensively transcribed and produces many long non-coding RNAs (lncRNAs). These lncRNAs are more than 200 nucleotides in length and are not translated into functional proteins. LncRNAs regulate the biological behavior of cancer cells and are associated with the pathogenesis and progression of various cancers (Zhang et al., 2022). Several reports have demonstrated that lncRNAs are associated with cuproptosis. The genes and lncRNAs involved in this process have been identified, and this has led to further exploration into their roles in neoplasm development and invasion via transcriptional modifications (Loewen et al., 2014). Emerging evidence suggests that the dysregulation of lncRNAs in LUAD is widely involved in tumor cell proliferation, invasion, and metastasis, as well as shaping the TME (Cobine and Brady, 2022). Studying cuproptosis-related lncRNAs may provide further insight into the role of this pathway in cancer including the PI3K/AKT, NF-κB, p53, and Notch pathways (Ritchie et al., 2015). Additionally, lncRNAs are largely associated with drug resistance in tumors (Dong et al., 2019). Whether lncRNAs are related to tumor invasion and migration remains unclear, and the pathways should be explored. In this study, we analyzed the cuproptosis-related genes (CG) in LUAD. We also generated a model of carcinogenesis-related lncRNAs (CR) to predict the prognosis of LUAD.

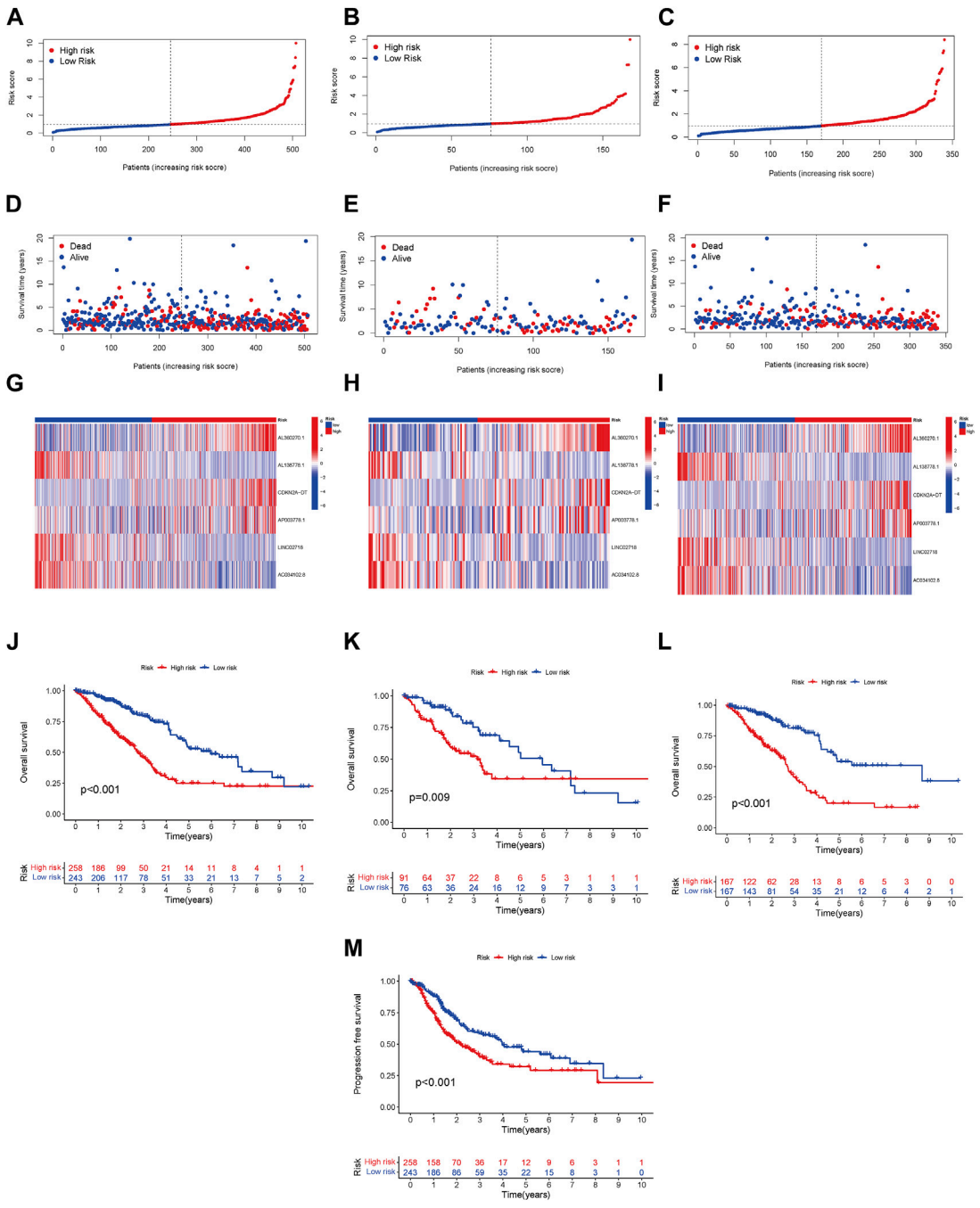

FIGURE 2
Prognosis model linked with risk in LRG and HRG. The overall survival (OS) risk scores (including all samples, test, and training groups) **(A–C)**. Survival characteristics in three cohorts (including all samples, test, and training groups) **(D–F)**. The heatmaps of 6 lncRNA expressions, (including all samples, test, and training groups) **(G–I)**. The LUAD patients' OS in three cohorts (including all samples, test, and training groups) **(J–L)**. The LUAD patients' PFS in all samples **(M)**.

2 Materials and methods

2.1 Data collection and identification of CRs

We extracted data from The Cancer Genome Atlas (TCGA) and GEO datasets using Perl (version 5.30.0–64 bit). The software R (version 4.0.1) and GraphPad Prism (version 8.0.2) were used for data analysis.

2.2 Creation and validation of cuproptosis-related lncRNAs

The lncRNAs in the CGs were screened using the Pearson correlation method. The candidate CR ($p < 0.05$) was selected for further analysis. Univariate Cox regression analysis was conducted to identify lncRNAs that were linked to the prognosis. These lncRNAs were mapped by the "limma," for the classifying the

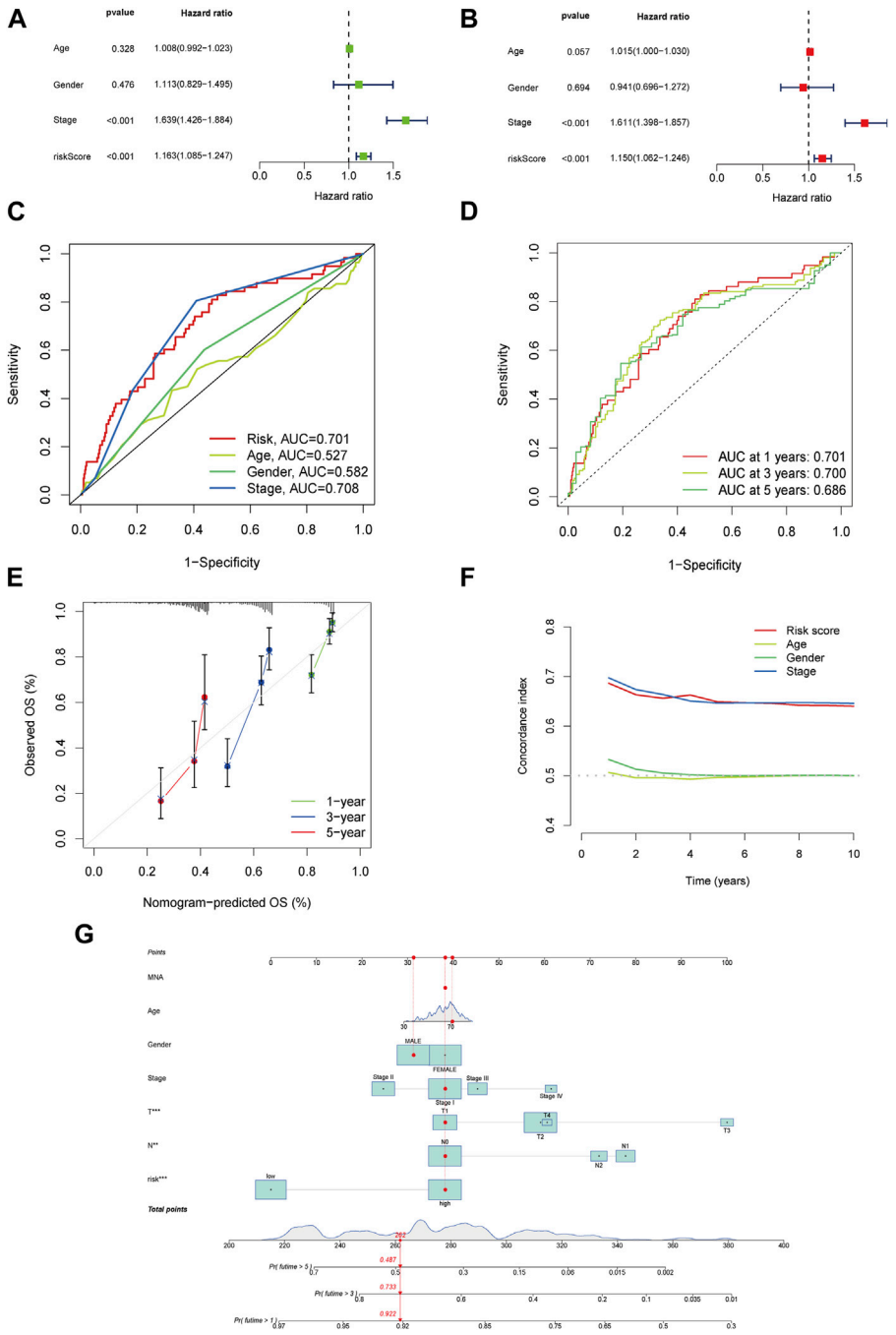

FIGURE 3
The risk model's accuracy and the nomogram's validation. Univariate analysis for the clinical features compared with the risk score **(A)**. Multivariate analysis for risk scores and clinical characteristics **(B)**. ROC curves summarized the risk characteristic for 1 year, 3 years, and 5 years **(C)**. ROC curves' characteristics in age, sex, and stage in the clinical model **(D)**. Calibration curves test the accuracy in this model at 1 year, 3 years, and 5 years **(E)**. Zero-10 years' C-index curve **(F)**. A nomogram shows 1 year, 3 years, and 5 years' OS in LUAD patients based on risk scores along with clinicopathological characteristics **(G)**.

lncRNAs; "ggplot2," for drawing the graph; "heatmap," for classifying the CRs; "survminer," for survival analysis and visualization; "timeROC," for calculating the cut-off point and the area; and "caret" packages for model prediction and testing. By applying the least absolute shrinkage and selection operator (LASSO) analysis to these lncRNAs, we identified the most suitable group of prognostic lncRNAs. After multi-Cox regression analysis, we established a 6-lncRNAs-risk model as follows (Eq. (1)):

$$\text{Risk score} = \sum i = lnCoef\,(i) \times Expr\,(i) \quad (1)$$

where Coef (i) refers to each lncRNA's regression coefficient in the multiple Cox regression analysis, and Expr (i) refers to each

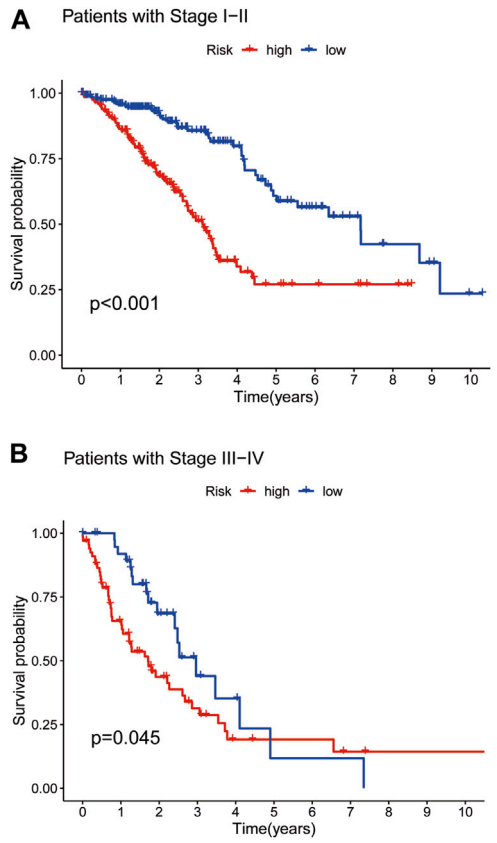

FIGURE 4
The Kaplan–Meier survival curves in low- and high-risk populations by TNMstage. Analysis of OS of patients with stage I–II in two groups **(A)**. Analysis of OS of patients with stage III–IV in two groups **(B)**.

lncRNA's normalized expression level. We categorized the above-mentioned lncRNAs into a low-risk group (LRG) with a hazard ratio (HR) < 1 and a high-risk group (HRG) with an HR > 1.

2.3 Construction of nomogram and calibration

The 1-, 3-, and 5-year overall survival (OS) in all samples was presented by figures drawn using the "survival," for analyzing the survival of the cases, "regplot," for fitting the regression model and "rms," for significance analysis of output variables. We applied risk scores to different clinicopathological factors, and a calibration curve was drawn according to the Hosmer-Lemeshow method.

2.4 Principal component, Gene Ontology, and KEGG analyses

To observe the different spatial distributions in the LRG and HRG, we used principal component analysis (PCA) to investigate the expression status of CRs in patients with LUAD. Firstly, we applied the Gene Ontology (GO) analysis (GO; http://www.geneontology.org/) by using "clusterProfiler" for gene enrichment; "colorspace" "stringi", "ggplot2", "CRclize" and "RcolorBrewer" for drawing the circle-map. Finally, we showed the difference of cellular components, molecular functions, and molecular biological processes. The Kyoto Encyclopedia of Genes and Genomes (KEGG; http://www.genome.jp/kegg/) pathways that were differentially expressed were analyzed by using "clusterProfiler", "enrichplot", "ggplot2", "dplyr" and "ComplexHeatmap". We considered the enriched biological functions, processes, and pathways significant when $p < 0.05$.

2.5 Tumor-immune-related function analysis

We determined the immune infiltration profile by using the "limma," for processing the gene expression matrix and "BiocManager" for visualization of data.

2.6 Tumor mutational burden and therapeutic drug correlation sensitivity analysis

Pearl was used to download the mutation data. "Map tools" was used to capture the mutational characteristics of the tumor mutational burden (TMB) and survival in LRG and HRG. All Tumor Immune Dysfunction and Exclusion (TIDE) files were obtained from http://tide.dfci.harvard.edu. We utilized "pRRophetic" for predicting the correlation between the half-limiting dose (IC50 values) and the risk scores. Finally, the sensitivity of the suitable treatment drugs was determined.

2.7 Validation of CRs under *in vitro* conditions

Based on the transcriptional sequences of the six lncRNAs, six qPCR primers were designed for each. All the sequences for these CRs have been explained below (5′-3′):

AL360270.1 F: CAGTCATACCACCCTGAACAC.
R: GGATTAACCAGGCCCAACC.
AL138778.1 F: AGTCTGCAGGAGAAATGACTGG.
R: AAAAGTGCCTTGGCAAGCAG.
CDKN2A-DT F: AGCGTGGACAGGAGCATCTC.
R: GGCTGTGAGGTTGCGAATGAC.
AP003778.1 F: TAGGTTATCTGGCAGCAACTTCAC.
R: GCACTTACTCCATTCACGCATTC.
LINC02718 F: AGCCGACTGTGGGACCTTG.
R: GCATCTGCTCCTTCCATCTTCTAC.
AC034102.8 F: GTGGTGGTGTGGCTCATTGTG.
R: TGGCTCCTGTGGCTGTATCTG.
GAPDH F: GGTGGTCTCCTCTGACTTCAACA.
R: GTTGCTGTAGCCAAATTCGTTGT.

To validate the above CRs, we used 16 pairs of adenocarcinomas and their para-carcinoma tissues to determine the different expression levels of lncRNAs in this model.

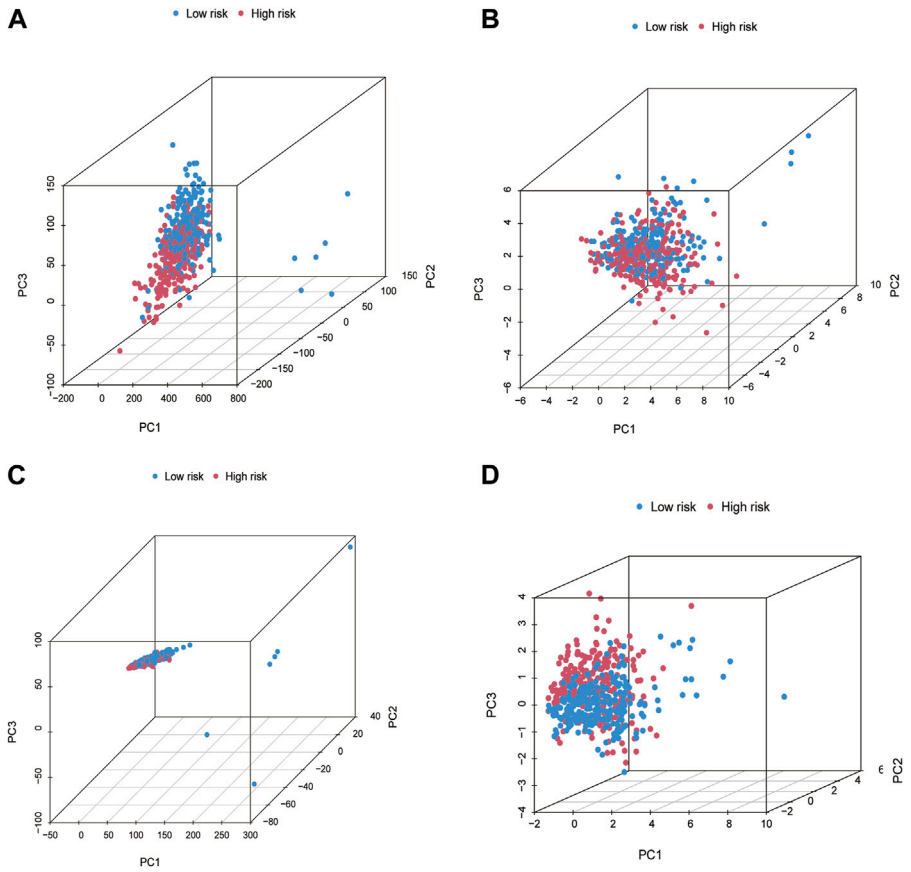

FIGURE 5
The principal component analysis (PCA) for patients in LRG and HRG. PCA in All genes **(A)**. Cuproptosis genes **(B)**. Cuproptosis-related lncRNAs **(C)**. Risk lncRNAs alone **(D)**.

For further confirmation, we selected nine types of adenocarcinomas in cell lines, including BEAS2B, A549, PC9, HCC827, H1299, H1650, H1975, H358, and H441. We selected the lowest and highest lncRNAs in our model to compare their relative expression levels in the 9 cell lines.

We isolated RNA from 16 pairs of tumors and para-carcinoma tissues. Information on the samples is shown in Supplementary Table S1. cDNA was prepared for CRs and GAPDH. Real-time qPCR was performed to determine the expression levels of the six lncRNAs in all samples. All staining was based on the SYBR Green Master (ROX, Roche; United States).

2.8 Cell culture and reagents

Human BEAS-2B (BEAS-2B was used for comparison), A549, PC9, HCC827, H1299, H1650, H1975, H358, and H441 cell lines were obtained from The American Type Culture Collection. Cells were maintained in Roswell Park Memorial Institute (RPMI) 1,640 medium (Gibco, United States) containing 10% fetal bovine serum (FBS) (Sigma, United States), streptomycin (50 g/mL) (Sigma, United States), and penicillin (100 U/mL) (Hyclone, United States). Cells were cultured in a incubator with 37°C humidified and 5% CO_2 incubator (SANYO, Japan).

2.9 Plasmid construction and lentivirus packaging

The AL138778.1 and AL360270.1 transcripts were cloned into the pCDH lentiviral vector, and lentiviral shRNAs targeting AL138778.1 and shRNA targeting AL360270.1 were obtained from Genechem (Shanghai, China). The lentiviral vectors were used according to the manufacturer's instructions.

2.10 RT-PCR analysis

RNAs were extracted from cells using TRIzol reagent (Invitrogen). After the synthesis of cDNA, RT-PCR was repeated three times. In order to determine whether targeted drugs could influence the expression of the six CRs, we performed axitinib (10 nM) incubations with the wild-type A549 cell line for 6 h in a 24-well plate and then performed qPCR to determine the change in the six lncRNAs (Wang et al., 2019).

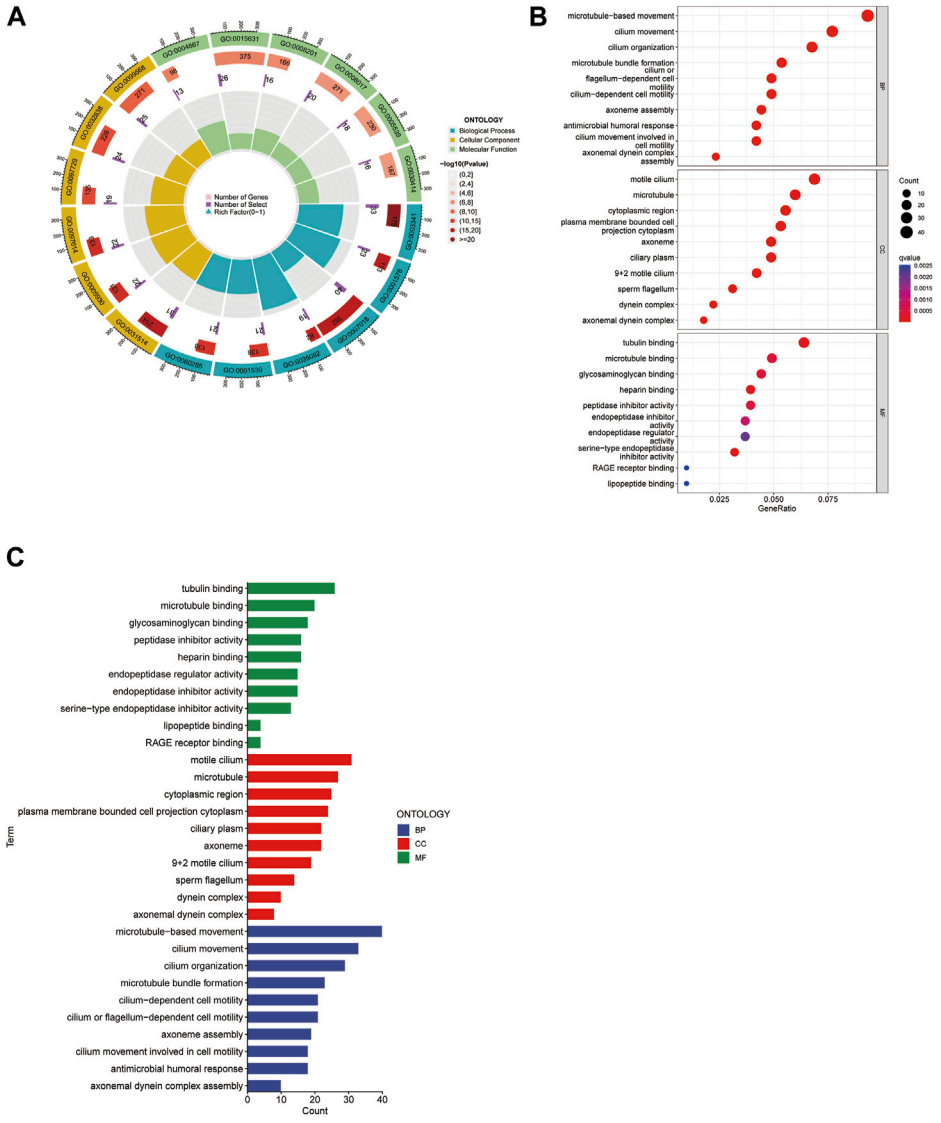

FIGURE 6
Gene Ontology (GO) analysis. The circle map presents the overview of the whole process **(A)**. The bubble map showed both the component and the **q** value **(B)**. It reveals predominant cellular components, molecular biological processes, and molecular functions **(C)**.

2.11 Scratch wound and transwell assay-the wound healing assay

We constructed the AL138778.1 knock-down and AL138778.1 control vector, and the AL360270.1 knock-down and AL138778.1 control vector in the A549 cell line. We then inoculated the cells (1×10^5/well) into a 24-well culture plate and cultivated them in an environment of 37°C, 5% CO_2 for 24 h. The culture solution was discarded, and a 10 μL pipette tip was used to scratch the inoculated cells. The cells were then gently washed twice with PBS, and 1 mL RPMI 1640 medium was added. A photograph of each scratch was taken at 0 and 24 h. Each experiment was conducted in 3-line parts and repeated five times. We measured and calculated the migration distance from the original site to the wounded area over 24 h. We placed the cells (5×10^4 cells/well) in a Matrigel plate well containing serum-free RPMI 1640 medium. The lower chamber was then filled with 500 μL of complete medium (RPMI 1640 with 10% FBS). The cells that did not pass the well were lightly cleaned with a cotton swab after incubation at 37°C for 24 h. Glutaraldehyde (5%) was then added in the lower chamber, and the cells were allowed to fix for 10 min. Crystal violet (1%) in 2% ethanol was used to stain the cells at room temperature (approximate temperature range from 15°C to 20°C) for 20 min. We used inverted microscope (OLYMPAS, Japan) to photograph five different sites and counted the numbers in a 10× view average for comparison.

2.12 Western blot analysis

We chose the following proteins that are closely related to migration in lung cancer (Bremnes et al., 2002): N-cadherin,

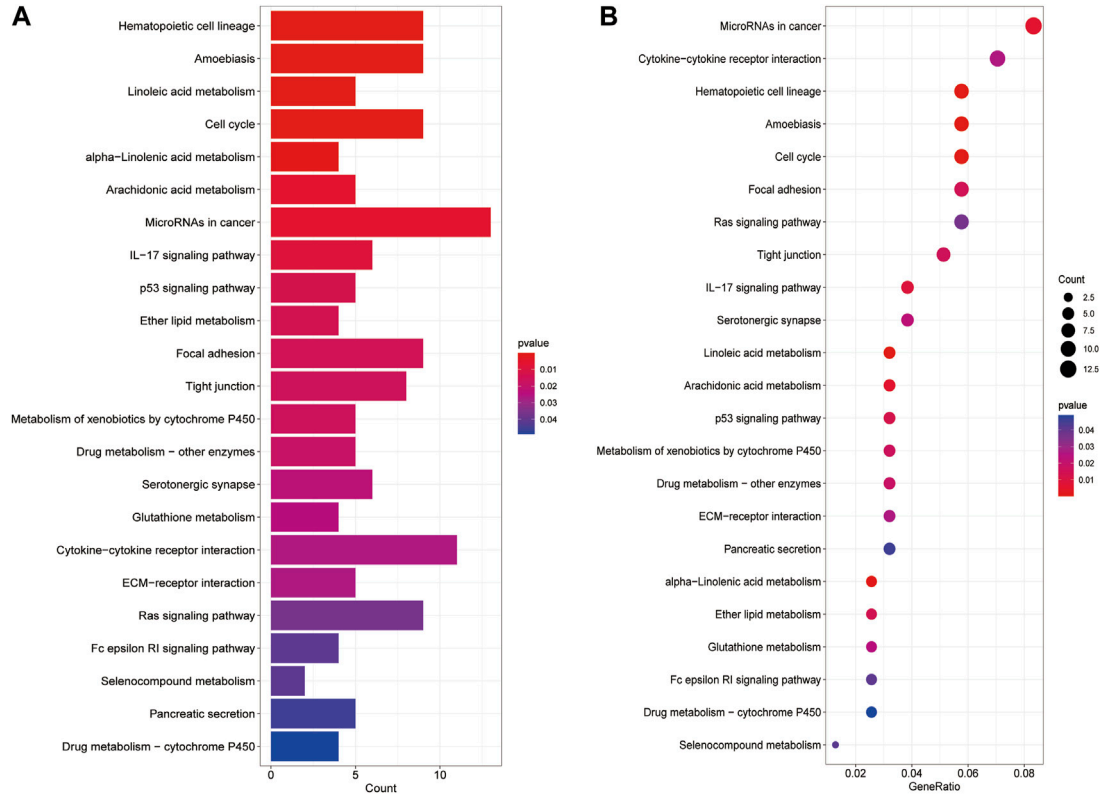

FIGURE 7
KEGG analysis shows significantly enriched KEGG pathways **(A, B)**.

E-cadherin, Vimentin, Snail, and Sox2. All data were normalized to those of GAPDH. We washed the cells three times with PBS, and then lysed them. After SDS-PAGE, the proteins were transferred onto polyvinylidene difluoride (PVDF) membranes by Western blotting. Skimmed milk (4%) was used to block the blots for 1 hour, and the primary monoclonal antibodies against the proteins (N-cadherin, E-cadherin, Vimentin, Snail, Sox2, and GAPDH) were added and incubated at 4°C overnight. Membranes were incubated with secondary antibodies (1: 1000 dilution) for 1 hour at room temperature. The membrane strips were then exposed to enhanced chemiluminescence and a fixer (1:1). The details of all the antibodies are shown in Supplementary Table S1.

3 Results

3.1 lncRNAs from Co-expressional cuproptosis-related genes

After risk score analysis, all LUAD cases in the test (n = 339) and training groups (n = 168) were separated into LRG and HRG. The basic clinical factors are presented in Table 1. A total of 16,876 lncRNAs from 19 cuproptosis-related genes (CG) were selected using Pearson correlation analysis. Univariate Cox regression analysis was used to identify the lncRNAs related to cuproptosis. Finally, 13 eligible CRs were selected ($p < 0.05$; Figure 1A). The co-expression network of LUAD is shown in Figure 1B. An expression heatmap of the six lncRNAs in the LRG and HRG is shown in Figure 1E.

3.2 Construction of the predictive signature

We used the "caret," "glmnet" to perform a LASSO analysis in the training group to choose lncRNAs that possessed the best prognostic value (Figures 1C,D). Using the results from Eq. (1), the value of each lncRNA was calculated (Eq. (2)):

$$\begin{aligned}\text{"risk scores"} = {} & \text{AL360270.1} \times (0.672984389012466) \\ & + \text{AL138778.1} \times (-0.998712907510809) + \text{"CDKN2A} \\ & - \text{DT"} \times (0.603568904030502) \\ & + \text{AP003778.1} \times (0.250123284609668) \\ & + \text{LINC02718} \times (-0.528689990460446) \\ & + \text{AC034102.8} \times (-0.472815056249193) \end{aligned} \quad (2)$$

We conducted a patient prognostic analysis for the LRG and HRG. In the three cohorts (all samples, test, and training groups), the risk scores were significantly higher in the HRG (Figures 2A–C). The survival time in the LRG was longer than that of the HRG in all three cohorts (Figures 2D,E). The heatmap shows the expression status and correlation of the six lncRNAs in the three cohorts. Patients in the LRG showed a negative relationship with the risk

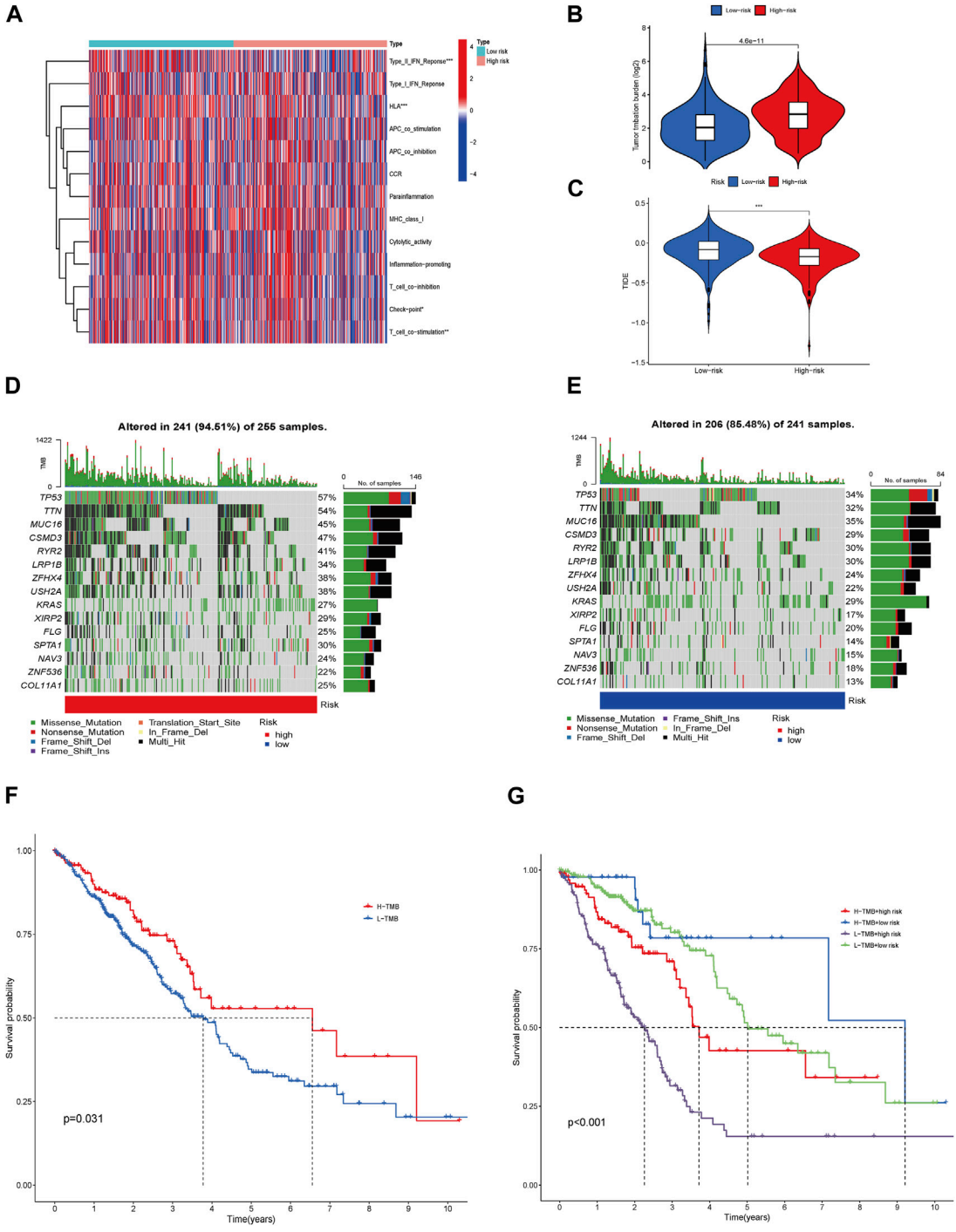

FIGURE 8
Immune-related function, Genetic alterations, TMB, TIDE, and Therapeutic Drug Sensitivity. Heatmap for various immune-related cells in LRG and HRG **(A)**. TMB in the LRG and HRG **(B)**. TIDE in the two groups **(C)**. Waterfall plots described the somatic mutation features in HRG **(D)**. Waterfall plots described the somatic mutation features in LRG **(E)**. Kaplan–Meier survival curves between low- and high-TMB groups **(F)**. The Kaplan–Meier survival curves between the 4 groups **(G)**.

factors AL360270.1, CDKN2A-DT, and AP003778.1. In contrast, patients in the HRG showed a positive relationship with these factors (Figures 2G,H). Patients in the LRG had a better OS than those in the HRG in all groups (Figures 2J–L). Patients in the LRG also benefited from improved progression-free survival (PFS) compared to those in the HRG (Figure 2M).

3.3 The risk score presented an indicative value in this signature

Based on the Cox regression analysis, the risk score was more efficient than other characteristics ([analysis of univariation: HR = 1.163, 95% CI = 1.085–1.247, $p < 0.001$] and [analysis of

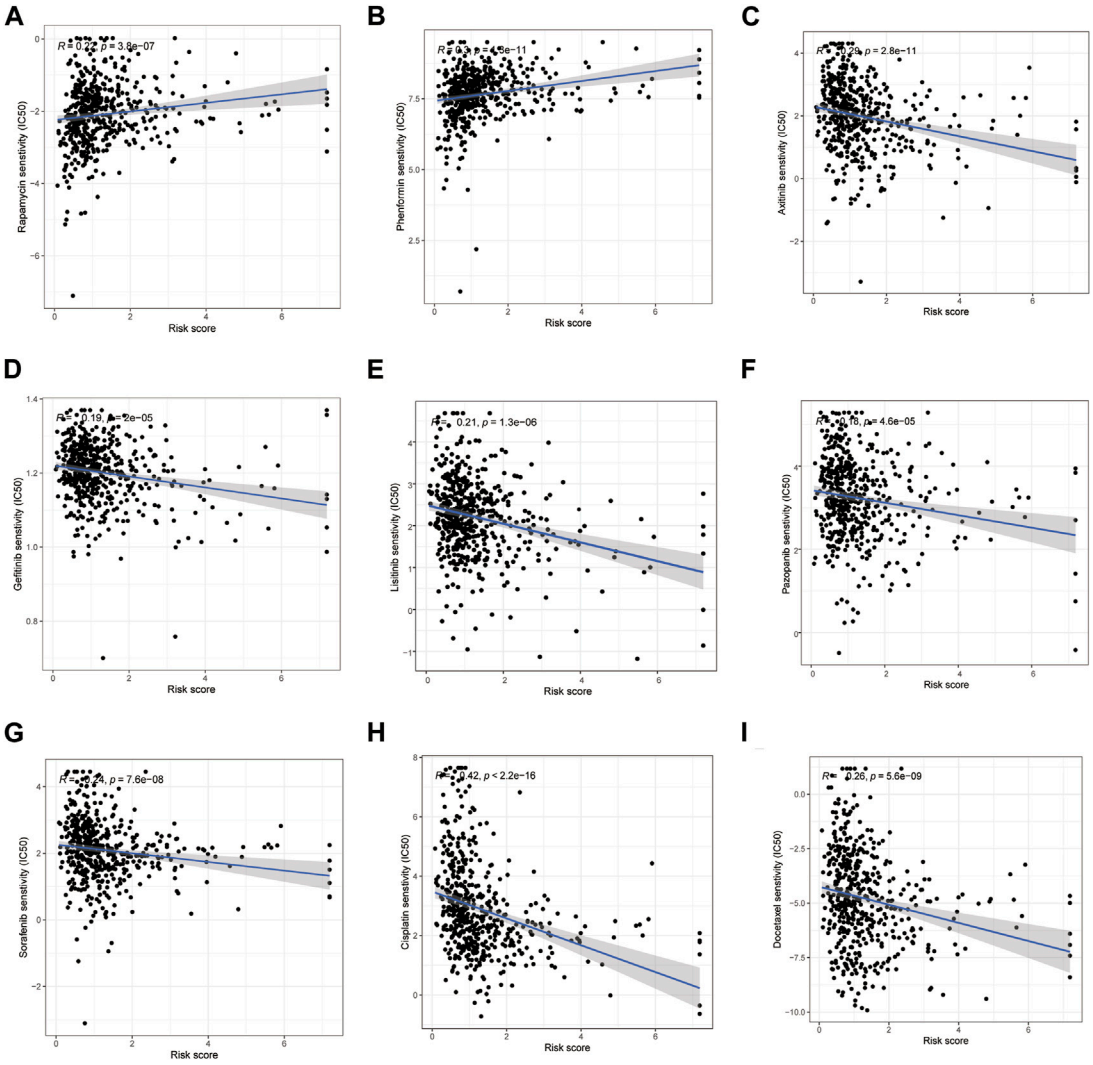

FIGURE 9
Correlation between the risk score and drug sensitivity. Drugs owned positive relation with the risk scores **(A, B)**. Drugs owned a negative relation with the risk scores **(C–I)**.

multivariation: HR = 1.150, 95% CI = 1.062–1.246, $p < 0.001$]), as shown in Figures 3A,B. The ROC curve also highlighted the sensitivity and specificity of the risk score, which was more efficient than those of age and sex (Figure 3C; risk score: AUC = 0.701). Similarly, the model presented a predictive value with high sensitivity (Figure 3D; AUC of 1 year = 0.701, AUC of 3 years = 0.700, and AUC of 5 years = 0.686).

3.4 Validation and accuracy of the risk model and nomogram

The calibration curves agreed well with the predictors and nomogram (Figure 3E). In the risk model, the C-index was higher than age and sex, especially in the 8th –10th years (Figure 3F). All samples at one, three, and 5 years were included in the nomogram and combined with their characteristics and risk scores (Figure 3G). In addition, the ROC and nomogram analyses demonstrated the accuracy of the signature.

3.5 Survival curves based on TNM stage

To further validate survival, we divided patient prognosis into stages (stages I–II and stages III–IV) for the survival probability analysis. The LRG benefited more than the HRG (Figures 4A,B; $p < 0.001$, $p = 0.045$, respectively).

3.6 Establishment and presentation of the principal component analysis

We used PCA to determine all gene expression profiles, CR and cuproptosis genes, and risk model lncRNAs in both groups.

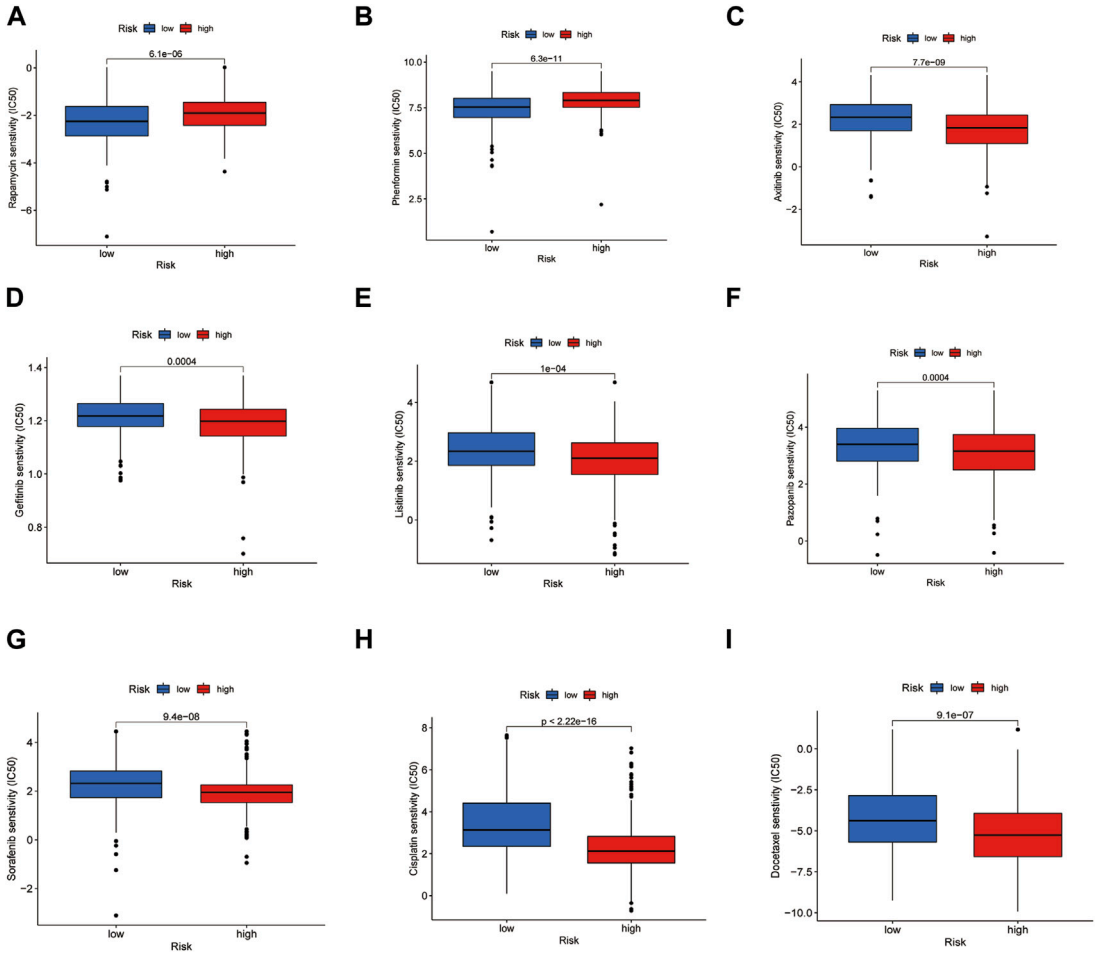

FIGURE 10
Drug sensitivity in LRG and HRG. Drugs were suitable for the HRG **(A, B)**. Drugs were suitable for the LRG **(C–I)**.

The outcomes indicated that all six CRs had the ability to differentiate between the LRG and HRG. The connection distance of each sample is large, and the sample composition is different (Figures 5A–D).

3.7 Analysis of biological pathways

We analyzed biological pathways using the GO and KEGG databases to demonstrate the different functions of cuproptosis-related genes (CGs). In GO analysis, the biological procedures, and functions of CGs mainly included tubulin binding, motile cilia in Molecular Function (MF) microtubules in Cellular Component (CC), microtubule-based movement, and cilium movement in Biological Process (BP) (Figures 6A–C). In the KEGG pathway enrichment analysis, the genes were predominantly involved in lipopeptide binding, RAGE receptor binding, endopeptidase regulatory activity, and endopeptidase inhibitors. In addition, arachidonic acid metabolism, linoleic acid metabolism, the p53 signaling pathway, and the metabolism of xenobiotics by cytochrome P450 also showed strong relevance to the model (Figures 7A,B).

3.8 Analysis of immune-related function, genetic alterations, TMB, TIDE, and sensitivity of the therapeutic drug

The immune-related functions are shown in a heatmap (Figure 8A); the inflammation-promoting, T cell co-inhibition, and immune checkpoint processes demonstrated a negative correlation in the HRG and a positive correlation in the LRG, whereas the difference in other immune cell types was small but not discrepant. The tumor mutation burden in HRG was higher than that in LRG, indicating a chemotherapy limitation for HRG (Figure 8B). The TIDE scores were higher in the LRG than in the HRG (Figure 8C); therefore, immunotherapy may not be appropriate for the LRG. Different somatic mutation changes were analyzed, and 15 highly mutated genes were selected. Mutations in TP53, TTN, MUC16, and CSMD3 are the most frequent in LUAD. Patients in the HRG presented with a higher TMB (94.51%) than those in the LRG (85.48%) (Figures 8D,E). Patients with a high TMB may benefit from 10 years of survival ($p = 0.031$). LRG patients with high TMB had the best OS, whereas HRG patients with low TMB had the worst 10-year OS ($p < 0.001$) (Figures 8F,G).

By comparing the drug sensitivities, differences were found in the half-limiting doses of LRG and HRG for several drugs. The sensitivities of

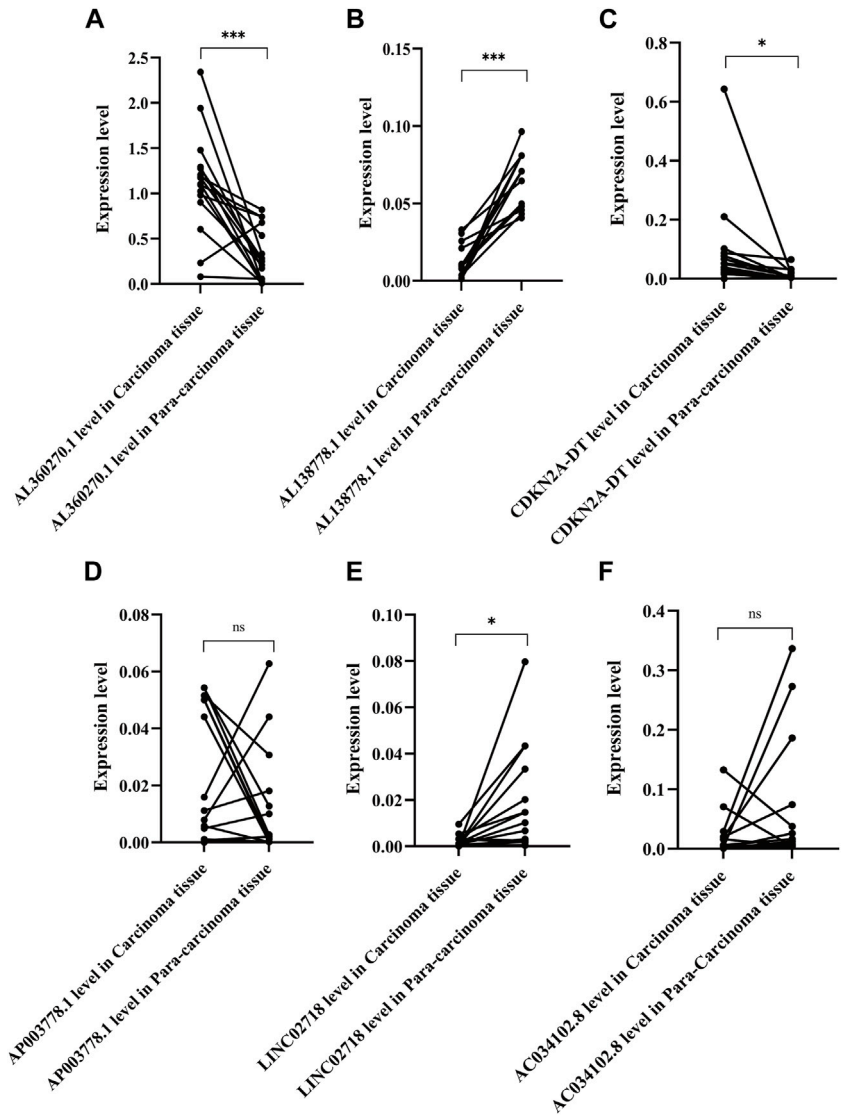

FIGURE 11
Expression level of the six lncRNAs of the model in 16 pair of adenocarcinoma and their para-carcinoma tissue. ***: **: $p < 0.001$, $p < 0.01$, ns: non-significant. **(A)**. Expression level of AL360270.1 in carcinoma and para-carcinoma tissue (C/P); **(B)**. Expression level of AL138778.1 in (C/P); **(C)**. Expression level of CDKN2A-DT in (C/P); **(D)**. Expression level of AP003778.1 in (C/P); **(E)**. Expression level of LINC02718 in (C/P); **(F)**. Expression level of AC034102.8 in (C/P).

the drugs in the two groups are shown in Figure 9. Among these drugs, rapamycin and phenformin showed a positive correlation with a higher risk score (Figures 9A,B) and greater sensitivity in the HRG (Figures 10A,B). However, targeted drugs such as axitinib, gefitinib, linsitinib, pazopanib, and sorafenib, and chemotherapeutic drugs such as cisplatin and docetaxel showed a negative correlation with higher risk scores (Figures 9C–I). These drugs were more effective in the LRG (Figures 10C–I).

3.9 Confirmation experiments

We chose 16 pairs of adenocarcinomas and their para-carcinoma tissues to perform qPCR, which was tissue preservation solution. Basic and clinical characteristics of the 16 adenocarcinoma pairs were shown in Supplementary Table S1. The highest risk factor, AL360270.1, was expressed at higher levels in tumor tissues than in para-carcinoma tissues ($p < 0.001$) (Figure 11A). The protective factor AL138778.1 was significantly lower in tumor tissue than in para-carcinoma tissue (Figure 11B; $p < 0.001$). The expression of CDKN2A-DT was higher in tumor tissues than in normal tissues (Figure 11C; $p < 0.05$). The expression of LINC02718 was lower in tumor tissues than in para-carcinoma tissues (Figure 11E; $p < 0.05$). These four factors showed the same trend in differential expression as in the model. However, AP003778.1 and LINC02718 did not show any differential expression patterns in the sample test (Figures 11D,F).

According to the GO analysis, we found that the risk factors were closely related to cell movement and potential migration trends; therefore, we conducted a relative analysis of these six lncRNAs.

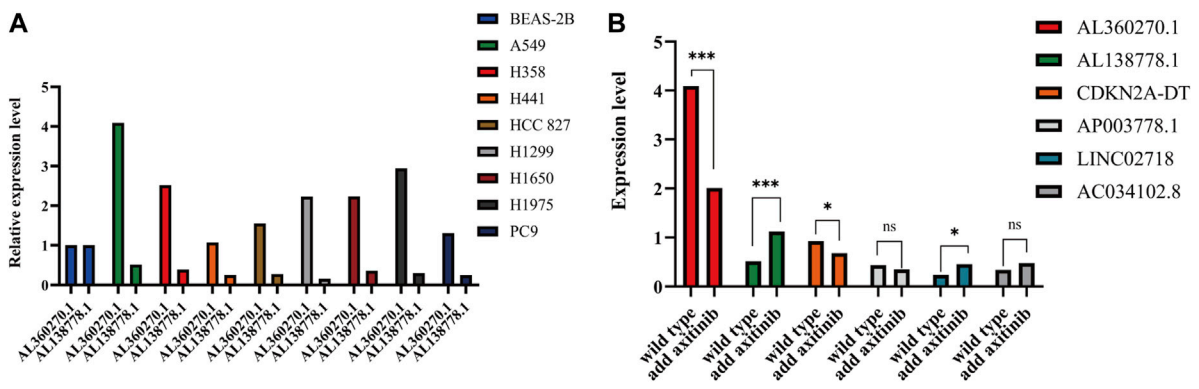

FIGURE 12
(A). Expression level of AL138778.1 and AL360270.1 in 9 lung adenocarcinoma cell lines. **(B)**. In A549 cell line, the expression level of 6 lncRNAs grouped by wild and treated with axitinib.

AL138778.1 × (−0.998712907510809) and AL360270.1 × (0.672984389012466) were the most protective and malignant factors in our model. As for AL138778.1, a lower expression level was observed in tumor tissues than in para-carcinoma tissues. We selected nine LUAD cell lines, BEAS-2B, A549, PC9, HCC827, H1299, H1650, H1975, H358, and H441, to perform RT-qPCR and compare the expression levels of these two factors (Figure 12A). All the cell lines showed a higher expression level of AL360270.1 and a lower expression level of AL138778.1 than that of the BEAS-2B cell line.

To further confirm the selection of the potential target drug, we applied axitinib (10 nM) to wild-type A549 cells for 6 h in 24-well plates and then performed qPCR to determine the changes in the six lncRNAs. The results showed that AL360270.1, and AL138778.1, mutated significantly when compared to the wild type, which lowered the risk aspect. This trend was consistent with the model (Figure 12B).

The A549 cell line showed the highest expression levels (Figure 12A). Therefore, we chose to perform scratch wound and Transwell assays by knocking down AL138778.1, and AL360270.1. We constructed the AL138778.1 knock-down cell line that was compared with the AL138778.1 control cell line, and the AL360270.1 knock-down cell line that was compared with the AL360270.1 control cell line.

After 24 h, the AL138778.1 knock-down cell line showed more migration ability than the control (Figure 13A). The relative migration rate = (migrated cell surface area/total surface area)×100. The relative migration rate was 46.08% vs. 12.75% ($p < 0.001$). A clear difference was observed (Figure 13B). Additionally, after 24 h, the AL360270.1 knock-down cell line showed less migration ability than the control (Figure 13A) The relative migration rate was 8.52% vs 23.98% ($p < 0.001$). A clear difference was observed (Figure 13D).

In the Transwell experiments, we found a significant difference between AL138778.1 knock-down and the control cell lines after 24 h of cultivation (Figure 13A). The AL138778.1 knockdown group showed a higher cell number on the Matrigel side than that of the control group (735 vs 452, $p < 0.001$) at ×10 magnification, indicating that AL138778.1 can protect the migration and metastasis of the tumor to some extent (Figure 13C).

In the Transwell experiments for AL360270.1 knock-down and its control set, a significant difference existed after 24 h of cultivation (Figure 13A). The AL360270.1 knock-down group showed fewer cells on the Matrigel side than that of the control group (326 vs 511, $p < 0.001$) at ×10 magnification. The results also indicated that AL360270.1 promotes tumor migration and metastasis (Figure 13E).

To further confirm this conclusion, we analyzed five protein factors related to CGs (Supplementary Figure S1). In the AL138778.1 knockdown group, there were higher expression levels of N-cadherin, Vimentin, Snail, and Sox2 and a lower expression level of E-cadherin than in the AL138778.1 control group (Figure 14). These results imply that the AL138778.1 knock-down cell line was more likely to metastasize than the AL138778.1 control cell line. In the AL360270.1 knock-down group, there was a lower expression level of N-cadherin, Vimentin, Snail, and Sox2, and a higher expression level of E-cadherin than in the AL360270.1 control group (Figure 14). These results indicated that the AL360270.1 knockdown group was less likely to metastasize than the AL360270.1 control group.

4 Discussion

A higher accumulation of Cu in cells can lead to severe consequences (Kim et al., 2008). Nevertheless, it has been reported that it is feasible to control normal intracellular Cu levels to selectively damage tumor cells (Masaldan et al., 2018). Several genes identified in this study, such as CDKN2A and ATP7A, have confirmed the feasibility of anti-tumor therapy in previous research. For example, the gene CDKN2A screened from TCGA, was shown to suppress tumor proliferation and influence cell cycle control (Rayess et al., 2012). The Cu transporter ATP7A is vital for the activation of lysyl oxidase (LOX) enzymes. Silencing ATP7A can inhibit LOX activity, which may trigger the loss of LOX-dependent metastatic mechanisms (Shanbhag et al., 2019).

However, intracellular Cu levels are related to metabolic and transportation mechanisms (Cobine and Brady, 2022). Studies

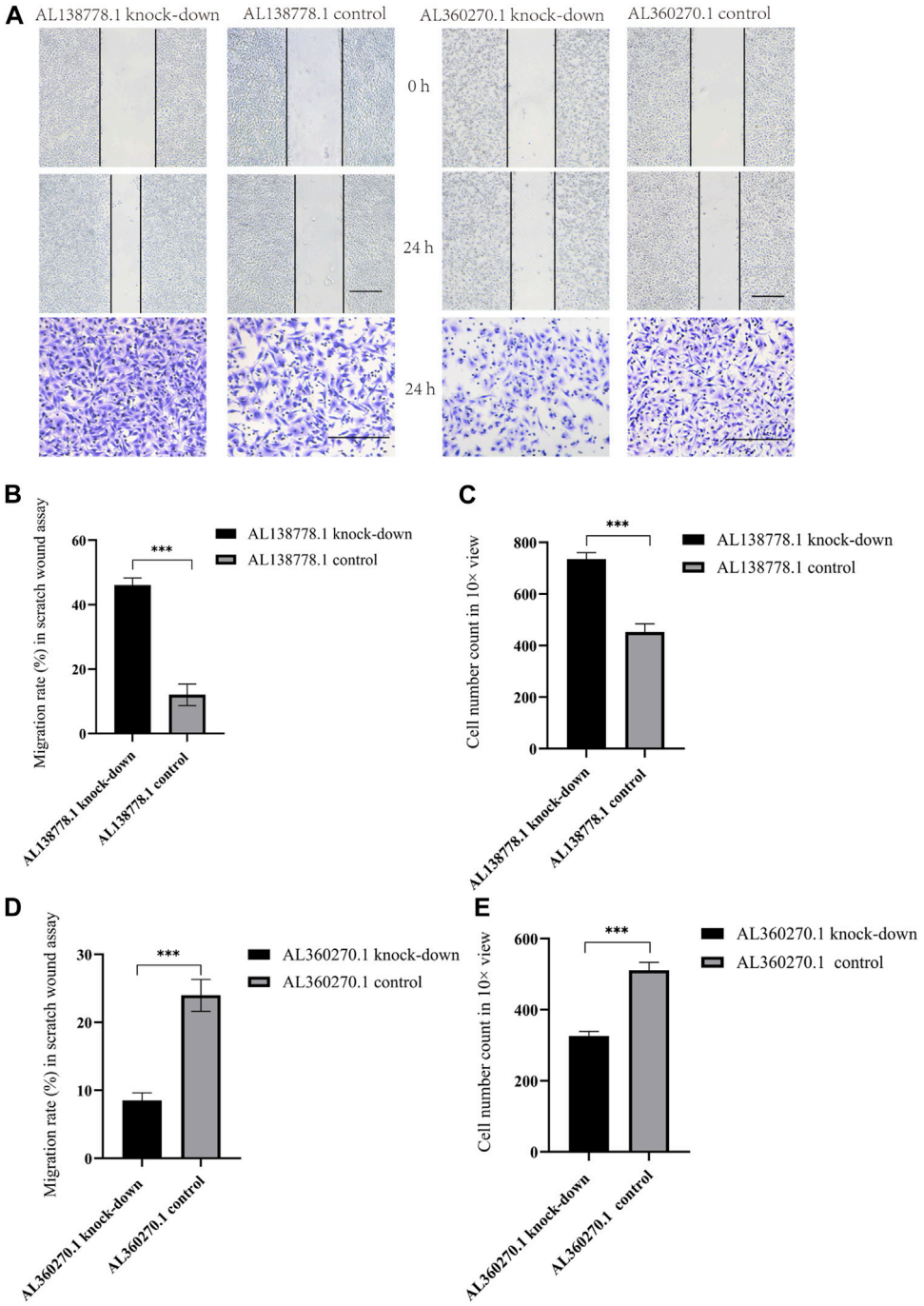

FIGURE 13
(A). The major figure above were scratch wound assay and transwell in A549 cell line grouped by AL138778.1 knock-down vs. control, AL360270.1 knock-down vs. control. The transverse black line were the standard ruler of all figures. **(B)**. Migration rate (%) in scratch wound assay in AL138778.1 knock-down vs. control; **(C)**. Average Cell number count in 10× view in transwell for AL138778.1 knock-down vs. control; **(D)**. Migration rate (%) in scratch wound assay in AL360270.1 knock-down vs. control; **(E)**. Average cell number count in 10× view in transwell for AL360270.1 knock-down vs. control. ***: **: $p < 0.001$, $p < 0.01$, ns: non-significant.

have revealed an unconventional cell death mechanism most frequently influenced by protein lipoylation during the TCA cycle (Kahlson and Dixon, 2022). We found that cilium movement and microtubule bundle formation had the highest frequency in our model, which is consistent with the fact that microtubule clusters foster cell invasion in malignant tumors (Lupo et al., 2016). KEGG analysis showed that microRNAs, IL-17, and the p53 signaling pathway were the most abundant and enriched in cuproptosis-associated processes, which may potentially affect the oxidative stress even the prognosis in LUAD patients (Filaire et al., 2013). The involvement of the p53 signaling pathway in tumor suppression has been confirmed

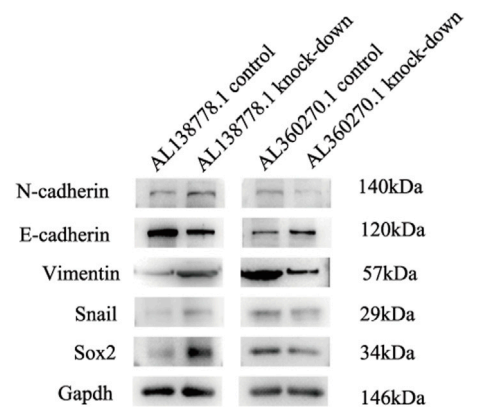

FIGURE 14
Western blot for migration features in A549 cell line grouped by AL138778.1 knock-down vs. control, AL360270.1 knock-down vs. control. The following items included N-cadherin, E-cadherin, Vimentin, Snail, Sox2, and proofed by Gapdh.

in various cell lines (Huang, 2021). As shown in the map tools of the two groups, TP53 missense mutations were the most frequent. Recent studies on immune cell infiltration and the tumor microenvironment have provided insights into immune cells. Researchers have demonstrated that higher levels of NK cells can suppress the proliferation of CD8+T cells and affect immune regulation (Sierra et al., 2021). The differentiation of T cells can affect the prognosis of patients with LUAD to some extent (Yu et al., 2020). Although the status of immune cells has outstanding value in anti-tumor therapy, the heat map of the expression and function of immune-related cells did not show a significant difference between the two groups. Patients in the HRG had lower TIDE scores than those in the LRG, indicating that immunotherapy may be limited to the HRG. Thus, in our model, patients in the LRG were more suitable candidates for targeted therapy. Consistent with our study, other studies have concluded that the clinical value of pazopanib could be more prominent in patients with higher risk factors (Xu et al., 2022). In addition, the IC50 drug susceptibility analysis suggested that patients in the HRG were more sensitive to phenformin, which can be used to target cancer cells and prevent relapse and metastasis (Krishnamurthy et al., 2014). Qin et al. have identified a novel prospective therapeutic target for cuproptosis (Qin et al., 2023). Similarly, our study used targeted drugs for LRG. Although patients with LRG exhibit a higher TIDE, which may lead to a poorer prognosis and less immunotherapy efficacy (Blumenschein, 2008), sorafenib, axitinib, pazopanib, and linsitinib may bring clinical benefits, which have been proven in previous trials (Leighl et al., 2017; Sun et al., 2018).

The lncRNAs affect the process of tumor metastasis by regulating the cell cuproptosis sensitivity such as CDKN2A, GLS and MTF1 (Xie et al., 2023). We demonstrated the predictive value of six CRs, including AL360270.1, AL138778.1, CDKN2A-DT, AP003778.1, LINC02718, and AC034102.8. Similarly, Liu et al. showed that the lncRNA AC034102.8 was a potential marker influencing the survival of patients with LUAD by pyroptosis (Liu et al., 2022). However, for these factors in our model, qPCR did not show differential expression in the carcinoma and para-carcinoma tissues. This may be due to AC034102.8 demonstrating a lower coefficient in the model. Although few studies have mentioned their function, AL138778.1 and AL360270.1 displayed their different capabilities for tumor migration and cell movement, which were in accordance with our model. Several studies have shown that CDK2N-DT promotes cancer (Tan et al., 2011). Similarly, our *in vitro* experiment also showed a high expression trend in carcinoma tissues when compared to that of para-carcinoma tissues. In addition, the transcription versions of AP003778.1, LINC02718, and AC034102.8 were long and mutable, so the lncRNA may vary among different versions. The function of these models may therefore change to some extent. This may be one of the reasons why the coefficient factor of these three lncRNAs (AP003778.1, LINC02718, and AC034102.8) was lower than that of the other three (AL360270.1, AL138778.1, and CDKN2A-DT).

Cu accumulation in cells can trigger tumor progression, and the GO analysis in our study highlighted microtubule-based movement, cilium movement, cilium organization, and cellular motility, which is different from the proposals based on previous studies that focused on the tricarboxylic acid cycle (Babak and Ahn, 2021). Although the relative expression of AL138778.1, AL360270.1, AP003778.1, and AC034102.8 has been reported in other studies, our study suggests that AL360270 is associated with the promotion of tumor metastasis and that AL138778.1 plays a role in the inhibition of metastasis. Scratch and Transwell experiments proved that the best and worst lncRNAs in our model were associated with cell movement and migration. Two of them have sufficient strength to balance the characteristics in our model, despite the potential influence of other lncRNAs. We chose N-cadherin, E-cadherin, Vimentin, Snail, and Sox2 to further confirm the feasibility of our model, because all these factors are closely related to the metastasis traits in LUAD (Han et al., 2022). Higher expression of N-cadherin, Vimentin, Snail, and Sox2 and lower expression of E-cadherin are always associated with tumor metastasis (Na et al., 2020). In addition, a correlation analysis of Cuproptosis genes with snail and Sox2 was conducted (Supplementary Figure S1). These Cuproptosis genes were closely related to AL138778.1 and AL360270.1 (Figure 1E). Therefore, we hypothesized that these five proteins may differ between AL138778.1 and AL360270.1 knock-down/control cell lines. After Western blotting, these factors were indeed found to be different in AL138778.1 and AL360270.1 knockdown/control cell lines, which further confirmed the migration features of our model.

However, this study had some limitations. Although we have validated the accuracy of our model, further experiments covering both *in vitro* and *in vivo* conditions are required. Second, larger public databases are needed to obtain more biological information to build up our evidence for this model. In future studies, these CRs should be validated in patients to test their target lncRNAs, and immunohistochemical analyses should be performed to determine the differences in related immune cells between the two groups.

5 Conclusion

We identified and validated six CR profiles (AL360270.1, AL138778.1, CDKN2A-DT, AP003778.1, LINC02718, and AC034102.8) by using various analytical methods and models. These CRs have clinical significance in predicting LUAD and may be used to evaluate the prognosis of patients with LUAD undergoing therapy.

Data availability statement

The original contributions presented in the study are included in the article/Supplementary Materials, further inquiries can be directed to the corresponding authors.

Ethics statement

The studies involving human participants were reviewed and approved by Ethics Committee of Tianjin Medical University Cancer Institute and Hospital (approval number: bc2022232). The patients/participants provided their written informed consent to participate in this study.

Author contributions

Conceptualization, MZ, ZX, and ZZ; methodology, ZZ; software, MZ and ZX; validation, ZF; formal analysis, MZ and ZX; investigation, MZ and ZX; resources, MZ and ZX; data curation, all authors; writing: original draft preparation, all authors; writing: review and editing, all authors; visualization, ZZ; supervision, ZZ; project administration, ZZ; funding acquisition, ZZ. All authors contributed to the article and approved the submitted version.

Acknowledgments

We thank those who assisted with the data resources and all the learners who contributed to the database.

Conflict of interest

The authors declare that the research was conducted in the absence of any commercial or financial relationships that could be construed as a potential conflict of interest.

Publisher's note

Supplementary material

The Supplementary Material for this article can be found online at: https://www.frontiersin.org/articles/10.3389/fphar.2023.1236655/full#supplementary-material

References

Babak, M. V., and Ahn, D. (2021). Modulation of intracellular copper levels as the mechanism of action of anticancer copper complexes: clinical relevance. *Biomedicines* 9 (8), 852. doi:10.3390/biomedicines9080852

Blumenschein, G. (2008). Sorafenib in lung cancer: clinical developments and future directions. *J. Thorac. Oncol.* 3 (2), S124–S127. doi:10.1097/JTO.0b013e318174e085

Brady, D. C., Crowe, M. S., Greenberg, D. N., and Counter, C. M. (2017). Copper chelation inhibits BRAFV600E-driven melanomagenesis and counters resistance to BRAFV600E and MEK1/2 inhibitors. *Cancer Res.* 77 (22), 6240–6252. doi:10.1158/0008-5472.CAN-16-1190

Bremnes, R. M., Veve, R., Hirsch, F. R., and Franklin, W. A. (2002). The E-cadherin cell-cell adhesion complex and lung cancer invasion, metastasis, and prognosis. *Lung Cancer* 36 (2), 115–124. doi:10.1016/s0169-5002(01)00471-8

Cobine, P. A., and Brady, D. C. (2022). Cuproptosis: cellular and molecular mechanisms underlying copper-induced cell death. *Mol. Cell* 82 (10), 1786–1787. doi:10.1016/j.molcel.2022.05.001

Dong, H., Hu, J., Zou, K., Ye, M., Chen, Y., Wu, C., et al. (2019). Activation of LncRNA TINCR by H3K27 acetylation promotes Trastuzumab resistance and epithelial-mesenchymal transition by targeting MicroRNA-125b in breast Cancer. *Mol. Cancer* 18 (1), 3. doi:10.1186/s12943-018-0931-9

Filaire, E., Dupuis, C., Galvaing, G., Aubreton, S., Laurent, H., Richard, R., et al. (2013). Lung cancer: what are the links with oxidative stress, physical activity and nutrition. *Lung Cancer* 82 (3), 383–389. doi:10.1016/j.lungcan.2013.09.009

Gautschi, O., Menon, R., Bertrand, M., Murer, C., and Diebold, J. (2020). Capmatinib and osimertinib combination therapy for EGFR-mutant lung adenocarcinoma. *J. Thorac. Oncol.* 15 (1), e13–e15. doi:10.1016/j.jtho.2019.07.027

Han, J. H., Kim, Y. K., Kim, H., Lee, J., Oh, M. J., Kim, S. B., et al. (2022). Snail acetylation by autophagy-derived acetyl-coenzyme A promotes invasion and metastasis of KRAS-LKB1 co-mutated lung cancer cells. *Cancer Commun.* 42 (8), 716–749. doi:10.1002/cac2.12332

Huang, J. (2021). Current developments of targeting the p53 signaling pathway for cancer treatment. *Pharmacol. Ther.* 220, 107720. doi:10.1016/j.pharmthera.2020.107720

Ishida, S., Andreux, P., Poitry-Yamate, C., Auwerx, J., and Hanahan, D. (2013). Bioavailable copper modulates oxidative phosphorylation and growth of tumors. *Proc. Natl. Acad. Sci. U. S. A.* 110 (48), 19507–19512. doi:10.1073/pnas.1318431110

Kahlson, M. A., and Dixon, S. J. (2022). Copper-induced cell death. *Science* 375 (6586), 1231–1232. doi:10.1126/science.abo3959

Kim, B.-E., Nevitt, T., and Thiele, D. J. (2008). Mechanisms for copper acquisition, distribution and regulation. *Nat. Chem. Biol.* 4 (3), 176–185. doi:10.1038/nchembio.72

Krishnamurthy, S., Ng, V. W. L., Gao, S., Tan, M. H., and Yang, Y. Y. (2014). Phenformin-loaded polymeric micelles for targeting both cancer cells and cancer stem cells *in vitro* and *in vivo*. *Biomaterials* 35 (33), 9177–9186. doi:10.1016/j.biomaterials.2014.07.018

Leighl, N. B., Rizvi, N. A., de Lima, L. G., Arpornwirat, W., Rudin, C. M., Chiappori, A. A., et al. (2017). Phase 2 study of erlotinib in combination with linsitinib (OSI-906) or placebo in chemotherapy-naive patients with non-small-cell lung cancer and activating epidermal growth factor receptor mutations. *Clin. Lung Cancer* 18 (1), 34–42. doi:10.1016/j.cllc.2016.07.007

Liu, J., Liu, Q., Shen, H., Liu, Y., Wang, Y., Wang, G., et al. (2022). Identification and validation of a three pyroptosis-related lncRNA signature for prognosis prediction in lung adenocarcinoma. *Front. Genet.* 13, 838624. doi:10.3389/fgene.2022.838624

Loewen, G., Jayawickramarajah, J., Zhuo, Y., and Shan, B. (2014). Functions of lncRNA HOTAIR in lung cancer. *J. Hematol. Oncol.* 7, 90. doi:10.1186/s13045-014-0090-4

Lupo, B., Vialard, J., Sassi, F., Angibaud, P., Puliafito, A., Pupo, E., et al. (2016). Tankyrase inhibition impairs directional migration and invasion of lung cancer cells by affecting microtubule dynamics and polarity signals. *BMC Biol.* 14, 5. doi:10.1186/s12915-016-0226-9

Masaldan, S., Clatworthy, S. A. S., Gamell, C., Smith, Z. M., Francis, P. S., Denoyer, D., et al. (2018). Copper accumulation in senescent cells: interplay between copper transporters and impaired autophagy. *Redox Biol.* 16, 322–331. doi:10.1016/j.redox.2018.03.007

Na, T.-Y., Schecterson, L., Mendonsa, A. M., and Gumbiner, B. M. (2020). The functional activity of E-cadherin controls tumor cell metastasis at multiple steps. *Proc. Natl. Acad. Sci. U. S. A.* 117 (11), 5931–5937. doi:10.1073/pnas.1918167117

Qin, Y., Liu, Y., Xiang, X., Long, X., Chen, Z., Huang, X., et al. (2023). Cuproptosis correlates with immunosuppressive tumor microenvironment based on pan-cancer multiomics and single-cell sequencing analysis. *Mol. Cancer* 22 (1), 59. doi:10.1186/s12943-023-01752-8

Rayess, H., Wang, M. B., and Srivatsan, E. S. (2012). Cellular senescence and tumor suppressor gene p16. *Int. J. Cancer* 130 (8), 1715–1725. doi:10.1002/ijc.27316

Ritchie, M. E., Phipson, B., Wu, D., Hu, Y., Law, C. W., Shi, W., et al. (2015). Limma powers differential expression analyses for RNA-sequencing and microarray studies. *Nucleic Acids Res.* 43 (7), e47. doi:10.1093/nar/gkv007

Sciegienka, S. J., Solst, S. R., Falls, K. C., Schoenfeld, J. D., Klinger, A. R., Ross, N. L., et al. (2017). D-penicillamine combined with inhibitors of hydroperoxide metabolism enhances lung and breast cancer cell responses to radiation and carboplatin via H2O2-mediated oxidative stress. *Free Radic. Biol. Med.* 108, 354–361. doi:10.1016/j.freeradbiomed.2017.04.001

Sequist, L. V., Yang, J. C.-H., Yamamoto, N., O'Byrne, K., Hirsh, V., Mok, T., et al. (2013). Phase III study of afatinib or cisplatin plus pemetrexed in patients with metastatic lung adenocarcinoma with EGFR mutations. *J. Clin. Oncol.* 31 (27), 3327–3334. doi:10.1200/JCO.2012.44.2806

Shanbhag, V., Jasmer-McDonald, K., Zhu, S., Martin, A. L., Gudekar, N., Khan, A., et al. (2019). ATP7A delivers copper to the lysyl oxidase family of enzymes and promotes tumorigenesis and metastasis. *Proc. Natl. Acad. Sci. U. S. A.* 116 (14), 6836–6841. doi:10.1073/pnas.1817473116

Sierra, J. M., Secchiari, F., Nuñez, S. Y., Iraolagoitia, X. L. R., Ziblat, A., Friedrich, A. D., et al. (2021). Tumor-experienced human NK cells express high levels of PD-L1 and inhibit $CD8^+$ T cell proliferation. *Front. Immunol.* 12, 745939. doi:10.3389/fimmu.2021.745939

Solmonson, A., Faubert, B., Gu, W., Rao, A., Cowdin, M. A., Menendez-Montes, I., et al. (2022). Compartmentalized metabolism supports midgestation mammalian development. *Nature* 604 (7905), 349–353. doi:10.1038/s41586-022-04557-9

Sun, J.-M., Lee, K. H., Kim, B.-S., Kim, H. G., Min, Y. J., Yi, S. Y., et al. (2018). Pazopanib maintenance after first-line etoposide and platinum chemotherapy in patients with extensive disease small-cell lung cancer: a multicentre, randomised, placebo-controlled phase II study (KCSG-LU12-07). *Br. J. Cancer* 118 (5), 648–653. doi:10.1038/bjc.2017.465

Tan, C., Xu, H.-Y., Zhang, C.-Y., Zhang, H., Chen, C. M., Zhang, W. M., et al. (2011). Effect of CYP1A1 MSPI polymorphism on the relationship between TP53 mutation and CDKN2A hypermethylation in non-small cell lung cancer. *Archives Med. Res.* 42 (8), 669–676. doi:10.1016/j.arcmed.2011.11.008

Tsang, T., Posimo, J. M., Gudiel, A. A., Cicchini, M., Feldser, D. M., and Brady, D. C. (2020). Copper is an essential regulator of the autophagic kinases ULK1/2 to drive lung adenocarcinoma. *Nat. Cell Biol.* 22 (4), 412–424. doi:10.1038/s41556-020-0481-4

van den Berghe, P. V. E., and Klomp, L. W. J. (2009). New developments in the regulation of intestinal copper absorption. *Nutr. Rev.* 67 (11), 658–672. doi:10.1111/j.1753-4887.2009.00250.x

Wang, M., Wang, X., Li, Y., Xiao, Q., Cui, X. H., Xiao, G. D., et al. (2019). Nutlin-3-Induced sensitization of non-small cell lung cancer stem cells to axitinib-induced apoptosis through repression of akt1/wnt signaling. *Oncol. Res.* 27 (9), 987–995. doi:10.3727/096504018X15424918479652

Xie, J., Yang, Y., Gao, Y., and He, J. (2023). Cuproptosis: mechanisms and links with cancers. *Mol. Cancer* 22 (1), 46. doi:10.1186/s12943-023-01732-y

Xu, S., Liu, D., Chang, T., Wen, X., Ma, S., Sun, G., et al. (2022). Cuproptosis-associated lncRNA establishes new prognostic profile and predicts immunotherapy response in clear cell renal cell carcinoma. *Front. Genet.* 13, 938259. doi:10.3389/fgene.2022.938259

Yu, Y., Chang, Z., Han, C., Zhuang, L., Zhou, C., Qi, X., et al. (2020). Long non-coding RNA MINCR aggravates colon cancer via regulating miR-708-5p-mediated Wnt/β-catenin pathway. *Biomed. Pharmacother. = Biomedecine Pharmacother.* 129, 110292. doi:10.1016/j.biopha.2020.110292

Zhang, G., Sun, J., and Zhang, X. (2022). A novel Cuproptosis-related LncRNA signature to predict prognosis in hepatocellular carcinoma. *Sci. Rep.* 12 (1), 11325. doi:10.1038/s41598-022-15251-1

frontiers | Frontiers in Oncology

TYPE Case Report
PUBLISHED 13 October 2023
DOI 10.3389/fonc.2023.1193503

OPEN ACCESS

EDITED BY
Yiming Meng,
China Medical University, China

REVIEWED BY
Gianluca Tedaldi,
Scientific Institute of Romagna for the Study and Treatment of Tumors (IRCCS), Italy
Grigoriy Yanus,
N.N. Petrov National Medical Research Center of Oncology, Russia

*CORRESPONDENCE
Eric H. Bernicker
ehbernick@gmail.com

RECEIVED 25 April 2023
ACCEPTED 18 September 2023
PUBLISHED 13 October 2023

CITATION
Hodges A, Sun K, Sheu TG and Bernicker EH (2023) Lung adenocarcinoma in a patient with Lynch syndrome: a case report and literature review.
Front. Oncol. 13:1193503.
doi: 10.3389/fonc.2023.1193503

Lung adenocarcinoma in a patient with Lynch syndrome: a case report and literature review

Alan Hodges[1,2], Kai Sun[3], Tiffany G. Sheu[4] and Eric H. Bernicker[3]*

[1]Texas A&M School of Medicine, Bryan, TX, United States, [2]Houston Methodist Research Institute, Center for Immunotherapy Research, Houston, TX, United States, [3]Houston Methodist Neal Cancer Center, Houston, TX, United States, [4]Department of Pathology and Genomic Medicine, Houston Methodist Hospital, Houston, TX, United States

This article presents a case of a 62-year-old Vietnamese woman with a history of Lynch syndrome (LS), who developed lung adenocarcinoma with *EGFR* L858R mutation. LS is an autosomal dominant cancer predisposition syndrome caused by a pathogenic germline variant in DNA mismatch repair genes, often leading to microsatellite instability. While LS is primarily associated with gastrointestinal, endometrial, ovarian, and urologic tract cancers, lung cancer accounts for less than 1% of LS-related cancers, with only six cases of LS-related lung cancer previously reported in the literature. The patient underwent multiple lines of treatment for her lung adenocarcinoma, including tyrosine kinase inhibitors, stereotactic body radiation therapy, pemetrexed and pembrolizumab, amivantamab, and fam-trastuzumab deruxtecan, but all resulted in only a partial response followed by a progressive disease. This case highlights the complex interplay of genetic cancer predisposition syndromes and the development of spontaneous driver mutations in the disease course and the subsequent management of tumors arising in these patients.

KEYWORDS

Lynch syndrome, NSCLC, MLH1, immune checkpoint therapy, ctDNA

1 Introduction

Lynch syndrome (LS) is a genetically defined disease entity often associated with the clinical syndrome hereditary non-polyposis colon cancer, an autosomal dominant cancer predisposition syndrome. Patients with LS have an increased risk of a wide array of malignancies, most commonly gastrointestinal cancer, endometrial cancer, ovarian cancer, and urologic tract cancer (1). LS is caused by an autosomal dominant, pathogenic, germline variant in one of the DNA mismatch repair (MMR) genes (*MSH2*, *MLH1*, *MSH6*, or *PMS2)* or *EPCAM*, which leads to epigenetic silencing of *MSH2* (2). Pathogenic variants in the MMR genes are relatively frequent, with an estimated prevalence of 1 in 279 (3), and thus LS represents one of the most prevalent cancer predisposition syndromes (4).

The resulting deficiency in MMR due to LS gene variants results in the accumulation of errors throughout the genome, including in short, repeated, microsatellite regions, a phenomenon termed microsatellite instability high (MSI-H). MSI-H is a hallmark of tumors associated with LS (5), and LS contributes to a significant proportion of MSI-H tumors across tumor types (6). Notably, there is significant heterogeneity in MSI prevalence between tumor types in LS patients, with a high MSI prevalence observed in ureteral, colorectal, and ovarian tumors (100%, 98%, and 94%, respectively) and a low MSI prevalence in tumors such as renal and primary brain tumors (25% and 0%, respectively) (7, 8). This MSI prevalence heterogeneity may have important treatment implications for LS-related tumors, as MSI-H tumors are more likely to respond to immune checkpoint therapy (7, 9), whereas the role of IC therapies in microsatellite-stable disease in LS patients is less clear (10).

Lung cancer is the most frequently diagnosed cancer and leading cause of cancer death (11), with cigarette smoking contributing significantly to the prevalence of the disease. While driver mutations are identified in tumors of both smokers and non-smokers, driver mutations are widely prevalent in the disease of non-smokers, occurring in 70% and 95% in cohorts of NSCLC and lung adenocarcinoma, respectively (12, 13). Among driver mutations in NSCLC, epidermal growth factor receptor (*EGFR*) mutations are the most common (13). Targeting *EGFR* mutations with tyrosine kinase inhibitors (TKIs) has revolutionized the therapeutic landscape of metastatic NSCLC. However, many patients eventually progress despite the initial good response and will receive chemotherapy-based second-line treatment. Despite the immune checkpoint blockade showing promising results in the second-line treatment of metastatic NSCLC (14, 15), those with EGFR mutations are unlikely to respond to immune checkpoint blockade (16, 17).

Less than 1% of lung cancer is associated with LS, and screening for LS is not recommended. Only six cases of lung cancer arising in patients with LS have been reported. *EGFR* mutation in LS-related lung cancer is even a rarer reported event. Here we report a case of incidentally discovered lung adenocarcinoma developing in a patient with a previous diagnosis of LS. Additionally, we review the leterature on lung cancer related to LS and the subset of this population with *EGFR*-mutated tumors.

2 Case presentation

A 62-year-old Vietnamese woman, non-smoker, presented with dysphagia and odynophagia. She had a history of colon cancer that was treated with hemicolectomy and adjuvant chemotherapy at age 53 and stage I right upper lobe lung adenocarcinoma that was treated with lobectomy at age 57 in Vietnam. The family's oncologic history was significant for colon cancer in her paternal grandmother and aunt. She was found to have left tongue squamous cell carcinoma by biopsy. During the staging of tongue squamous cell carcinoma, she was found to have one 1-cm right upper lobe nodule and one 1-cm left upper lobe nodule. The biopsy of the right upper lobe nodule revealed lung adenocarcinoma (Figure 1). Molecular testing showed *EGFR* L858R mutation—negative for *ALK* rearrangement, *BRAF*, and *MET* mutations. PD-L1 by 22C3 pharmDx was negative. A positron emission tomography/computed tomography scan showed moderate fluorodeoxyglucose uptake in both lesions, which are concerning for malignancy. Her family history was significant for colon cancer in her son at age 35 who was later found to carry the pathogenic germline *MLH1* variant. Due to the patient's history of multiple malignancies and her family history, genetic testing was performed, which revealed a pathogenic germline *MLH1* variant, and the patient was subsequently diagnosed with LS.

She underwent left partial glossectomy and lymph node dissection for her stage II tongue squamous cell carcinoma. She then completed stereotactic body radiation therapy (SBRT, 50 Gy in five fractions) to both the left and right upper lobe lung lesions. However, she was found to have enlarged left lung nodules and new pleural effusion on surveillance scans 2 years after her SBRT treatment. The sampled pleural fluid contained cytologic features of adenocarcinoma. A ctDNA analysis by Guardant360 (18) was performed, but it only revealed BRCA2 variance of unknown significance. Given the *EGFR* mutation status on the initial tissue biopsy, she was started on osimertinib. She had stable disease for 6 months but then developed worsening pleural effusion and new bone lesions (Figures 2A, B). A repeat ctDNA was performed, and it showed *ERBB2* (G778_P780dup) and *TP53* (M237I) mutations at a very low frequency. Her treatment was switched to pemetrexed and pembrolizumab doublet. Platinum chemotherapy was omitted given her history of ischemic stroke and performance status. During the period following an initial partial response, she also received elective total hysterectomy and bilateral salpingo-oophorectomy for risk reduction. At 7 months after the initiation of the pemetrexed and pembrolizumab doublet, her disease progressed. The patient was then started on the EGFR/MET bispecific antibody amivantamab (Rybrevant), again showing partial response followed by a progressive disease after 7 months. Another ctDNA was conducted, and it revealed *ERBB2* and *TP53* mutations at low frequency. Notably, none of the ctDNA tests showed MSI-H disease but was significant for a *MLH1* A681T mutation at approximately 50% allele frequency (47.8%), which was likely from her LS-defining germline heterozygosity. The patient was subsequently started on fam-trastuzumab deruxtecan (Enhertu) for three cycles. At 1 month following the final cycle of fam-trastuzumab deruxtecan, the patient developed fatal acute respiratory failure secondary to pulmonary edema (Figure 3).

3 Discussion

We report the case of a patient with LS who was diagnosed with NSCLC with *EGFR* mutation and had a short response to EGFR-targeted tyrosine kinase inhibitor and subsequent immune checkpoint inhibitor. To our knowledge, this is the second reported case of NSCLC with *EGFR* mutation in patients with LS and the first reported case with a long-term clinical outcome.

LS is known as one of the most common forms of inherited cancer predisposition (3). Although LS is classically associated with increased risks of a wide array of malignancies (1), NSCLC is not

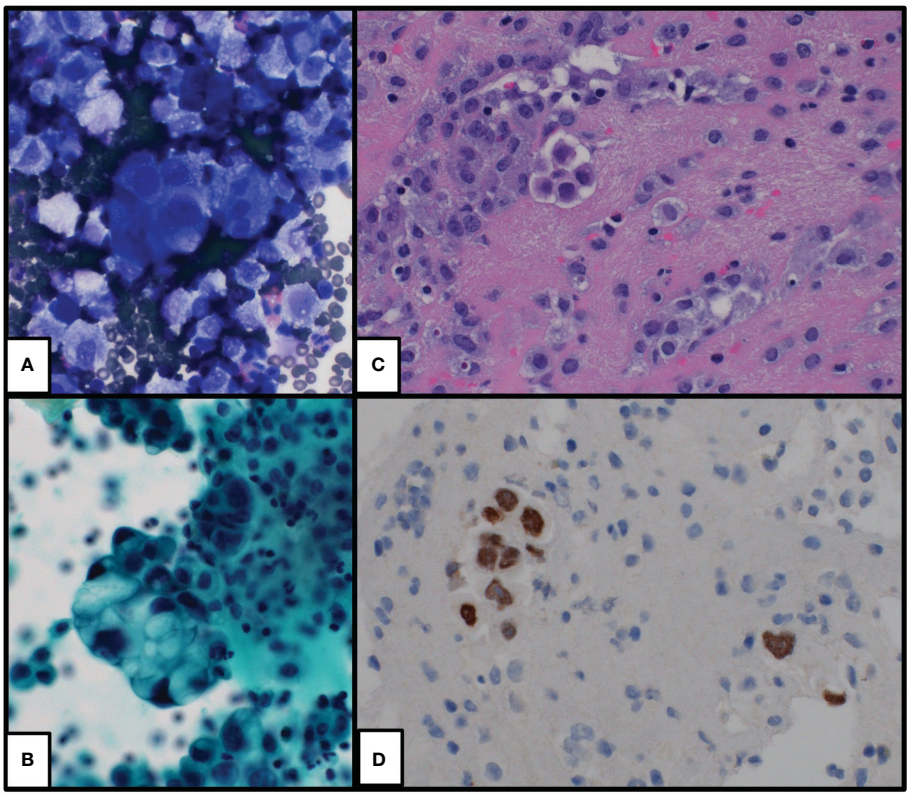

FIGURE 1
Cytologic preparations of initial pleural effusion which show groups and single malignant cells with morphologic and immunophenotypic findings supportive of lung adenocarcinoma. **(A)** DiffQuik-stained cytospin preparation at ×400, **(B)** Pap-stained cytospin preparation at ×400, **(C)** hematoxylin and eosin-stained cell block preparation at ×400, and **(D)** TTF1 immunohistochemical stain at ×400.

traditionally believed to be one of them. Sun et al. (19) analyzed the germline mutational status of 1,179 paired samples of lung cancer tumor tissue and normal lung tissue, and only six of 1,179 (0.5%) patients were found to have germline MMR gene pathogenic variants. Takamochi et al. (20) analyzed the MSI status in 366 patient samples, and only one tumor sample was found to have MSI-H, and this patient had no background of LS. A larger study by Warth et al. (21) also confirmed low MSI-H frequency (0.8%) in patients with lung adenocarcinoma. These studies indicate that lung cancer with MMR germline pathogenic variants or MSI-H is a rare and sporadic event, and screening for LS in patients newly diagnosed with lung cancer will be low-yield and likely be cost-ineffective.

However, there have been several case reports of lung cancer that developed in patients with LS (Table 1). Including our case, all cases were diagnosed with lung adenocarcinoma with low or negative PD-L1 expression. MSH2 germline mutation was the most common mutation, followed by MLH1 mutation. In total, five of seven (71.4%) patients were found to have loss of MMR expression on tumor tissues; none of these five patients had *EGFR* mutation, and three out of these five patients had either remission or stable disease as the best response to second-line immune checkpoint inhibitors. Moreover, two of seven (28.6%) patients had tumors that harbored *EGFR* mutation, but neither tumor had loss of MMR expression. In the study by Warth et al. (21), two of four (50%) patients who had MSI-H tumors also harbored *EGFR* mutations, and in the study by Sun et al. (19), two of six (33.3%) patients who had germline MMR mutation harbored *EGFR* mutations. The prevalence of *EGFR* mutations in lung cancer patients with LS from the case reports and studies mentioned above is 35.3% (6/17), which is higher than that of 10%–20% observed in Europe and North America populations (28).

Even though our patient harbored *EGFR* mutation, her response to osimertinib and immune checkpoint inhibitor with chemotherapy was short-lasting. Li et al. (29) reported the association between a stronger MLH1 expression and a higher *EGFR* mutation frequency. The authors predicted that the overexpression of MLH1 could be a potential marker for sensitivity to EGFR TKIs. If true, patients with LS with a loss of MLH1 expression would likely demonstrate a suboptimal response to EGFR TKIs. Moreover, although patients with LS are expected to have an increased response to immune checkpoint inhibitors, a decreased response to immune checkpoint inhibitors is observed in *EGFR*-mutated NSCLC at large (30) and likely contributed to the failure of immune checkpoint therapy in this patient. Furthermore, MMR deficiency in tumors arising in LS patients cannot be presumed, especially in non-typical LS tumor types, and therefore individualized testing of tumors may be warranted to guide the use of IC therapies in these patients.

This case also highlights the need to carefully weigh the decision to pursue risk reduction surgery, weighing the pathogenicity of

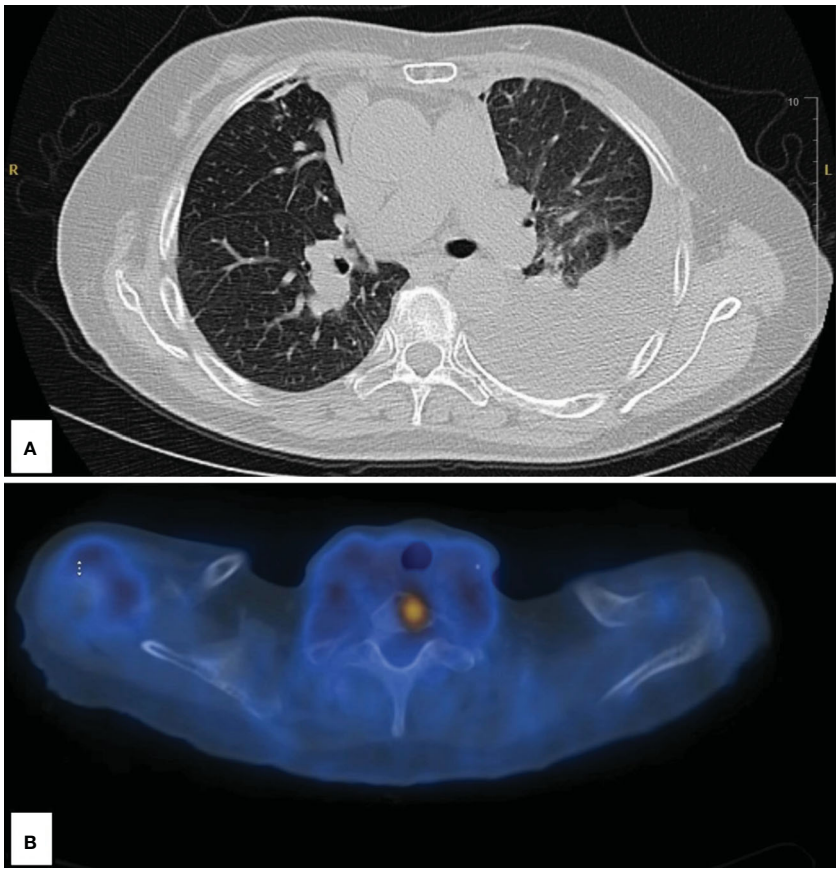

FIGURE 2
Imaging following disease progression at 2 years' status post-stereotactic body radiation therapy. **(A)** Large left pleural effusion and left lower lobe atelectasis. **(B)** Abnormal fluorodeoxyglucose uptake in the upper spine; SUV of 5.5.

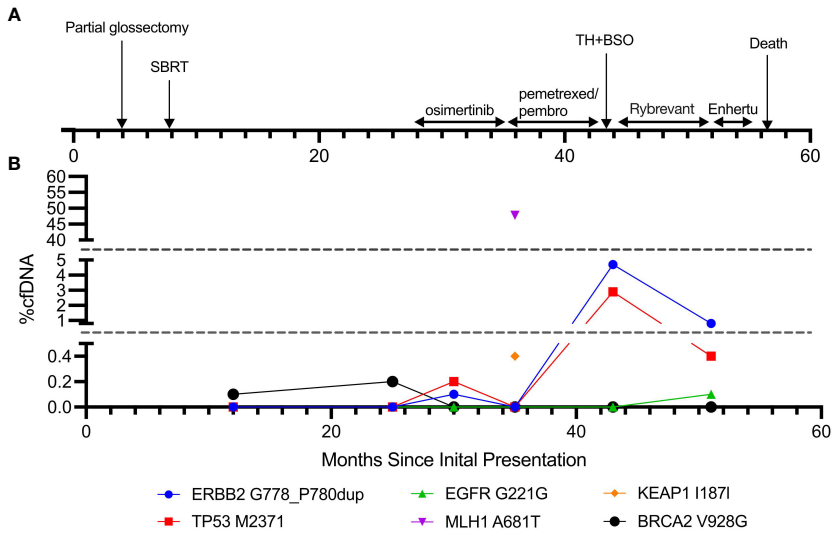

FIGURE 3
Timeline of the disease course and cfDNA trends. **(A)** Timeline of clinical course and treatment modalities. **(B)** cfDNA composition throughout the disease course.

TABLE 1 Summary of patients with Lynch syndrome who developed lung cancer.

	Age/ gender	Germline gene pathogenic variant	Other malignancies	Lung cancer histology	MMR (D/P)	MSI	PD-L1 level	*EGFR* mutation	Outcome
Canney et al. (22)	59/M	*MSH2*	Colon cancer	NSCLC	D*	Not reported	Not reported	Not reported	Not reported
Kawashima et al. (23)	68/M	*MSH2*	Colon, rectal, and prostate	NSCLC	D (loss of MSH2 and MSH6)	S	3%	No	Long-lasting response to nivolumab >22 months
Masuzawa et al. (24)	36/M	*MLH1*	None	NSCLC	D (loss of MLH1 and PMS2)	H	1%–24%	No	Long-lasting response to nivolumab >20 months
Nolan et al. (25)	64/M	*MSH2*	Colon and bladder	NSCLC	D (loss of MSH2)†	H	Not reported	No	Alive after surgery
Maccaroni et al. (26)	74/F	*MSH6*	Ovarian and rectal	NSCLC	D (loss of MSH6 on brain met)	H	Negative	No	4 months of SD on pembrolizumab, disease progression and death at 6 months
Hissong et al. (27)	66/F	*MSH2*	Endometrial	NSCLC	P	S	5%	*EGFR* L858A	Not reported
Our case	62/F	*MLH1*	Colon, tongue	NSCLC	Not reported	S	Negative	*EGFR* L858R	Deceased following failure of multiple lines of therapy

*Two lung lesions were identified: one had loss of MSH2 and MSH6 expression, and the other one was MMR proficient.
†Two lung lesions were identified: one had loss of MSH2 expression and was MSI-H, and the other one was MMR proficient.

different LS variants and the patient's underlying comorbidities as recommended by the NCCN (31). Moreover, in patients with current and stable malignancies, the risks of exacerbating the disease through unrelated risk reduction surgeries must be considered (32, 33).

4 Conclusion

NSCLC is not among the malignancies that are commonly associated with LS. In patients with LS who developed NSCLC, *EGFR* mutation seems to be more prevalent and should be checked as in patients without LS. Despite the MSI-H status that is commonly seen in LS with an associated expected good response to immune checkpoint blockade, these patients with *EGFR* mutations and LS tend to have a poor response to immune checkpoint inhibitors.

Data availability statement

The original contributions presented in the study are included in the article/supplementary material. Further inquiries can be directed to the corresponding author.

Ethics statement

Written informed consent was obtained from the individual(s) for the publication of any potentially identifiable images or data included in this article.

Author contributions

AH, KS, and EB each contributed to data gathering, analysis, and manuscript preparation. KS and EB contributed to the clinical care of the patient. TS provided the pathology analysis. All authors contributed to the article and approved the submitted version.

Acknowledgments

The authors would like to thank the patient and her family and the clinical team involved in patient's care.

Conflict of interest

The authors declare that the research was conducted in the absence of any commercial or financial relationships that could be construed as a potential conflict of interest.

Publisher's note

References

1. Watson P, Vasen HFA, Mecklin JP, Bernstein I, Aarnio M, Järvinen HJ, et al. The risk of extra-colonic, extra-endometrial cancer in the Lynch syndrome. *Int J Cancer.* (2008) 123(2):444–9. doi: 10.1002/ijc.23508

2. Rebuzzi F, Ulivi P, Tedaldi G. Genetic predisposition to colorectal cancer: how many and which genes to test? *IJMS* (2023) 24(3):2137. doi: 10.3390/ijms24032137

3. Win AK, Jenkins MA, Dowty JG, Antoniou AC, Lee A, Giles GG, et al. Prevalence and penetrance of major genes and polygenes for colorectal cancer. *Cancer Epidemiol Biomarkers Prev* (2017) 26(3):404–12. doi: 10.1158/1055-9965.EPI-16-0693

4. Peltomäki P, Nyström M, Mecklin JP, Seppälä TT. Lynch syndrome genetics and clinical implications. *Gastroenterology* (2023) 164(5):783–99. doi: 10.1053/j.gastro.2022.08.058

5. Peltomäki P, Lothe RA, Aaltonen LA, Pylkkänen L, Nyström-Lahti M, Seruca R, et al. Microsatellite instability is associated with tumors that characterize the hereditary non-polyposis colorectal carcinoma syndrome. *Cancer Res* (1993) 53(24):5853–5.

6. Latham A, Srinivasan P, Kemel Y, Shia J, Bandlamudi C, Mandelker D, et al. Microsatellite instability is associated with the presence of lynch syndrome pan-cancer. *JCO* (2019) 37(4):286–95. doi: 10.1200/JCO.18.00283

7. Therkildsen C, Jensen LH, Rasmussen M, Bernstein I. An update on immune checkpoint therapy for the treatment of lynch syndrome. *Clin Exp Gastroenterol* (2021) 14:181–97. doi: 10.2147/CEG.S278054

8. Gylling AHS, Nieminen TT, Abdel-Rahman WM, Nuorva K, Juhola M, Joensuu EI, et al. Differential cancer predisposition in Lynch syndrome: insights from molecular analysis of brain and urinary tract tumors. *Carcinogenesis* (2008) 29(7):1351–9. doi: 10.1093/carcin/bgn133

9. Le DT, Durham JN, Smith KN, Wang H, Bartlett BR, Aulakh LK, et al. Mismatch repair deficiency predicts response of solid tumors to PD-1 blockade. *Science* (2017) 357(6349):409–13. doi: 10.1126/science.aan6733

10. Bari S, Kim RD, Wang X, Matejcic M, Muzaffar J. Outcomes of Lynch syndrome (LS) patients treated with immune checkpoint inhibitors (ICI). *JCO* (2020) 38 (15_suppl):1548–8. doi: 10.1200/JCO.2020.38.15_suppl.1548

11. Bray F, Ferlay J, Soerjomataram I, Siegel RL, Torre LA, Jemal A. Global cancer statistics 2018: GLOBOCAN estimates of incidence and mortality worldwide for 36 cancers in 185 countries. *CA Cancer J Clin* (2018) 68(6):394–424. doi: 10.3322/caac.21492

12. Mack PC, Klein MI, Ayers KL, Zhou X, Guin S, Fink M, et al. Targeted next-generation sequencing reveals exceptionally high rates of molecular driver mutations in never-smokers with lung adenocarcinoma. *Oncologist.* (2022) 27(6):476–86. doi: 10.1093/oncolo/oyac035

13. Sholl LM, Aisner DL, Varella-Garcia M, Berry LD, Dias-Santagata D, Wistuba II, et al. Multi-institutional oncogenic driver mutation analysis in lung adenocarcinoma: the lung cancer mutation consortium experience. *J Thorac Oncol* (2015) 10(5):768–77. doi: 10.1097/JTO.0000000000000516

14. Leighl NB, Hellmann MD, Hui R, Carcereny E, Felip E, Ahn MJ, et al. Pembrolizumab in patients with advanced non-small-cell lung cancer (KEYNOTE-001): 3-year results from an open-label, phase 1 study. *Lancet Respir Med* (2019) 7 (4):347–57. doi: 10.1016/S2213-2600(18)30500-9

15. Jemielita T, Li XN, Piperdi B, Zhou W, Burke T, Chen C. Overall survival with second-line pembrolizumab in patients with non-small-cell lung cancer: randomized phase III clinical trial versus propensity-adjusted real-world data. *JCO Clin Cancer Inform.* (2021) 5:56–65. doi: 10.1200/CCI.20.00099

16. Lee CK, Man J, Lord S, Links M, Gebski V, Mok T, et al. Checkpoint inhibitors in metastatic EGFR-mutated non-small cell lung cancer-A meta-analysis. *J Thorac Oncol* (2017) 12(2):403–7. doi: 10.1016/j.jtho.2016.10.007

17. Lisberg A, Cummings A, Goldman JW, Bornazyan K, Reese N, Wang T, et al. A phase II study of pembrolizumab in EGFR-mutant, PD-L1+, tyrosine kinase inhibitor naïve patients with advanced NSCLC. *J Thorac Oncol* (2018) 13(8):1138–45. doi: 10.1016/j.jtho.2018.03.035

18. Aggarwal C, Thompson JC, Black TA, Katz SI, Fan R, Yee SS, et al. Clinical implications of plasma-based genotyping with the delivery of personalized therapy in metastatic non–small cell lung cancer. *JAMA Oncol* (2019) 5(2):173. doi: 10.1001/jamaoncol.2018.4305

19. Sun S, Liu Y, Eisfeld AK, Zhen F, Jin S, Gao W, et al. Identification of germline mismatch repair gene mutations in lung cancer patients with paired tumor-normal next generation sequencing: A retrospective study. *Front Oncol* (2019) 9:550. doi: 10.3389/fonc.2019.00550

20. Takamochi K, Takahashi F, Suehara Y, Kitano S, Sato E, Kohsaka S, et al. A microsatellite instability analysis using the promega panel in lung adenocarcinoma. *Chest* (2016) 150(4):715A. doi: 10.1016/j.chest.2016.08.810

21. Warth A, Körner S, Penzel R, Muley T, Dienemann H, Schirmacher P, et al. Microsatellite instability in pulmonary adenocarcinomas: a comprehensive study of 480 cases. *Virchows Arch* (2016) 468(3):313–9. doi: 10.1007/s00428-015-1892-7

22. Canney A, Sheahan K, Keegan D, Tolan M, Hyland J, Green A. Synchronous lung tumours in a patient with metachronous colorectal carcinoma and a germline MSH2 mutation. *J Clin Pathol* (2009) 62(5):471–3. doi: 10.1136/jcp.2008.063008

23. Kawashima Y, Nishikawa S, Ninomiya H, Yoshida R, Takano N, Oguri T, et al. Lung adenocarcinoma with lynch syndrome and the response to nivolumab. *Intern Med* (2019) 58(10):1479–84. doi: 10.2169/internalmedicine.1673-18

24. Masuzawa K, Asakura T, Ikemura S, Yasuda H, Kawada I, Takaoka S, et al. Long-lasting response to nivolumab for a patient with lynch syndrome–associated lung adenocarcinoma. *JCO Precis Oncol* (2020) 4):74–8. doi: 10.1200/PO.19.00156

25. Nolan L, Eccles D, Cross E, Crawford G, Beck N, Bateman A, et al. First case report of Muir-Torre syndrome associated with non-small cell lung cancer. *Fam Cancer.* (2009) 8(4):359–62. doi: 10.1007/s10689-009-9247-7

26. Maccaroni E, Lenci E, Agostinelli V, Cognigni V, Giampieri R, Mazzanti P, et al. *Lynch syndrome-associated lung cancer: pitfalls of an immunotherapy-based treatment strategy in an unusual tumor type. Exploration of Targeted Anti-tumor Therapy* (2021). Available at: https://www.explorationpub.com/Journals/etat/Article/100244.

27. Hissong E, Baek I, Costa V, Beneck D, Saxena A, Solomon JP, et al. Identification of a microsatellite stable, EGFR-mutant lung adenocarcinoma developing in a patient with lynch syndrome. *JCO Precis Oncol* (2020) 4:818–22. doi: 10.1200/PO.20.00074

28. Melosky B, Kambartel K, Häntschel M, Bennetts M, Nickens DJ, Brinkmann J, et al. Worldwide prevalence of epidermal growth factor receptor mutations in non-small cell lung cancer: A meta-analysis. *Mol Diagn Ther* (2022) 26(1):7–18. doi: 10.1007/s40291-021-00563-1

29. Li M, Zhang Q, Liu L, Lu W, Wei H, Li RW, et al. Expression of the mismatch repair gene hMLH1 is enhanced in non-small cell lung cancer with EGFR mutations. *PloS One* (2013) 8(10):e78500. doi: 10.1371/journal.pone.0078500

30. Hastings K, Yu HA, Wei W, Sanchez-Vega F, DeVeaux M, Choi J, et al EGFR mutation subtypes and response to immune checkpoint blockade treatment in non-small-cell lung cancer. *Ann Oncol* (2019) 30(8):1311–20. doi: 10.1093/annonc/mdz141

31. National Comprehensive Cancer Network. *Genetic/familial high-risk assessment: colorectal*. Available at: https://www.nccn.org/professionals/physician_gls/pdf/genetics_colon.pdf.

32. Ceelen W, Pattyn P, Mareel M. Surgery, wound healing, and metastasis: Recent insights and clinical implications. *Crit Rev Oncology/Hematology.* (2014) 89(1):16–26. doi: 10.1016/j.critrevonc.2013.07.008

33. Tohme S, Simmons RL, Tsung A. Surgery for cancer: A trigger for metastases. *Cancer Res* (2017) 77(7):1548–52. doi: 10.1158/0008-5472.CAN-16-1536

frontiers | Frontiers in Immunology

TYPE Original Research
PUBLISHED 22 December 2023
DOI 10.3389/fimmu.2023.1304529

OPEN ACCESS

EDITED BY
Yiming Meng,
China Medical University, China

REVIEWED BY
Shaochuan Liu,
Tianjin Medical University Cancer Institute and Hospital, China
Rodwell Mabaera,
Dartmouth Hitchcock Medical Center, United States
Jie Dong,
Nanjing University, China
Min Wei,
Nanjing University, China, in collaboration with reviewer JD

*CORRESPONDENCE
Jun Chen
huntercj2004@qq.com
Zuoqing Song
thoracic_expert@aliyun.com

†These authors have contributed equally to this work

RECEIVED 29 September 2023
ACCEPTED 11 December 2023
PUBLISHED 22 December 2023

CITATION
Liu R, Zhu G, Sun Y, Li M, Hu Z, Cao P, Li X, Song Z and Chen J (2023) Neutrophil infiltration associated genes on the prognosis and tumor immune microenvironment of lung adenocarcinoma.
Front. Immunol. 14:1304529.
doi: 10.3389/fimmu.2023.1304529

Neutrophil infiltration associated genes on the prognosis and tumor immune microenvironment of lung adenocarcinoma

Renwang Liu[1,2†], Guangsheng Zhu[1,2†], Yonglin Sun[3†], Mingbiao Li[2], Zixuan Hu[1,2], Peijun Cao[1,2], Xuanguang Li[1,2], Zuoqing Song[1,2*] and Jun Chen[1,2*]

[1]Department of Lung Cancer Surgery, Tianjin Medical University General Hospital, Tianjin, China, [2]Tianjin Key Laboratory of Lung Cancer Metastasis and Tumour Microenvironment, Lung Cancer Institute, Tianjin Medical University General Hospital, Tianjin, China, [3]Gynecology and Obstetrics Department, Tianjin Third Central Hospital, Tianjin, China

The neutrophils exhibit both anti-tumor and pro-tumor effects in cancers. The correlation between neutrophils and tumor development in lung adenocarcinoma (LUAD) is still uncertain, possibly due to a lack of specific neutrophil infiltration evaluation methods. In this study, we identified 30 hub genes that were significantly associated with neutrophil infiltration in LUAD through data mining, survival analysis, and multiple tumor-infiltrating immune cells (TICs) analysis, including TIMER, CIBERSORT, QUANTISEQ, XCELL, and MCPCOUNTER. Consensus clustering analysis showed that these 30 hub genes were correlated with clinical features in LUAD. We further developed a neutrophil scoring system based on these hub genes. The neutrophil score was significantly correlated with prognosis and tumor immune microenvironment (TIME) in LUAD. It was also positively associated with PD-L1 expression and negatively associated with tumor mutational burden (TMB). When combined with the neutrophil score, the predictive capacity of PD-L1 and TMB for prognosis was significantly improved. Thus, the 30 hub genes might play an essential role in the interaction of neutrophils and LUAD, and the neutrophil scoring system might effectually assess the infiltration of neutrophils. Furthermore, we verified the expression of these 30 genes in the LUAD tumor tissues collected from our department. We further found that overexpressed TNFAIP6 and TLR6 and downregulated P2RY13, SCARF1, DPEP2, PRAM1, CYP27A1, CFP, GPX3, and NCF1 in LUAD tissue might be potentially associated with neutrophils pro-tumor effects. The following *in vitro* experiments demonstrated that TNFAIP6 and TLR6 were significantly overexpressed, and P2RY13 and CYP27A1 were significantly downregulated in LUAD cell lines, compared to BEAS-2B cells. Knocking down TNFAIP6 in A549 and PC9 resulted in the upregulation of FAS, CCL3, and ICAM-1, and the downregulation of CCL2, CXCR4, and VEGF-A in neutrophils when co-culturing with the conditioned medium (CM) from LUAD cells. Knocking

down TNFAIP6 in LUAD also led to an elevated early apoptosis rate of neutrophils. Therefore, overexpressed TNFAIP6 in LUAD cancer cells might lead to neutrophils "N2" polarization, which exhibited pro-tumor effects. Further research based on the genes identified in this pilot study might shed light on neutrophils' effects on LUAD in the future.

KEYWORDS

neutrophil infiltration, tumor associated neutrophil, tumor immune microenvironment, LUAD, bioinformatics analysis, survival analysis

1 Introduction

Neutrophils are humans' most abundant innate immune cells, accounting for 50-70% of all leukocytes (1, 2). It mainly participates in host defense through phagocytosis, degranulation and release of proteases, secretion of various chemokines and cytokines, and forming neutrophil extracellular traps (NETs) via NETosis to resist the invasion and reproduction of pathogenic bacteria (3, 4). The neutrophils can also be recruited and infiltrated into tumor microenvironments as tumor-associated neutrophils (TANs) (5, 6).

TANs have emerged as significant prognostic biomarkers in various cancers, such as bronchioloalveolar and renal carcinoma (7–9). It plays an essential role in tumor development and presents significant heterogeneity. On the one hand, TANs may promote tumor occurrence by generating reactive oxygen species (ROS) (10), releasing neutrophil elastase (NE) to accelerate tumor growth (11), secreting matrix metalloproteinase-9 (MMP-9) to induce angiogenesis (12), and forming NETs to facilitate tumor metastasis (13). On the other hand, TANs also exhibit anti-tumor properties, including direct killing of nascent tumor cells (14), releasing Arg1 to stimulate TRAIL expression and induce tumor cell apoptosis (15), and recruiting and activating T cells for tumor cell eradication (16, 17).

In non-small cell lung cancer (NSCLC), the abundance of neutrophils holds prognostic significance. Patients with higher neutrophil-to-lymphocyte ratios (NLR) exhibited reduced progression-free survival (PFS) and overall survival (OS) (18, 19). Early-stage NSCLC patients with heightened CD66b-positive neutrophil infiltration faced an increased likelihood of postoperative recurrence (20). However, in different subtypes of NSCLC, TANs demonstrated distinct roles (21). For instance, *Mehrdad Rakaee* et al. found that the proportion of CD66b-positive TANs presented opposing prognostic impacts between squamous cell carcinoma (SCC) and adenocarcinoma (ADC) (22). *Xinyan Liu* et al. also found that the TANs infiltration did not correlate with prognosis in lung adenocarcinoma (LUAD) (23).

These unclear effects of TANs in LUAD may be due to a lack of specific methods for assessing TANs. The underlying mechanisms of TANs' effect on LUADs also remain unknown. Thus, in this study, we identified 30 hub genes closely associated with neutrophil infiltration in LUADs using bioinformatics approaches. Then, by using these hub genes, we constructed a specific LUADs' TANs infiltration scoring system and analyzed its correlation with prognosis and tumor immune microenvironment. This pilot study might provide valuable insights into exploring TANs effects on LUADs.

2 Materials and methods

2.1 Data acquisition and differentially expressed genes analysis

All LUAD patients' data, including gene expression and clinical pathological features, were downloaded from The Cancer Genome Atlas (TCGA) database. The neutrophils-specific expressed genes were downloaded from The Human Protein Atlas (THPA) database (https://www.proteinatlas.org/). Gene microarray data and clinical information of 181 tumor samples in external validation were obtained from the Gene Expression Omnibus (GEO) dataset (https://www.ncbi.nlm.nih.gov/geo/query/acc.cgi?acc=GSE50081) (24). The log2(x+0.001) transforming was performed in each expression value. R software (version 3.6.4) was used to analyze differential expression and clinical characteristics.

2.2 Tumor-infiltrating immune cells analysis

Five independent TICs analysis methods, including TIMER (25), MCPCOUNTER (26), XCELL (27), CIBERSORT (28), and QUANTISEQ (29), were performed to assess neutrophil infiltration.

The tumor-associated immune comprehensive score was assessed via ImmunoPhenoScore (IPS) in R package IOBR (version 0.99.9) (30).

2.3 Neutrophil scoring construction and clustering analysis

The principal component analysis (PCA) algorithm was used for establishing neutrophil scoring according to the selected 30 hub genes. The formula was: Neutrophil_score=$\sum PC1_i+PC2_i$. The consensus clustering analysis was performed via the ConsensusClusterPlus package in R software.

2.4 Survival analysis

The bioinformatics survival analysis was performed as previously described (31). Briefly, the CoxPH in R software was used for univariate Cox regression analysis to screen genes and to establish the Cox proportional hazards regression model. MaxStat in R was used to calculate the best cut-off value and survfit in R to analyze the differences in OS and PFS between each group.

2.5 Mutations and tumor mutational burden

All the level 4 Simple Nucleotide Variation datasets in TCGA were downloaded from GDC (https://portal.gdc.cancer.gov/) (32) and processed by MuTect2. The alterations were analyzed in both high and low neutrophil score groups. The TMB was calculated by the tmb function from the R package maftools (version 2.8.05).

2.6 Tissue specimens and qPCR

Ten fresh lung adenocarcinoma specimens with paired adjacent normal tissue samples were collected from Tianjin Medical University General Hospital between May 2023 and June 2023. The basic information of these ten patients was listed in Supplementary Table 1. The expression of the 30 hub genes in both cancer and normal tissue was detected by qPCR. The procedure of qPCR was described previously (33). Briefly, TRIzol Reagent (Invitrogen, USA) was used for total RNA extraction. Power SYBR Green PCR Master Mix (Applied Biosystems, USA) was used for the reaction after reverse transitions. The primer sequences in this study were listed in Supplementary Table 2.

2.7 Cell culture and transfection

The cell culture and transfections were performed as described previously (31). All the cell lines were purchased from the American Tissue Culture Collection (ATCC). The cells were maintained in RPMI 1640 medium (Gibco, USA). The si-TNFAIP6 (SIGS0003862-1), si-TLR6 (SIGS0000949-1), and si NCs (siN0000001-1-5) were purchased from RiboBio (Guangzhou, China). The si-RNA or si-NC was transfected into cells by Lipofectamine 2000 (Invitrogen, United States) under the manufacturer's instructions.

2.8 Immunohistochemistry staining

IHC staining was performed as described previously (34). Briefly, the tissue slices underwent deparaffinization, followed by antigen retrieval in 5 mM Tris-HCl for 10 mins using microwave pretreatment. The 3% H2O2 was used to quench endogenous peroxidase activity, and the non-specific binding sites were blocked by serum. After incubated with anti-TNFAIP6 primary antibody (1:200, Proteintech, China) at 4°C overnight, the slides were washed and followed by horseradish peroxidase (HRP) labeled secondary antibody incubation for 30 mins at room temperature. Then, the slides were stained with diaminobenzidine and counterstained with hematoxylin. All stained slides were scanned by the Pannoramic MIDI (3DHISTECH, Hungary) and visualized in CaseViewer2.4 software (3DHISTECH, Hungary). The mages were scored automatically by Aipathwell software (Servicebio, Wuhan, China).

2.9 Neutrophils isolation

The peripheral blood was collected from healthy volunteers in EDTA-coated tubes. The isolation of neutrophils was using Polymorphprep (Axis-Shield, UK) under the manufacturer's instructions. Fast Giemsa Stain Kit (Yeasen, China) was used to determine the purity of the isolated neutrophils. The neutrophils were maintained in RPMI 1640.

2.10 Neutrophil polarization detection

The cancer cells were washed thrice with serum-free medium after growing to ~80% confluence. Then, after incubating in a serum-free medium for 24h, the conditioned medium (CM) was collected. $1X10^6$ neutrophils were seeded on 6-well plates with RPMI 1640 medium, adding 10% si-TNFAIP6 or si-NC LUAD cells CM. After 16h at 37°C, the total RNA and protein were collected. The expression of Fas cell surface death receptor (FAS), C-C motif chemokine ligand 3 (CCL3), intercellular adhesion molecule 1 (ICAM-1), C-C motif chemokine ligand 2 (CCL2), C-X-C motif chemokine receptor 4 (CXCR4) and vascular endothelial growth factor A (VEGF-A) were detected.

2.11 Western blot

Western blot was performed as previously described (35). Primary antibodies used were: anti-TNFAIP6 (1:1000, Proteintech, China), anti-TLR6 (1:1000, ABclonal, China), anti-FAS (1:3000, Proteintech, China), anti-CCL3 (1:1000, Proteintech,

China), anti-ICAM-1 (1:3000, Proteintech, China), anti-CCL2 (1:3000, Proteintech, China), anti-CXCR4 (1:3000, Proteintech, China), anti-VEGFA (1:2000, Proteintech, China), anti-β-Tubulin (1:20000, Proteintech, China) and anti-GAPDH (1:2000, Servicebio, China).

2.12 Annexin V- PI assay

The Annexin V- PI assay was performed as previously described (36). Briefly, after being stained with the Annexin V-FITC and PI (BD Biosciences, CA, USA) for 15 mins, the cells were analyzed using the Agilent Novocyte 2000R flow cytometer (Agilent Technologies, USA).

2.13 Cell counting Kit-8 assay

CCK8 assay was performed as previously described (31). Briefly, 4000 cells of each cell line were seeded in a 96-well plate. 10μl CCK8 (APExBIO, USA) was added to each well after 24h, 48h, and 72h incubation. Then, the OD values were detected after 1h incubation.

2.14 CM collection and protein precipitation

The CM was collected and centrifuged at 1000g for 5 minutes. The supernatant was centrifugated for 30 minutes using the Amicon® Ultra-15 Centrifugal Filter Unit (3 KDa, Millipore, USA). Afterward, the concentrated liquor was mixed with an equal volume of 50% Trichloroacetic acid (TCA) solution and incubated on ice for 2 hours. Then, the protein precipitation was obtained after centrifuged at 2000g and 4°C for 5 minutes and washed twice with 1ml of pre-chilled (-20°C) acetone.

2.15 In-solution digestion

The precipitated proteins were suspended in 100 mM NH_4HCO_3 and incubated overnight at 37°C with trypsin (Promega, USA). Subsequently, the solutions were heated at 56°C for 1h with 5mM dithiothreitol, followed by alkylation in the dark for 45 min with 15mM iodoacetamide. The unreacted iodoacetamide was then neutralized at room temperature for 30 min with 30mM cysteine. A second trypsin digestion was performed at 37°C for 4h and stopped with 10% TFA. The resulting solutions were dried using SpeedVac and desalted using a μ-C18 Ziptip (Millipore, USA).

2.16 Liquid chromatography-tandem mass spectrometry analysis

After desalting, each tryptic digest was dissolved in HPLC buffer A (0.1% (v/v) formic acid in water) and injected into a nano-LC system (EASY-nLC 1200, Thermo Fisher Scientific, USA). Each sample was separated using a C18 column (75μm inner-diameter×25 cm, 3 μm C18) with a 130 min HPLC gradient at a flow rate of 300 nL/min. The gradient consisted of the following steps: 5% to 7% solvent B (0.1% formic acid in 80% acetonitrile) in 2 min, 7% to 22% solvent B in 78 min, 22% to 38% solvent B in 38 min, 38% to 100% solvent B in 3 min, and hold at 100% solvent B for 9 min. The HPLC eluate was directly electrosprayed into an Orbitrap Eclipse Tribrid mass spectrometer (Thermo Fisher Scientific, USA). The spray voltage was set to 2.2 kV, the funnel RF level was set at 40, and the ion transfer tube temperature was set at 320°C. Mass spectrometric analysis was performed in a data-dependent (DDA) mode with a 2s cycle, and data acquisition was carried out using Xcalibur (v.4.5). The orbitrap mass analyzer was utilized as the MS1 detector with a resolution of 60,000 and a scan range of 350–1500 m/z. The normalized AGC target and maximum injection time were set at 100%/50 ms for MS1, and 100%/22 ms for MS2. The orbitrap mass analyzer was employed as the MS2 detector with a resolution of 15000. Precursor ions with charges of +2 to +5 were selected for MS2, and a dynamic exclusion time of 55s was set. The MS2 isolation window was 1.6Da, and precursor fragmentation was achieved using a normalized HCD (higher-energy collision-induced dissociation) collision energy of 30%.

2.17 Database search

Proteome Discoverer (PD) 3.0 was used to search the MS/MS data, with a maximum false discovery rate (FDR) of 1% for peptides. Peptide sequences were searched with trypsin specificity, allowing a maximum of two missed cleavages. Fixed modification of carbamidomethylation on cysteine was specified, and the minimal peptide length was set to six. Variable modifications included methionine oxidation and acetylation on the N-terminal and lysine residues. The mass tolerances for precursor ions were set at ±10 ppm and ±0.02 Da for MS/MS.

2.18 Label-free quantification

Protein abundance was determined by summing the abundances of unique+trazor peptides, and the PD3.0-derived abundance ratio was used for protein quantitation. The fold difference per protein was calculated from the average abundance (normalized) in all replicates, and the t-test was applied to assess the statistical significance. The abundance was required in at least two replicates for protein quantification to be considered.

2.19 Statistical analysis

Statistical analysis was performed by R software (version 3.6.4) or SPSS version 23. T-tests were used for the data with homogeneity of variance. Mann-Whitney U-tests were used for the data without homogeneity of variance. Wilcoxon Rank Sum and Signed Rank

Tests were used for unpaired data. Kruskal tests were used for samples with multiple groups. The correlation analysis was performed using Pearson's correlation coefficient. The survival analysis was tested by Log-rank test. P-value <0.05 was considered significant.

3 Results

3.1 Screening of the hub genes associated with neutrophil infiltration in LUAD

All LUAD data were extracted from the TCGA database. The neutrophil infiltration in each sample was scored via five independent methods: TIMER, CIBERSORT, QUANTISEQ, XCELL, and MCPCOUNTER. Then, all patients were divided into low and high infiltration groups. Thirty patients with low infiltration (Figure 1A) and 24 with high infiltration (Figure 1B) were identified in all five methods.

Then, the DEG analysis was performed between the two groups (Figure 1C). Among these DEGs, 287 genes were confirmed as significantly associated with PFS. After intersecting these 287 genes and neutrophils-specific elevated genes retrieved from THPA, 30 genes were selected as hub genes ultimately (Figure 1D). The official symbols and univariate Cox regression analysis of these 30 hub genes were listed in Table 1. The results of other PFS-associated DEGs were shown in Supplementary Table 3.

3.2 Consensus clustering analysis based on the 30 hub genes

Using the screened 30 hub genes mentioned above, we performed consensus clustering analysis on all LUAD patients in TCGA, dividing them into three groups - A, B, and C (Figure 2A). Each gene showed differential expression among the three groups (Figure 2B). Group A mainly exhibited lower expression of the 30 genes, Group B had significantly higher expression, and Group C displayed intermediate levels (Figure 2C, *top panel*). The groups also showed significant differences in gender distribution (P=0.00043) and TNM staging (P=0.001) (Figure 2C, *bottom panel*). Moreover, significant differences in prognosis were observed, with Group C having the lowest PFS (P<0.001) and OS (P=0.001) (Figures 2D, E). Additionally, each group exhibited differential prognostic trends in disease-free survival (DFS) (P=0.072) and significant differences in disease-specific survival (DSS) (P=0.002) (Supplementary Figures 1A, B).

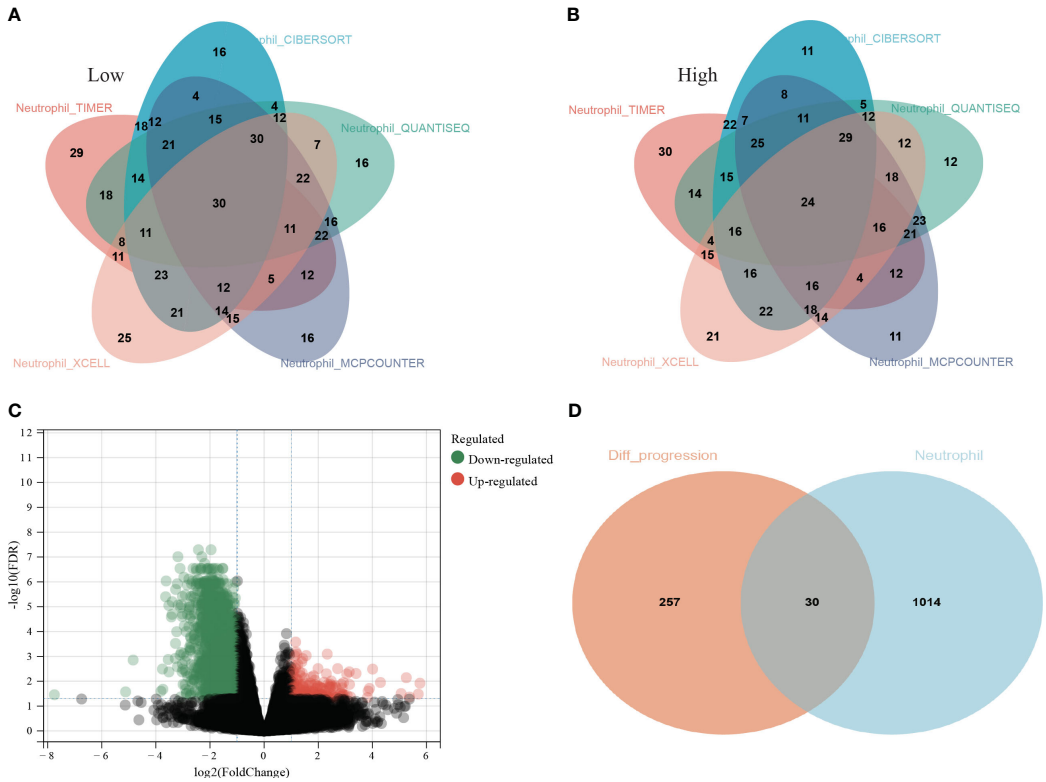

FIGURE 1
Screening process of the thirty hub genes. **(A)** Thirty lung adenocarcinoma (LUAD) patients from TCGA database were identified as low neutrophil infiltration according to TIMER, CIBERSORT, QUANTISEQ, XCELL, and MCPCOUNTER analysis; **(B)** twenty-four LUAD patients were identified as high neutrophil infiltration; **(C)** The differentially expressed genes (DEGs) between high and low neutrophil infiltration patients; **(D)** 287 genes among the DEGs were associated with PFS (*orange circle*) and 1044 genes specifically elevated in neutrophils were download from THPA (*cyan circle*). Thirty genes were ultimately selected as hub genes associated with neutrophil infiltration in LUAD (*overlap region*).

10.3389/fimmu.2023.1304529

TABLE 1 Official symbols and univariate Cox regression analysis of the 30 hub genes.

Official symbols of the 30 hub genes	Hazard ratio (HR)	HR 0.95L	HR 0.95H	P-value
RNF175	0.794973	0.638474	0.989833	0.040236
CFP	0.813738	0.671622	0.985927	0.035319
SCARF1	0.835366	0.713439	0.97813	0.02544
DPEP2	0.844535	0.717108	0.994604	0.042888
PRAM1	0.849817	0.729501	0.989976	0.03668
NCF1	0.858761	0.73832	0.99885	0.048281
GPX3	0.866249	0.77219	0.971764	0.01435
TLR2	0.870601	0.780534	0.97106	0.012882
P2RY13	0.872838	0.767962	0.992037	0.037308
CYP27A1	0.873393	0.77547	0.983683	0.025673
TMEM130	0.896336	0.818025	0.982143	0.018964
ALPL	0.925434	0.864133	0.991084	0.026685
C4BPA	0.938682	0.886638	0.993782	0.029683
TNFAIP6	1.137979	1.013886	1.27726	0.028231
NAMPT	1.143029	1.01787	1.283578	0.023864
PLAUR	1.161761	1.027196	1.313953	0.016978
SOD2	1.167791	1.003731	1.358666	0.044624
ITGA5	1.169639	1.027687	1.331198	0.017612
RGS2	1.174756	1.043412	1.322634	0.007757
MBOAT2	1.180258	1.023182	1.361448	0.022937
DDX58	1.188232	1.0098	1.398193	0.037761
ITPRIP	1.193036	1.002325	1.420033	0.047023
RELL1	1.195204	1.032019	1.384192	0.017277
MCTP1	1.209421	1.030428	1.419507	0.019978
PCSK5	1.20998	1.021865	1.432725	0.027047
FOSL2	1.22138	1.045147	1.42733	0.011891
MXD1	1.237342	1.056558	1.449059	0.008226
TLR6	1.258264	1.055564	1.499889	0.010367
SLC2A14	1.289774	1.030839	1.613751	0.02604
KIAA0825	1.47937	1.18471	1.847316	0.000549

3.3 Neutrophil infiltration scoring in LUAD

3.3.1 Validation of neutrophil scoring model

The neutrophil scoring model was developed using the PCA algorithm depending on the 30 hub genes. All LUAD patients from TCGA were divided into high and low neutrophil score groups. Five independent TICs analysis methods were used to validate the effectiveness of this new scoring model. Results showed that patients with high scores showed significantly increased neutrophil infiltration scores in TIMER, MCPCOUNTER, and QUANTISEQ (P<0.001 for all) (Figure 3A). In XCELL, high-score patients exhibited lower neutrophil infiltration (P=0.011) (Figure 3A). In CIBERSORT, there was no difference between the two groups (Figure 3A).

We further assessed the neutrophil scores in the three patient groups mentioned in the consensus clustering analysis. Results showed that Group A had the lowest scores, followed by Group C, and Group B had the highest scores, with significant differences among the groups (Figure 3B). The scores aligned with their gene expression profiles. Meanwhile, consistent with the clustering analysis, Group C had the highest proportion of recurrences (Figure 3C).

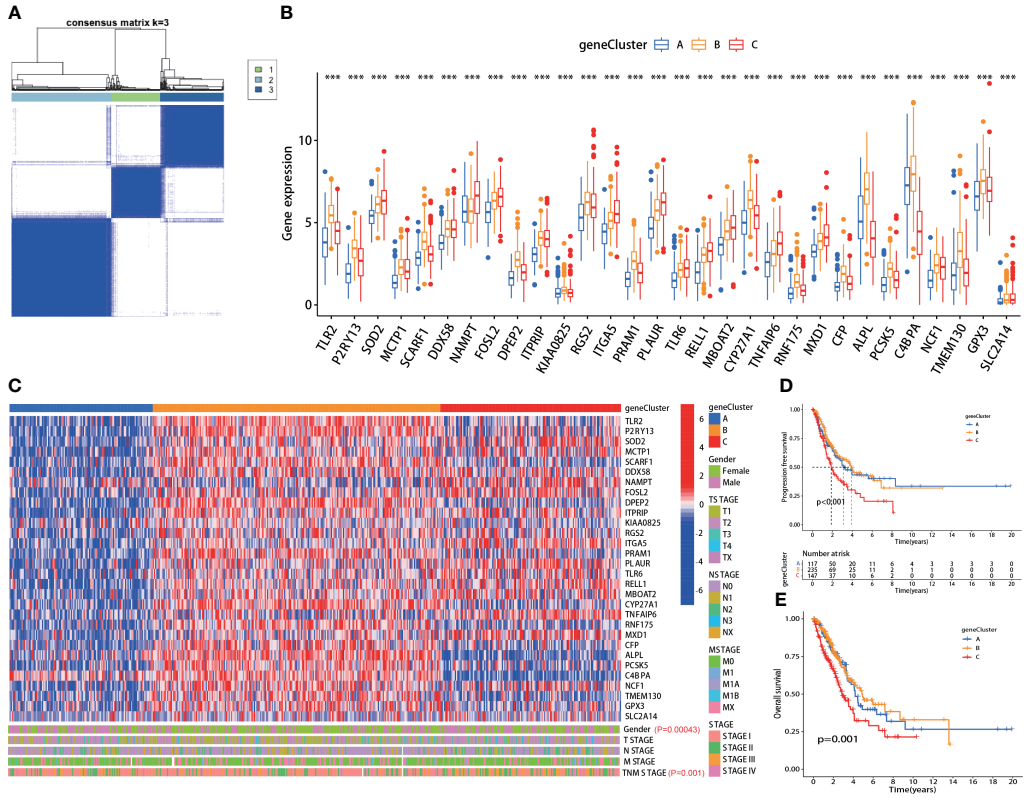

FIGURE 2
The hub genes correlated with clinical characteristics in lung adenocarcinoma (LUAD). **(A)** All LUAD patients in TCGA were divided into A, B, and C groups by consensus clustering analysis according to the 30 hub genes; **(B)** The expression of each hub gene was significantly different among the three groups; **(C)** *Top panel*: heatmap of the 30 hub genes in each group; *Bottom panel*: each group exhibited different clinical features in gender and TNM staging; **(D, E)** The A, B and C group patients showed significant difference in PFS (p<0.001) and OS (p=0.001). ***:p-value < 0.001.

3.3.2 Neutrophil scoring positively correlated with prognosis

Survival analysis revealed that patients with low neutrophil scores presented significantly lower PFS (P<0.001), OS (P<0.001), DFS (P=0.017), and DSS (P<0.001) (Figures 3D–G). The low-scoring group also showed a higher recurrence rate than the high-scoring group (47% vs. 32%) (Figure 3H). Following stratified analyses demonstrated that low neutrophil score patients also exhibited significantly lower PFS in aged over 65 (P<0.001), female (P=0.006), male (P=0.034), and stages I-II (P=0.006) class (Supplementary Figure 2). Neutrophil scores were significantly lower in recurrent patients than in non-recurrent patients (P=0.0039) (Figure 3I). Meanwhile, the low neutrophil score group also presented significantly worse OS (P=0.0038) (Supplementary Figure 3) in data derived from GSE50081.

3.3.3 Neutrophil scoring correlated with PD-L1 and TMB and promoted their prognosis-predicting capability

Patients with high neutrophil sore presented higher PD-L1 expression (P<0.001) (Figure 4A). Further correlation analysis demonstrated that neutrophil score was significantly positively correlated with PD-L1 expression in LUADs (R=0.38, P<0.001) (Figure 4A). TMB, on the contrary, presented significant reverse results as negatively correlated with neutrophil score (R=-0.31, P<0.001) (Figure 4C). The genetic mutation status of the two groups was also basically consistent with TMB, as 273 of 281 (97.15%) in the low-score group and 190 of 222 (85.59%) in the high-score group exhibited gene mutations (Figure 4B).

Interestingly, the neutrophil scoring might improve the prognosis-predicting capability of PD-L1 and TMB in lung adenocarcinoma. Patients with high PD-L1 expression had slightly worse PFS than those with low PD-L1 expression (P=0.039), while there was no significant difference between high and low TMB patients (P=0.139) (Supplementary Figure 4). When combined with neutrophil scoring, respectively, significant differences were observed among each group in both PD-L1 (P<0.001) (Figure 4D) and TMB (P<0.001) (Figure 4E).

3.3.4 Neutrophil scoring correlated with tumor immune microenvironment (TIME) in lung adenocarcinoma

IPS was performed between the high and low neutrophil score groups. We found that the high-scoring group presented significantly higher effector cells (EC) and major histocompatibility complex (MHC) scores and lower checkpoints (CP) and suppressor cells (SC) scores (Figure 5A). The IPS total score was also higher in the high-scoring group (Figure 5A).

10.3389/fimmu.2023.1304529

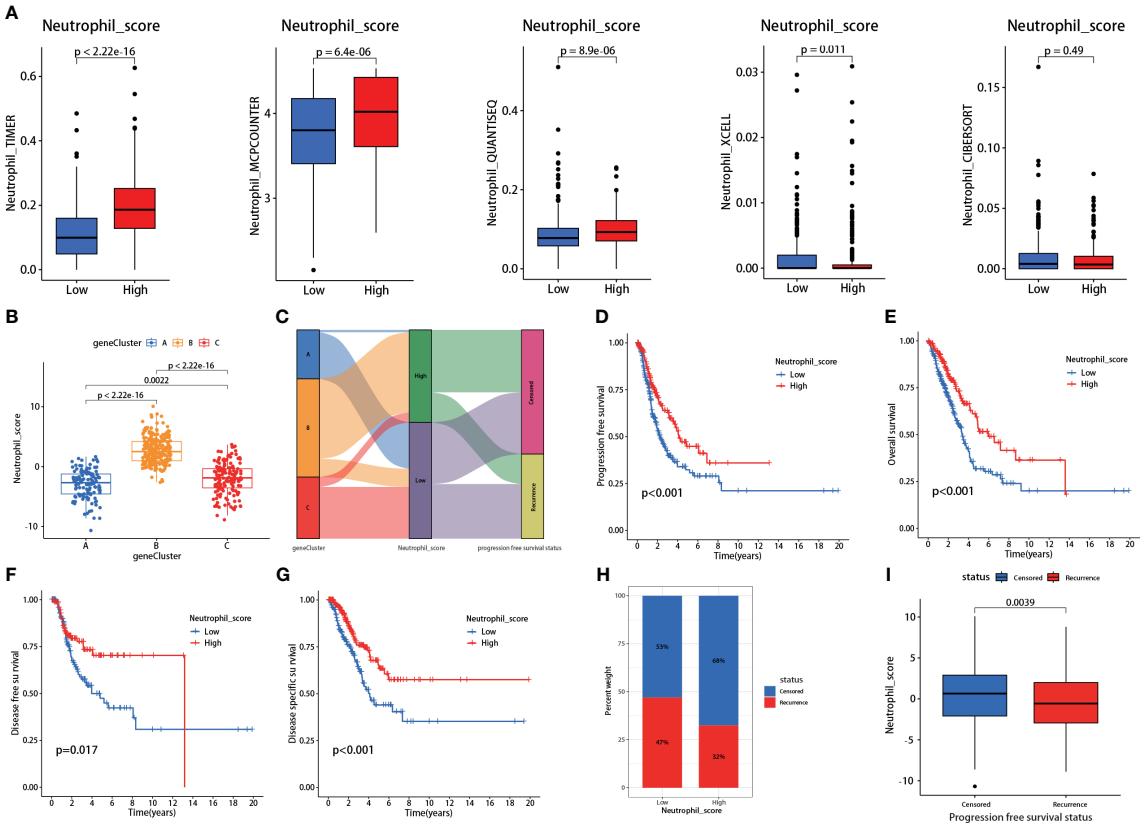

FIGURE 3
Validations and prognosis predicting effects of the neutrophil scoring model. **(A)** Based on the hub genes, a new neutrophil scoring model was developed by PCA algorithm and validated via five independent tumor-infiltrating immune cells (TICs) analysis methods; **(B)** Each group from consensus clustering analysis exhibited a significant difference in neutrophil sore; **(C)** Group C presented the highest proportion of recurrences; **(D–G)** low neutrophil score patients exhibited significantly lower PFS (P<0.001), OS (P<0.001), DFS (P=0.017), and DSS (P<0.001); **(H)** Low neutrophil score patients presented higher recurrence rate (47% vs 32%); **(I)** Recurrent patients also exhibited lower neutrophil score (P=0.0039).

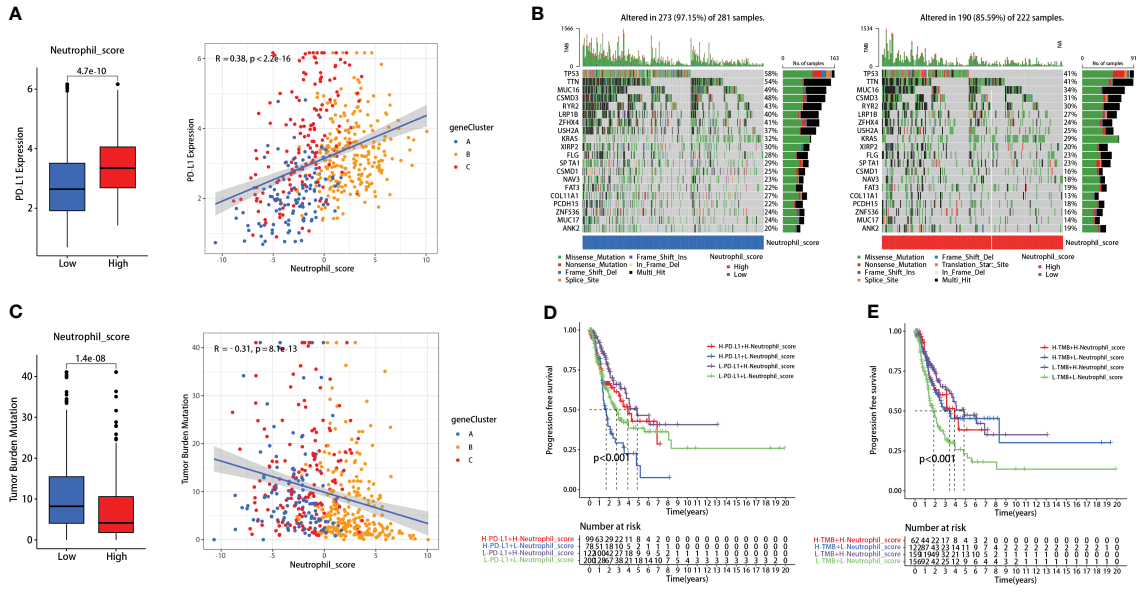

FIGURE 4
Neutrophil score correlated with PD-L1 and tumor mutational burden (TMB). **(A)** Neutrophil score positively correlated with PD-L1; **(B)** 273 of 281 (97.15%) low-score patients and 190 of 222 (85.59%) high-score patients exhibited gene mutations; **(C)** Neutrophil score negatively correlated with TMB; **(D)** Neutrophil score significantly promoted the FPS predicting effectiveness of PD-L1; **(E)** It also promoted the effectiveness of TMB.

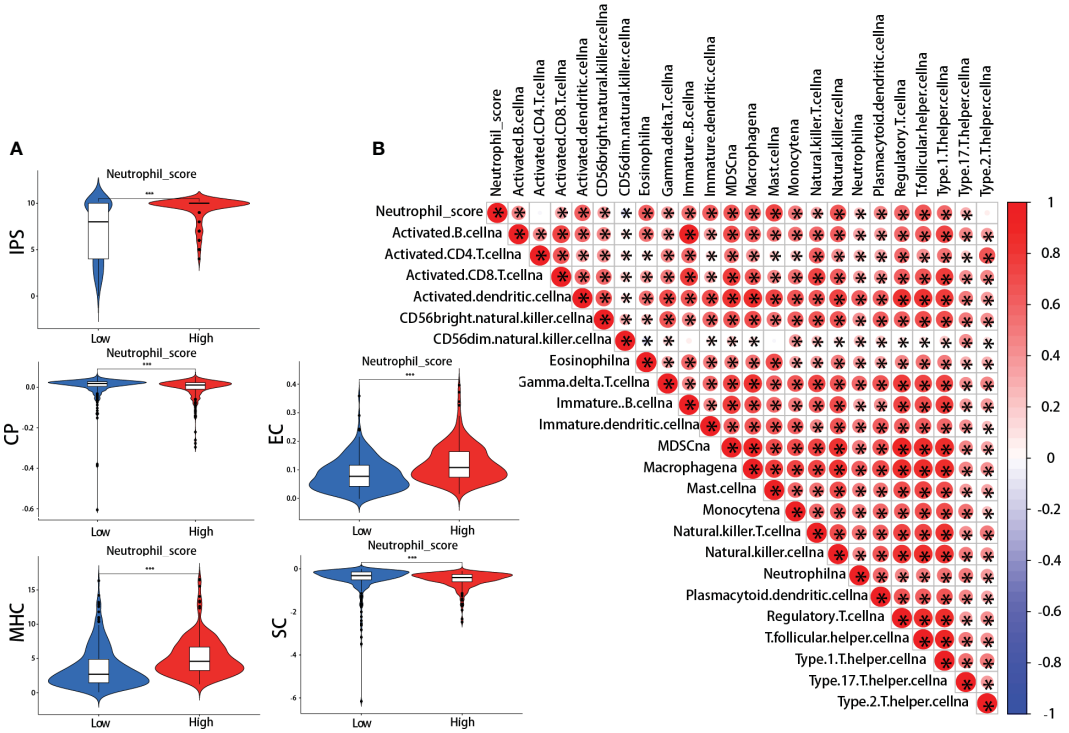

FIGURE 5
Neutrophil score and tumor immune microenvironment (TIME). **(A)** ImmunoPhenoScore (IPS): the high-scoring group presented higher total IPS, effector cells (EC), and major histocompatibility complex (MHC) scores, and lower checkpoints (CP) and suppressor cells (SC) scores; **(B)** The correlations between neutrophil score and other cells in TIME. *: p-value < 0.05; ***:p-value < 0.001.

Meanwhile, further analysis revealed that neutrophil score was closely related to the infiltration of other immune cells, including cytotoxic CD8 + T cells, effector CD4 + T cells, natural killer cells (NK), Tregs, myeloid-derived suppressor cells (MDSCs), and macrophages (Figure 5B). The neutrophil scoring was broadly correlated with TIME in lung adenocarcinoma.

3.4 Ten genes, including TNFAIP6, might be correlated with the pro-tumor effects of TANs

TANs exhibit both pro-tumor and anti-tumor effects in the tumor microenvironment. We performed the following procedures to screen for the genes closely associated with the pro-tumor effects of TANs. Firstly, we analyzed the differential expression of the 30 hub genes between tumor and normal tissues in LUAD patients from the TCGA database (Figure 6A). We also collected paired cancer and normal tissues from our department's surgical resections of LUAD patients. The differential expression of these 30 hub genes was further validated in those fresh specimens via qPCR (Figure 6B). The hazard ratio of each hub gene has been assessed via univariate Cox regression, as mentioned above (Table 1).

After taking the intersection, we found that TNFAIP6 and TLR6 were not only overexpressed in cancer tissue but also indicated poorer prognosis (Figure 6C). The P2RY13, SCARF1, DPEP2, PRAM1, CYP27A1, CFP, GPX3, and NCF1 were low expressed in cancer tissue and indicated better prognosis (Figure 6C). We speculated that dysregulation of these ten genes might indicate the pro-tumor effects of TANs in lung adenocarcinoma.

3.5 TNFAIP6 overexpressed in lung adenocarcinoma cells and might promote neutrophil "N2" polarization *in vitro*

In order to further screen the potential genes differentially expressed in tumor cells specifically, instead of TICs in TIME, we used qPCR to test the expression of all the ten genes in the A549, PC9, and H1975 cell lines with the BEAS-2B cell line as a control. The results showed that TNFAIP6, TLR6, P2RY13, and CYP27A1 were significantly differentially expressed in all A549, PC9, and H1975 cell lines (Figure 7A; Supplementary Figure 5). The TNFAIP6 protein was significantly overexpressed in cancer tissue compared to normal pulmonary tissue, according to the IHC examination (Figure 7B). Then, the TNFAIP6 was knocked down in both A549 and PC9 cells (Supplementary Figure 6). The CCK8 assay showed that TNFAIP6 might not affect the proliferation of A549 and PC9 cells (Supplementary Figure 7). After co-culturing healthy human neutrophils with the conditioned medium (Figure 7C), we found that knocking down TNFAIP6 in A549 and PC9 led to the elevated expression of FAS, CCL3, and ICAM-1 in neutrophils while reducing the expression of CCL2, CXCR4, and

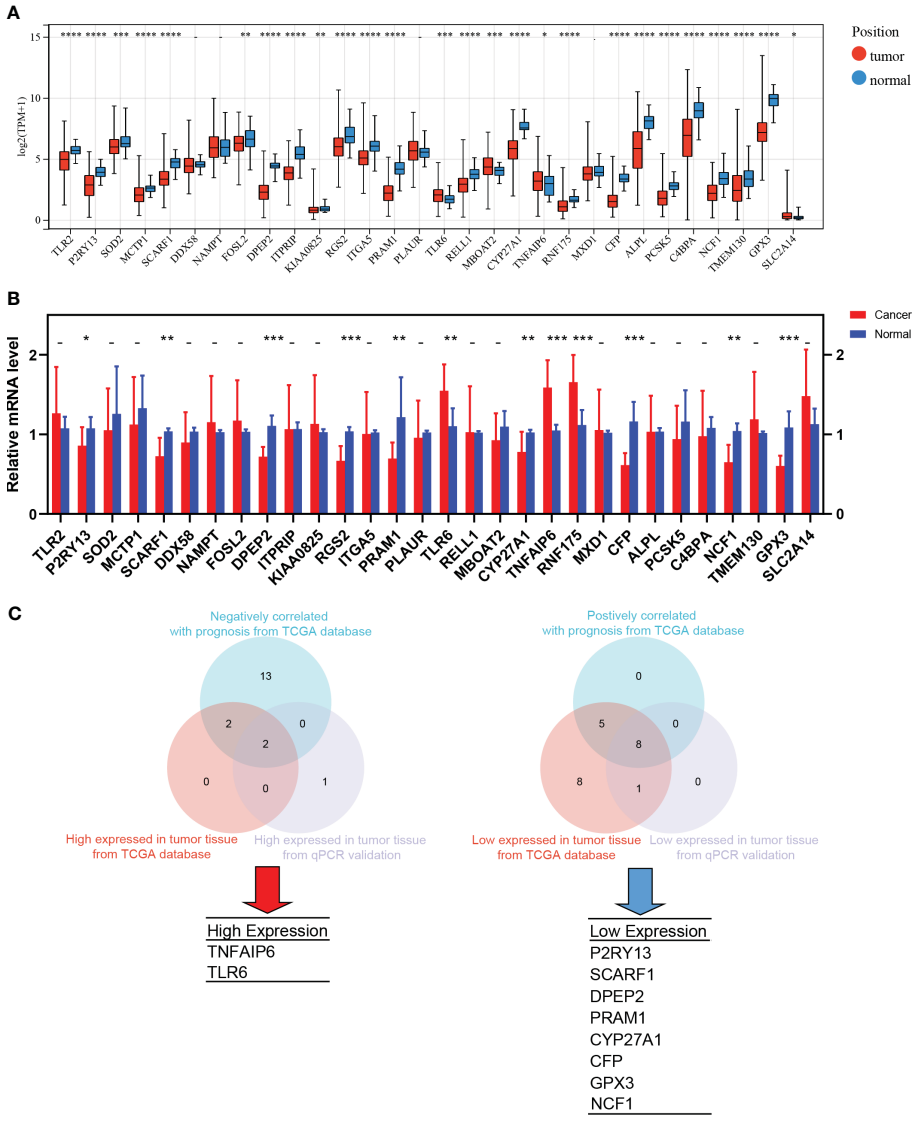

FIGURE 6
The screening process of pro-tumor effects associated genes. **(A)** Differential expression of the 30 hub genes between tumor and normal tissues in LUAD from TCGA; **(B)** The differential expression was further validated in the fresh samples collected from our department; **(C)** The strategy and results of the pro-tumor effects associated genes screening. *: p-value < 0.05; **: p-value < 0.01; ***:p-value < 0.001; ****: p-value < 0.0001.

VEGF-A (Figures 7D, E). The CM derived from TNFAIP6 knock-downed A549 and PC9 cells also promoted the early apoptosis rate of neutrophils (Figure 7F). Furthermore, the LC-MS/MS analysis showed that eight cytokines, including glucose-6-phosphate isomerase (GPI), C-X-C motif chemokine ligand 5 (CXCL5), macrophage migration inhibitory factor (MIF), secreted phosphoprotein 1 (SPP1), C-X-C motif chemokine ligand 1 (CXCL1), colony stimulating factor 1 (CSF1), transforming growth factor beta 2 (TGFB2), and CCL2, were secreted into the CMs. The label-free quantification showed that the secretion of SPP1 (P=0.012) and CCL2 (P<0.001) was significantly decreased in si TNFAIP6 CM (Table 2).

4 Discussion

The effects of TANs on lung adenocarcinoma remain unclear (22, 23). The specific gene sets that can assess neutrophil infiltration are still uncertain. In this study, we employed the five most widely used TICs analysis methods, based on the TCGA database, to explore the DEGs between high and low neutrophil infiltration patients. Then, by intersecting DEGs, prognosis effects, and neutrophils-specific expressed genes from THPA, we preliminarily identified 30 hub genes (Figure 1; gene symbols were listed in Table 1). Then, subsequent consensus clustering analysis validated that these hub genes might be widely associated

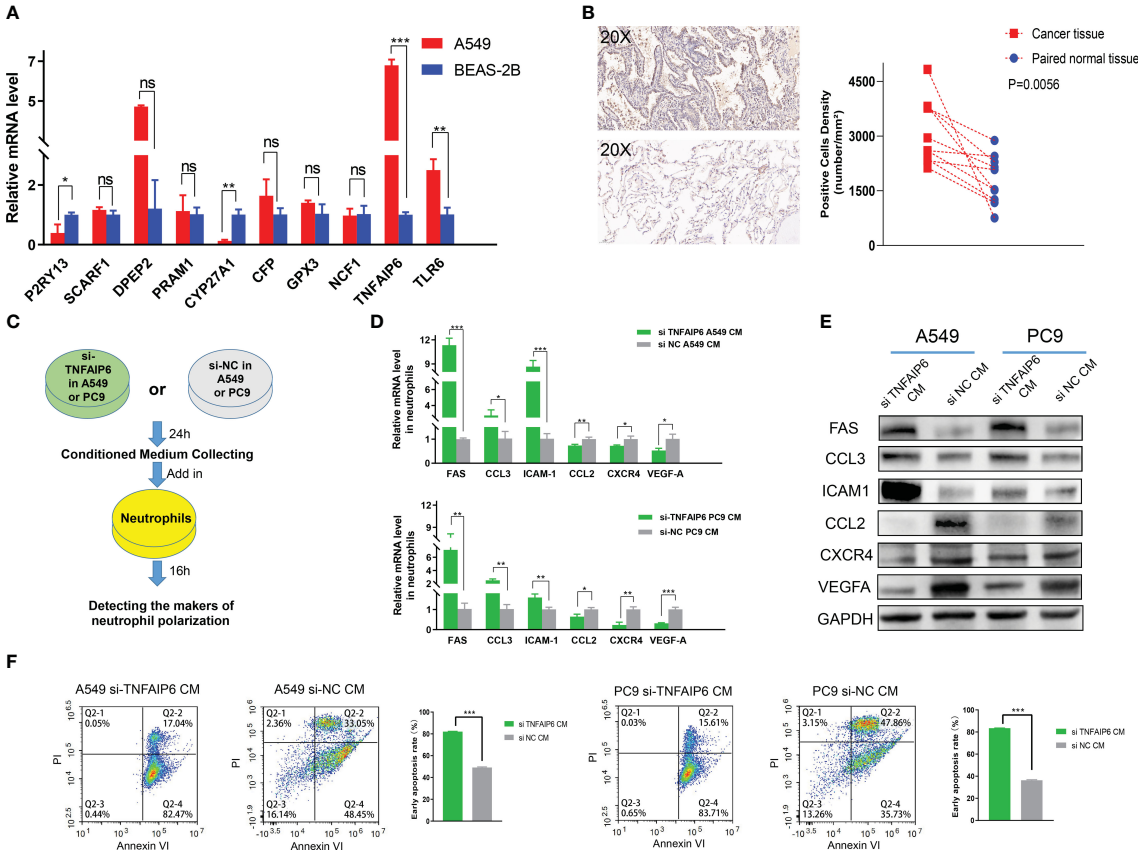

FIGURE 7
TNFAIP6 and pro-tumor effects. **(A)** TNFAIP6, TLR6, P2RY13, and CYP27A1 were significantly dysregulated in all A549, PC9, and H1975 cells (results of PC9 and H1975 shown in Supplementary Figure 5), compared to BEAS-2B cells; **(B)** Immunohistochemical (IHC) staining of TNFAIP6. *Left panel*: typical IHC staining images of lung adenocarcinoma (LUAD) tissue (*top part*) and normal tissue (*bottom part*); *Right panel*: statistical analysis showed TNFAIP6 significantly overexpressed in LUAD tissues; **(C)** Flowchart of the co-culturing procedure; **(D, E)** Knocking down TNFAIP6 in A549 and PC9 resulted in upregulating of FAS, CCL3, and ICAM-1 and downregulating of CCL2, CXCR4, and VEGF-A in neutrophils; **(F)** Knocking down TNFAIP6 in A549 (*left panel*, P<0.001) and PC9 (*right panel*, P<0.001) significantly evaluated the early apoptosis rate of neutrophils. ns: p-value≥0.05; *: p-value<0.05; **: p-value < 0.01; ***:p-value < 0.001.

TABLE 2 Label-free quantification of the differentially secreted cytokines between si NC and si TNFAIP6 A549 cells.

Cytokines	Abundance Ratio: (si NC)/(si TNFAIP6)	Abundance Ratio Adj. P-Value	Abundance Ratio Variability [%]	Score Sequest HT:
GPI	0.698	0.844103815	40.99	1682.79
CXCL5	0.531	0.499366075	58.51	1276.87
MIF	0.555	0.57501736	39.93	396.26
SPP1*	2.737	0.012491252	65.39	391.73
CXCL1	1.058	0.872092929	66.63	239.71
CSF1	0.523	0.479401422	17.95	202.3
TGFB2	1.394	0.555152029	21.94	136.31
CCL2***	4.485	4.62414E-05	17.6	63.43

PS: * 0.05>P>0.01, ***P<0.001.

with clinical pathological features and prognosis in LUAD (Figure 2; Supplementary Figure 1).

The specific neutrophil infiltration scoring in LUAD has not been reported yet. Thus, based on these 30 hub genes, we developed a comprehensive scoring system that might be able to evaluate the neutrophil infiltration in LUADs precisely. The following multiple-method validation revealed that this scoring system effectively reflected neutrophil infiltration status and correlated with essential clinical characteristics (Figures 3A–C).

Due to the dual effects of neutrophils on cancers, the prognosis prediction in LUAD by traditional neutrophil infiltration scoring methods was ambiguous. For example, *Xinyan Liu* et al. reported no significant association between neutrophil infiltration and prognosis in LUAD (23). In contrast, *Mehrdad Rakaee* et al. reported that high neutrophil infiltration density suggests a poor prognosis in LUAD (22). Unlike other TICs analysis methods, our neutrophil infiltration scoring system was developed based on the prognosis-related hub genes. It was significantly associated with PFS, OS, DFS, DSS, and recurrence rate in LUADs (Figures 3D–I). Meanwhile, we further validated the prognosis predictive capability of the scoring system in an independent cohort, resulting in similar outcomes (Supplementary Figure 3).

Our neutrophil scoring system might apply to immune checkpoint inhibitors (ICIs) efficacy prediction. Over the past decade, research outcomes regarding ICIs have revolutionized the lung cancer treatment landscape (37). For instance, Pembrolizumab has significantly improved the 5-year survival rate of advanced NSCLC patients and has been approved for first-line treatment in patients with PD-L1 tumor proportion score (TPS) ≥1% and without EGFR/ALK gene alterations (38, 39). Recent studies have underscored the pivotal role of TANs in the anti-tumor immune response, showing their capacity to disrupt ICI responses and their correlation with ICIs acquired resistance (40). Our results showed that the neutrophil score positively correlated with PD-L1 expression and negatively correlated with TMB (Figures 4A, C). PD-L1 and TMB are vital biomarkers for predicting ICI efficacy (41, 42). Our neutrophil infiltration scoring system maintained a significant association with PD-L1 and TMB and presented independence from these two biomarkers. These results indicated the potential predictive role of neutrophil sore in ICI treatment efficacy.

Meanwhile, the prognostic significance of PD-L1 and TMB in LUAD remains uncertain. Although the overexpressed PD-L1 was reported to be significantly associated with poor prognosis (43), the predictive effect of TMB on prognosis is less robust (44, 45). Consistent with these researches, our data also exhibited similar limitations of PD-L1 and TMB (Supplementary Figure 4). As the neutrophil soring might be independent of both PD-L1 and TMB, as discussed above, we combined these effects. Our neutrophil soring significantly improved the prognostic prediction of PD-L1 and TMB, respectively (Figures 4D, E).

The potential predictive value of neutrophil score for ICI efficacy and prognosis of LUAD patients might be attributed to the broad crosstalk between TANs and other cells in TIME (46). The TIME mainly comprises CD8 + T cells, CD4 + T cells, NK, Tregs, MDSCs, macrophages, etc (47). These cells can influence neutrophil infiltration and function by secreting chemokines to recruit neutrophils, inducing "N2" polarization, etc (1, 48). The TANs, on the other hand, also affect other cells in TIME, such as forming NETs to diminish the cytotoxic effects of CD8+ T cells on tumor cells (49). Our results indicated similar crosstalk effects on the bioinformatics level, as the neutrophil score was significantly associated with the IPS score and other TICs in LUAD (Figure 5).

Based on neutrophil sore potential values, we believed the 30 hub genes might be strongly associated with the infiltration of neutrophils in LUAD. They might extensively participate in the mechanisms of the neutrophil effect on cancer cells and TIME. As mentioned earlier, TANs exhibit a significant dual role in promoting and inhibiting tumor growth, named pro-tumor and anti-tumor effects. To further explore which specific genes are associated with TANs' pro-tumor effects, we integrated bioinformatics analyses, tissue validation, and prognosis analysis in the following investigations.

The results showed that the high expression of TNFAIP6 and TLR6, as well as the low expression of P2RY13, SCARF1, DPEP2, PRAM1, CYP27A1, CFP, GPX3, and NCF1 might be closely associated with pro-tumor effects (Figure 6). Thus, we speculated that these genes might be likely crucial regulators or key downstream targets in TANs' tumor-promoting activities.

Lung cancer tissue comprises tumor cells, extracellular matrix, immune cells, etc. The dysregulation of these ten genes might manifest in various cell types within the tumor tissue. Therefore, to preliminary identify genes that potentially have specific differential expression in tumor cells, we detected the expression of these ten genes in adenocarcinoma cell lines, including A549, PC9, and H1975. The BEAS-2B cell lines, which were isolated from normal human bronchial epithelium, were selected as the control group. Significant upregulation of TNFAIP6 and TLR6 and downregulation of P2RY13 and CYP27A1 were observed in all three adenocarcinoma cell lines (Figure 7A; Supplementary Figure 5).

TNFAIP6, also known as TSG-6 (50), exhibited anti-inflammatory effects in myocardial infarction and trauma repair (51). The role of TNFAIP6 in tumors was rarely reported. Several studies showed that TNFAIP6 can promote metastasis in gastric and colorectal cancers (52, 53). Its elevated expression has also been significantly associated with poor prognosis in urothelial carcinomas (54). The effect of TNFAIP6 on lung cancer and its TIME has not been reported yet. We knocked down TNFAIP6 expression in lung adenocarcinoma cells by siRNA (Supplementary Figure 6) and co-cultured neutrophils within its conditioned medium (Figure 7C). The results showed that FAS, CCL3, and ICAM-1 were significantly upregulated, and CCL2, CXCR4, and VEGF-A were downregulated in neutrophils (Figures 7D, E).

Various studies have employed FAS, CCL3, ICAM-1, CCL2, CXCR4, and VEGF-A as biomarkers to characterize "N1" and "N2" neutrophil phenotypes (55, 56). Among these, FAS, also known as CD95, is a transmembrane protein that triggers the apoptosis signaling pathway upon binding with FASL (57). *Z.G. Fridlender* et al. revealed that FAS was significantly overexpressed in "N1" polarized neutrophils (48). ICAM-1, an intercellular adhesion molecule that plays a pivotal role in inflammation, was also significantly elevated in "N1" polarized neutrophils, according to investigations conducted by *Mareike Ohms* et al. *in vitro* (58, 59).

CCL3, also known as macrophage inflammatory protein-1α (MIP-1α), might play dual effects in TIME (60). On one hand, its chemotactic function on dendritic cells and CD8+ T cells significantly promoted the anti-tumor effects of immune cells (61). On the other hand, CCL3 also recruited Tregs and MDSCs within the TIME to facilitate immune evasion (62). However, high expression of CCL3 was usually recognized as "N1" polarization in neutrophils (55, 56, 63).

Conversely, overexpressed CXCR4 might indicate "N2" polarization in neutrophils. *Chenghui Yang* et al. reported that aged neutrophils, characterized by high CXCR4 expression, promoted NETs formation, contributing to breast cancer lung metastasis (64). VEGFA, one of the VEGF family proteins, is primarily secreted by neutrophils (65). By binding to VEGFR2 and mediating multiple signaling pathways, VEGFA stimulates angiogenesis and promotes cancer progression in multiple cancers (66). Therefore, elevated VEGFA in neutrophils usually indicates "N2" polarization.

CCL2, known as monocyte chemoattractant protein-1 (MCP-1), primarily functions in monocyte chemotaxis (67). Although CCL2 was once considered to stimulate host anti-tumor responses in a T-lymphocyte-independent manner, it was recently widely recognized for its significant pro-tumor effects (68). Patients overexpressing CCL2 in cancer presented a worse prognosis (69). It also promoted proliferation and enhanced stemness in cancer cells (70, 71). *Shao-Lai Zhou* et al. reported that TANs secreted CCL2 to recruit macrophages and Tregs, promoting hepatocellular carcinoma proliferation (72). Overexpressed CCL2 in neutrophils might promote its pro-tumor effects.

Thus, according to the above literature reports and our experimental results, we speculated that TNFAIP6 overexpressed in lung cancer might induce the "N2" polarization and pro-tumor effects on neutrophils. The "N2" polarization of neutrophils also exhibited a lower apoptosis rate in TIME (63, 73). Our results showed that the neutrophil's early apoptosis rate was significantly evaluated when treated with si TNFAIP6 CM, further validating our speculation (Figure 7F).

There are several limitations in this study. Firstly, we identified the 30 hub genes closely associated with neutrophil infiltration in LUAD and developed a scoring system correlating with prognosis. However, the scoring system solely assessed the infiltration of neutrophils. It was unable to distinguish whether TANs exhibited anti-tumor or pro-tumor effects. The relationship between neutrophil infiltration and prognosis is intricate. Solely evaluating the infiltration might lead to unexpected outcomes in some patients. For instance, in our study, patients in Cluster A, despite having lower scores than Cluster C (Figure 3B), exhibited better PFS and OS outcomes (Figures 2D, E). Therefore, we further identified 10 out of these 30 hub genes potentially associated with the pro-tumor function of TANs preliminarily. Although the results might be subject to bias, further multi-omic, high-throughput, and multidimensional studies based on these 10 genes could potentially explore evaluation methods capable of simultaneously reflecting TAN infiltration and function.

Meanwhile, our *in vitro* experiments revealed significant upregulation of TNFAIP6 in lung adenocarcinoma cells, which could potentially lead to the "N2" polarization of neutrophils. However, the underlying mechanisms remain unclear. Hence, we performed LC-MS/MS analysis in the CMs. By LFQ, we found that TNFAIP6 significantly stimulated the secretion of CCL2 and SPP1 in LUAD cells (Table 2). As discussed above, CCL2 might promote neutrophil "N2" polarization in TIME. SPP1, also known as osteopontin (OPN), is secreted by various cells and plays a crucial role in immune regulation (74, 75). Patients with overexpressed SPP1 in lung cancer presented a poor prognosis (76). The SPP1 also stimulated NETs formation to promote cancer progression (77). Thus, the effects of TNFAIP6 might be attributed to CCL2 and SPP1 secretion. The specific regulatory mechanism requires further investigation. Furthermore, we detected the effects of TNFAIP6 on cancer cell viability by CCK8 assays. Results showed that TNFAIP6 might not or slightly promote LUAD cell proliferation (Supplementary Figure 7). Whether TNFAIP6 directly affects cancer cell proliferation also needs further validation.

In addition, whether and how differential expressing TLR6, P2RY13, and CYP27A1 in LUAD cells promote neutrophils' pro-tumors effects still requires further investigation. Neutrophils contribute to tumor progression through various mechanisms, including N2 polarization, NETs formation, inhibition of NK and CD8+ T cell cytotoxicity, and secretion of pro-angiogenic cytokines (1). Our results in this study indicated that TNFAIP6 might stimulate the neutrophils' pro-tumor effects by inducing "N2" polarization. However, whether TLR6, P2RY13, and CYP27A1 operate through similar mechanisms remains unclear. For instance, no significant alteration in neutrophil polarization was observed when co-cultured with the CM derived from TLR6 knocking down LUAD cells (Supplementary Figure 8). Further comprehensive studies may reveal the underlying mechanisms.

In conclusion, TANs play a crucial role in lung adenocarcinoma. Thirty hub genes identified in this study might broadly participate in the neutrophil effects on LUADs. The neutrophil scoring system, developed based on these 30 hub genes, could effectively predict prognosis and potentially reflect the ICI efficacy and TIME situations in LUADs. 10 of 30 hub genes were further screened as significantly associated with pro-tumor effects of TANs. TNFAIP6, as one of these pro-tumor genes, was significantly overexpressed in lung adenocarcinoma cells and might lead to the "N2" polarization of neutrophils *in vitro*. Further research on these hub genes, provided in this pilot study, may unravel the mechanisms of TANs affecting the TIME and development of LUADs.

Data availability statement

The raw data supporting the conclusions of this article will be made available by the authors, without undue reservation.

Ethics statement

The studies involving humans were approved by Ethical Committee of Tianjin Medical University General Hospital. The

studies were conducted in accordance with the local legislation and institutional requirements. The participants provided their written informed consent to participate in this study.

Author contributions

RL: Conceptualization, Funding acquisition, Investigation, Methodology, Visualization, Writing – original draft, Writing – review & editing, Data curation, Project administration, Software, Validation. GZ: Conceptualization, Data curation, Formal analysis, Investigation, Methodology, Software, Validation, Visualization, Writing – review & editing, Writing – original draft. YS: Conceptualization, Data curation, Investigation, Methodology, Software, Validation, Visualization, Writing – original draft, Writing – review & editing. ML: Conceptualization, Investigation, Methodology, Validation, Visualization, Writing – review & editing. ZH: Investigation, Software, Visualization, Writing – review & editing. PC: Conceptualization, Data curation, Writing – review & editing. XL: Conceptualization, Investigation, Methodology, Writing – review & editing. ZS: Conceptualization, Investigation, Validation, Writing – review & editing. JC: Conceptualization, Funding acquisition, Methodology, Writing – review & editing.

Funding

The author(s) declare financial support was received for the research, authorship, and/or publication of this article. This study was supported by grants from the Tianjin Key Medical Discipline (Specialty) Construction Project [TJLCZJ2021-12] and the National Natural Science Foundation of China [82303537].

Conflict of interest

The authors declare that the research was conducted in the absence of any commercial or financial relationships that could be construed as a potential conflict of interest.

The reviewer SL declared a shared affiliation with the authors to the handling editor at the time of review.

Publisher's note

Supplementary material

The Supplementary Material for this article can be found online at: https://www.frontiersin.org/articles/10.3389/fimmu.2023.1304529/full#supplementary-material

SUPPLEMENTARY FIGURE 1
DFS and DSS of the patients grouped by consensus clustering analysis. Lung adenocarcinoma patients were grouped by consensus clustering analysis based on the 30 hub genes. Each group exhibited differential prognostic trends in DFS (P=0.072) **(A)** and significant differences in DSS (P=0.002) **(B)**.

SUPPLEMENTARY FIGURE 2
Stratified analyses in PFS of the patients with different neutrophil scores. **(A)** No significant difference in PFS was found in the patients aged less than 65 (P=0.098); **(B–E)** Low neutrophil score patients exhibited significantly lower PFS in aged over 65 (P<0.001), female (P=0.006), male (P=0.034), and stages I-II (P=0.006) class; **(F)** For stages III-IV patients, low neutrophil score exhibited lower PFS tendency (P=0.229).

SUPPLEMENTARY FIGURE 3
Survival analysis of neutrophil score in data from GSE50081. **(A)** The overall survival analysis between low and high neutrophil score groups; **(B)** The receiver operating characteristic curve of the neutrophil score.

SUPPLEMENTARY FIGURE 4
Survival analysis of PD-L1 and TMB in lung adenocarcinoma (LUAD). **(A)** Lower PD-L1 expression in LUAD patients presented better PFS (P=0.039); **(B)** No significant differences were found between low and high TMB patients.

SUPPLEMENTARY FIGURE 5
The expression of all the ten genes in PC9 and H1975 cells, compared to BEAS-2B cells. The TNFAIP6, TLR6, P2RY13, and CYP27A1 were significantly differently expressed in both PC9 **(A)** and H1975 **(B)** cells.

SUPPLEMENTARY FIGURE 6
Knocking down TNFAIP6 in A549 and PC9. **(A)** Si TNFAIP6-2 has strongly inhibited the mRNA expression in A549 cells; **(B)** Si TNFAIP6-2 was selected to transfect into A549 and PC9 and validated by WB.

SUPPLEMENTARY FIGURE 7
CCK8 assay. TNFAIP6 might not affect the proliferation of A549 **(A)** and PC9 **(B)** cells.

SUPPLEMENTARY FIGURE 8
TLR6 in lung adenocarcinoma cells might not affect the polarization of neutrophils. **(A)** Si TLR6-1 strongly inhibited the mRNA expression in A549 cells; **(B)** Si TLR6-1 was selected to transfect into A549 and PC9 and validated by WB; **(C)** Knocking down TLR6 in A549 did not affect the expression of FAS, CCL3, ICAM-1, CCL2, CXCR4, and VEGF-A in neutrophils; **(D)** Although knocking down TLR6 in PC9 unregulated the expression of CCL3 (indicating "N1" polarization), it also elevated the expression of CCL2 (indicating "N2" polarization) in neutrophils. Meanwhile, no significant difference was observed in the expression of FAS, ICAM-1, CXCR4, and VEGF-A.

References

1. Coffelt SB, Wellenstein MD, de Visser KE. Neutrophils in cancer: neutral no more. *Nat Rev Cancer* (2016) 16:431–46. doi: 10.1038/nrc.2016.52

2. Bronte V, Brandau S, Chen SH, Colombo MP, Frey AB, Greten TF, et al. Recommendations for myeloid-derived suppressor cell nomenclature and characterization standards. *Nat Commun* (2016) 7:12150. doi: 10.1038/ncomms12150

3. Thanabalasuriar A, Scott BNV, Peiseler M, Willson ME, Zeng Z, Warrener P, et al. Neutrophil extracellular traps confine pseudomonas aeruginosa ocular biofilms and restrict brain invasion. *Cell Host Microbe* (2019) 25:526–536 e524. doi: 10.1016/j.chom.2019.02.007

4. Mantovani A, Cassatella MA, Costantini C, Jaillon S. Neutrophils in the activation and regulation of innate and adaptive immunity. *Nat Rev Immunol* (2011) 11:519–31. doi: 10.1038/nri3024

5. Aruga A, Aruga E, Cameron MJ, Chang AE. Different cytokine profiles released by CD4+ and CD8+ tumor-draining lymph node cells involved in mediating tumor regression. *J Leukoc Biol* (1997) 61:507–16. doi: 10.1002/jlb.61.4.507

6. Uribe-Querol E, Rosales C. Neutrophils in cancer: two sides of the same coin. *J Immunol Res* (2015) 2015:983698. doi: 10.1155/2015/983698

7. Wislez M, Rabbe N, Marchal J, Milleron B, Crestani B, Mayaud C, et al. Hepatocyte growth factor production by neutrophils infiltrating bronchioloalveolar subtype pulmonary adenocarcinoma: role in tumor progression and death. *Cancer Res* (2003) 63:1405–12.

8. Jensen HK, Donskov F, Marcussen N, Nordsmark M, Lundbeck F, von der Maase H. Presence of intratumoral neutrophils is an independent prognostic factor in localized renal cell carcinoma. *J Clin Oncol* (2009) 27:4709–17. doi: 10.1200/JCO.2008.18.9498

9. Trellakis S, Bruderek K, Dumitru CA, Gholaman H, Gu X, Bankfalvi A, et al. Polymorphonuclear granulocytes in human head and neck cancer: enhanced inflammatory activity, modulation by cancer cells and expansion in advanced disease. *Int J Cancer* (2011) 129:2183–93. doi: 10.1002/ijc.25892

10. Canli O, Nicolas AM, Gupta J, Finkelmeier F, Goncharova O, Pesic M, et al. Myeloid cell-derived reactive oxygen species induce epithelial mutagenesis. *Cancer Cell* (2017) 32:869–883 e865. doi: 10.1016/j.ccell.2017.11.004

11. Houghton AM, Rzymkiewicz DM, Ji H, Gregory AD, Egea EE, Metz HE, et al. Neutrophil elastase-mediated degradation of IRS-1 accelerates lung tumor growth. *Nat Med* (2010) 16:219–23. doi: 10.1038/nm.2084

12. Nozawa H, Chiu C, Hanahan D. Infiltrating neutrophils mediate the initial angiogenic switch in a mouse model of multistage carcinogenesis. *Proc Natl Acad Sci USA* (2006) 103:12493–8. doi: 10.1073/pnas.0601807103

13. Kaltenmeier C, Simmons RL, Tohme S, Yazdani HO. Neutrophil extracellular traps (NETs) in cancer metastasis. *Cancers (Basel)* (2021) 13. doi: 10.3390/cancers13236131

14. Blaisdell A, Crequer A, Columbus D, Daikoku T, Mittal K, Dey SK, et al. Neutrophils oppose uterine epithelial carcinogenesis via debridement of hypoxic tumor cells. *Cancer Cell* (2015) 28:785–99. doi: 10.1016/j.ccell.2015.11.005

15. Koga Y, Matsuzaki A, Suminoe A, Hattori H, Hara T. Neutrophil-derived TNF-related apoptosis-inducing ligand (TRAIL): a novel mechanism of antitumor effect by neutrophils. *Cancer Res* (2004) 64:1037–43. doi: 10.1158/0008-5472.CAN-03-1808

16. Eruslanov EB, Bhojnagarwala PS, Quatromoni JG, Stephen TL, Ranganathan A, Deshpande C, et al. Tumor-associated neutrophils stimulate T cell responses in early-stage human lung cancer. *J Clin Invest* (2014) 124:5466–80. doi: 10.1172/JCI77053

17. Ponzetta A, Carriero R, Carnevale S, Barbagallo M, Molgora M, Perucchini C, et al. Neutrophils driving unconventional T cells mediate resistance against murine sarcomas and selected human tumors. *Cell* (2019) 178:346–360 e324. doi: 10.1016/j.cell.2019.05.047

18. Diem S, Schmid S, Krapf M, Flatz L, Born D, Jochum W, et al. Neutrophil-to-Lymphocyte ratio (NLR) and Platelet-to-Lymphocyte ratio (PLR) as prognostic markers in patients with non-small cell lung cancer (NSCLC) treated with nivolumab. *Lung Cancer* (2017) 111:176–81. doi: 10.1016/j.lungcan.2017.07.024

19. Tanizaki J, Haratani K, Hayashi H, Chiba Y, Nakamura Y, Yonesaka K, et al. Peripheral blood biomarkers associated with clinical outcome in non-small cell lung cancer patients treated with nivolumab. *J Thorac Oncol* (2018) 13:97–105. doi: 10.1016/j.jtho.2017.10.030

20. Ilie M, Hofman V, Ortholan C, Bonnetaud C, Coelle C, Mouroux J, et al. Predictive clinical outcome of the intratumoral CD66b-positive neutrophil-to-CD8-positive T-cell ratio in patients with resectable nonsmall cell lung cancer. *Cancer* (2012) 118:1726–37. doi: 10.1002/cncr.26456

21. Peng W, Sheng Y, Xiao H, Ye Y, Kwantwi LB, Cheng L, et al. Lung adenocarcinoma cells promote self-migration and self-invasion by activating neutrophils to upregulate Notch3 expression of cancer cells. *Front Mol Biosci* (2021) 8:762729. doi: 10.3389/fmolb.2021.762729

22. Rakaee M, Busund LT, Paulsen EE, Richardsen E, Al-Saad S, Andersen S, et al. Prognostic effect of intratumoral neutrophils across histological subtypes of non-small cell lung cancer. *Oncotarget* (2016) 7:72184–96. doi: 10.18632/oncotarget.12360

23. Liu X, Wu S, Yang Y, Zhao M, Zhu G, Hou Z. The prognostic landscape of tumor-infiltrating immune cell and immunomodulators in lung cancer. *BioMed Pharmacother* (2017) 95:55–61. doi: 10.1016/j.biopha.2017.08.003

24. Der SD, Sykes J, Pintilie M, Zhu CQ, Strumpf D, Liu N, et al. Validation of a histology-independent prognostic gene signature for early-stage, non-small-cell lung cancer including stage IA patients. *J Thorac Oncol* (2014) 9:59–64. doi: 10.1097/JTO.0000000000000042

25. Li T, Fan J, Wang B, Traugh N, Chen Q, Liu JS, et al. TIMER: A web server for comprehensive analysis of tumor-infiltrating immune cells. *Cancer Res* (2017) 77:e108–10. doi: 10.1158/1538-7445.AM2017-108

26. Becht E, Giraldo NA, Lacroix L, Buttard B, Elarouci N, Petitprez F, et al. Estimating the population abundance of tissue-infiltrating immune and stromal cell populations using gene expression. *Genome Biol* (2016) 17:218. doi: 10.1186/s13059-016-1070-5

27. Aran D, Hu Z, Butte AJ. xCell: digitally portraying the tissue cellular heterogeneity landscape. *Genome Biol* (2017) 18:220. doi: 10.1186/s13059-017-1349-1

28. Newman AM, Liu CL, Green MR, Gentles AJ, Feng W, Xu Y, et al. Robust enumeration of cell subsets from tissue expression profiles. *Nat Methods* (2015) 12:453–7. doi: 10.1038/nmeth.3337

29. Finotello F, Mayer C, Plattner C, Laschober G, Rieder D, Hackl H, et al. Molecular and pharmacological modulators of the tumor immune contexture revealed by deconvolution of RNA-seq data. *Genome Med* (2019) 11:34. doi: 10.1186/s13073-019-0638-6

30. Zeng D, Ye Z, Shen R, Yu G, Wu J, Xiong Y, et al. IOBR: multi-omics immuno-oncology biological research to decode tumor microenvironment and signatures. *Front Immunol* (2021) 12:687975. doi: 10.3389/fimmu.2021.687975

31. Liu R, Zhu G, Li M, Cao P, Li X, Zhang X, et al. Systematic pan-cancer analysis showed that RAD51AP1 was associated with immune microenvironment. *Tumor Stemness Prognosis Front Genet* (2022) 13:971033. doi: 10.3389/fgene.2022.971033

32. Beroukhim R, Mermel CH, Porter D, Wei G, Raychaudhuri S, Donovan J, et al. The landscape of somatic copy-number alteration across human cancers. *Nature* (2010) 463:899–905. doi: 10.1038/nature08822

33. Li Y, Zhang H, Gong H, Yuan Y, Li Y, Wang C, et al. miR-182 suppresses invadopodia formation and metastasis in non-small cell lung cancer by targeting cortactin gene. *J Exp Clin Cancer Res* (2018) 37:141. doi: 10.1186/s13046-018-0824-1

34. Xie G, Li Y, Jiang Y, Ye X, Tang J, Chen J. Silencing HIPPI suppresses tumor progression in non-small-cell lung cancer by inhibiting DNA replication. *Onco Targets Ther* (2021) 14:3467–80. doi: 10.2147/OTT.S305388

35. Li Y, Zhang H, Li Y, Zhao C, Fan Y, Liu J, et al. MiR-182 inhibits the epithelial to mesenchymal transition and metastasis of lung cancer cells by targeting the Met gene. *Mol Carcinog* (2018) 57:125–36. doi: 10.1002/mc.22741

36. Li Y, Li Y, Zhang H, Shi R, Zhang Z, Liu H, et al. EML4-ALK-mediated activation of the JAK2-STAT pathway is critical for non-small cell lung cancer transformation. *BMC Pulm Med* (2021) 21:190. doi: 10.1186/s12890-021-01553-z

37. Doroshow DB, Sanmamed MF, Hastings K, Politi K, Rimm DL, Chen L, et al. Immunotherapy in non-small cell lung cancer: facts and hopes. *Clin Cancer Res* (2019) 25:4592–602. doi: 10.1158/1078-0432.CCR-18-1538

38. Garon EB, Hellmann MD, Rizvi NA, Carcereny E, Leighl NB, Ahn MJ, et al. Five-year overall survival for patients with advanced non-small-cell lung cancer treated with pembrolizumab: results from the phase I KEYNOTE-001 study. *J Clin Oncol* (2019) 37:2518–27. doi: 10.1200/JCO.19.00934

39. Mok TSK, Wu YL, Kudaba I, Kowalski DM, Cho BC, Turna HZ, et al. Pembrolizumab versus chemotherapy for previously untreated, PD-L1-expressing, locally advanced or metastatic non-small-cell lung cancer (KEYNOTE-042): a randomised, open-label, controlled, phase 3 trial. *Lancet* (2019) 393:1819–30. doi: 10.1016/S0140-6736(18)32409-7

40. Faget J, Peters S, Quantin X, Meylan E, Bonnefoy N. Neutrophils in the era of immune checkpoint blockade. *J Immunother Cancer* (2021) 9. doi: 10.1136/jitc-2020-002242

41. Zhou F, Qiao M, Zhou C. The cutting-edge progress of immune-checkpoint blockade in lung cancer. *Cell Mol Immunol* (2021) 18:279–93. doi: 10.1038/s41423-020-00577-5

42. Gaule P, Smithy JW, Toki M, Rehman J, Patell-Socha F, Cougot D, et al. A quantitative comparison of antibodies to programmed cell death 1 ligand 1. *JAMA Oncol* (2017) 3:256–9. doi: 10.1001/jamaoncol.2016.3015

43. Zhang M, Li G, Wang Y, Wang Y, Zhao S, Haihong P, et al. PD-L1 expression in lung cancer and its correlation with driver mutations: a meta-analysis. *Sci Rep* (2017) 7:10255. doi: 10.1038/s41598-017-10925-7

44. Galvano A, Gristina V, Malapelle U, Pisapia P, Pepe F, Barraco N, et al. The prognostic impact of tumor mutational burden (TMB) in the first-line management of advanced non-oncogene addicted non-small-cell lung cancer (NSCLC): a systematic review and meta-analysis of randomized controlled trials. *ESMO Open* (2021) 6:100124. doi: 10.1016/j.esmoop.2021.100124

45. Hellmann MD, Paz-Ares L, Bernabe Caro R, Zurawski B, Kim SW, Carcereny Costa E, et al. Nivolumab plus ipilimumab in advanced non-small-cell lung cancer. *N Engl J Med* (2019) 381:2020–31. doi: 10.1056/NEJMoa1910231

46. Genova C, Dellepiane C, Carrega P, Sommariva S, Ferlazzo G, Pronzato P, et al. Therapeutic implications of tumor microenvironment in lung cancer: focus on immune checkpoint blockade. *Front Immunol* (2021) 12:799455. doi: 10.3389/fimmu.2021.799455

47. Lv B, Wang Y, Ma D, Cheng W, Liu J, Yong T, et al. Immunotherapy: reshape the tumor immune microenvironment. *Front Immunol* (2022) 13:844142. doi: 10.3389/fimmu.2022.844142

48. Fridlender ZG, Sun J, Kim S, Kapoor V, Cheng G, Ling L, et al. Polarization of tumor-associated neutrophil phenotype by TGF-beta: "N1" versus "N2" TAN. *Cancer Cell* (2009) 16:183–94. doi: 10.1016/j.ccr.2009.06.017

49. Teijeira A, Garasa S, Gato M, Alfaro C, Migueliz I, Cirella A, et al. CXCR1 and CXCR2 chemokine receptor agonists produced by tumors induce neutrophil extracellular traps that interfere with immune cytotoxicity. *Immunity* (2020) 52:856–871 e858. doi: 10.1136/jitc-2020-SITC2020.0755

50. Maruotti N, Annese T, Cantatore FP, Ribatti D. Macrophages and angiogenesis in rheumatic diseases. *Vasc Cell* (2013) 5:11. doi: 10.1186/2045-824X-5-11

51. Dyer DP, Salanga CL, Johns SC, Valdambrini E, Fuster MM, Milner CM, et al. The anti-inflammatory protein TSG-6 regulates chemokine function by inhibiting chemokine/glycosaminoglycan interactions. *J Biol Chem* (2016) 291:12627–40. doi: 10.1074/jbc.M116.720953

52. Zhang X, Xue J, Yang H, Zhou T, Zu G. TNFAIP6 promotes invasion and metastasis of gastric cancer and indicates poor prognosis of patients. *Tissue Cell* (2021) 68:101455. doi: 10.1016/j.tice.2020.101455

53. Liu B, Liu T, Liu Y, Feng X, Jiang X, Long J, et al. TSG-6 promotes Cancer Cell aggressiveness in a CD44-Dependent Manner and Reprograms Normal Fibroblasts to create a Pro-metastatic Microenvironment in Colorectal Cancer. *Int J Biol Sci* (2022) 18:1677–94. doi: 10.7150/ijbs.69178

54. Chan TC, Li CF, Ke HL, Wei YC, Shiue YL, Li CC, et al. High TNFAIP6 level is associated with poor prognosis of urothelial carcinomas. *Urol Oncol* (2019) 37:293 e211–293 e224. doi: 10.1016/j.urolonc.2018.12.009

55. Wang G, Joel MDM, Yuan J, Wang J, Cai X, Ocansey DKW, et al. Human umbilical cord mesenchymal stem cells alleviate inflammatory bowel disease by inhibiting ERK phosphorylation in neutrophils. *Inflammopharmacology* (2020) 28:603–16. doi: 10.1007/s10787-019-00683-5

56. Guimaraes-Bastos D, Frony AC, Barja-Fidalgo C, Moraes JA. Melanoma-derived extracellular vesicles skew neutrophils into a pro-tumor phenotype. *J Leukoc Biol* (2022) 111:585–96. doi: 10.1002/JLB.3A0120-050RR

57. Waring P, Mullbacher A. Cell death induced by the Fas/Fas ligand pathway and its role in pathology. *Immunol Cell Biol* (1999) 77:312–7. doi: 10.1046/j.1440-1711.1999.00837.x

58. Bui TM, Wiesolek HL, Sumagin R. ICAM-1: A master regulator of cellular responses in inflammation, injury resolution, and tumorigenesis. *J Leukoc Biol* (2020) 108:787–99. doi: 10.1002/JLB.2MR0220-549R

59. Ohms M, Moller S, Laskay T. An attempt to polarize human neutrophils toward N1 and N2 phenotypes in *vitro*. *Front Immunol* (2020) 11:532. doi: 10.3389/fimmu.2020.00532

60. Maurer M, von Stebut E. Macrophage inflammatory protein-1. *Int J Biochem Cell Biol* (2004) 36:1882–6. doi: 10.1016/j.biocel.2003.10.019

61. Ntanasis-Stathopoulos I, Fotiou D, Terpos E. CCL3 signaling in the tumor microenvironment. *Adv Exp Med Biol* (2020) 1231:13–21. doi: 10.1007/978-3-030-36667-4_2

62. Qin R, Ren W, Ya G, Wang B, He J, Ren S, et al. Role of chemokines in the crosstalk between tumor and tumor-associated macrophages. *Clin Exp Med* (2023) 23:1359–73. doi: 10.1007/s10238-022-00888-z

63. Piccard H, Muschel RJ, Opdenakker G. On the dual roles and polarized phenotypes of neutrophils in tumor development and progression. *Crit Rev Oncol Hematol* (2012) 82:296–309. doi: 10.1016/j.critrevonc.2011.06.004

64. Yang C, Wang Z, Li L, Zhang Z, Jin X, Wu P, et al. Aged neutrophils form mitochondria-dependent vital NETs to promote breast cancer lung metastasis. *J Immunother Cancer* (2021) 9. doi: 10.1136/jitc-2021-002875

65. Loffredo S, Borriello F, Iannone R, Ferrara AL, Galdiero MR, Gigantino V, et al. Group V secreted phospholipase A(2) induces the release of proangiogenic and antiangiogenic factors by human neutrophils. *Front Immunol* (2017) 8:443. doi: 10.3389/fimmu.2017.00443

66. Claesson-Welsh L, Welsh M. VEGFA and tumour angiogenesis. *J Intern Med* (2013) 273:114–27. doi: 10.1111/joim.12019

67. Yoshimura T, Leonard EJ. Identification of high affinity receptors for human monocyte chemoattractant protein-1 on human monocytes. *J Immunol* (1990) 145:292–7. doi: 10.4049/jimmunol.145.1.292

68. Conti I, Rollins BJ. CCL2 (monocyte chemoattractant protein-1) and cancer. *Semin Cancer Biol* (2004) 14:149–54. doi: 10.1016/j.semcancer.2003.10.009

69. Korbecki J, Kojder K, Siminska D, Bohatyrewicz R, Gutowska I, Chlubek D, et al. CC chemokines in a tumor: A review of pro-cancer and anti-cancer properties of the ligands of receptors CCR1, CCR2, CCR3, and CCR4. *Int J Mol Sci* (2020) 21. doi: 10.3390/ijms21218412

70. Lu B, Zhou Y, Su Z, Yan A, Ding P. Effect of CCL2 siRNA on proliferation and apoptosis in the U251 human glioma cell line. *Mol Med Rep* (2017) 16:3387–94. doi: 10.3892/mmr.2017.6995

71. Tsuyada A, Chow A, Wu J, Somlo G, Chu P, Loera S, et al. CCL2 mediates cross-talk between cancer cells and stromal fibroblasts that regulates breast cancer stem cells. *Cancer Res* (2012) 72:2768–79. doi: 10.1158/0008-5472.CAN-11-3567

72. Zhou SL, Zhou ZJ, Hu ZQ, Huang XW, Wang Z, Chen EB, et al. Tumor-associated neutrophils recruit macrophages and T-regulatory cells to promote progression of hepatocellular carcinoma and resistance to sorafenib. *Gastroenterology* (2016) 150:1646–1658 e1617. doi: 10.1053/j.gastro.2016.02.040

73. Zhang X, Shi H, Yuan X, Jiang P, Qian H, Xu W. Tumor-derived exosomes induce N2 polarization of neutrophils to promote gastric cancer cell migration. *Mol Cancer* (2018) 17:146. doi: 10.1186/s12943-018-0898-6

74. Mazzali M, Kipari T, Ophascharoensuk V, Wesson JA, Johnson R, Hughes J. Osteopontin–a molecule for all seasons. *QJM* (2002) 95:3–13. doi: 10.1093/qjmed/95.1.3

75. Weber GF, Cantor H. The immunology of Eta-1/osteopontin. *Cytokine Growth Factor Rev* (1996) 7:241–8. doi: 10.1016/S1359-6101(96)00030-5

76. Matsubara E, Yano H, Pan C, Komohara Y, Fujiwara Y, Zhao S, et al. The significance of SPP1 in lung cancers and its impact as a marker for protumor tumor-associated macrophages. *Cancers (Basel)* (2023) 15. doi: 10.3390/cancers15082250

77. Shen XT, Xie SZ, Xu J, Yang LY, Qin LX. Pan-cancer analysis reveals a distinct neutrophil extracellular trap-associated regulatory pattern. *Front Immunol* (2022) 13:798022. doi: 10.3389/fimmu.2022.798022

frontiers | Frontiers in Oncology

TYPE Case Report
PUBLISHED 15 February 2024
DOI 10.3389/fonc.2024.1329152

OPEN ACCESS

EDITED BY
Yiming Meng,
China Medical University, China

REVIEWED BY
Ming Yi,
Zhejiang University, China
Alvin Liu,
University of Washington, United States

*CORRESPONDENCE
Guangxin Zhang
guangxinzhang@jlu.edu.cn

RECEIVED 28 October 2023
ACCEPTED 25 January 2024
PUBLISHED 15 February 2024

CITATION
Li Q, Zhang G, Yang H and Li J (2024) Rare case report: a case of histological type transformation of lung cancer caused by neoadjuvant immunotherapy.
Front. Oncol. 14:1329152.
doi: 10.3389/fonc.2024.1329152

Rare case report: a case of histological type transformation of lung cancer caused by neoadjuvant immunotherapy

Quanqing Li, Guangxin Zhang*, Hao Yang and Jindong Li

Department of Thoracic of the Second Hospital of Jilin University, Changchun, Jilin, China

Lung cancer remains the leading cause of cancer-related mortality, with 1.8 million deaths per year. Small cell lung cancer and non-small cell lung cancer (NSCLC) are the main cancer types. Approximately 85% of cases are NSCLC, including adenocarcinoma, squamous cell carcinoma, and large cell carcinoma. In this reported treatment case, the tumor histological type changed after targeted therapy, which has not been previously well documented. The patient was a 67-year-old woman diagnosed with squamous cell carcinoma via bronchoscopy. She received five neoadjuvant immune monotherapies. The lesion shrank but then progressed, with a diagnosis of small cell carcinoma via bronchoscopy. This finding suggests that tumor acquisition of resistance as manifested by cancer-type changes needs consideration and study in the application of this particular type of immunotherapy.

KEYWORDS

histological type transformation, neoadjuvant immunotherapy, small cell lung cancer, drug resistance, squamous cell lung carcinoma

Introduction

Immunotherapeutic agents such as sintilimab (anti-PD-1) are antibodies that promote immune system activation and exhibit good efficacy in the first-line treatment of non-small cell lung cancer (NSCLC). Squamous cell carcinoma responds very well to this preoperative immunotherapy (1). Some reactions such as fever and fatigue are observed, most of which are primary or secondary treatment-related adverse events (TRAEs) (2), although serious grade III TRAEs are rare. A related study has revealed that histological transformation into small cell lung cancer (SCLC) from NSCLC is a potential mechanism in therapeutic resistance (3). Herein, we describe the relevant medical history, examination and diagnosis, and treatment regimens of a patient to improve our understanding of this disease, avoid potential misdiagnosis, and provide a basis for a more standardized care of lung cancer patients.

10.3389/fonc.2024.1329152

Case presentation

The patient was a 67-year-old woman. Seven months ago, she exhibited no obvious reasons for cough or white sputum. At times, she coughed up blood. She did not receive systematic diagnosis and treatment. One month later, she felt suffocation in the anterior chest area with poor breathing; again, she did not pay attention to these signs. Only after the gradual worsening of the symptoms did she visit our hospital. Chest computed tomography (CT, Figure 1A) revealed the presence of a soft tissue mass in the left hilum of her lung. The lesion was 32 × 25 mm in size, with uneven density and a CT value of 32 HU. It was protruding into the bronchus of the upper lobe of the left lung. There was bronchial wall thickening, distal lumen obstruction, and many mediastinal lymph nodes. Bronchoscopy (Figure 1B) revealed mucosal swelling at the opening of the left upper lobe, superficial irregular hyperplasia, lumen occlusion, lesions involving the upper and lower interlobar ridges, and lumen stenosis at the opening of the left lower lobe. Pathological examination of the opening of the left upper lobe revealed a tumor morphology consistent with squamous cell carcinoma (non-keratinizing type). The patient had a smoking history of 20 years and a smoking index of 400 years. A physical examination found no obvious abnormality. Tumor marker (sample number 20230324HYA001) analysis showed the following: abnormal prothrombin, 39.740 mAU/ml (reference value: 11.12–32.01 mAU/ml); cytokeratin 19 fragment at 2.42 ng/ml (reference value: 0–2.08 ng/ml); and premenopausal ROMA value of 12.00% (reference value: 0%–7.4%); the other markers were normal. Head-enhanced magnetic resonance imaging, abdominal CT, whole-body bone scan, and other auxiliary examinations suggested no metastasis or surgical contraindications. The tumor stage was T2aNxM0, and the clinical stage was IB as per the guidelines for primary lung cancer diagnosis and treatment of the China Health Commission (2022 edition). As a result, surgery was indicated. The preoperative pulmonary function test suggested mild obstructive ventilatory dysfunction. However, after being informed of the surgical risks, the patient and her family declined surgery. As a substitute, preoperative chemotherapy combined with neoadjuvant immunotherapy sintilimab and gemcitabine–platinum-containing drug for squamous cell carcinoma was prescribed as per the first-line drug treatment guidelines for primary lung cancer diagnosis and

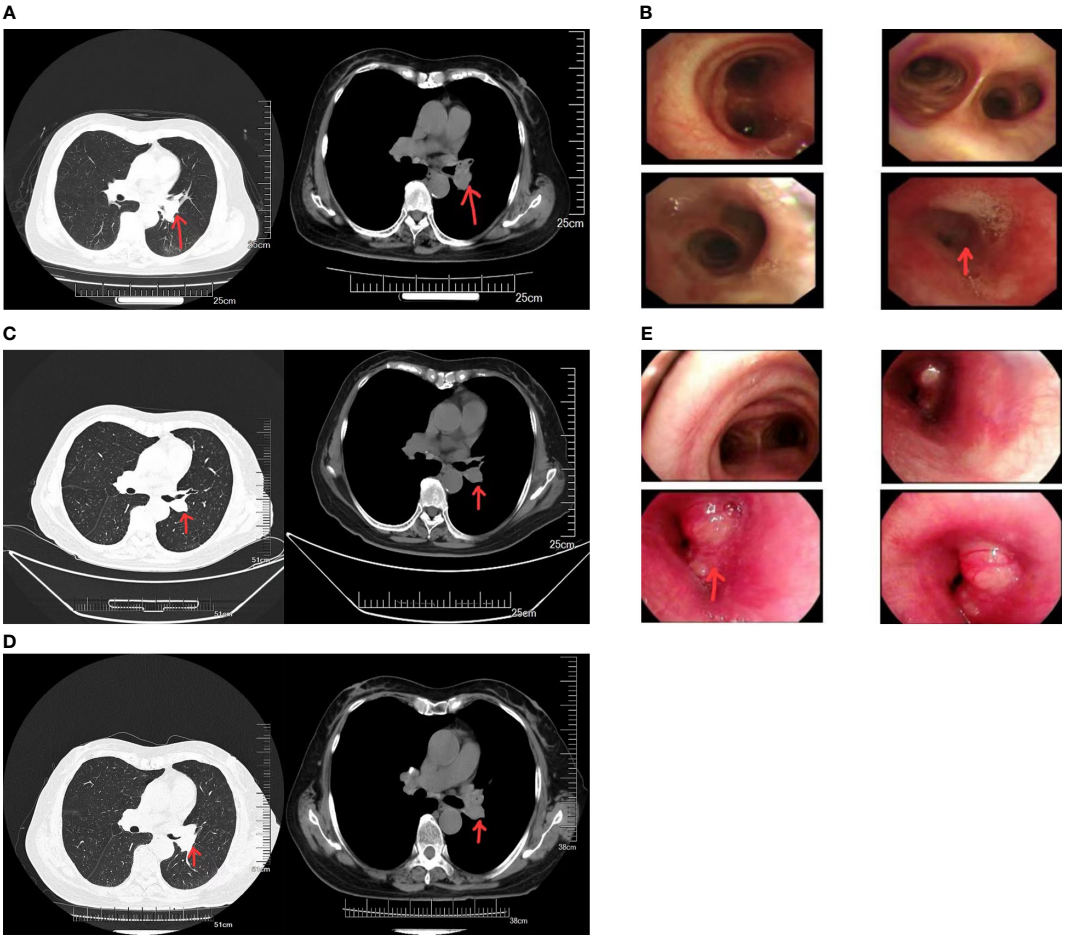

FIGURE 1
(A) Computed tomography (CT) images of the patient before neoadjuvant therapy. **(B)** Results of the first bronchoscopy. **(C)** CT images of the patient after three cycles of sintilimab immunotherapy. **(D)** CT images of the patient after five cycles of sintilimab immunotherapy. **(E)** Results of the second bronchoscopy.

treatment (2022 edition). Prior to chemotherapy, the patient scored 50 on the Karnofsky Performance Scale (KPS), which precluded chemotherapy, and only immunotherapy was administered. Due to economic issues, the PD-1 test was not performed. In the end, sintilimab immunotherapy was carried out for 21 days as one cycle. The lung cancer guidelines do not specify the number of immunotherapy cycles. The patient's symptoms significantly improved after three cycles. Chest CT (Figure 1C) showed that the tumor size was reduced to 21 × 24 mm. From the good result of neoadjuvant immunotherapy, surgery was recommended again. Yet, the patient and her family refused it again due in part to the good effects of immunotherapy, plus cost consideration and other related reasons. Therefore, maintenance treatment was administered as per the primary lung cancer diagnosis and treatment guidelines, which can be selected for patients who attain disease control after first-line treatment. If no disease progression and tolerable adverse reactions are obtained from using these immune checkpoint inhibitors, these treatment cycles can be administered for 2 years. However, after the fourth cycle of sintilimab, the symptoms began to worsen. Before the fifth cycle, chest CT (Figure 1D) revealed that the tumor size had increased to 31 × 24 mm. Bronchoscopy (Figure 1E) revealed that the lumen was blocked by new growth in the lower portion of the left main bronchus, with an irregular layer of cell proliferation. The lower portion of the left main bronchus was biopsied. Pathology revealed bronchial carcinoma. Immunohistochemical staining combined with morphology supported the diagnosis of small cell carcinoma. At this time, the patient scored 60 on KPS. Considering that the patient could likely tolerate the side effects of chemotherapy, etoposide plus nedaplatin was recommended. After chemotherapy, chest high-resolution CT revealed a reduced lesion size of 20 × 18 mm, suggesting that the tumor had responded to the new treatment regimen.

Discussion

Currently, drug resistance arising during treatment is a major treatment-related concern for patients with NSCLC. We summarized some differences in treatment resistance between the use of epidermal growth factor receptor tyrosine kinase inhibitors (EGFR-TKIs) and anti-PD-1, as well as the mechanisms in tumor histology changes as a result to provide insight for counteracting drug resistance in NSCLC treatment in the future.

Transformation of NSCLC into SCLC and T790M point mutation in EGFR-TK during EGFR-TKI treatment

In patients with active EGFR, EGFR-TKIs can rapidly shrink the primary tumor; nevertheless, resistance appears in approximately 12 months (4, 5). The most obvious reason for resistance is the T790M point mutation in exon 20 that increases ATP affinity (6). The other is the transformation of EGFR-positive NSCLC into SCLC (7, 8). In a retrospective study, 58 patients with NSCLC and EGFR mutations were enrolled. Among them, 93% of the patients received EGFR-TKIs; all patients received a median of more than two lines of treatment. Ninety-seven percent of the patients were found to harbor SCLC (9). Significantly, the original activated EGFR mutation was retained in the tumor tissues that transformed into SCLC, suggesting a direct lineage from NSCLC rather than sampling or an undiagnosed primary lesion (10). RB1 inactivation is an important marker for SCLC. Western blotting of repeated biopsy samples from patients with EGFR mutation-positive adenocarcinoma transformed into SCLC showed the absence of RB1 in all cases and not in those with EGFR mutation-positive NSCLC (11). However, RB1 expression loss or downregulation alone via experimental manipulation on TKI-resistant cancer cell lines with EGFR mutations did not result in NSCLC transformation into SCLC. EGFR-TKI treatment plus genetic mutations, such as RB1 and TP53 deletions, may act in concert to promote tumor differentiation into SCLC (11, 12).

Transformation of NSCLC into SCLC during PD-1 treatment

Anti-PD-1/PD-L1 interaction has become the paradigm of immune checkpoint inhibitor-based cancer treatment. It has successfully prolonged the survival of patients with advanced NSCLC. When tumor cells are detected by the body's immune system, proinflammatory molecules, chemokines, and innate immunity cells are congregated at the tumor sites causing antitumor responses (13). PD-1 is expressed in T cells, whereas PD-L1 is expressed in tumor cells. The PD-1/PD-L1 axis inhibits T-cell function (14), a process that could be interrupted by PD-1 antibodies (14, 15). A study has revealed that the emergence of PD-1 treatment resistance might be due to defects in antigen processing and presentation by tumor cells with the result that the immune system is no longer able to detect the tumor antigens and initiates tumor cytolysis. Human leukocyte antigen class I (HLA-I) can bind to specific peptides of intracellular proteins, express them on the cell surface, and present them to $CD8^+$ T cells. β2-microglobulin (B2M) is needed to maintain stable HLA-I expression, and mutations in B2M can hamper antigen presentation. Therefore, impairment in HLA-I-mediated antigen presentation could lead to resistance to checkpoint inhibitors (16). Therefore, the transformation of NSCLC into SCLC with defects in antigen presentation may be another route to resistance.

The treatment-induced transformation of adenocarcinoma into small cell carcinoma merits further investigation (17). Understanding the possible origin of the different lung cancer types is essential. In general, SCLC cells express neuroendocrine markers, such as neuron-specific enolase and progastrin-releasing peptide. Tumor cells with neuroendocrine expression could be derived from airway neuroendocrine cells localized in the central area near the lung hilum (18). Adenocarcinoma cells are derived primarily from type II pneumocytes, and carcinoma cells with

squamous differentiation from basal cells (19). Other studies have reported that EGFR mutation-positive adenocarcinoma cells can also be derived from alveolar type II cells. In fact, alveolar type II cells can produce both adenocarcinoma and SCLC (19–21). Therefore, EGFR mutation-positive lung cancer occurring in alveolar type II cells may be readily transformed into SCLC (7).

In the present case report, the patient is a woman with a long smoking history. Smokers are particularly susceptible to squamous cell carcinoma and small cell carcinoma (22, 23). The treatment regimens are different for these two cancer types. As per the primary lung cancer diagnosis and treatment guidelines (2022 edition), surgery remains the primary treatment modality for resectable squamous cell lung carcinoma. However, our patient forwent surgery for the reasons given above. In patients with advanced or unresectable NSCLC, patients undergoing PD-1 treatment showed longer progression-free survival, overall survival, and fewer adverse events than those undergoing platinum-based chemotherapy (24). Therefore, we chose the PD-1 inhibitor monotherapy to treat that patient. Encouraging results were obtained in the first three cycles of therapy, but the patient developed worsening symptoms and tumor growth after four cycles. We suspected tumor resistance or tumor hyperprogression needing clarification by pathology. Testing revealed small cell carcinoma suggesting a change in the histological type induced by therapy. We searched the relevant literature and retrieved 10 reports, where eight patients received nivolumab and two received pembrolizumab; these patients also received chemotherapy before immunotherapy (25). All these patients exhibited tumor histological type transformation after treatment. For patients with treatment-induced SCLC, no clear guidelines are available on whether further application of immunotherapeutic drugs will benefit them. Etoposide combined with platinum remains the primary treatment modality for SCLC (26). For this patient, we chose this method as the next treatment option. The prompt discovery of SCLC transformation prevented unnecessary surgical trauma and wrong medication which might aggravate her well-being. The pathogenesis of transformed SCLC should be explored. To date, no explanation is available on the specific mechanism underlying this phenomenon.

In the present case, another reason for the histological results of the two samplings might be the uncertainty of missing SCLC diagnosis in the preliminary pathology. Previous studies have found that 9 (2%) of 429 patients with SCLC had a combined subtype of small cell carcinoma plus squamous cell carcinoma or adenocarcinoma at the time of diagnosis (27). Existing clinical data and evidence suggest that SCLC has a shorter survival time with fewer choices of effective therapeutic intervention than NSCLC. Transformed SCLC is a result of tumor resistance (28). Extensive clinical research suggests that it is not rare for the transformation of NSCLC to SCLC when therapeutic drugs are used.

Conclusion

We present the case of a woman with dyspnea symptoms from central lung cancer. The first bronchoscopy revealed squamous cell carcinoma. After five cycles of sintilimab, re-examination revealed small cell carcinoma. Whether surgical resection, if carried out at first, could affect this patient's disease course is unknown.

Data availability statement

The original contributions presented in the study are included in the article/supplementary material. Further inquiries can be directed to the corresponding author.

Ethics statement

The studies involving humans were approved by the Ethics Committee of the Second Hospital of Jilin University. The studies were conducted in accordance with the local legislation and institutional requirements. The participants provided their written informed consent to participate in this study. Written informed consent was obtained from the individual(s) for the publication of any potentially identifiable images or data included in this article.

Author contributions

QL: Writing – original draft, Conceptualization. GZ: Supervision, Writing – review & editing, Validation. HY: Investigation, Writing – original draft. JL: Writing – review & editing, Validation.

Funding

The author(s) declare financial support was received for the research, authorship, and/or publication of this article. The present study was supported by grants (3D5222865429) from the Finance Department of Jilin Province.

Conflict of interest

The authors declare that the research was conducted in the absence of any commercial or financial relationships that could be construed as a potential conflict of interest.

Publisher's note

References

1. Gao S, Li N, Gao S, Xue Q, Ying J, Wang S, et al. Neoadjuvant PD-1 inhibitor (Sintilimab) in NSCLC. *J Thorac Oncol* (2020) 15(5):816–26. doi: 10.1016/j.jtho.2020.01.017

2. Forde PM, Chaft JE, Smith KN, Anagnostou V, Cottrell TR, Hellmann MD, et al. Neoadjuvant PD-1 blockade in resectable lung cancer. *N Engl J Med* (2018) 378 (21):1976–86. doi: 10.1056/NEJMoa1716078

3. Giaccone G, He Y. Current knowledge of small cell lung cancer transformation from non-small cell lung cancer. *Semin Cancer Biol* (2023) 94:1–10. doi: 10.1016/j.semcancer.2023.05.006

4. Mok TS, Wu T-L, Thongprasert S, Yang C-H, Chu D-T, Saijo N, et al. Gefitinib or carboplatin-paclitaxel in pulmonary adenocarcinoma. *N Engl J Med* (2009) 361 (10):947–57. doi: 10.1056/NEJMoa0810699

5. Ohashi K, Maruvka YE, Michor F, Pao W. Epidermal growth factor receptor tyrosine kinase inhibitor-resistant disease. *J Clin Oncol* (2013) 31(8):1070–80. doi: 10.1200/JCO.2012.43.3912

6. Yun CH, Mengwasser KM, Toms AV, Woo MS, Greulich H, Wong K-K, et al. The T790M mutation in EGFR kinase causes drug resistance by increasing the affinity for ATP. *Proc Natl Acad Sci U.S.A.* (2008) 105(6):2070–5. doi: 10.1073/pnas.0709662105

7. Oser MG, Niederst MJ, Sequist LV, Engelman JA. Transformation from non-small-cell lung cancer to small- cell lung cancer: molecular drivers and cells of origin. *Lancet Oncol* (2015) 16(4):e165–72. doi: 10.1016/S1470-2045(14)71180-5

8. Yu HA, Arcila ME, Rekhtman N, Sima CS, Zakowski MF, Pao W, et al. Analysis of tumor specimens at the time of acquired resistance to EGFR-TKI therapy in 155 patients with EGFR-mutant lung cancers. *Clin Cancer Res* (2013) 19(8):2240–7. doi: 10.1158/1078-0432.CCR-12-2246

9. Marcoux N, Gettinger SN, O'Kane G, Arbour KC, Neal JW, Husain H, et al. EGFR-Mutant adenocarcinomas that transform to small-cell lung cancer and other neuroendocrine carcinomas: clinical outcomes. *J Clin Oncol* (2019) 37(4):278–85. doi: 10.1200/JCO.18.01585

10. Fukui T, Tsuta K, Furuta K, Watanabe S-I, Asamura H, Ohe Y, et al. Epidermal growth factor receptor mutation status and clinicopathological features of combined small cell carcinoma with adenocarcinoma of the lung. *Cancer Sci* (2007) 98(11):1714–9. doi: 10.1111/j.1349-7006.2007.00600.x

11. Niederst MJ, Sequist LV, Poirier JT, Mermel CH, Lockerman EL, Garcia AR, et al. RB loss in resistant EGFR mutant lung adenocarcinomas that transform to small-cell lung cancer. *Nat Commun* (2015) 6:6377. doi: 10.1038/ncomms7377

12. Byers LA, Wang J, Nilsson MB, Fujimoto J, Saintigny P, Yordy J, et al. Proteomic profiling identifies dysregulated pathways in small cell lung cancer and novel therapeutic targets including PARP1. *Cancer Discovery* (2012) 2(9):798–811. doi: 10.1158/2159-8290.CD-12-0112

13. Dunn GP, Old LJ, Schreiber RD. The three Es of cancer immunoediting. *Annu Rev Immunol* (2004) 22:329–60. doi: 10.1146/annurev.immunol.22.012703.104803

14. Pardoll DM. The blockade of immune checkpoints in cancer immunotherapy. *Nat Rev Cancer* (2012) 12(4):252–64. doi: 10.1038/nrc3239

15. Zhou K, Li S, Zhao Y, Cheng K. Mechanisms of drug resistance to immune checkpoint inhibitors in non-small cell lung cancer. *Front Immunol* (2023) 14:1127071. doi: 10.3389/fimmu.2023.1127071

16. Gettinger S, Choi J, Hastings K, Truini A, Datar I, Sowell R, et al. Impaired HLA class I antigen processing and presentation as a mechanism of acquired resistance to immune checkpoint inhibitors in lung cancer. *Cancer Discovery* (2017) 7(12):1420–35. doi: 10.1158/2159-8290.CD-17-0593

17. Lim SM, Syn NL, Chul Cho B, Soo RA. Acquired resistance to EGFR targeted therapy in non-small cell lung cancer: Mechanisms and therapeutic strategies. *Cancer Treat Rev* (2018) 65:1–10. doi: 10.1016/j.ctrv.2018.02.006

18. Schoenfeld AJ, Chan JM, Kubota D, Sato H, Rizvi H, Daneshbod Y, et al. Tumor analyses reveal squamous transformation and off-target alterations as early resistance mechanisms to first-line Osimertinib in EGFR-mutant lung cancer. *Clin Cancer Res* (2020) 26(11):2654–63. doi: 10.1158/1078-0432.CCR-19-3563

19. Lin C, Song H, Huang C, Yao E, Gacayan R, Xu S-M, et al. Alveolar type II cells possess the capability of initiating lung tumor development. *PloS One* (2012) 7(12): e53817. doi: 10.1371/journal.pone.0053817

20. Sutherland KD, Proost N, Brouns I, Adriaensen D, Song J-Y, Berns A, et al. Cell of origin of small cell lung cancer: inactivation of Trp53 and Rb1 in distinct cell types of adult mouse lung. *Cancer Cell* (2011) 19(6):754–64. doi: 10.1016/j.ccr.2011.04.019

21. Mainardi S, Mijimolle N, Francoz S, Vicente-Dueñas C, Sánchez-García I, Barbacid M, et al. Identification of cancer initiating cells in K-Ras driven lung adenocarcinoma. *Proc Natl Acad Sci U.S.A.* (2014) 111(1):255–60. doi: 10.1073/pnas.1320383110

22. Brownson RC, Chang JC, Davis JR. Gender and histologic type variations in smoking-related risk of lung cancer. *Epidemiology* (1992) 3(1):61–4. doi: 10.1097/00001648-199201000-00012

23. Demedts IK, Vermaelen KY, van Meerbeeck JP. Treatment of extensive- stage small cell lung carcinoma: current status and future prospects. *EurRespir J* (2010) 35 (1):202–15. doi: 10.1183/09031936.00105009

24. Reck M, Rodríguez-Abreu D, Robinson AG, Hui R, Csőszi T, Fülöp A, et al. Pembrolizumab versus chemotherapy for PD-L1-pPositive non- small-cell lung cancer. *N Engl J Med* (2016) 375(19):1823–33. doi: 10.1056/NEJMoa1606774

25. Sehgal K, Varkaris A, Viray H, VanderLaan PA, Rangachari D, Costa DB, et al. Small cell transformation of non-small cell lung cancer on immune checkpoint inhibitors: uncommon or under-recognized? *J Immunother Cancer* (2020) 8(1): e000697. doi: 10.1136/jitc-2020-000697

26. Goldman JW, Dvorkin M, Chen Y, Reinmuth N, Hotta K, Trukhin D, et al. Durvalumab, with or without tremelimumab, plus platinum-etoposide versus platinum-etoposide alone in first-line treatment of extensive-stage small-cell lung cancer (CASPIAN): updated results from a randomised, controlled, open-label, phase 3 trial. *Lancet Oncol* (2021) 22(1):51–65. doi: 10.1016/S1470-2045(20)30539-8

27. Mangum MD, Greco FA, Hainsworth JD, Hande KR, Johnson DH. Combined small-cell and non-small-cell lung cancer. *J Clin Oncol* (1989) 7(5):607–12. doi: 10.1200/JCO.1989.7.5.607

28. Bar J, Ofek E, Barshack I, Gottfried T, Zadok O, Kamer I, et al. Transformation to small cell lung cancer as a mechanism of resistance to immunotherapy in non-small cell lung cancer. *Lung Cancer* (2019) 138:109–15. doi: 10.1016/j.lungcan.2019.09.025

frontiers | Frontiers in Oncology

TYPE Case Report
PUBLISHED 25 March 2024
DOI 10.3389/fonc.2024.1324057

OPEN ACCESS

EDITED BY
Elisa Frullanti,
University of Siena, Italy

REVIEWED BY
Waleed Kian,
The Institute of Oncology, Assuta Ashdod, Israel
Lena Horvath,
Innsbruck Medical University, Austria

*CORRESPONDENCE
Jianjun Zhang
JZhang20@mdanderson.org

RECEIVED 18 October 2023
ACCEPTED 29 January 2024
PUBLISHED 25 March 2024

CITATION
Li H, Hu X, Ning MS, Fuller GN, Stewart JM, Gilliam JC, Wu J, Le X, Vaporciyan AA, Lee JJ, Gibbons DL, Heymach JV, Futreal A and Zhang J (2024) Case report: Molecular profiling facilitates the diagnosis of a challenging case of lung cancer with choriocarcinoma features.
Front. Oncol. 14:1324057.
doi: 10.3389/fonc.2024.1324057

Case report: Molecular profiling facilitates the diagnosis of a challenging case of lung cancer with choriocarcinoma features

Hui Li[1,2], Xin Hu[3], Matthew S. Ning[4], Gregory N. Fuller[5], John M. Stewart[5], Jared C. Gilliam[6], Jia Wu[1,2], Xiuning Le[1], Ara A. Vaporciyan[7], J. Jack Lee[8], Don L. Gibbons[1,9], John V. Heymach[1], Andrew Futreal[3] and Jianjun Zhang[1,3]*

[1]Department of Thoracic/Head and Neck Medical Oncology, The University of Texas MD Anderson Cancer Center, Houston, TX, United States, [2]Department of Imaging Physics, The University of Texas MD Anderson Cancer Center, Houston, TX, United States, [3]Department of Genomic Medicine, The University of Texas MD Anderson Cancer Center, Houston, TX, United States, [4]Department of Thoracic Radiation Oncology, The University of Texas MD Anderson Cancer Center, Houston, TX, United States, [5]Department of Pathology, The University of Texas MD Anderson Cancer Center, Houston, TX, United States, [6]Caris Life Sciences, Phoenix, AZ, United States, [7]Department of Thoracic and Cardiovascular Surgery, The University of Texas MD Anderson Cancer Center, Houston, TX, United States, [8]Department of Biostatistics, The University of Texas MD Anderson Cancer Center, Houston, TX, United States, [9]Department of Molecular and Cellular Oncology, The University of Texas MD Anderson Cancer Center, Houston, TX, United States

Accurate diagnoses are crucial in determining the most effective treatment across different cancers. In challenging cases, morphology-based traditional pathology methods have important limitations, while molecular profiling can provide valuable information to guide clinical decisions. We present a 35-year female with lung cancer with choriocarcinoma features. Her disease involved the right lower lung, brain, and thoracic lymph nodes. The pathology from brain metastasis was reported as "metastatic choriocarcinoma" (a germ cell tumor) by local pathologists. She initiated carboplatin and etoposide, a regimen for choriocarcinoma. Subsequently, her case was assessed by pathologists from an academic cancer center, who gave the diagnosis of "adenocarcinoma with aberrant expression of β-hCG" and finally pathologists at our hospital, who gave the diagnosis of "poorly differentiated carcinoma with choriocarcinoma features". Genomic profiling detected a KRAS G13R mutation and transcriptomics profiling was suggestive of lung origin. The patient was treated with carboplatin/paclitaxel/ipilimumab/nivolumab followed by consolidation radiation therapy. She had no evidence of progression to date, 16 months after the initial presentation. The molecular profiling could facilitate diagnosing of challenging cancer cases. In addition, chemoimmunotherapy and local consolidation radiation therapy may provide promising therapeutic options for patients with lung cancer exhibiting choriocarcinoma features.

KEYWORDS

lung cancer with choriocarcinoma features, whole transcriptome sequencing, whole exome sequencing, immune checkpoint inhibitors, nivolumab, ipilimumab

Introduction

Lung cancer remains as the leading cause of cancer-related deaths worldwide. Non-small cell lung cancer (NSCLC) accounts for almost 85% of all lung cancers, with adenocarcinoma and squamous cell carcinoma as the most common histologic subtypes of NSCLCs (1). NSCLCs can present as other rare histologies (2). Accurate histopathological diagnosis is crucial, as treatment and prognosis vary among different subtypes (3). Currently, the histopathological diagnosis is primarily based on morphological characteristics and immunohistochemical patterns. Although it remains as the gold standard in cancer diagnosis, it has important limitations, particularly for rare lung cancer subtypes. This report highlights the role of molecular profiling in differential diagnosis of a rare lung cancer subtype.

Case presentation

A 35-year-old white female, never smoker, presented to the emergency room (ER) with complaints of a syncope episode and right arm pain in September 2022. She had been experiencing right-sided neuropathic symptoms for 2 months prior to ER visit. Computed tomography (CT) scan of the head revealed a left frontal hypodensity, and brain magnetic resonance imaging (MRI) showed a 2.0 x 1.6 x 1.6 cm peripherally enhancing lesion in the peripheral aspect of the left postcentral gyrus, which was suspected to be an intracranial abscess. Subsequently, the patient underwent frontal craniotomy. However, the pathology report revealed a pleomorphic epithelial tumor with extensive necrosis and scattered multinucleated cells. Immunohistochemical staining was positive for pancytokeratin, CK7, β-hCG and focal cytoplasmic staining for inhibin. The cells were negative for GATA3, CK20, TTF-1, and PAX 8. The Ki-67 was approximately 60%. These results were consistent with metastatic choriocarcinoma.

The patient's laboratory results were mostly unremarkable, with normal alpha-fetoprotein (AFP) levels. There was a slight elevation in serum β-hCG levels from 171 to 248 mIU/mL (Reference range 0-5 mIU/mL) during the first week following the frontal craniotomy. Further examinations, including pelvic and transvaginal ultrasound, abdominal and pelvic CT did not identify any masses. However, CT scan of the chest revealed a 4.0 x 4.4 cm opacity in the right lower lobe (Figures 1A, B), leading to an EBUS for the biopsy of the lung mass and mediastinal nodes. The results showed poorly differentiated

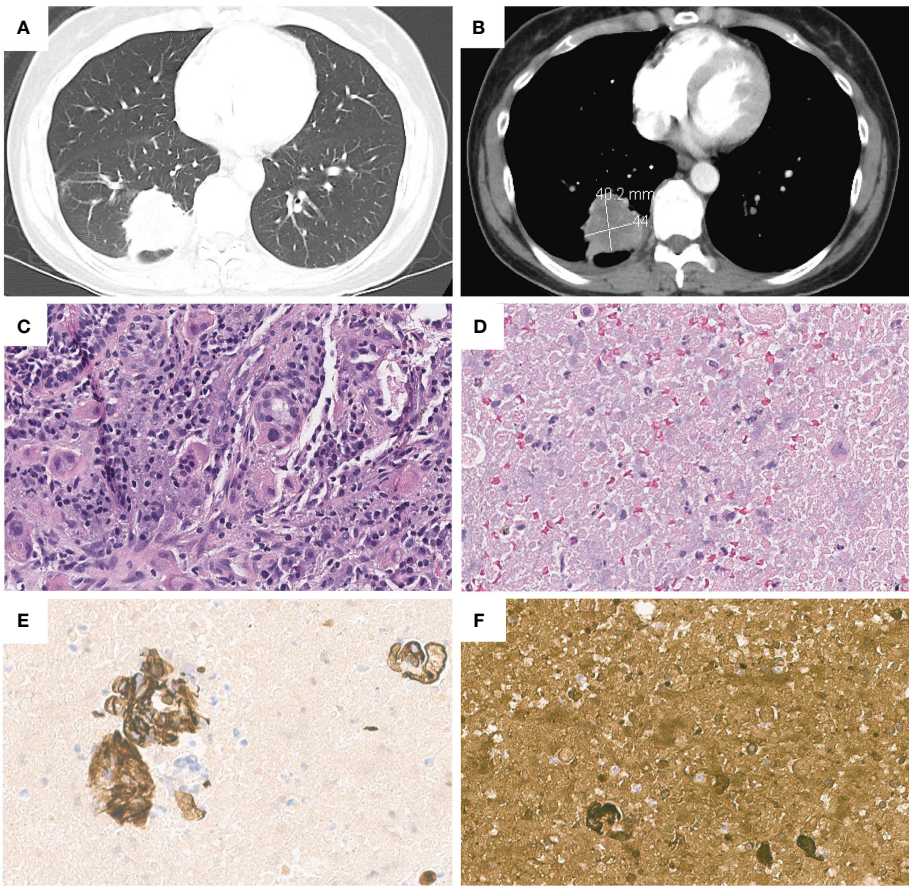

FIGURE 1
Chest contrast-enhanced computed tomography images revealed a 4.0*4.4 cm right lower lobe lung mass, in **(A)** lung window and **(B)** mediastinal window. Pathologic and immunohistochemical findings in lung cancer with choriocarcinoma features. **(C)** H&E staining of lung tumor. **(D)** H&E staining of metastatic lymph node(11R). Lymph node(11R) showed positive staining for **(E)** CK7 and **(F)** β-hCG.

carcinoma, compatible with choriocarcinoma. CK7 and β-hCG staining were positive and the tumor had morphologic features like the brain lesion (Figures 1C–F). PET/CT scan showed a hypermetabolic mass lesion in the right lower lobe along with hypermetabolic lymph nodes in the neck, mediastinum, bilateral hilar, and right axillary regions.

The patient was initially treated as metastatic choriocarcinoma and received one cycle of etoposide and cisplatin chemotherapy (EP) from her local oncologist. She proceeded to seek a second opinion at a university hospital, where the pathologists re-evaluated the tissues from the brain metastasis, right lower lobe mass, and subcarinal lymph node. Immunostaining was negative for CDX2, Glypican, TTF-1, P63, and Napsin, while positive for β-hCG, claudin-4 and Ber-Ep4. PD-L1 staining could not be completed due to insufficient tissue samples. The final diagnosis was "adenocarcinoma with aberrant expression of β-hCG" and the primary site of the tumor was undetermined. Finally, genomic profiling of brain metastasis revealed KRAS p.G13R and GNAS p.R201H mutations among others (Table 1). The same KRAS and GNAS mutations were also detected by liquid biopsy using Guardant 360 platform (Table 1).

The patient sought to a third opinion at our hospital. Our gynecologic oncologists reviewed her obstetric and gynecologic history and discovered that she had successfully delivered three children, each at full term without complications. Her most recent delivery was 4.5 years ago, and she had consistently experienced regular monthly periods without intermenstrual spotting. The peak serum β-hCG levels reached 287 mIU/mL (Reference range 0-5 mIU/mL) and declined to negative shortly after treatment. This was significantly lower than the typical β-hCG levels associated with choriocarcinoma, which can reach up to 100,000 mIU/mL. In addition, there was no indication of uterine or ovarian abnormalities on CT imaging. Thus, our gynecologic oncologists determined that the primary malignancy is unlikely to be of gynecologic origin. Our thoracic pathologists conducted a thorough review of the patient's slides, reporting it as poorly differentiated carcinoma with features of choriocarcinoma. However, there were different opinions among other pathologists, who were inclined to consider it as adenocarcinoma with β-hCG production.

Following the first cycle of etoposide and cisplatin, the primary tumor showed a slight increase in size, growing from 4.4cm to 5.0cm. Based on the patient's clinical, radiologic and molecular profiling results, the patient was transitioned to the CheckMate 9LA regimen (carboplatin/paclitaxel/ipilimumab/nivolumab) (4). The tumor size decreased 21% after two cycles of treatment. The serum β-hCG level declined to normal. Given her young age and relatively limited disease burden, the patient was referred to the radiation oncology team to consider local consolidation based on previous studies (5, 6). The patient underwent EBUS prior to radiation and fine needle aspiration, brushing tissue, and transbronchial biopsy of multiple thoracic lymph nodes from stations 11L, 4L, 2L, 2R, 4R, 11RS and 11RI came back negative for malignant cells. She subsequently underwent volumetric modulated arc therapy (VMAT) to the right lower lung and mediastinum in January 2023. The patient returned to her local oncologist. She discontinued chemotherapy and received ipilimumab and nivolumab until April 2023, and then continued with nivolumab monotherapy. Her most recent brain MRI and chest scan in January 2024 revealed good disease control without evidence of recurrence.

Of note, molecular profiling using whole transcriptome sequencing (WTS) and whole exome sequencing (WES) by Caris was also consistent with lung cancer diagnosis. The same KRAS G13R and

TABLE 1 Genetic profile results in lung cancer with choriocarcinoma features.

Biopsy Samples	Biomarkers	Details	Variant Allele Fraction
Brain metastasis	KRAS	p.G13R	17.8%
	GNAS	p.R201H	8.2%
	ERBB2(Her2)	p.R1053G	45.8%
	ANXA7	p.R479*	41.9%
	BAP1	p.V439M	7.2%
	TIGIT	p.V100M	46.7%
	WNK1	p.C733fs	10.5%
	ZRSR2	p.S447_R448insQS	39.0%
	Tumor Mutational Burden	3.7 mutations/Mb	–
	Microsatellite instability	Stable	–
Blood	KRAS	p.G13R	0.3%
	GNAS	p.R201H	0.2%
Lung tumor	KRAS	p.G13R	20.0%
	GNAS	p.R201H	9.0%
	ERBB2(Her2)	p.R1053G	50.0%
	BAP1	p.V439M	11.0%
	DDB2	p.R20K	44.0%
	DOT1L	p.S1061C	50.0%
	NSD3	p.R326W	48.0%
	POLQ	p.K58Q	48.0%
	THRAP3	p.H761R	48.0%
	TNFAIP3	p.R761H	40.0%
	ZRSR2	p.S447_R448insQS	61.0%
	Tumor Mutational Burden	Low, 1.0 mutations/Mb	–
	Microsatellite instability	Stable	–
	Genomic loss of Heterozygosity (LOH)	Low, 2.0% of tested genomic segments exhibited LOH	–

GNAS R201H among others were identified in lung tumor (Table 1). Additionally, a cancer-type similarity assessment that compared patient's tumor against the signatures across 21 distinct common cancer types in the Caris database revealed that the most likely cancer type was lung adenocarcinoma (Figure 2A).

Discussion

Choriocarcinoma is an aggressive tumor, which is classified into gestational and non-gestational choriocarcinoma. Gestational choriocarcinoma originates from trophoblastic cells and usually associates with pregnancy events including hydatidiform moles and production of β-hCG (7). Non-gestational choriocarcinoma typically is a mixed germ cell tumor, showing differentiation towards trophoblastic structures. Non-gestational choriocarcinoma has been reported in extragonadal sites. These tumors typically occur in midline locations such as the mediastinum, retroperitoneum, or brain (8). Interestingly, trophoblastic differentiation has been observed in tumors originating from various organs. This has led to a debate regarding whether these cancers should be classified as extragonadal choriocarcinoma (9, 10). These types of carcinomas have been reported in different organs, including liver, stomach, cervix, lung and others (11–14).

Lung cancer exhibiting choriocarcinoma features or trophoblastic differentiation is a rare occurrence, and it has been reported in some case reports (Supplementary Table 1). However, it's evident that there is substantial controversy among pathologists regarding the terminology used for this rare subtype of lung cancer, commonly referred to as "primary pulmonary choriocarcinoma (PPC)". Alternative terms such as "primary choriocarcinoma of the lung", "lung tumors with trophoblastic morphology" and "lung adenocarcinoma with choriocarcinomatous features" were also employed in published literature. In our case, the biopsies from brain metastasis were reported by local pathologists as "metastatic choriocarcinoma". Subsequent biopsies of the lung and lymph nodes were reported by local pathologists as "suggestive of choriocarcinoma". Pathologic consultations at two academic cancer centers reported it as adenocarcinoma with aberrant expression of β-hCG versus poorly differentiated carcinoma with

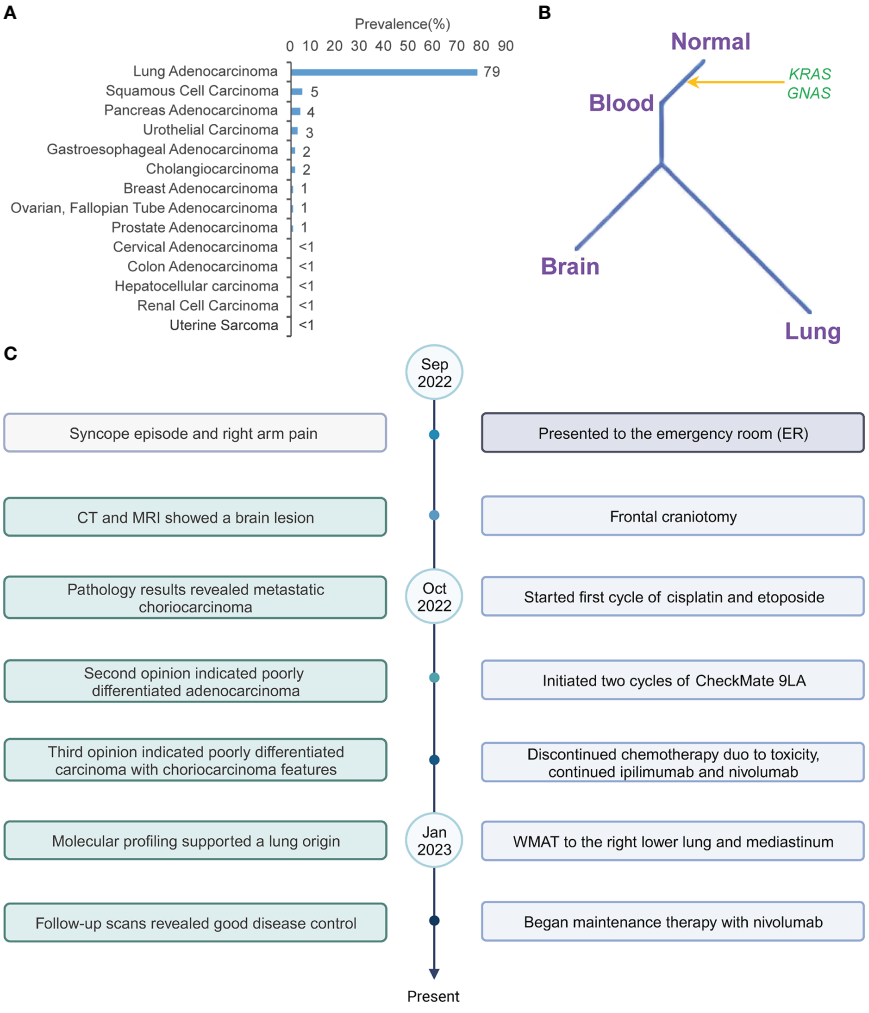

FIGURE 2
(A) The prevalence of cancer types based on the tumor's molecular signature, including all the mutations (Data from Caris). **(B)** Phylogenetic tree of lung cancer with choriocarcinoma features. **(C)** Timeline of the patient's diagnosis and treatments.

choriocarcinoma features or adenocarcinoma with β-hCG production.

Diagnosis of this rare subtype of lung cancer is challenging, especially in female patients. In addition to particular morphological feature and detection of β-hCG in cancer cells, it is imperative to rule out any prior gynecologic cancers and molar pregnancy in the patient's medical history (15). It's noteworthy that typical immunohistochemical markers found in lung adenocarcinoma, such as TTF-1 and Napsin A, were negative in lung cancer with choriocarcinoma features. TTF-1, that plays a crucial role in maintaining terminal respiratory unit cell function in the lung, and Napsin A, an aspartic proteinase involved in surfactant protein maturation (16) may provide valuable information facilitating the diagnosis of primary lung adenocarcinoma. However, they are not always positive in cancers of lung origins. Indeed, both markers were negative in our case, which was consistent with other reported cases (15, 17–19). Taken together, these highlight the profound challenges in identifying the tumor's origin of rare histologic subtypes.

Clinically, the absence of abnormal bleeding, uterine or ovarian abnormalities and low serum β-hCG levels in our case was against the initial diagnosis of metastatic choriocarcinoma by local pathologists. Although the primary site of the tumor could not be determined based on morphology and IHC staining, the molecular profiling including the cancer gene mutations and transcriptomic features was suggestive of lung origin. The notable mutations detected in this tumor included KRAS G13R and GNAS R201H. KRAS is one of the most common mutated oncogenes and frequently detected in colorectal adenocarcinoma, lung adenocarcinoma, multiple myeloma and pancreatic adenocarcinoma (20, 21). In lung adenocarcinoma, KRAS is the most prevalent cancer driver, with about 35.5% of patients harboring a KRAS mutation (22). On the other hand, KRAS mutations are rarely observed in either gestational or non-gestational choriocarcinomas originating from germ cells (23, 24). KRAS mutations have only been reported in extragonadal choriocarcinomas, such as duodenal choriocarcinoma (25). The tumor in our case carried a pathogenic KRAS G13R mutation, which was supportive of lung origin. Furthermore, the transcriptomic profiling data was also suggestive of lung origin (Figure 2A). Taken together, these results suggested that genetic profiling may facilitate the diagnosis and identification of organ origin of rare tumors such as lung cancer with choriocarcinoma features.

Due to its scarcity, the genomic landscape of lung cancer with choriocarcinoma features has not been defined. EGFR L858R, EGFR V774M (17, 18) and TP53 C275G, R273L, V73fs or D281E (17, 26–28) have been reported previously. The case in our study is the first case with KRAS mutation. Another interesting mutation is GNAS p.R201H, an oncogenic activating mutation in alpha-subunit of the stimulatory G protein (Gsα) that caused constitutive Gsα signaling. GNAS mutations have been identified in many epithelial tumors, such as pancreatic cancer and colon cancer. GNAS mutated tumors frequently harbored concurrent mutations in the Ras/Raf pathway, such as KRAS mutations (29). While uncommon, GNAS p.R201H mutation has been detected in lung adenocarcinoma (30). On the other hand, GNAS mutations are also rarely detected in gestational and non-gestational choriocarcinomas. We leveraged the molecular profiling data from lung tumors, brain metastasis and ctDNA to investigate the genomic evolutionary pattern in this case. All tumor samples carried identical KRAS and GNAS mutations, indicating that these mutations were early events in tumor development (Figure 2B).

Compared to other NSCLC subtypes, lung cancer with choriocarcinoma features is associated with a very poor prognosis, with a 5-year survival rate of less than 5% (31). This rare type of lung cancer tends to present with widespread metastases and to progress rapidly (15). Due to the rarity, there is no evidence to guide optimal treatment. Chemotherapy including BEP (bleomycin, etoposide and cisplatin) and EMA-CO (etoposide, methotrexate, actinomycin-D, cyclophosphamide, vincristine) (15, 32) is the commonly used therapeutic modality. Surgery or radiation in combination with chemotherapy was also employed for lung cancer with choriocarcinoma features of early stages (33).

Immune checkpoint inhibitors (ICIs) have revolutionized the therapeutic landscape across different cancer types including NSCLC. However, the use of ICIs in gestational choriocarcinoma remains under investigation. Notably, high levels of PD-L1 expression were observed in gestational choriocarcinoma (34), leading to the potential utilization of ICIs such as anti-PD1/PD-L1 as treatment options. Case reports and small sized clinical trials have explored the potential of ICIs, particularly pembrolizumab, for patients who progressed after initial chemotherapy (35, 36). Favorable outcomes, including complete responses, were observed in cases with strong PD-L1 expression (often 90%-100%) (37–43). Additionally, toripalimab and tirelizumab showed promise in chemo-resistant choriocarcinoma (44, 45).In a phase 2 clinical trial, the combination of camrelizumab and apatinib showed potential for chemo-resistant choriocarcinoma, with a 50% complete response rate (46). In the TROPHIMMUN trial, avelumab also demonstrated curative potential in 50% chemotherapy-resistant gestational trophoblastic tumors, including cases of choriocarcinoma (47). Despite these encouraging findings, the variability in response rates and long-term benefits of ICIs in gestational choriocarcinoma require further investigation.

Evidence concerning the using of ICIs in non-gestational choriocarcinoma, especially extragonadal cases, was limited. In a case report involving non-gestational choriocarcinoma, pembrolizumab was utilized as a second-line treatment following the initial EMA-CO regimen. Unfortunately, the patient experienced rapid progression and subsequently returned to chemotherapy. Despite attempting pembrolizumab once more, the treatment did not yield a favorable response (27). In a case of primary mediastinal choriocarcinoma, the patient initially achieved partial remission after two cycles of pembrolizumab but developed resistance. Despite attempting a combination treatment of pembrolizumab with chemotherapy, however, the treatment proved unsuccessful due to rapid disease progression (48). In contrast, a case involving primary neck choriocarcinoma achieved

a complete response when treated with a combination of pembrolizumab and chemotherapy (49). The effectiveness of ICIs in non-gestational choriocarcinoma showed varying outcomes and requires additional research.

Regarding lung cancer with choriocarcinoma features, its rarity has led to a lack of clinical trial data on the efficacy of ICIs. Only a few case reports have utilized ICIs in this rare subtype of lung cancer. Buza et al. reported a case in which the patient initiated first line treatment with carboplatin and paclitaxel for 6 cycles. PD-L1 immunostaining showed a 30% staining of tumor cells. However, during the follow-up period, the tumor experienced progression, leading to the administration of pembrolizumab. Unfortunately, the disease continued to progress and the patient passed away (11). Another case report explored nivolumab as a second line treatment following the initial administration of pemetrexed/cisplatin/bevacizumab. PD-L1 immunostaining exhibited positivity in more than 50% of cells. The patient achieved a partial response after completing the first 4 cycles of immunotherapy, but CT indicated disease progression after 1 year of treatment (50).

The integration of immunotherapy with chemotherapy has emerged as the primary treatment approach for NSCLC. However, the potential application of this combined treatment in lung cancer with choriocarcinoma features or even as a first-line option remains uncertain. A case study implementing the CheckMate 9LA regimen was conducted after a patient exhibited postoperative relapse. Following two months of treatment, the patient achieved a partial response and subsequently received nivolumab and ipilimumab as part of maintenance therapy. This positive response persisted throughout the 12-month follow-up period (51). To our knowledge, the patient in our study represents the second reported instance of receiving combined anti-PD-1/anti-CTLA-4 therapy and chemotherapy in lung cancer with choriocarcinoma features. After one cycle of EP and two cycles of CheckMate 9LA, the primary tumor exhibited a reduction in size. Subsequent maintenance treatment involving eight cycles of nivolumab and ipilimumab, followed by nivolumab monotherapy, a continuous decrease in tumor size was observed, while other sites remained stable. Her relatively small disease burden also made it possible for us to offer LCT, which may also have contributed to her good disease control. These encouraging results suggest that the combination of chemoimmunotherapy with local radiation therapy may provide a promising therapeutic option for patients with lung cancer with choriocarcinoma features (Figure 2C).

Conclusion

Lung cancer with choriocarcinoma features is a rare and aggressive malignancy. Determining the primary origin by traditional pathology assessment based on morphology and IHC is challenging. As a result, delayed diagnosis is common in patients with this rare subtype of lung cancer. In the era of precision medicine, the utilization of molecular profiling has proven highly informative and has significant diagnostic implications, particularly for cancer of rare histologies. The molecular information could not only facilitate identifying the origin of malignancy but may also guide decision making for treatment approaches on or off trials. For lung cancer with choriocarcinoma features, despite the lack of established treatment options, our case and others demonstrate the potential of chemoimmunotherapy in treating this subtype of lung cancer. In addition, local consolidation therapy could be considered for patients with small disease burden and good performance status.

Data availability statement

The data presented in the study are deposited in the GEO repository, accession number GSE261551.

Ethics statement

The studies involving humans were approved by The University of Texas MD Anderson Cancer Center. The studies were conducted in accordance with the local legislation and institutional requirements. The participants provided their written informed consent to participate in this study. Written informed consent was obtained from the individual(s) for the publication of any potentially identifiable images or data included in this article.

Author contributions

HL: Data curation, Formal analysis, Writing – original draft, Writing – review & editing. XH: Formal analysis, Writing – review & editing. MN: Writing – review & editing. GF: Writing – review & editing. JS: Writing – review & editing. JG: Writing – review & editing. JW: Writing – review & editing. XL: Writing – review & editing. AV: Writing – review & editing. JL: Writing – review & editing. DG: Writing – review & editing. JH: Writing – review & editing. AF: Writing – review & editing. JZ: Conceptualization, Funding acquisition, Supervision, Writing – review & editing.

Funding

The author(s) declare financial support was received for the research, authorship, and/or publication of this article. This work received support from the MD Anderson Lung Moon Shot Program, as well as generous support from Andrea Mugnaini and Edward LC Smith Fund.

Acknowledgments

The authors express their gratitude to the patient for her graciousness in allowing her case to be reported.

Conflict of interest

JZ reports research funding from Merck, Johnson & Johnson, and Novartis; and consultant fees from BMS, Johnson & Johnson, AstraZeneca, Geneplus, OrigMed, Novartis, Varian and Innovent, outside the submitted work. XL receives consulting/advisory fees from EMD Serono Merck KGaA, AstraZeneca, Spectrum Pharmaceutics, Novartis, Eli Lilly, Boehringer Ingelheim, Hengrui Therapeutics, Janssen, Blueprint Medicines, Sensei Biotherapeutics, Abion, and Abbvie, and Research Funding from Eli Lilly, EMD Serono, ArriVent, Teligene, Regeneron, and Boehringer Ingelheim. AV reports membership on the advisory board with AstraZeneca.

The remaining authors declare that the research was conducted in the absence of any commercial or financial relationships that could be construed as a potential conflict of interest.

This study received funding from MD Anderson Lung Moon Shot Program and Andrea Mugnaini and Edward LC Smith Fund. The funder was not involved in the study design, collection, analysis, interpretation of data, the writing of this article or the decision to submit it for publication.

Publisher's note

Supplementary material

The Supplementary Material for this article can be found online at: https://www.frontiersin.org/articles/10.3389/fonc.2024.1324057/full#supplementary-material

References

1. Gridelli C, Rossi A, Carbone DP, Guarize J, Karachaliou N, Mok T, et al. Non-small-cell lung cancer. *Nat Rev Dis Primers* (2015) 1(1):15009. doi: 10.1038/nrdp.2015.9

2. Nicholson AG, Tsao MS, Beasley MB, Borczuk AC, Brambilla E, Cooper WA, et al. The 2021 WHO classification of lung tumors: impact of advances since 2015. *J Thorac Oncol* (2022) 17(3):362–87. doi: 10.1016/j.jtho.2021.11.003

3. Howlader N, Forjaz G, Mooradian MJ, Meza R, Kong CY, Cronin KA, et al. The effect of advances in lung-cancer treatment on population mortality. *N Engl J Med* (2020) 383(7):640–9. doi: 10.1056/NEJMoa1916623

4. Paz-Ares L, Ciuleanu TE, Cobo M, Schenker M, Zurawski B, Menezes J, et al. First-line nivolumab plus ipilimumab combined with two cycles of chemotherapy in patients with non-small-cell lung cancer (CheckMate 9LA): an international, randomised, open-label, phase 3 trial. *Lancet Oncol* (2021) 22(2):198–211. doi: 10.1016/S1470-2045(20)30641-0

5. Gomez DR, Blumenschein GR Jr., Lee JJ, Hernandez M, Ye R, Camidge DR, et al. Local consolidative therapy versus maintenance therapy or observation for patients with oligometastatic non-small-cell lung cancer without progression after first-line systemic therapy: a multicentre, randomised, controlled, phase 2 study. *Lancet Oncol* (2016) 17(12):1672–82. doi: 10.1016/S1470-2045(16)30532-0

6. Gomez DR, Tang C, Zhang J, Blumenschein GR Jr., Hernandez M, Lee JJ, et al. Local consolidative therapy vs. Maintenance therapy or observation for patients with oligometastatic non-small-cell lung cancer: long-term results of a multi-institutional, phase II, randomized study. *J Clin Oncol* (2019) 37(18):1558–65. doi: 10.1200/jco.19.00201

7. Lurain JR. Gestational trophoblastic disease I: epidemiology, pathology, clinical presentation and diagnosis of gestational trophoblastic disease, and management of hydatidiform mole. *Am J Obstet Gynecol* (2010) 203(6):531–9. doi: 10.1016/j.ajog.2010.06.073

8. Johnson AM, Johnson CM, Khalil Z, Stitzel M, Teoh D. Case Report: Treatment of primary pulmonary choriocarcinoma with lung lobectomy and adjuvant chemotherapy. *Gynecol Oncol Rep* (2022) 43:101064. doi: 10.1016/j.gore.2022.101064

9. Yen C-J, Yen C-C, Tsai H-W. Postmolar metastatic choriocarcinoma mimicking primary lung cancer. *J Cancer Res Pract* (2019) 6(1):41–4. doi: 10.4103/jcrp.Jcrp_7_18

10. Cao X, Feng H, Liu S, Chen L. Analysis of clinical characteristics and prognosis of 68 patients with primary pulmonary choriocarcinoma. *BMC Pulm Med* (2023) 23(1):75. doi: 10.1186/s12890-023-02368-w

11. Buza N, Baine I, Hui P. Precision genotyping diagnosis of lung tumors with trophoblastic morphology in young women. *Mod Pathol* (2019) 32(9):1271–80. doi: 10.1038/s41379-019-0275-z

12. Fukagawa A, Fujita N, Ohira K, Fujimoto H, Goto N, Nozawa A. Primary hepatic choriocarcinoma in an 83-year-old woman. *Pathol Int* (2017) 67(8):425–30. doi: 10.1111/pin.12552

13. Kobayashi A, Hasebe T, Endo Y, Sasaki S, Konishi M, Sugito M, et al. Primary gastric choriocarcinoma: two case reports and a pooled analysis of 53 cases. *Gastric Cancer* (2005) 8(3):178–85. doi: 10.1007/s10120-005-0332-9

14. Longo R, Battaglia F, Gattuso D, De Sio L, Sarmiento R, Amici S, et al. Primary nongestational choriocarcinoma of the uterine cervix. *J Clin Oncol* (2011) 29(11):e301–2. doi: 10.1200/JCO.2010.33.2361

15. Nguyen HTT, Hoang HH, Le ATV. A case report of primary pulmonary choriocarcinoma in a man: successful combination of surgery and chemotherapy. *Case Rep Oncol* (2020) 13(2):923–8. doi: 10.1159/000508744

16. Ren X, Wen X, Ren YJ, Liu X, Wang J, Hao M, et al. Significance of thyroid transcription factor 1 and Napsin A for prompting the status of EGFR mutations in lung adenocarcinoma patients. *J Thorac Dis* (2022) 14(11):4395–404. doi: 10.21037/jtd-22-1265

17. Shigematsu Y, Nakano K, Uchibori K, Inamura K. EGFR-mutated pulmonary choriocarcinoma combined with adenocarcinoma. *J Thorac Oncol* (2022) 17(11):1318–22. doi: 10.1016/j.jtho.2022.07.1146

18. Onishi I, Kirimura S, Wakejima R, Okubo K, Odai T, Kakuta R, et al. Primary pulmonary choriocarcinoma with a genomic sequence. *Pathol Int* (2022) 72(2):141–3. doi: 10.1111/pin.13193

19. Dinis de Sousa M, Barata M, Miranda AR, Sequeira P, Oliveira A, Xavier L, et al. Beta-HCG secretion by a pulmonary pleomorphic carcinoma: A case report. *Respir Med Case Rep* (2021) 34:101528. doi: 10.1016/j.rmcr.2021.101528

20. Cook JH, Melloni GEM, Gulhan DC, Park PJ, Haigis KM. The origins and genetic interactions of KRAS mutations are allele- and tissue-specific. *Nat Commun* (2021) 12(1):1808. doi: 10.1038/s41467-021-22125-z

21. Timar J, Kashofer K. Molecular epidemiology and diagnostics of KRAS mutations in human cancer. *Cancer Metastasis Rev* (2020) 39(4):1029–38. doi: 10.1007/s10555-020-09915-5

22. Eklund EA, Wiel C, Fagman H, Akyurek LM, Raghavan S, Nyman J, et al. KRAS mutations impact clinical outcome in metastatic non-small cell lung cancer. *Cancers (Basel)* (2022) 14(9):2063. doi: 10.3390/cancers14092063

23. Jung SH, Choi YJ, Kim MS, Park HC, Han MR, Hur SY, et al. Distinct genomic profiles of gestational choriocarcinoma, a unique cancer of pregnant tissues. *Exp Mol Med* (2020) 52(12):2046–54. doi: 10.1038/s12276-020-00544-0

24. Fulop V, Mok SC, Genest DR, Szigetvari I, Cseh I, Berkowitz RS. c-myc, c-erbB-2, c-fms and bcl-2 oncoproteins. Expression in normal placenta, partial and complete mole, and choriocarcinoma. *J Reprod Med* (1998) 43(2):101–10.

25. Berry AC, Berry NA, Sobrado J, Mohan K, Berry B. S2894 Jaundice, elevated beta-human chorionic gonadotropin, and female gender: duodenal Choriocarcinoma, not pregnancy. *Off J Am Coll Gastroenterol | ACG* (2020) 115:S1517. doi: 10.14309/01.ajg.0000713624.51210.53

26. Zhang X, Ding B, Chen L, Huang X, Zhang K, Wang Z, et al. Primary pulmonary choriocarcinoma in male: report a case with genetic testing and review of the literature. *Transl Cancer Res* (2022) 11(6):1844–9. doi: 10.21037/tcr-21-2627

27. Kazemi NY, Langstraat C, John Weroha S. Non-gestational choriocarcinoma with hyperprogression on pembrolizumab: A case report and review of the literature. *Gynecol Oncol Rep* (2022) 39:100923. doi: 10.1016/j.gore.2022.100923

28. Ma Y, Wang C, Sun PL, Zhu Y, Huang ZK, Jin SX. A case of male primary pulmonary Choriocarcinoma. *Chin Med J (Engl)* (2018) 131(24):3001–3. doi: 10.4103/0366-6999.247205

29. Ritterhouse LL, Vivero M, Mino-Kenudson M, Sholl LM, Iafrate AJ, Nardi V, et al. GNAS mutations in primary mucinous and non-mucinous lung adenocarcinomas. *Mod Pathol* (2017) 30(12):1720–7. doi: 10.1038/modpathol.2017.88

30. Lv Y, Zhou C, Chen Z, Zhao X, Sun Y, Li J, et al. Response to trametinib in a nonsmall cell lung cancer patient with osimertinib resistance harboring GNAS R201C and R201H mutations: a case report. *Anticancer Drugs* (2022) 33(9):966–9. doi: 10.1097/CAD.0000000000001342

31. Serno J, Zeppernick F, Jakel J, Schrading S, Maass N, Meinhold-Heerlein I, et al. Primary pulmonary choriocarcinoma: case report and review of the literature. *Gynecol Obstet Invest* (2012) 74(2):171–6. doi: 10.1159/000336784

32. Snoj Z, Kocijancic I, Skof E. Primary pulmonary choriocarcinoma. *Radiol Oncol* (2017) 51(1):1–7. doi: 10.1515/raon-2016-0038

33. Kim JH, Cha MJ, Kim MK, Chung YJ, Lee EJ. Disseminated primary pulmonary choriocarcinoma successfully treated by chemotherapy: A case report and literature review. *Cancer Invest* (2020) 38(8-9):493–501. doi: 10.1080/07357907.2020.1804575

34. Zong L, Zhang M, Wang W, Wan X, Yang J, Xiang Y. PD-L1, B7-H3 and VISTA are highly expressed in gestational trophoblastic neoplasia. *Histopathology* (2019) 75 (3):421–30. doi: 10.1111/his.13882

35. Paydas S. Immune checkpoint inhibitor using in cases with gestational trophoblastic diseases. *Med Oncol* (2023) 40(3):106. doi: 10.1007/s12032-022-01941-3

36. Sharma N, Kundal R, Kaushal V. Immunobiology and immunotherapy of gestational trophoblastic disease. *Gynecology Obstetrics Clin Med* (2022) 2(2):76–81. doi: 10.1016/j.gocm.2022.04.008

37. Ghorani E, Kaur B, Fisher RA, Short D, Joneborg U, Carlson JW, et al. Pembrolizumab is effective for drug-resistant gestational trophoblastic neoplasia. *Lancet* (2017) 390(10110):2343–5. doi: 10.1016/S0140-6736(17)32894-5

38. Goldfarb JA, Dinoi G, Mariani A, Langstraat CL. A case of multi-agent drug resistant choriocarcinoma treated with Pembrolizumab. *Gynecol Oncol Rep* (2020) 32:100574. doi: 10.1016/j.gore.2020.100574

39. Clair KH, Gallegos N, Bristow RE. Successful treatment of metastatic refractory gestational choriocarcinoma with pembrolizumab: A case for immune checkpoint salvage therapy in trophoblastic tumors. *Gynecol Oncol Rep* (2020) 34:100625. doi: 10.1016/j.gore.2020.100625

40. Huang M, Pinto A, Castillo RP, Slomovitz BM. Complete serologic response to pembrolizumab in a woman with chemoresistant metastatic choriocarcinoma. *J Clin Oncol* (2017) 35(27):3172–4. doi: 10.1200/jco.2017.74.4052

41. Paspalj V, Polterauer S, Poetsch N, Reinthaller A, Grimm C, Bartl T. Long-term survival in multiresistant metastatic choriocarcinoma after pembrolizumab treatment: A case report. *Gynecol Oncol Rep* (2021) 37:100817. doi: 10.1016/j.gore.2021.100817

42. Wong AJ, Finch L, Pearson JM, Pinto A, Huang M. Retreatment of chemotherapy-resistant metastatic choriocarcinoma with immunotherapy. *Gynecol Oncol Rep* (2022) 40:100955. doi: 10.1016/j.gore.2022.100955

43. Matthews BJ, Froehlich A, Goicochea L, Levinson K. Postmenopausal mixed gestational trophoblastic neoplasia with complete response to immunotherapy - A case report. *Gynecol Oncol Rep* (2023) 46:101168. doi: 10.1016/j.gore.2023.101168

44. Liu X, Li X, Qu H, Zhang S, Zhang R, Du Z. Effectiveness and safety of toripalimab combination therapies for patients with chemo-resistant choriocarcinoma. *Front Oncol* (2022) 12:815917. doi: 10.3389/fonc.2022.815917

45. Chen Y, Ye H, Tang J, Weng Y, Zhang J, Liu J. Case report: first-line immune checkpoint inhibitor plus chemotherapy for oral metastasis in a patient with ultra high-risk gestational choriocarcinoma. *Cancer Manag Res* (2022) 14:1867–75. doi: 10.2147/CMAR.S351165

46. Cheng H, Zong L, Kong Y, Wang X, Gu Y, Cang W, et al. Camrelizumab plus apatinib in patients with high-risk chemorefractory or relapsed gestational trophoblastic neoplasia (CAP 01): a single-arm, open-label, phase 2 trial. *Lancet Oncol* (2021) 22(11):1609–17. doi: 10.1016/S1470-2045(21)00460-5

47. You B, Bolze P-A, Lotz J-P, Massardier J, Gladieff L, Joly F, et al. Avelumab in patients with gestational trophoblastic tumors with resistance to single-agent chemotherapy: cohort A of the TROPHIMMUN phase II trial. *J Clin Oncol* (2020) 38(27):3129–37. doi: 10.1200/jco.20.00803

48. Pan W, Hou J. Pembrolizumab for treatment of a male with primary mediastinal choriocarcinoma: a case report. *Transl Cancer Res* (2022) 11(9):3416–20. doi: 10.21037/tcr-22-766

49. Han C, Zhou Y, Ma JA, Liu J, Jiang YN, Zhang HX. A promising treatment option for refractory male primary choriocarcinoma: report of two cases. *Transl Cancer Res* (2020) 9(4):3054–60. doi: 10.21037/tcr.2020.02.05

50. Ochi M, Miyamoto S, Terada Y, Furuhata Y, Awano N, Izumo T, et al. The significant antitumor activity of nivolumab in lung adenocarcinoma with choriocarcinomatous features. *Intern Med* (2018) 57(12):1773–7. doi: 10.2169/internalmedicine.0002-17

51. Iso H, Hisakane K, Terashi N, Mikami E, Matsuki S, Sonokawa T, et al. A remarkable response to combination chemotherapy with nivolumab and ipilimumab in a patient with primary pulmonary choriocarcinoma: a case report. *Transl Cancer Res* (2023) 12(8):2212–8. doi: 10.21037/tcr-23-221

Frontiers in Genetics

Highlights genetic and genomic inquiry relating to all domains of life

The most cited genetics and heredity journal, which advances our understanding of genes from humans to plants and other model organisms. It highlights developments in the function and variability of the genome, and the use of genomic tools.

Discover the latest Research Topics

See more →

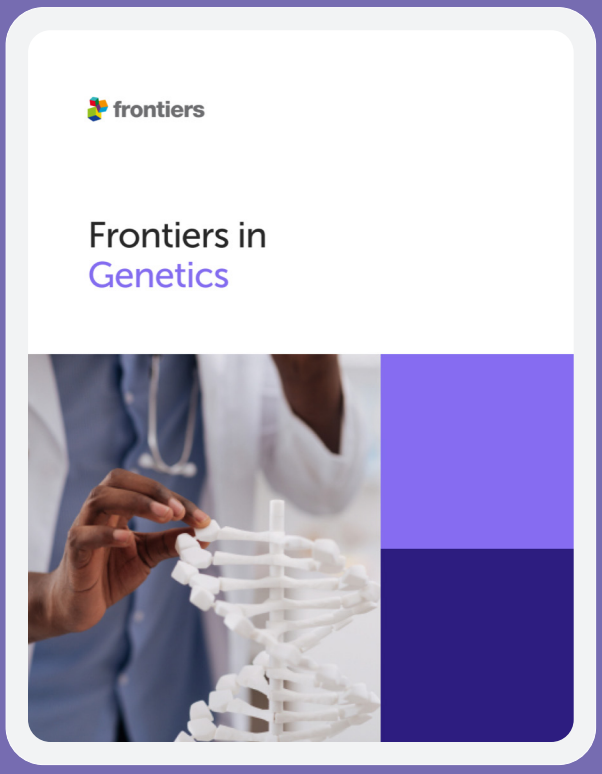

Frontiers

Avenue du Tribunal-Fédéral 34
1005 Lausanne, Switzerland
frontiersin.org

Contact us

+41 (0)21 510 17 00
frontiersin.org/about/contact